

UCRL-16455

University of California
Ernest O. Lawrence
Radiation Laboratory

DECAY PROPERTIES OF THE Ξ HYPERON
AND Ξ^* RESONANCES

TWO-WEEK LOAN COPY

*This is a Library Circulating Copy
which may be borrowed for two weeks.
For a personal retention copy, call
Tech. Info. División, Ext. 5545*

34a

R

UNIVERSITY OF CALIFORNIA

Lawrence Radiation Laboratory
Berkeley, California

AEC Contract No. W-7405-eng-48

DECAY PROPERTIES OF THE Ξ HYPERON
AND Ξ^* RESONANCES

Deane Whitney Merrill, Jr.
(Ph. D. Thesis)

September 10, 1966

DECAY PROPERTIES OF THE Ξ HYPERON
AND Ξ^* RESONANCES

Contents

Abstract	viii
I. Introduction	1
II. Theory	
A. Non-Leptonic Hyperon Decay	3
1. Coordinate Systems and Relativistic Transformations	4
2. Density Matrix Formalism	4
3. Description of Initial Spin State	7
4. Spin $J \rightarrow$ Spin $J' +$ Spin 0	10
B. Maximum-Likelihood Analysis of Data.	22
III. Description of K-63 Beam	25
IV. Selection of K-63 Events	
A. Preliminary Analysis	30
B. Selection Criteria	31
1. Ξ^- Events	31
2. Ξ^0 Events	38
V. Properties of the Ξ^- and Ξ^0 Hyperons	49
A. Spin Analysis	
1. Preliminary Considerations	49
2. $(2J + 1)$ Spin Factor	52
3. Analysis of Monte Carlo Events.	54
4. Discussion	66
B. Decay Parameters	
1. Maximum-Likelihood Analysis	69
2. Discussion	75
C. Decay Distributions	84

VI.	Properties of Ξ^* (1530)	90
A.	Final States Analyzed	90
1.	$\Xi K\pi$ Final States	90
2.	$\Xi K\pi\pi$ Final States	92
B.	Electromagnetic Mass Difference	95
1.	Selection and Fitting of Events	95
2.	Determination of Ξ^* Masses and Mass Difference	96
3.	Possible Systematic Errors	99
4.	Discussion	105
C.	Spin and Parity	111
VII.	Properties of Ξ^* (1817)	117
A.	Analysis of Ξ^* (1817) \rightarrow Ξ^* (1530) + π	118
B.	Discussion	124
	Acknowledgments	126
	Appendices	
A.	Current Status of K-63 Data Analysis	127
B.	Scanning Biases and Other Systematic Errors	130
C.	Checkerboard Theorem for N-Body Final States	149
D.	Approximate K-63 Path Length and Beam Contamination	152
E.	Analysis of Monte Carlo Events	155
	Footnotes and References	165

LIST OF ILLUSTRATIONS

<u>Fig.</u>	<u>Title</u>
II-1.	Angles and coordinate systems in Ξ production and decay
III-1.	Schematic layout of K-63 beam
III-2.	Profiles of K-63 beam
III-3.	Cocked mass slit
IV-1.	Resolution of ambiguities by ionization
IV-2.	Confidence levels, Type-72 events
IV-3.	Classification of events by confidence levels
IV-4.	Distribution of $\log_{10} R$, $K^- + p \rightarrow \Xi^0 + K^+ + \pi^-$, 1.7-2.1 BeV/c
IV-5.	Distribution of $\log_{10} R$, $K^- + p \rightarrow \Xi^0 + K^+ + \pi^-$, 2.45-2.7 BeV/c
IV-6.	Distribution of $\log_{10} R$, $K^- + p \rightarrow \Xi^0 + K^0$, 1.7-2.1 BeV/c
IV-7.	Distribution of $\log_{10} R$, $K^- + p \rightarrow \Xi^0 + K^0$, 2.45-2.7 BeV/c
IV-8.	Distribution of $\log_{10} R$, $K^- + p \rightarrow \Xi^0 + K^0 + \pi^+ + \pi^-$, 2.45-2.7 BeV/c
V-1.	Plot of $w = \ln \mathcal{L}$ vs $(2J+1)$, 3278 Ξ^- events
V-2.	Distribution of $X = \Delta \ln \mathcal{L}$, 15 $\Xi^{-,0}$ subsamples and unpolarized Monte Carlo samples
V-3.	Distribution of $X = \Delta \ln \mathcal{L}$, polarized Monte Carlo samples
V-4.	Comparison of X_{obs} and $P(X, J)$, 4080 $\Xi^{-,0}$ events and 3130 Ξ^- events
V-5.	Comparison of X_{obs} and $P(X, J)$, 649 Ξ^0 events and 3779 $\Xi^{-,0}$ events
V-6.	Plot of X vs $ t_{10} $, 45 Ξ^- subsamples and 7 Ξ^0 subsamples
V-7.	Plot of $w = \ln \mathcal{L}$ vs Φ_{Ξ^0} , 649 Ξ^0 events
V-8.	Correlation between α_{Ξ} and α_{Λ} , 4080 $\Xi^{-,0}$ events
V-9.	Measurements of Ξ decay parameters
V-10.	Lee SU(3) triangle and $ \Delta I = 1/2$ rule
V-11.	Distribution of $\hat{p} \cdot \hat{\Lambda}$, 4080 Ξ^- and Ξ^0 events
V-12.	Observed Ξ decay distribution, 4080 Ξ^- and Ξ^0 events
V-13.	Observed Ξ decay distribution, 649 Ξ^0 events
V-14.	Observed Ξ decay distribution, $J = 1/2$ Monte Carlo events
V-15.	Observed Ξ decay distribution, $J = 3/2$ Monte Carlo events
VI-1.	Dalitz plot, $\Xi K \pi$ final states

LIST OF ILLUSTRATIONS (Cont.)

<u>Fig.</u>	<u>Title</u>
VI-2.	Observed $\Xi\pi$ mass distribution, $\Xi K\pi$ final states
VI-3.	Plot of $m^2(K\pi)$ vs $m^2(\Xi\pi)$, $\Xi K\pi\pi$ final states
VI-4.	Observed $\Xi\pi$ mass distribution, $\Xi K\pi\pi$ final states
VI-5.	Observed $\Lambda\pi\pi$ mass distribution, $\Xi K\pi$ final states
VI-6.	Dependence of $m(\Xi^*)$ and $m(\Lambda\pi)$ upon assumed $m(\Xi)$
VI-7.	Predicted c.m. mass differences in spin-1/2 octet and spin-3/2 decuplet
VI-8.	Comparison of decuplet mass splittings with SU(3) predictions
VI-9.	Values of $w = \ln \mathcal{L}$ for $\Xi^*(1530)$ spin and parity hypotheses
VII-1.	Plot of $m^2(\Xi\pi)$ vs $m^2(\Xi\pi\pi)$, $\Xi K\pi\pi$ final states
VII-2.	Plot of c.m. energy vs $\cos \alpha \equiv [\hat{\Xi}^*(1530) \cdot \hat{\Xi}^*(1817)]$, $\Xi K\pi\pi$ final states
VII-3.	Distribution of $[\hat{\Xi}^*(1530) \cdot \hat{n}]$ and $[\hat{\Xi} \cdot \hat{\Xi}^*(1530)]$, $\Xi K\pi\pi$ final states
B-1.	Coordinate systems used in discussion of systematic errors
B-2.	Observed Ξ production distribution, K-63 Ξ^- events
B-3.	Observed Ξ decay distribution, K-63 Ξ^- events
B-4.	Distribution of Ξ lab momenta, K-63 Ξ^- events
B-5.	Distribution of Λ lab momenta, K-63 Ξ^- events
B-6.	Distribution of K-63 Ξ^- events in bubble chamber
B-7.	Distribution of $(\hat{\Lambda} \cdot \hat{K})$ and $(\hat{\Lambda} \cdot \hat{\Xi})$, 4080 Ξ^- and Ξ^0 events
C-1.	Illustration of N-body Checkerboard Theorem
E-1.	Distribution of a_{Ξ} , Ξ samples and Monte Carlo samples
E-2.	Distribution of a_{Ξ} , Monte Carlo samples
E-3.	Distributions of t_{10} , Ξ samples and Monte Carlo samples
E-4.	Distributions of t_{10} , Monte Carlo samples
E-5.	Distributions of Φ_{Ξ} , Ξ samples and Monte Carlo samples
E-6.	Distributions of Φ_{Ξ} , Monte Carlo samples

LIST OF TABLES

<u>Table</u>	<u>Title</u>
IV-I.	Classification of passing type-72 events.
IV-II.	Classification of passing type-74 events.
IV-III.	Classification of passing type-12 events.
IV-IV.	Ambiguities among Ξ^0 candidates.
IV-V.	Estimate of π^- -produced background in unambiguous K-63 Ξ^0 sample.
V-I.	Final states and momenta of Ξ^- and Ξ^0 events analyzed.
V-II.	Search for $J = 3/2$ moments in Ξ decay.
V-III.	Subsamples used in Ξ spin analysis.
V-IV.	Determination of $C_{1/2}$ and $C_{3/2}$ from analysis of Monte Carlo events.
V-V.	Estimates of Ξ spin probabilities.
V-VI.	Subsamples used in Ξ decay parameter analysis.
V-VII.	Decay parameters, Ξ^- and Ξ^0 data analyzed separately.
V-VIII.	Decay parameters, Ξ^- and Ξ^0 data combined.
V-IX.	Decay parameters, comparison of experimental results.
V-X.	Non-leptonic hyperon decay amplitudes.
VI-I.	Events used in $\Xi^*(1530)$ mass-difference analysis.
VI-II.	Resonance parameters of Ξ^{*0} and Ξ^{*-} .
VI-III.	Analysis of 93 $\Xi^- K^0 \pi^+$ events with visible K^0 decay.
VI-IV.	Comparison of predicted and observed e. m. mass splittings.
VI-V.	Values of $w = \ln \mathcal{L}$ and t_{LM} for $\Xi^*(1530)$ subsamples (a)-(d).
VI-VI.	Values of $w = \ln \mathcal{L}$ and t_{LM} for combined $\Xi^*(1530)$ sample.
A-I.	Status of K-63 data analysis, September 1965.
A-II.	Percentage of K-63 data analyzed.
B-I.	Estimated Ξ and Λ escape losses.
B-II.	Effect of Ξ^- scanning bias correction.
D-I.	Approximate K-63 path length and percent beam contamination.
E-I.	Analysis of Monte Carlo events.

DECAY PROPERTIES OF THE Ξ HYPERON
AND Ξ^* RESONANCES

Deane Whitney Merrill, Jr.

Lawrence Radiation Laboratory
University of California
Berkeley, California

September 10, 1966

ABSTRACT

A sample of 2500 Ξ^- and 500 Ξ^0 hyperons, produced in ΞK , $\Xi K\pi$, and $\Xi K\pi\pi$ final states by K^- (in H_2) at incident momenta of 1.7 to 2.7 BeV/c, has been analyzed. The data are from an exposure (K-63) of 26 events/ μb in the 72-inch bubble chamber; approximately 85% of the Ξ^- events and 60% of the Ξ^0 events have been analyzed. For the Ξ , we determine the spin and decay parameters a_{Ξ} and $\Phi_{\Xi} = \tan^{-1}(\beta_{\Xi}/\gamma_{\Xi})$. Combining our data with 900 Ξ^- and 150 Ξ^0 events from an earlier experiment (K-72),* we obtain the following results:

Ξ spin: $J = 1/2$ favored over $J = 3/2$ by ≈ 2.5 standard deviations;

Ξ decay parameters (assuming $a_{\Lambda} = 0.647 \pm 0.048$):

$$a_{\Xi^-} = -0.398 \pm 0.041, \Phi_{\Xi^-} = 9.8^\circ \pm 9.0^\circ;$$

$$a_{\Xi^0} = -0.413 \pm 0.104.$$

We observe $\Xi^*(1530)$ and $\Xi^*(1817)$; our data are insufficient for analysis of suggested Ξ^* resonances at 1705 and 1933 MeV. We measure the $\Xi^*(1530)$ electromagnetic mass difference $\Delta m = m(\Xi^{*-}) - m(\Xi^{*0}) = 2.0 \pm 3.2$ MeV. Using data, part of which has already been described,[†] we find for $\Xi^*(1530)$:

$J \geq 3/2$ favored over $J = 1/2$ (the $J = 1/2$ hypothesis is $\approx 3.5\%$ as probable as the $J = 3/2$ hypothesis);

$J^P = 3/2^+$ favored over $3/2^-$ by ≈ 2.8 standard deviations.

For $\Xi^*(1817)$ decaying into $\Xi^*(1530) + \pi$, the hypotheses $J^P = 1/2^+$, $1/2^-$, $3/2^-$, $5/2^+$, $7/2^-$, etc. (corresponding to $\ell = 1, 2, 0$ and $2, 1$ and 3 , and 2 and 4 , respectively) are favored over other hypotheses, but results are inconclusive due to large background.

*J. Peter Berge, Philippe Eberhard, J. Richard Hubbard, Deane W. Merrill, Janice Button-Shafer, Frank T. Solmitz, and M. Lynn Stevenson, Phys. Rev. 147, 945 (1966); and J. Richard Hubbard, Properties of the Neutral Cascade Hyperon (Ph. D. Thesis), UCRL-11510, April 1966.

†Janice Button-Shafer, James S. Lindsey, Joseph J. Murray, and Gerald A. Smith, Phys. Rev. 142, 883 (1966).

I. INTRODUCTION

The Ξ^- hyperon was first observed in cosmic ray experiments in 1952.¹ Five years later, Alvarez et al. observed the first Ξ^0 in the Laboratory's 15-inch bubble chamber.² Since that time the Ξ doublet has played a central role in the development of elementary particle physics. It was soon recognized that the eight baryons $N^{+,0}, \Lambda, \Sigma^{+,0,-}, \Xi^{0,-}$ have similar characteristics, and various attempts were made to relate their observed properties. The most successful scheme yet devised is that of Gell-Mann³ and Ne'eman,⁴ SU(3), in which the baryons are represented as members of a unitary octet. Their predictions relating the baryon masses, magnetic moments, lifetimes, decay parameters, and production cross sections are in good agreement with experiment. In addition, SU(3) correctly relates many properties of mesons and other baryons and has predicted in advance the existence and quantum numbers of several new particles.

In 1964 a generalization of SU(3), known as SU(6), was introduced.^{5,6} The SU(6) scheme not only incorporates all the predictions of SU(3), but in addition relates the properties of particles belonging to different SU(3) multiplets. Higher symmetry schemes [U(12) and others] yield further predictions. The testing of the predictions of SU(3) and the higher symmetry schemes continues to be a most active area of research in experimental high-energy physics. A better knowledge of the properties of the Ξ hyperon and Ξ^* resonances will allow more sensitive tests to be made.

At the time of this writing, more than 5000 Ξ^- and 800 Ξ^0 have been photographed in bubble chambers, two-thirds of them in the Laboratory's 72-inch bubble chamber. This report represents the most comprehensive analysis so far of 2500 Ξ^- and 500 Ξ^0 in the K-63 experiment. We present the first discussion of the following in K-63: (i) the separation of Ξ^0 final states from background; (ii) the $\Xi^*(1530)$ electromagnetic mass difference; (iii) Ξ^- and Ξ^0 spin and decay parameters, from data including multibody final states. (The Ξ spin and decay parameters are also analyzed in a combined sample including 900 Ξ^- and 150 Ξ^0 from the K-72 experiment.) Analysis of K-72 data,⁷⁻⁹ and partial analysis

of K-63 Ξ^- data^{9, 10} has been previously reported. The decay properties of Ξ^{*+} (1530) and Ξ^{*0} (1817) have been analyzed in earlier published work;¹¹⁻¹³ in these areas we have analyzed a larger data sample, but no essential modification of earlier results is indicated.

The analysis of K-63 Ξ data is far from complete; 10% of the Ξ^- events and 40% of the Ξ^0 events remain to be measured (see Appendix A), and the analysis of Ξ production properties, lifetimes, leptonic decay modes, and the Ξ e. m. mass difference has not been started. It is hoped that information presented in this report will be useful to experimenters working with K-63 Ξ data in the future.

In this analysis such topics as escape losses and scanning biases are discussed (see Appendix B), but corrections have not been applied directly to the data (except in the analysis of Sec. V.A.1). The systematic errors introduced by such effects in no case exceed stated statistical errors; however, specific corrections for scanning biases, at least for Ξ^- events, should be considered in further analysis of these data.

Here we compare our experimental results with theoretical predictions and with results from other experiments. Conclusions are presented separately for each topic investigated, rather than being relegated to a separate chapter.

II. THEORY

A. Non-Leptonic Hyperon Decay

In this paper we shall discuss the decay properties of the Ξ hyperon, the $\Xi^*(1530)$, and the $\Xi^*(1817)$. The Ξ decays weakly, principally via the non-leptonic modes

$$\text{and } \Xi^- \rightarrow \Lambda + \pi^- \quad (\text{II-1a})$$

$$\Xi^0 \rightarrow \Lambda + \pi^0 \quad (\text{II-1b})$$

The $\Xi^*(1530)$ decays strongly via

$$\Xi^*(1530) \rightarrow \Xi + \pi \quad (\text{II-2})$$

and the $\Xi^*(1817)$ decays strongly, principally via^{11, 12, 14-17}

$$\text{and } \Xi^*(1817) \rightarrow \Lambda + \bar{K} \quad (\text{II-3a})$$

$$\Xi^*(1817) \rightarrow \Xi^*(1530) + \pi \quad (\text{II-3b})$$

We may schematically represent all of these processes by

$$F_J \rightarrow F_{J'} + B_0,$$

where F_J , $F_{J'}$, and B_0 are a fermion of spin J , a fermion of spin J' , and a spinless boson, respectively.

The angular distributions in a decay process of this type have been investigated by a number of authors, including (among others) Ademollo and Gatto,¹⁸ Gatto and Stapp,¹⁹ Capps,²⁰ Byers and Fenster,²¹ Button-Shafer,²² Zemach,²³ and Berman and Jacob.²⁴ We shall lean most heavily on the work of Byers and Fenster, who use the language of irreducible tensors T_{LM} to develop a sensitive test for the spin J of F_J , for the special case $J' = 1/2$. We shall also use Button-Shafer's work, which is an extension of the Byers-Fenster formalism, to treat the case $J' = 3/2$.

The Byers-Fenster formalism has several appealing features:

- (i) the initial spin state of F_J is described with a minimum number of parameters, without assumptions regarding the mechanisms that produced F_J ;
- (ii) the mechanism describing the decay of F_J is described with a minimum number of parameters in terms of helicity amplitudes;
- (iii) the spin state of $F_{J'}$ is expressed in terms of expectation values of a minimum number of spin operators. As a result, one can readily formulate tests to extract complete information (about the spin and

decay properties of F_J) from a given set of observed events.

1. Coordinate Systems and Relativistic Transformations

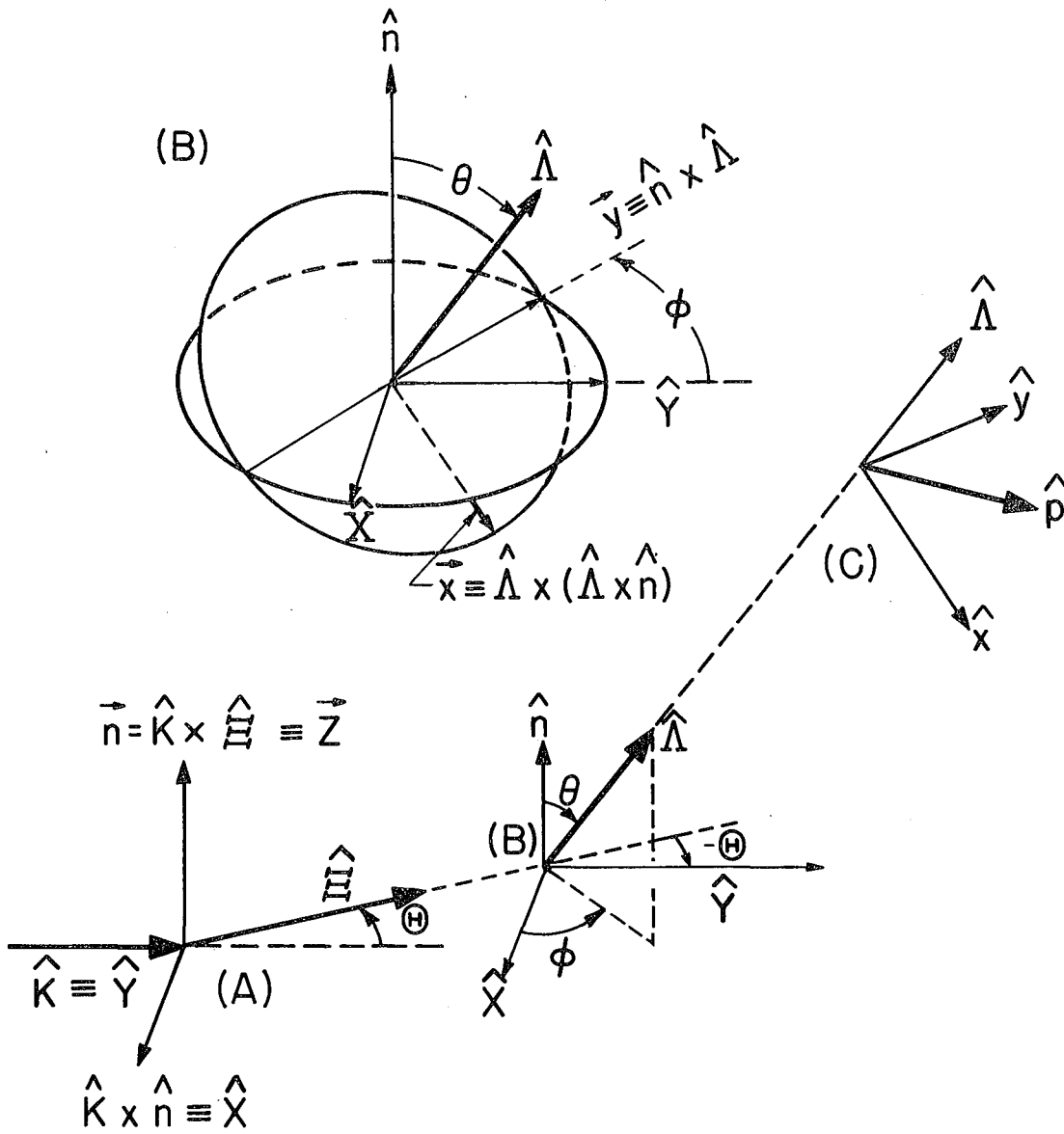
Figure II-1 illustrates Ξ production and decay via the sequence (A) $K^- + p \rightarrow \Xi + K$; (B) $\Xi \rightarrow \Lambda + \pi$; (C) $\Lambda \rightarrow p + \pi$. In the c.m. frame (A), the axes X, Y, Z, and the Ξ production angle Θ are defined in terms of the incoming K^- direction \hat{K} and the outgoing Ξ direction $\hat{\Xi}$. In the Ξ rest frame (B), the Λ direction $\hat{\Lambda}$ is defined in terms of angles θ and ϕ . In the Λ rest frame (C), the Λ polarization \vec{P}_Λ and the proton direction \hat{p} are described with reference to axes x and y, illustrated in the expanded view (upper left) of system (B).

In a particle's own rest frame, its spin state, and the angular distribution of its decay products, are conveniently expressed in terms of tensors formed from the three components of a spin operator \vec{S} . A complication arises when one wishes to describe multistep production and decay processes similar to that of Fig. II-1. Nevertheless, the nonrelativistic three-dimensional description of spin states may be used even in the relativistic region, provided the observed momenta of the reaction are transformed successively through all intermediate rest frames, via successive direct Lorentz transformations.^{25, 26} Three successive transformations are required, for example, to transform the momentum \vec{p} of the decay proton from the lab frame into the Λ rest frame.

The processes (II-2) and (II-3) are described in a fashion exactly analogous to that illustrated in Fig. II-1 for the process (II-1). In each case the production normal $\hat{n} = \hat{Z}$ is defined by $\vec{n} = \hat{K} \times \hat{F}_J$, where \hat{F}_J is the direction of F_J in the production c.m. The choice of axes $\hat{Y} = \hat{K}$, $\hat{X} = \hat{K} \times \hat{n}$ is arbitrary; one could choose instead $\hat{Y} = \hat{F}_J$, $\hat{X} = \hat{F}_J \times \hat{n}$, which we have done in analyzing decays of Ξ^* (1530) and Ξ^* (1817).

2. Density Matrix Formalism

The density matrix formalism yields a correct description of an experimental situation in which the decaying particles are not in a pure quantum-mechanical spin state. We review some basic concepts of the density matrix formalism before switching over to the convenient language of Byers and Fenster.²¹



MUB-5077-A

Fig. II-1

Considered in its rest frame, a particle F_J of spin J in any pure spin state \underline{n} may be represented by a wave function $|\psi^n\rangle$ of the form

$$|\psi^n\rangle = \sum_{j=-1}^{2J+1} a_j^n |\psi^j\rangle, \quad (\text{II-4})$$

where the expansion coefficients $a_j^n = \langle \psi^j | \psi^n \rangle$ are complex numbers, and where the $|\psi^j\rangle$ are the $(2J+1)$ eigenfunctions of the operator J_z , the component of angular momentum along some arbitrary z -axis. An ensemble of particles in various pure states \underline{n} may be represented by a density matrix ρ_{jk} of the form

$$\rho_{jk} = \sum_{\underline{n}} P_{\underline{n}} \left[|\psi^n\rangle \langle \psi^n| \right]_{jk} = \sum_{\underline{n}} P_{\underline{n}} a_j^n a_k^{n*}, \quad (\text{II-5})$$

where $P_{\underline{n}}$ is the probability of observing a particle in the \underline{n} th pure spin state.

The expectation value of any operator Q , for the ensemble as a whole, is equal to

$$\text{Av}(Q) = \frac{\text{Tr}(Q\rho)}{\text{Tr}(\rho)} = \frac{\sum_{\underline{n}} P_{\underline{n}} \langle \psi^n | Q | \psi^n \rangle}{\sum_{\underline{n}} P_{\underline{n}} \langle \psi^n | \psi^n \rangle}. \quad (\text{II-6})$$

Normalization of $|\psi^n\rangle$ so that $\langle \psi^n | \psi^n \rangle = 1$ implies that

$$\text{Tr}(\rho) = 1, \quad \text{Av}(Q) = \text{Tr}(Q\rho). \quad (\text{II-7})$$

Consider an ensemble of particles F_J , each decaying into a particle $F_{J'}$ of spin J' and a particle B_0 of spin zero. The density matrix describing the initial spin state is ρ_i , of dimensionality $(2J+1)$; the density matrix describing the final spin state is ρ_f , of dimensionality $(2J'+1)$. If the decay process is described by an operator M defined so that

$$|\psi^f\rangle = M|\psi^i\rangle, \quad (\text{II-8})$$

where $|\psi^i\rangle$ and $|\psi^f\rangle$ are a pure initial spin state and its corresponding final spin state, respectively, then the final state density matrix is equal to

$$\rho_f = M \rho_i M^\dagger. \quad (\text{II-9})$$

Given knowledge of ρ_i and M , one can calculate expectation values of

any operator Q' on the final-state ensemble, by taking

$$Av(Q') = \frac{\text{Tr}(Q' \rho_f)}{\text{Tr}(\rho_f)} . \quad (\text{II-10})$$

The rules established above may be applied any number of times to investigate angular distributions in complex decay chains. For example, the final-state density matrix for the proton in the decay sequence

$$\Xi^* \rightarrow \Xi + \pi; \quad \Xi \rightarrow \Lambda + \pi; \quad \Lambda \rightarrow p + \pi \quad (\text{II-11})$$

is equal to

$$\rho_f(\text{proton}) = M'' M' M \rho_i(\Xi^*) M^\dagger (M')^\dagger (M'')^\dagger , \quad (\text{II-12})$$

where M , M' , and M'' describe the decay of the Ξ^* , Ξ , and Λ , respectively.

3. Description of Initial Spin State

Using the language of Byers and Fenster,²¹ we expand the initial-state density matrix ρ_i in terms of irreducible tensor operators T_{LM} :

$$\rho_i \Big]_{jk} = \frac{1}{2J+1} \sum_{L=0}^{2J} \sum_{M=-L}^L (2L+1) t_{LM}^* T_{LM} \Big]_{jk} , \quad (\text{II-13})$$

where the quantities $t_{LM} = \text{Tr}(\rho_i T_{LM})$ are expectation values of the T_{LM} . The T_{LM} are normalized so that

$$\text{Tr}(T_{LM} T_{L'M'}^\dagger) = \frac{2J+1}{2L+1} \delta_{LL'} \delta_{MM'} , \quad (\text{II-14})$$

and are formed from spin operators S_x , S_y , and S_z , as the spherical harmonics Y_{LM} are formed from coordinates x , y , and z . [For example, $T_{11} \propto (S_x + iS_y)$, in analogy with $Y_{11} \propto (x + iy)$.] The tensor operators T_{LM} and the expectation values t_{LM} obey the relations

$$T_{L, -M} = (-)^M T_{LM}^\dagger$$

and

$$t_{L, -M} = (-)^M t_{LM}^* .$$

Hence t_{L0} is real. The normalization conditions (II-7) and (II-14) imply that $t_{00} = 1$. The matrix representation of the T_{LM} depends upon

the dimensionality $(2J+1)$ of the spin space, and also upon the choice of basis vectors used to define the space. In a representation where T_{L0} is diagonal, the matrix elements of the T_{LM} are real, and equal to Clebsch-Gordan coefficients:

$$\begin{aligned} T_{LM} \Big]_{M'' M'} &= C(JLJ; M' M) \delta_{M'', M'+M} \\ &= (-)^{J-M'} \left(\frac{2J+1}{2L+1} \right)^{1/2} C(JJL; M'', -M') \delta_{M, M''-M'} \end{aligned} \quad (\text{II-15})$$

(The notation for the Clebsch-Gordan coefficients corresponds to $C(j_1 j_2 j_3; m_1 m_2)$, where $\vec{j}_1 + \vec{j}_2 = \vec{j}_3$ and $m_1 + m_2 = m_3$.)

Noting that t_{10} is related to the expectation value of the spin operator S_z by

$$t_{10} = \left[\frac{1}{J(J+1)} \right]^{1/2} \langle S_z \rangle, \quad (\text{II-16})$$

one obtains an upper limit for $|t_{10}|$, for any spin J :

$$|t_{10}| \leq \left[\frac{J}{J+1} \right]^{1/2}. \quad (\text{II-17})$$

Similar relations may be derived for other t_{LM} . An additional restriction on the permitted range of the t_{L0} is imposed by the requirement that the diagonal elements of the density matrix be real and non-negative. Substituting appropriate values of the matrix elements $T_{LM} \Big]_{jk}$ into Eq. (II-13), one obtains the following inequalities:

For $J = 1/2$:

$$1 \pm \sqrt{3} t_{10} \geq 0. \quad (\text{II-18})$$

For $J = 3/2$:

$$\begin{aligned} 1 \pm 3 \sqrt{\frac{3}{5}} t_{10} + \sqrt{5} t_{20} \pm \sqrt{\frac{7}{5}} t_{30} &\geq 0 \\ 1 \pm \sqrt{\frac{3}{5}} t_{10} - \sqrt{5} t_{20} \mp 3 \sqrt{\frac{7}{5}} t_{30} &\geq 0. \end{aligned} \quad (\text{II-19})$$

For $J = 5/2$:

$$\begin{aligned} 1 \pm 3 \sqrt{\frac{5}{7}} t_{10} + 5 \sqrt{\frac{5}{14}} t_{20} \pm \sqrt{\frac{35}{6}} t_{30} + 3 \sqrt{\frac{3}{14}} t_{40} \pm \sqrt{\frac{11}{42}} t_{50} &\geq 0 \\ 1 \pm 9 \sqrt{\frac{1}{35}} t_{10} - \sqrt{\frac{5}{14}} t_{20} \mp 7 \sqrt{\frac{7}{30}} t_{30} - 9 \sqrt{\frac{3}{14}} t_{40} \mp 5 \sqrt{\frac{11}{42}} t_{50} &\geq 0 \\ 1 \pm 3 \sqrt{\frac{1}{35}} t_{10} - 2 \sqrt{\frac{10}{7}} t_{20} \mp 2 \sqrt{\frac{14}{15}} t_{30} + 3 \sqrt{\frac{6}{7}} t_{40} \pm 5 \sqrt{\frac{22}{21}} t_{50} &\geq 0. \end{aligned} \quad (\text{II-20})$$

If all t_{L0} having $L > 1$ are zero, these various inequalities reduce to the condition

$$|t_{10}| \leq \frac{1}{3} \sqrt{\frac{J+1}{J}}. \quad (\text{II-21})$$

The inequalities (II-17) and (II-21) are equivalent to the two inequalities of Lee and Yang:²⁸

$$|\langle \cos \theta \rangle| \equiv |\langle \hat{F}_J \cdot \hat{n} \rangle| \leq \frac{1}{2J+2} \quad (\text{II-22})$$

and

$$|\langle \cos \theta \rangle| \leq \frac{1}{6J}. \quad (\text{II-23})$$

Equation (II-23) holds only if no powers higher than $(\cos \theta)$ appear in the F_J decay distribution $I(\theta, \phi)$. Further inequalities restricting the values of the t_{LM} have been pointed out by Byers and Fenster,²¹ and others, but in our analysis these inequalities provide no new information.

In certain cases some of the t_{LM} may vanish due to symmetries in the production process. For example, we show in Appendix C that for particles J produced in a parity-conserving reaction of the type



the expectation values t_{LM} describing the spin state of the particles J in their rest frame vanish for odd M , provided:

- (i) the axis of quantization of the t_{LM} is the production normal $\vec{z} = \hat{A} \times \hat{J}$;
- (ii) the beam and target particles (A and B) are unpolarized, and averages are taken over the spin states of the final-state particles C, D, E, etc.;
- (iii) averages are taken over all directions of C, D, E, etc.

(This is a generalization of Capps' Checkerboard Theorem, which has been demonstrated by Capps²⁹ and by Byers and Fenster²¹ for two-body production reactions of the type $A + B \rightarrow J + C$. The name is due to the appearance of the density matrix when elements corresponding to odd- M t_{LM} vanish.)

4. Spin J → Spin J' + Spin 0

As stated earlier, the initial and final state density matrices ρ_i and ρ_f are related by

$$\rho_f = M \rho_i M^\dagger, \quad (\text{II-25})$$

where M is the transition matrix for the process

$$F_J \rightarrow F_{J'} + B_0, \quad (\text{II-26})$$

defined so that

$$|\psi^f\rangle = M |\psi^i\rangle. \quad (\text{II-27})$$

In the "helicity" coordinate system (x, y, z) having its z -axis along $\hat{F}_{J'}$, the direction of $F_{J'}$ ($\hat{F}_{J'} = \hat{\Lambda}$ in Fig. II-1), the orbital angular momentum of the two-particle final state can have no z -component, so that an initial state $|\psi^i\rangle \equiv |J, \lambda\rangle$ (having z -component of angular momentum λ) can couple only with the final state $|\psi^f\rangle \equiv |J', \lambda'\rangle$ having $\lambda' = \lambda$. Hence in the helicity representation the transition matrix M is diagonal.

Because of the symmetries in the production reaction, we choose to express the initial-state density matrix ρ_i in the (X, Y, Z) coordinate system, having as its Z -axis the production normal \hat{n} . (See Fig. II-1). Hence M must consist of two parts: a rotation matrix $R(\phi, \theta, 0)$ transforming ρ_i into the helicity representation,³⁰ and the diagonalized transition matrix M' describing the actual decay. That is,

$$\rho_f = M' R(\phi, \theta, 0) \rho_i R^\dagger(\phi, \theta, 0) (M')^\dagger \quad (\text{II-28})$$

where M' and ρ_f are represented in the helicity system (x, y, z) and ρ_i in the production system (X, Y, Z) .

The element of the complete decay matrix $M \equiv M' R(\phi, \theta, 0)$ may be written³²

$$M_{\lambda m} = A_\lambda [(2J+1)/4\pi]^{1/2} D_{m\lambda}^{J*}(\phi, \theta, 0), \quad (\text{II-29})$$

where λ is the projection of spin J (and J') on the helicity z -axis, and m is the projection of spin J on the production Z -axis. The "helicity amplitudes" A_λ are the elements of the diagonalized transition matrix M' , each representing the probability amplitude for the process (with helicity λ)

$$D^J |J, \lambda\rangle \rightarrow |J', \lambda\rangle + B_0. \quad (\text{II-30})$$

The functions $D^J_{m_1 m_2}(\alpha, \beta, \gamma)$, sometimes called "symmetric top functions," are matrix elements of the rotation operator $R(\alpha, \beta, \gamma)$ in the spin-J representation:

$$D^J_{m_1 m_2}(\alpha, \beta, \gamma) \equiv \langle J, m_1 | \exp(-\frac{i}{\hbar} \alpha J_z) \exp(-\frac{i}{\hbar} \beta J_y) \exp(-\frac{i}{\hbar} \gamma J_z) | J, m_2 \rangle. \quad (\text{II-31})$$

In the representation where J_z is diagonal,

$$D^J_{m_1 m_2}(\alpha, \beta, \gamma) = \exp(-im_1 \alpha) d^J_{m_1 m_2}(\beta) \exp(-im_2 \gamma) \quad (\text{II-32})$$

where

$$d^J_{m_1 m_2}(\beta) = \langle J, m_1 | \exp(-\frac{i}{\hbar} \beta J_y) | J, m_2 \rangle. \quad (\text{II-33})$$

The quantities $D^L_{M0}(\phi, \theta, 0)$ are related to the spherical harmonics $Y_{LM}(\theta, \phi)$ by³¹

$$D^L_{M0}(\phi, \theta, 0) = \left(\frac{4\pi}{2L+1} \right)^{1/2} Y_{LM}(\theta, \phi). \quad (\text{II-34})$$

The quantities $D^L_{M1}(\phi, \theta, 0)$ may be calculated easily by means of (II-32) and the relations³¹

$$d^L_{M1}(\theta) = [L(L+1)]^{-1/2} \left\{ \begin{array}{l} -M(1+\cos\theta) d^L_{M0}(\theta)/\sin\theta \\ -[(L-M)(L+M+1)]^{1/2} d^L_{M+1,0}(\theta) \end{array} \right\} \quad (\text{II-35})$$

$$d^L_{-M\lambda}(\theta) = (-)^{L+\lambda} d^L_{M\lambda}(\pi-\theta). \quad (\text{II-36})$$

In general, the decay process $F_J \rightarrow F_{J'} + B_0$ can proceed via several different partial waves ℓ , where ℓ may assume values from $|J-J'|$ to $|J+J'|$. In strong decay, only those partial waves consistent with parity conservation contribute to the decay amplitude. In terms of the

usual complex partial-wave decay amplitudes a_ℓ , the helicity amplitudes of Eq. (II-29) have the form³³

$$A_\lambda = (-)^{\lambda-J'} \sum_{\ell} a_\ell C(JJ' \ell; \lambda, -\lambda) \quad (\text{II-37})$$

subject to a normalization constraint

$$\sum_{\lambda} |A_\lambda|^2 = 1. \quad (\text{II-38})$$

For example, for $J' = 1/2$,

$$A_{\pm 1/2} = \frac{a \pm b}{[2(|a|^2 + |b|^2)]^{1/2}} \quad (\text{II-39})$$

where $a = a_{J-1/2}$ and $b = a_{J+1/2}$.

Combining Eqs. (II-13), (II-15), (II-28), and (II-29), one obtains a rather unwieldy expression for ρ_f in terms of the helicity amplitudes A_λ and the t_{LM} describing the initial spin state of F_J . Byers and Fenster²¹ and Button-Shafer²² simplify the expression by utilizing the orthogonality properties of the $\mathcal{D}_{M\lambda}^J$ functions and Clebsch-Gordan coefficients. The general form of an element of ρ_f (in the helicity representation) is³⁴

$$\begin{aligned} \rho_f \Big]_{\lambda\lambda'} &\equiv \langle J', \lambda | \rho_f | J', \lambda' \rangle = (-)^{J-\lambda'} (A_\lambda A_{\lambda'}^* / 4\pi) (2J+1)^{1/2} \\ &\times \sum_{L=0}^{2J} \sum_{M=-L}^L \left[(2L+1)^{1/2} C(JJL; \lambda, -\lambda') t_{LM}^* \mathcal{D}_{M, \lambda-\lambda'}^{L*}(\phi, \theta, 0) \right], \end{aligned} \quad (\text{II-40})$$

which is valid for any spin J and J' (integer as well as half-integer). We note that only the $\mathcal{D}_{M, \lambda-\lambda'}^{L*}(\phi, \theta, 0)$ having integral indices L, M , and $(\lambda-\lambda')$ appear in Eq. (II-40).

Having arrived at an expression for the final-state density matrix, one may calculate the angular distribution of the decay process

$F_J \rightarrow F_{J'} + B_0$ as

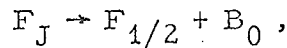
$$I(\theta, \phi) = \text{Tr}(\rho_f) = \sum_{\lambda=-J'}^{J'} \left[\rho_f \right]_{\lambda\lambda} \quad (\text{II-41})$$

A complete description of the spin state of $F_{J'}$, as a function of θ and ϕ is obtained by calculating the quantities (for $0 \leq L \leq 2J'$ and $-L \leq M \leq L$)

$$I t_{LM}(\theta, \phi) = \text{Tr}(\rho_f T_{LM}) = \sum_{\lambda, \lambda'=-J'}^{J'} \left[\rho_f \right]_{\lambda\lambda'} \left[T_{LM} \right]_{\lambda'\lambda} \quad (\text{II-42})$$

In Sec. II.A.4.a we evaluate (II-41) and (II-42) for the special case $J' = 1/2$, following the work of Byers and Fenster.²¹ In Sec. II.A.4.b we discuss some of the results obtained by Button-Shafer for the special case of strong decay with $J' = 3/2$.²²

a. Spin $J \rightarrow$ spin $1/2 +$ spin 0 . By considering the special case $J' = 1/2$, we may apply the theory already presented to reactions of the type



where $F_{1/2}$ is a spin-1/2 fermion. We shall consider the weak decay process



and the strong decay processes



(where spin $1/2$ is assumed for the Ξ).

For weak decay, the two partial waves $a \equiv a_{J-\frac{1}{2}}$

and $b \equiv a_{J+\frac{1}{2}}$ can contribute to the transition matrix M . One

customarily defines

$$\alpha + i\beta \equiv (\text{Re} + i\text{Im})[2ab^*/(|a|^2 + |b|^2)] \quad (\text{II-45})$$

$$\gamma \equiv (|a|^2 - |b|^2) / (|a|^2 + |b|^2)$$

so that $\alpha^2 + \beta^2 + \gamma^2 = 1$. Alternatively, the parameters β and γ may be expressed in terms of independent parameters α and Φ :

$$\gamma + i\beta \equiv [1 - \alpha^2]^{1/2} e^{i\Phi}.$$

For strong decay, only the one partial wave consistent with parity conservation can contribute, whereby $\alpha = \beta = 0$, $\gamma = \pm 1$, and $\Phi = 0$ or π .

The final-state density matrix may be written as

$$\rho_f = \frac{I(\theta, \phi)}{2} \begin{bmatrix} 1 + \vec{P} \cdot \hat{z} & \vec{P} \cdot \hat{x} - i \vec{P} \cdot \hat{y} \\ \vec{P} \cdot \hat{x} + i \vec{P} \cdot \hat{y} & 1 - \vec{P} \cdot \hat{z} \end{bmatrix}, \quad (\text{II-46})$$

where \vec{P} is the polarization of $F_{1/2}$, and (x, y, z) are helicity axes (see Fig. II-1). Equating matrix elements of (II-40) and (II-46), and using Eqs. (II-34), (II-39), (II-45), and the relation

$$C(\text{J} \text{J} \text{L}; \frac{1}{2}, -\frac{1}{2}) = (-)^{2\text{J}+\text{L}} C(\text{J} \text{J} \text{L}; -\frac{1}{2}, \frac{1}{2}), \quad (\text{II-47})$$

one arrives at the result^{21,9}

$$I(\theta, \phi) = \left[\sum_{\substack{L=0 \\ L \text{ even}}}^{2\text{J}-1} + \alpha \sum_{\substack{L=1 \\ L \text{ odd}}}^{2\text{J}} \right] \sum_{M=-L}^L n_{L0}^{\text{J}} t_{LM} Y_{LM}^*(\theta, \phi) \quad (\text{II-48a})$$

$$\vec{P} \cdot \hat{z} = \left[\alpha \sum_{\substack{L=0 \\ L \text{ even}}}^{2\text{J}-1} + \sum_{\substack{L=1 \\ L \text{ odd}}}^{2\text{J}} \right] \sum_{M=-L}^L n_{L0}^{\text{J}} t_{LM} Y_{LM}^*(\theta, \phi) \quad (\text{II-48b})$$

$$\vec{I}\vec{P} \cdot \hat{x} + i \vec{I}\vec{P} \cdot \hat{y} = (-\gamma + i\beta) (2J+1) \sum_{\substack{L=1 \\ L \text{ odd}}}^{2J} \sum_{M=-L}^L n_{L0}^J t_{LM} \mathcal{D}_{M1}^L(\phi, \theta, 0) \quad (\text{II-48c})$$

$$\times [(2L+1)/4\pi]^{1/2} [L(L+1)]^{-1/2},$$

where

$$n_{L0}^J \equiv (-)^{J-\frac{1}{2}} [(2J+1)/4\pi]^{1/2} C(JJL; \frac{1}{2}, -\frac{1}{2}). \quad (\text{II-49})$$

As an aid to computation, one may re-express Eqs. (II-48) as sums over non-negative M-values only, and rewrite the \mathcal{D}_{M1}^L functions in terms of the familiar spherical harmonics Y_{LM} :³⁵

$$I(\theta, \phi) = \left[\sum_{\substack{L=0 \\ L \text{ even}}}^{2J-1} + \alpha \sum_{\substack{L=1 \\ L \text{ odd}}}^{2J} \right] n_{L0}^J \left[\sum_{\substack{M=0 \\ (1 \text{ term})}} + 2 \sum_{M=1}^L \right] Y_{LM}(\theta, 0) \operatorname{Re} \left(t_{LM} e^{-iM\phi} \right) \quad (\text{II-50a})$$

$$\vec{I}\vec{P} \cdot \hat{z} = \left[\alpha \sum_{\substack{L=0 \\ L \text{ even}}}^{2J-1} + \sum_{\substack{L=1 \\ L \text{ odd}}}^{2J} \right] n_{L0}^J \left[\sum_{\substack{M=0 \\ (1 \text{ term})}} + 2 \sum_{M=1}^L \right] Y_{LM}(\theta, 0) \operatorname{Re} \left(t_{LM} e^{-iM\phi} \right) \quad (\text{II-50b})$$

$$\begin{aligned} \vec{I}\vec{P} \cdot \hat{x} + i\vec{I}\vec{P} \cdot \hat{y} &= (2J+1) (-\gamma + i\beta) \sum_{\substack{L=1 \\ L \text{ odd}}}^{2J} n_{L0}^J [L(L+1)]^{-1} \\ &\times \left[\sum_{\substack{M=0 \\ (1 \text{ term})}} + 2 \sum_{M=1}^L \right] \left[A_{LM}(\theta) \operatorname{Re} \left(t_{LM} e^{-iM\phi} \right) + i B_{LM}(\theta) \operatorname{Im} \left(t_{LM} e^{-iM\phi} \right) \right] \end{aligned} \quad (\text{II-50c})$$

where $A_{LM}(\theta) \equiv -MY_{LM}(\theta, 0) \cot \theta - [(L-M)(L+M+1)]^{1/2} Y_{L, M+1}(\theta, 0)$
 and $B_{LM}(\theta) \equiv -MY_{LM}(\theta, 0)/\sin \theta$

for any L and M, even or odd.

Experimentally, the polarization \vec{P} of $F_{1/2}$ may be observed through scattering or, if $F_{1/2}$ decays weakly, through the angular distribution of its decay products. For the two-step decay process

$$\Xi \rightarrow \Lambda + \pi; \quad \Lambda \rightarrow p + \pi,$$

the joint angular distribution of the Λ (in the Ξ rest frame) and of the decay proton (in the Λ rest frame) is given by

$$\begin{aligned} I(\hat{\Lambda}, \hat{p}) &\propto I(\hat{\Lambda}) [1 + a_{\Lambda} \vec{P}_{\Lambda}(\hat{\Lambda}) \cdot \hat{p}] \\ &= I(\theta, \phi) + a_{\Lambda} [I \vec{P}_{\Lambda} \cdot \hat{\Lambda} (\hat{p} \cdot \hat{\Lambda}) + I \vec{P}_{\Lambda} \cdot \hat{x} (\hat{p} \cdot \hat{x}) + I \vec{P}_{\Lambda} \cdot \hat{y} (\hat{p} \cdot \hat{y})], \end{aligned} \quad (\text{II-51})$$

where the Λ angular distribution $I(\theta, \phi)$ and the Λ polarization components $I \vec{P}_{\Lambda} \cdot \hat{x}$, $I \vec{P}_{\Lambda} \cdot \hat{y}$, and $I \vec{P}_{\Lambda} \cdot \hat{z} \equiv I \vec{P}_{\Lambda} \cdot \hat{\Lambda}$ are given by Eqs. (II-48).

The distribution in $(\hat{p} \cdot \hat{\Lambda})$ is obtained by integrating (II-51) over θ, ϕ , and $\phi_p \equiv \tan^{-1} [(\hat{p} \cdot \hat{y})/(\hat{p} \cdot \hat{x})]$:

$$\mathcal{J}(\hat{p} \cdot \hat{\Lambda}) \propto 1 + a_{\Lambda} a_{\Xi} (\hat{p} \cdot \hat{\Lambda}); \quad (\text{II-52})$$

this relation holds for any spin J. Thus a spin-independent estimate of a_{Ξ} is possible even if all t_{LM} with $L > 0$ are zero.

The presence of non-zero t_{LM} with $L > 0$ permits a more accurate (and spin-dependent) determination of a_{Ξ} . If the Ξ has spin 1/2 and polarization $P_{\Xi} \equiv \vec{P}_{\Xi} \cdot \hat{n} = \sqrt{3} t_{10}$, the distribution function (II-51) reduces to the familiar form

$$\begin{aligned} I(\hat{\Lambda}, \hat{p}) &\propto 1 + a_{\Xi} P_{\Xi} \cos \theta + a_{\Lambda} (\hat{p} \cdot \hat{\Lambda}) [a_{\Xi} + P_{\Xi} \cos \theta] \\ &\quad + a_{\Lambda} P_{\Xi} \sin \theta [\beta_{\Xi} \hat{p} \cdot \hat{y} - \gamma_{\Xi} \hat{p} \cdot \hat{x}]. \end{aligned} \quad (\text{II-53})$$

Equations (II-48), (II-50), and (II-51) hold also for the reactions

$$\Xi^*(1817) \rightarrow \Lambda + \bar{K}; \Lambda \rightarrow p + \pi, \quad (\text{II-54})$$

and (if spin 1/2 is assumed for the Ξ)

$$\Xi^*(1530) \rightarrow \Xi + \pi; \Xi \rightarrow \Lambda + \pi, \quad (\text{II-55})$$

provided the appropriate substitutions are made:

<u>Reaction</u>	<u>F_J</u>	<u>$F_{1/2}$</u>	<u>Decay fermion</u>	<u>$(\alpha, \beta, \gamma)_{F_J}$</u>	<u>$\alpha_{F_{1/2}}$</u>
$\Xi \rightarrow \Lambda + \pi;$ $\Lambda \rightarrow p + \pi$	Ξ	Λ	p	$(\alpha_{\Xi}, \beta_{\Xi}, \gamma_{\Xi})$	α_{Λ}
$\Xi^*(1817) \rightarrow \Lambda + \bar{K};$ $\Lambda \rightarrow p + \pi$	$\Xi^*(1817)$	Λ	P	$(0, 0, \pm 1)$	α_{Λ}
$\Xi^*(1530) \rightarrow \Xi + \pi;$ $\Xi \rightarrow \Lambda + \pi$	$\Xi^*(1530)$	Ξ	Λ	$(0, 0, \pm 1)$	α_{Ξ}

Coordinate systems and angles are defined as in Fig. II-1, after the corresponding unit vectors are substituted in place of $\hat{\Xi}$, $\hat{\Lambda}$, and \hat{p} . The choice $\gamma_{F_J} = \pm 1$ is appropriate for $J^P = 1/2^+$, $3/2^{\pm}$, $5/2^+$, etc., where P is the parity of F_J relative to that of $F_{1/2}$. The relative parity P cannot be determined unless at least one odd-L t_{LM} is non-zero.

For either strong or weak decay, three features of the decay distribution enable one, in principle, to determine the spin J: (i) a lower limit for J is established by the maximum complexity of the observed distribution; i.e. $J \geq L_{\max}/2$ where L_{\max} is the L-value of the highest non-zero t_{LM} ; (ii) if $|t_{10}|$ or any other $|t_{LM}|$ exceeds its J-dependent bounds, an upper limit for J may be established by inequalities similar to the Lee-Yang inequalities (II-22) and (II-23); (iii) if any odd-L t_{LM} are non-zero, a best value of the factor $(2J+1)$ of Eq. (II-48c) may be determined experimentally.

b. Strong decay: Spin $J \rightarrow$ spin $3/2$ + spin 0 . The strong decay process

$$F_J \rightarrow F_{3/2} + B_0 \quad (\text{II-56})$$

(where $F_{3/2}$ is a spin- $3/2$ fermion) has been discussed by Button-Shafer,²² Zemach,²³ and Berman and Jacob,²⁴ among others. We utilize the formalism of Button-Shafer, who extends the Byers-Fenster theory to obtain a complete and general description of the decay process (II-56). All equations are discussed more extensively in Ref. 22, except for the introduction here of the parameter λ_0 (Eq. II-68) and of the momentum-barrier treatment of higher l -waves.

A variety of tests may be performed to determine the spin and parity of F_J ; we shall describe here only those used in our analysis of the reaction

$$\Xi^*(1817) \rightarrow \Xi^*(1530) + \pi; \Xi^*(1530) \rightarrow \Xi + \pi, \quad (\text{II-57})$$

which we denote symbolically by

$$F_J \rightarrow F_{3/2} + B_0; F_{3/2} \rightarrow F_{1/2} + B_0. \quad (\text{II-58})$$

As was shown earlier, the spin state of $F_{3/2}$ may be represented by a 4×4 density matrix ρ_f whose elements $\rho_f]_{\lambda\lambda'} \equiv \langle \frac{3}{2}, \lambda | \rho_f | \frac{3}{2}, \lambda' \rangle$ (in the helicity representation) are given by Eq. (II-40). In particular, the diagonal elements are

$$\rho_f]_{\lambda\lambda} = \sum_{L=0}^{2J} \sum_{M=-L}^L t_{LM}^* |A_\lambda|^2 n_{L0}^{(2\lambda)} Y_{LM}(\theta, \phi), \quad (\text{II-59})$$

where the t_{LM} describe the spin state of F_J , and where θ and ϕ define the direction of $F_{3/2}$ in the F_J rest frame. The helicity amplitudes A_λ are given by Eq. (II-37), and the J -dependent constants $n_{L0}^{(2\lambda)}$ by the relation

$$n_{L0}^{(2\lambda)} = (-)^{J-\lambda} [(2J+1)/4\pi]^{1/2} C(JJL; \lambda, -\lambda). \quad (\text{II-60})$$

The angular distribution of $F_{3/2}$ (in the F_J rest frame) is

$$\begin{aligned}
 I(\theta, \phi) &= \text{Tr}(\rho_f) \\
 &= 2 \sum_{\substack{L=0 \\ L \text{ even}}}^{2J-1} \sum_{M=-L}^L \left[|A_{3/2}|^2 n_{L0}^{(3)} + |A_{1/2}|^2 n_{L0}^{(1)} \right] t_{LM} Y_{LM}^*(\theta, \phi).
 \end{aligned}
 \tag{II-61}$$

A lower limit on the spin J is established by the maximum complexity of the observed $I(\theta, \phi)$ distribution; i. e., if the data require non-zero t_{LM} through order L , then $J \geq L/2$. No spin information is obtained from Eq. (II-61) if all t_{LM} having $L > 0$ are consistent with zero. One finds that $I(\theta, \phi)$ has a particularly simple form if ϕ is ignored and only the lower ℓ -wave included.³⁶

If $F_{3/2}$ subsequently decays strongly via $F_{3/2} \rightarrow F_{1/2} + B_0$, the angular distribution of $F_{1/2}$ (in the $F_{3/2}$ rest frame) is given by the Byers-Fenster formalism of Sec. II.A.4.a:

$$\mathcal{I}(\psi) = \frac{1}{4\pi} I(\theta, \phi) \left[1 - \sqrt{5} \langle T_{20} \rangle_{F_{3/2}}(\theta, \phi) P_2(\cos \psi) \right],
 \tag{II-62}$$

where ψ is the angle of $F_{1/2}$ relative to the $F_{3/2}$ direction of flight, where $P_2(x) \equiv \frac{3}{2}x^2 - \frac{1}{2}$, and where we have ignored the azimuthal orientation of $F_{1/2}$. The quantity

$$\begin{aligned}
 I \langle T_{20} \rangle_{F_{3/2}}(\theta, \phi) &= \text{Tr}(\rho_f T_{20}) \\
 &= 2(5)^{-1/2} \sum_{\substack{L=0 \\ L \text{ even}}}^{2J-1} \sum_{M=-L}^L \left[|A_{3/2}|^2 n_{L0}^{(3)} - |A_{1/2}|^2 n_{L0}^{(1)} \right] t_{LM} Y_{LM}^*(\theta, \phi)
 \end{aligned}
 \tag{II-63}$$

represents the T_{20} component of $F_{3/2}$ polarization referred to helicity axes, i. e., the $F_{3/2}$ spin alignment along its direction of flight.

Combining Eqs. (II-61) through (II-63) and integrating over θ and ϕ (the angles describing the direction of $F_{3/2}$), we are left with only those terms containing t_{00} , so that³⁷

$$I(\psi) \propto 1 + a_2 P_2(\cos \psi) = 1 + a_2 (3 \cos^2 \psi - 1)/2, \quad (\text{II-64})$$

where

$$a_2 = (|A_{1/2}|^2 - |A_{3/2}|^2) \times (|A_{1/2}|^2 + |A_{3/2}|^2)^{-1}. \quad (\text{II-65})$$

(We have used the relation $n_{00}^{(1)} = n_{00}^{(3)}$.) After integration over θ and ϕ , the azimuthal distribution of $F_{1/2}$ about the $F_{3/2}$ line of flight is isotropic.

If $J = 1/2$, then $A_{3/2} = 0$, so that $a_2 = 1.0$ regardless of the parity of J . If $J \geq 3/2$, the helicity amplitudes A_λ have the following form for various $\Xi^*(1817)$ spin and parity assumptions J^P [where P is the parity of $\Xi^*(1817)$ relative to that of $\Xi^*(1530)$]:

$$J^P = 3/2^-, 5/2^+, 7/2^-, \text{ etc.} :$$

$$A_{1/2} \propto a(3J-3/2)^{1/2} - c(J+3/2)^{1/2} \quad (\text{II-66a})$$

$$A_{3/2} \propto a(J+3/2)^{1/2} + c(3J-3/2)^{1/2} \quad (\text{II-66b})$$

$$J^P = 3/2^+, 5/2^-, 7/2^+, \text{ etc.} :$$

$$A_{1/2} \propto b(J-1/2)^{1/2} - d(3J+9/2)^{1/2} \quad (\text{II-67a})$$

$$A_{3/2} \propto b(3J+9/2)^{1/2} + d(J-1/2)^{1/2}, \quad (\text{II-67b})$$

where a, b, c , and d are complex amplitudes for decay via partial waves $l = J-3/2, J-1/2, J+1/2$, and $J+3/2$ respectively. One may show that a_2 is of the form

$$a_2 = S \cos \lambda_0 - T \sin \lambda_0 \cos \Delta\phi, \quad (\text{II-68})$$

where $S, T, \Delta\phi$, and $\cos \lambda_0$ have the following values and where

$$|a|^2 + |c|^2 = 1, \quad |b|^2 + |d|^2 = 1, \quad \sin \lambda_0 \geq 0:$$

J^P	S	T	$\Delta\phi$	$\cos \lambda_0$
$3/2^-, 5/2^+, 7/2^-, \text{ etc.}$	$ a ^2 - c ^2$	$2 a c $	$\delta_c - \delta_a$	$(2J-3)/4J$
$3/2^+, 5/2^-, 7/2^+, \text{ etc.}$	$ b ^2 - d ^2$	$2 b d $	$\delta_d - \delta_b$	$(-2J-5)/(4J+4)$

We note that $-1 \leq a_2 \leq 1$, regardless of the magnitudes and relative phases of a, b, c , and d . If only the lower partial wave (a or b) contributes (for those cases having $J > 1/2$), a_2 has the following values:³⁷

J^P	a_2	J^P	a_2
$1/2^+$	1.00	$1/2^-$	1.00
$3/2^-$	0.00	$3/2^+$	-0.80
$5/2^+$	0.20	$5/2^-$	-0.71
$7/2^-$	0.29	$7/2^+$	-0.67
limit $J \rightarrow \infty$	0.50	limit $J \rightarrow \infty$	-0.50

One expects the rate of decay via partial wave ℓ to be suppressed (relative to 1.0 for $\ell = 0$) by a factor of the order of³⁸

$$(qR)^2 [1 + (qR)^2]^{-1} \quad \text{for } \ell = 1 \quad (\text{II-69a})$$

$$(qR)^4 [9 + 3(qR)^2 + (qR)^4]^{-1} \quad \text{for } \ell = 2 \quad (\text{II-69b})$$

$$(qR)^6 [225 + 45(qR)^2 + 6(qR)^4 + (qR)^6]^{-1} \quad \text{for } \ell = 3, \quad (\text{II-69c})$$

where q is the momentum of $F_{3/2}$ in the F_J rest frame, and R is a characteristic radius of interaction, of the order of $(2m_\pi)^{-1}$. (For the decay process $\Xi^*(1817) \rightarrow \Xi^*(1530) + \pi$, $q = 230 \text{ MeV}/c \approx 1/R$.) Taking $qR \approx 1$, we estimate $|D^2| / |S^2| \approx 0.08$ and $|F^2| / |P^2| \approx 0.007$, where S, P, D , and F are decay amplitudes for $\ell = 0, 1, 2$, and 3 , respectively. Even with complete ignorance of the relative phase $\Delta\phi$, we may specify the permitted range of the coefficient a_2 , allowing for the presence of higher partial waves:

$\frac{J^P}{}$	Partial waves ℓ	a_2
$1/2^+$	1	1.0
$1/2^-$	2	1.0
$3/2^-$	0, 2	0.0 ± 0.5
$3/2^+$	1, 3	-0.8 ± 0.1
$5/2^+$	1, 3	0.2 ± 0.2

Decay via the higher partial wave is negligible for higher spin hypotheses.

B. Maximum-Likelihood Analysis of Data

The likelihood function $\mathcal{L} \equiv \mathcal{L}(x_i | a)$ may be defined as the probability of obtaining a set of N observations x_1, x_2, \dots, x_N , given a theoretical model described by a number of parameters which we denote collectively by a . For example, if the quantities x_i are angles describing the decay of N events, then the likelihood function is given by

$$\mathcal{L}(x_i | a) = \prod_{i=1}^N f(x_i, a) \quad (\text{II-70})$$

where $f(x_i, a)$ is an expected angular decay distribution, i. e., the probability of observing x_i , given a .

We consider \mathcal{L} as a function $\mathcal{L}(a_1, a_2, \dots, a_m)$ of m variable parameters a_1, a_2, \dots, a_m . A maximum-likelihood analysis consists of varying the parameters a_i to achieve a maximum in \mathcal{L} , at which point the final values a_{i0} of the parameters a_i constitute a description of the experimental data. At the maximum,

$$\mathcal{L} = \mathcal{L}_{\max} = \mathcal{L}(a_{10}, a_{20}, \dots, a_{m0}) \quad (\text{II-71})$$

If $w \equiv \ln \mathcal{L}$, a maximum in w (and in \mathcal{L}) is achieved when

$$\frac{\partial w}{\partial a_1} = \frac{\partial w}{\partial a_2} = \dots = \frac{\partial w}{\partial a_m} = 0 \quad (\text{II-72})$$

Near the maximum, by a Taylor's expansion,

$$w \approx w_{\max} - \frac{1}{2} \chi^2 \quad (\text{II-73})$$

and

$$L \approx L_{\max} \exp \left(- \frac{1}{2} \chi^2 \right) \quad (\text{II-74})$$

where

$$\chi^2 = - \sum_{j,k} (a_j - a_{j0}) \frac{\partial^2 w}{\partial a_j \partial a_k} (a_k - a_{k0}) \quad (\text{II-75})$$

if partial derivatives higher than those of the second order are small.

The value of w_{\max} increases by 0.5, on the average, for each additional unnecessary parameter a_i that is allowed to vary; an increase of more than this amount indicates that the additional degree of freedom is necessary to describe the data. For example, an increase of 2.5 for three additional degrees of freedom corresponds to a χ^2 of 5.0 for three degrees of freedom, or a probability of $\approx 15\%$ that the data were correctly described by the smaller number of parameters.

Accordingly, we may define the standard deviation error δa_i of any parameter a_i as that change in a_i which causes w to decrease by 0.5 from its maximum value w_{\max} . (To properly account for correlations between parameters, w should be remaximized with respect to all other parameters as a_i is varied.) A change in a_i which causes w to decrease by an amount X is equivalent to an n -standard-deviation effect, where $n = (2X)^{1/2}$.

In the above definition of δa_i , nothing is assumed about the form of L as a function of a_i . Now if the parameters a_i are suitably chosen, and if N (the number of observations) is sufficiently large, the likelihood function may be quite nearly Gaussian in the vicinity of the maximum; i. e., Eqs. (II-73) and (II-74) are good approximations, and the second derivatives $\partial^2 w / \partial a_j \partial a_k$ are approximately independent of a_1, a_2, \dots, a_m . If this is the case, the error δa_i of any parameter a_i (as defined previously) is approximately equal to $(G_{ii})^{1/2}$, where $(G^{-1})_{jk} \equiv - \frac{\partial^2 w}{\partial a_j \partial a_k}$. (We note that $w \propto N$, so $\delta a_i \propto N^{-1/2}$, as required.)

In this report we analyze Ξ and Ξ^* decay distributions, using the maximum-likelihood method. For Ξ decay, the distribution function $f(x, a)$ is the function $I(\hat{\Lambda}, \hat{p})$ of (II-51), normalized so that $\ln \mathcal{L} = 0$ for an isotropic distribution. Continuous parameters (a_Λ , a_Ξ , Φ_Ξ , and t_{LM}) are determined (with errors) by maximizing $w = \ln \mathcal{L}$ and inverting the second derivative matrix; discrete parameters (J and L_{\max}) are investigated by comparing values of $\ln \mathcal{L}$ obtained under different spin assumptions.³⁹

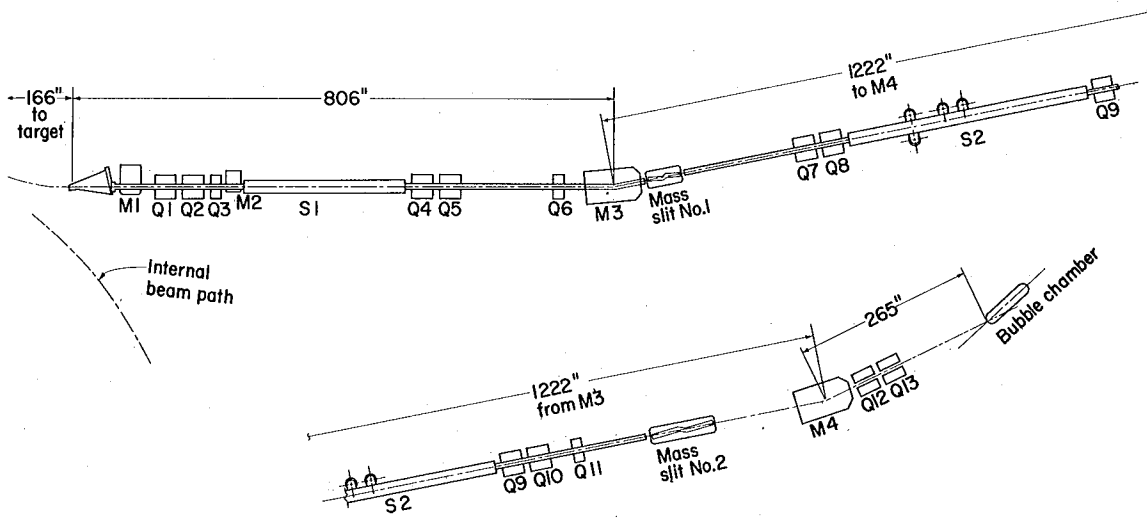
The analysis of Ξ^* decay distributions is similar, except that the continuous parameters a_{F_J} and Φ_{F_J} are replaced by a discrete parameter ($\gamma_{F_J} = \pm 1$) specifying the parity of F_J (the Ξ^*).

III. DESCRIPTION OF K-63 BEAM

The data analyzed in this report were obtained from photographs of $K^- + p$ interactions in the Laboratory's 72-inch bubble chamber. Most of the data are from a 1.7 to 2.7 BeV/c separated K^- beam (K-63) designed by Joseph J. Murray with the assistance of Janice Button-Shafer; however, our analysis of Ξ decay properties includes data from an earlier beam, K-72.^{7, 8}

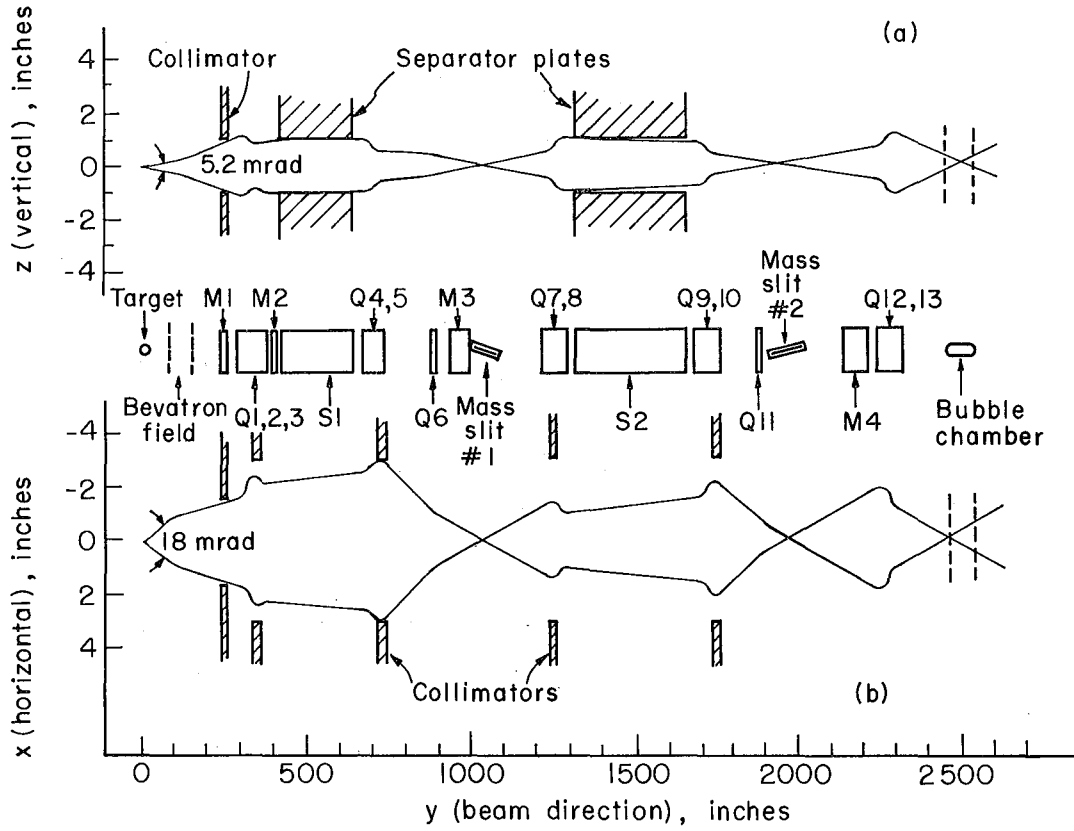
Figures III-1 and III-2 illustrate the general features of the K-63 beam, which has been described in detail elsewhere.⁴⁰⁻⁴² The Bevatron internal proton beam (operating at 6.1 BeV, 4.2×10^{12} protons/pulse) strikes a copper target 4 in. long by 1/8-in. wide by 1/16-in. high. The secondary beam channel accepts ≈ 0.10 msr at an angle of 0° . Momentum selection ($\approx \pm 1.5\%$ about the nominal momentum) is performed by collimators at mass slit 1, after horizontal dispersion in M3. Electrostatic separators S1 and S2 separate K^- from background (mostly π^-) in two stages, in the vertical plane. These separators, of the glass cathode type described in Ref. 43, maintain a potential of 500 kV across a 2-inch gap. At the two mass slits, K^- and π^- are focused into images 1/16-in. high separated by $\approx 1/8$ -in. The K^- pass through the slits to the bubble chamber, whereas the π^- , passing through uranium in the slit jaws (see Fig. III-3), lose $\geq 8\%$ of their momentum and are swept aside by the bending magnet M4.

The rather broad momentum bite, required for adequate K^- flux at the bubble chamber, necessitated the use of special cocked mass slits, a design feature utilized for perhaps the first time. One of these slits (#1) is illustrated in Fig. III-3; slit #2 is similar in design but more nearly parallel to the beam direction. Particles are focused at various distances y along the beam axis, the higher momentum particles being focused further downstream. The bending magnet M3 introduces horizontal dispersion, and the mass slit is placed so that a particle of any momentum (in the 3% interval) is focused at some point along the mass slit. The beam is so designed that images in the horizontal and vertical planes approximately coincide and "track" linearly with momentum to follow the mass slit.



MU-36827

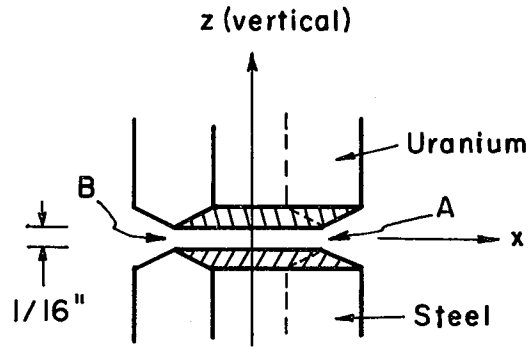
Fig. III-1



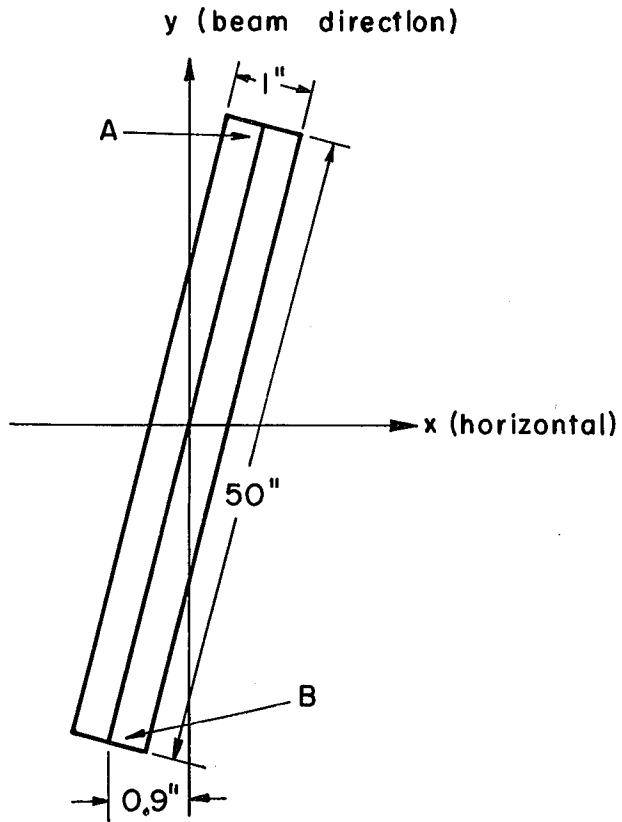
MUB 13866

Fig. III-2

(a)



(b)



MUB 13867

Fig. III-3

The critical design requirements necessitated the use of many quadrupoles, which were carefully corrected for small aberrations.⁴⁴ Optimum quadrupole positions and currents were calculated with a special analog computer designed by Murray.⁴¹ The beam was turned on in July 1963.

Over an 18-month period, 2376 rolls (averaging ≈ 630 frames/roll) of K^- film were photographed, including: (a) 897 rolls at 2.45 to 2.7 BeV/c; (b) 235 rolls at 2.1 BeV/c; (c) 249 rolls at 1.7 BeV/c;⁴⁵ (d) 26 rolls at 2.9 BeV/c, which had unacceptably low K^- yield and high background; (e) 321 rolls at 2.0 BeV/c, for UCLA; (f) 425 rolls at 2.1 BeV/c, with lead plates in the chamber; and (g) 223 rolls in D_2 (no lead plates), at 2.1 and 2.63 BeV/c. Only the data from (a), (b), and (c), amounting to ≈ 26 events/microbarn, are discussed in this report; in this exposure, we observe 6 to 10 beam tracks per frame, including 15 to 35% non- K^- background. The path length and π^- background at each momentum, estimated from observed numbers of 3-prong events, are presented in Appendix D.

The same beam setup was used for a π^- exposure from 1.6 to 4.2 BeV/c. Data from this experiment (π^-63) were useful in assessing the effects of π^- contamination in the K-63 beam, as will be explained in Sec. IV.B.2.

IV. SELECTION OF K-63 EVENTS

A. Preliminary Analysis

After being topologically scanned, the events of the K-63 experiment were measured either on one of the Franckenstein measuring projectors or on one of SMP's (scanning and measuring projectors).⁴⁶

The measured events were processed on the IBM 7094 or 7044 with the standard data-analysis programs of the Alvarez group--PANAL, PACKAGE, WRING, AFREET, and DST-EXAM. Failing events (events failing to fit acceptably any kinematic hypothesis) were remeasured and, when necessary, re-examined at the scanning table. For ambiguous events, ionization information was used wherever possible to distinguish between competing hypotheses. Except as otherwise noted, the standard analysis procedure was used without modification.⁴⁷⁻⁴⁹

The actual fitting of the events, done by PACKAGE, begins with a three-dimensional reconstruction of each measured track; appropriate corrections are made for energy loss, optical distortions, and non-uniformity of the magnetic field. The measured momenta and angles of each track at a production or decay vertex are adjusted to give a best fit to each of several particle-assignment hypotheses, and a χ^2 is calculated. Events having more than one visible vertex are fit one vertex at a time, beginning with the final decay vertex and ending with the production vertex. In certain types of events, for example in Ξ^0 production and decay, tracks from two different vertices are fit simultaneously. When more than one unseen neutral particle is present at the production vertex, the invariant mass of the unobserved particles is calculated.

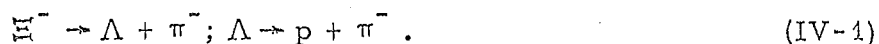
In DST-EXAM, the χ^2 from individual vertices are combined to form an overall confidence level (c.l.) for each of several production-and-decay hypotheses, including missing-mass hypotheses.⁵⁰ Confidence levels of hypotheses contradicted by ionization information are set equal to zero.

B. Selection Criteria

In this section we describe and evaluate the criteria used in selecting Ξ^- and Ξ^0 events. In Table A-I (Appendix A) we show the numbers of events passing these criteria, from K-63 data processed as of September 1965.

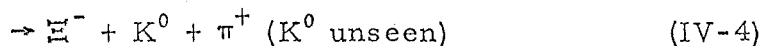
1. Ξ^- Events

The only Ξ^- events analyzed were those in which both the Ξ^- and Λ decayed visibly, via

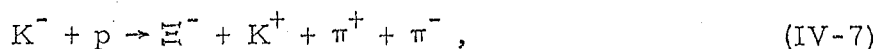


Such events occur with the following topologies (code numbers refer to the event type classification of Ref. 48):

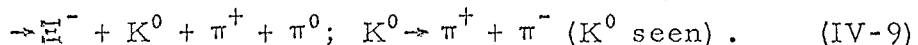
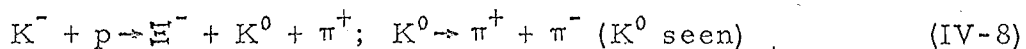
Event-type 72 (vee with two prongs and negative decay vertex):



Event-type 74 (vee with four prongs and negative decay vertex):



Event-type 12 (two vees, two prongs, and negative decay vertex):



In fitting each of the hypotheses (IV-2) to (IV-9), we made a 3C fit at the Λ decay vertex, and a 3C fit at the K^0 decay vertex where a K^0 was observed. The fitted Λ momentum was used in a 4C fit (3C for events having short Ξ^-) at the Ξ^- decay vertex. Finally the fitted Ξ^- momentum was used in a 4C fit, a 1C fit, or a missing-mass

calculation at the production vertex. Both possible assignments were tested for the K^+ and π^+ of (IV-7), and for the Λ and K^0 of (IV-8) and (IV-9).

Confidence levels were calculated in DST-EXAM for each of the hypotheses listed. For event-type 72, the following competing hypotheses, not involving a Ξ^- with visible Λ decay, were also tested:

$$K^- + p \rightarrow \Xi^- + K^0 + \pi^+; \quad \Xi^- \rightarrow \Lambda + \pi^-; \quad K^0 \rightarrow \pi^+ + \pi^- (\Lambda \text{ unseen})$$

(IV-10)

$$\rightarrow \Xi^- + K^0 + \pi^+ + \pi^0; \quad \Xi^- \rightarrow \Lambda + \pi^-; \quad K^0 \rightarrow \pi^+ + \pi^- (\Lambda \text{ unseen})$$

(IV-11)

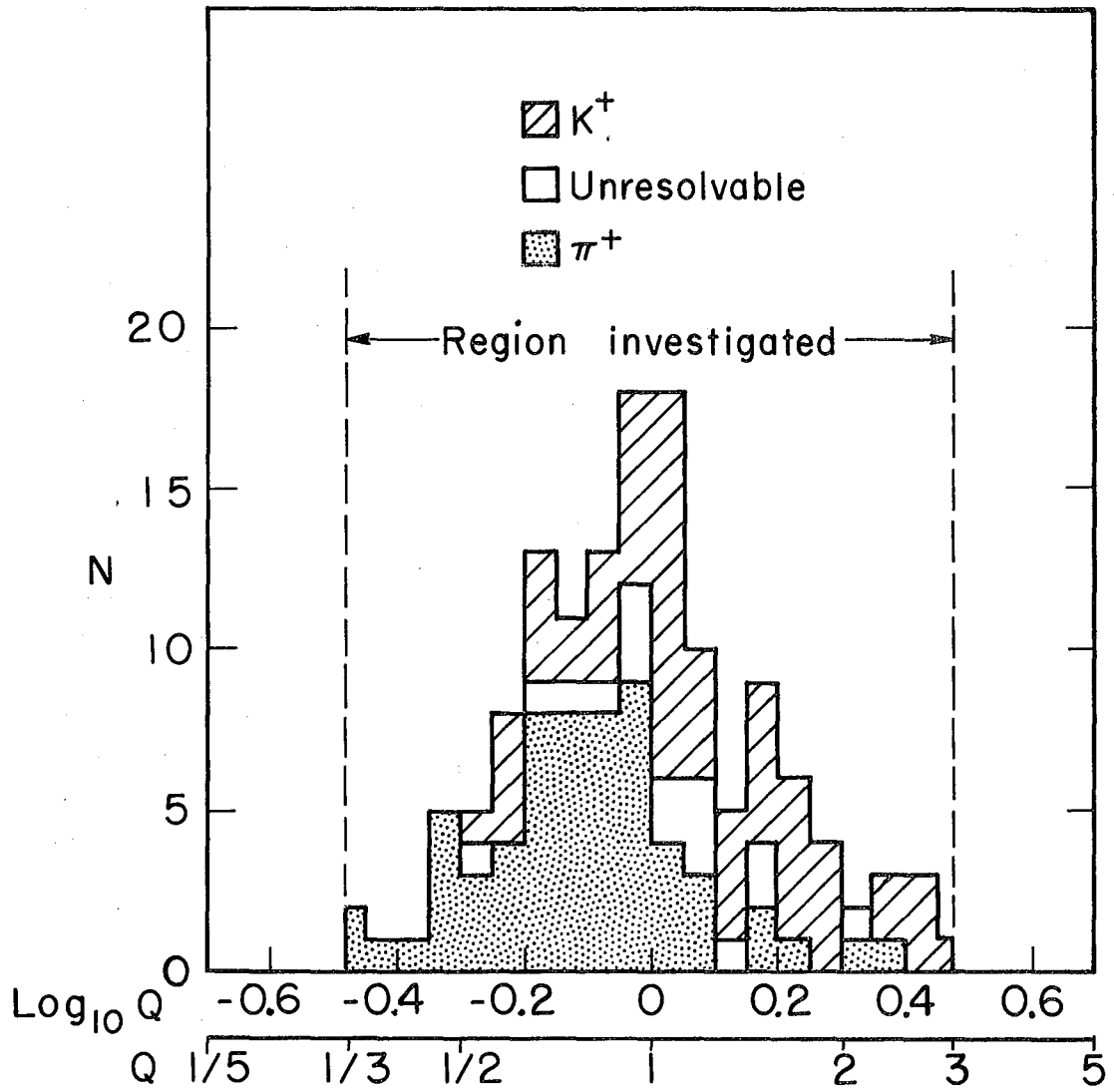
$$\rightarrow \Sigma^- + K^+ + K^0; \quad \Sigma^- \rightarrow n + \pi^-; \quad K^0 \rightarrow \pi^+ + \pi^- . \quad (IV-12)$$

No competing hypotheses were tested for event-type 74 or 12.

For most events, an unambiguous choice between competing hypotheses could be made on the basis of calculated confidence levels (c.l.) alone. Most of the remaining ambiguities (for example, ambiguities between $\Xi^- K^+ \pi^0$ and $\Xi^- K^0 \pi^+$ final states) could be resolved, at the scanning table, by identification of the positive track at the production vertex as either K^+ or π^+ .

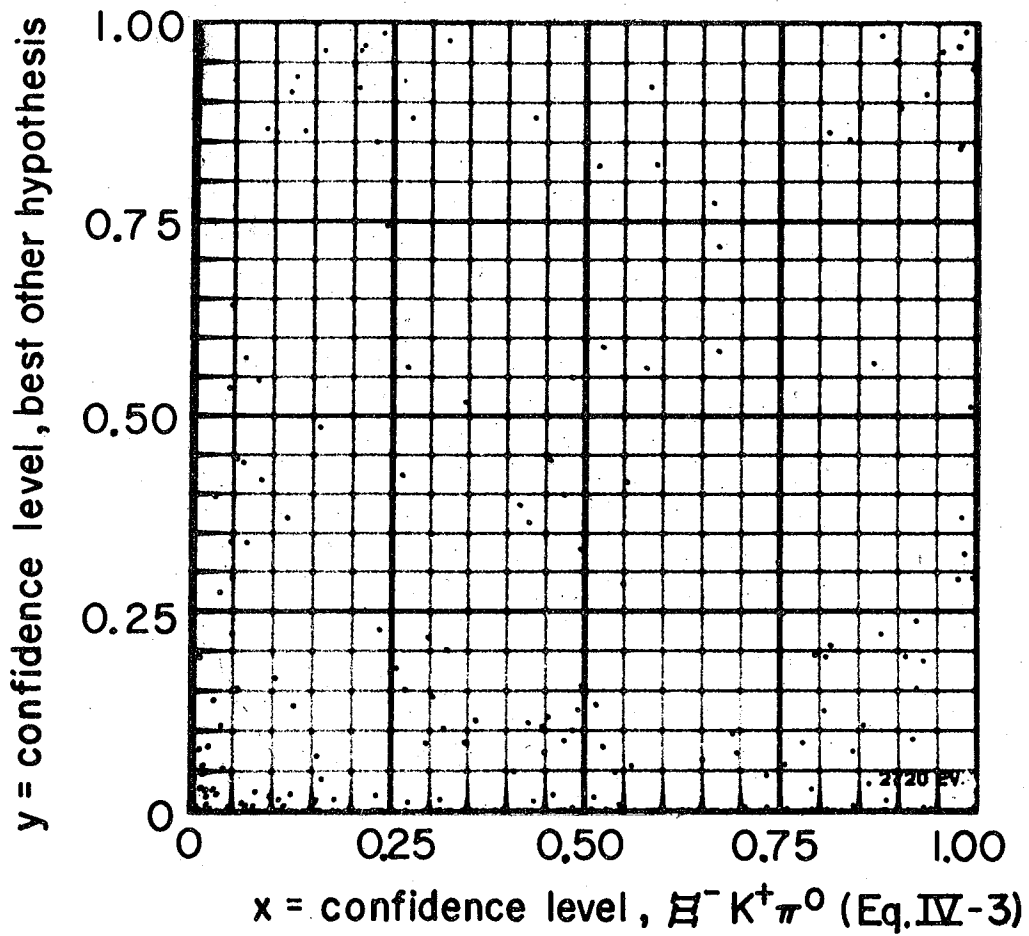
Partial results of the ionization study are illustrated in Fig. IV-1, where we have plotted the number of events vs $Q \equiv \text{c.l. (best } K^+ \text{ hypothesis)}/\text{c.l. (best } \pi^+ \text{ hypothesis)}$. We find that in the region investigated ($1/3 \leq Q \leq 3$), 33/122 or 27% of the resolvable events would have been assigned to the wrong hypothesis on the basis of the calculated c.l. alone; outside the region investigated we expect to find few, if any, wrongly assigned events.

In Fig. IV-2 we present a confidence-level plot for 2720 type-72 events, obtained after application of available ionization information. Only passing events (greatest c.l. ≥ 0.005) are included. Each event is represented by a point (x,y), where x is the c.l. of one hypothesis X [in this case Eq. (IV-3)] and y is the c.l. of the best other hypothesis



MUB 13868

Fig. IV-1



MUB 13869

Fig. IV-2

tested. Events falling below the 45° line are those designated as hypothesis X. Most events are unambiguously hypothesis X($y = 0$) or unambiguously not hypothesis X($x = 0$); those near the 45° line either could not be resolved by ionization or have not yet been examined at the scanning table. We have examined similar plots for each of the hypotheses (IV-2) through (IV-9); in no case are ambiguities more numerous than in Fig. IV-2.⁵¹

For purposes of further discussion we arbitrarily classify events according to the following criteria:

Failing events: greatest c.l. < 0.005 .

Ξ^- candidates: greatest c.l. (≥ 0.005) is from one of the hypotheses (IV-2) through (IV-9) involving a Ξ^- with visible Λ decay.

Non- Ξ^- candidates (type 72 only): greatest c.l. is from one of the competing hypotheses (IV-10) through (IV-12).

Only Ξ^- candidates are considered further. These are classified as follows:

Unambiguous: greatest c.l. $\geq 10 \times$ (second greatest c.l.), and greatest c.l. ≥ 0.05 ;

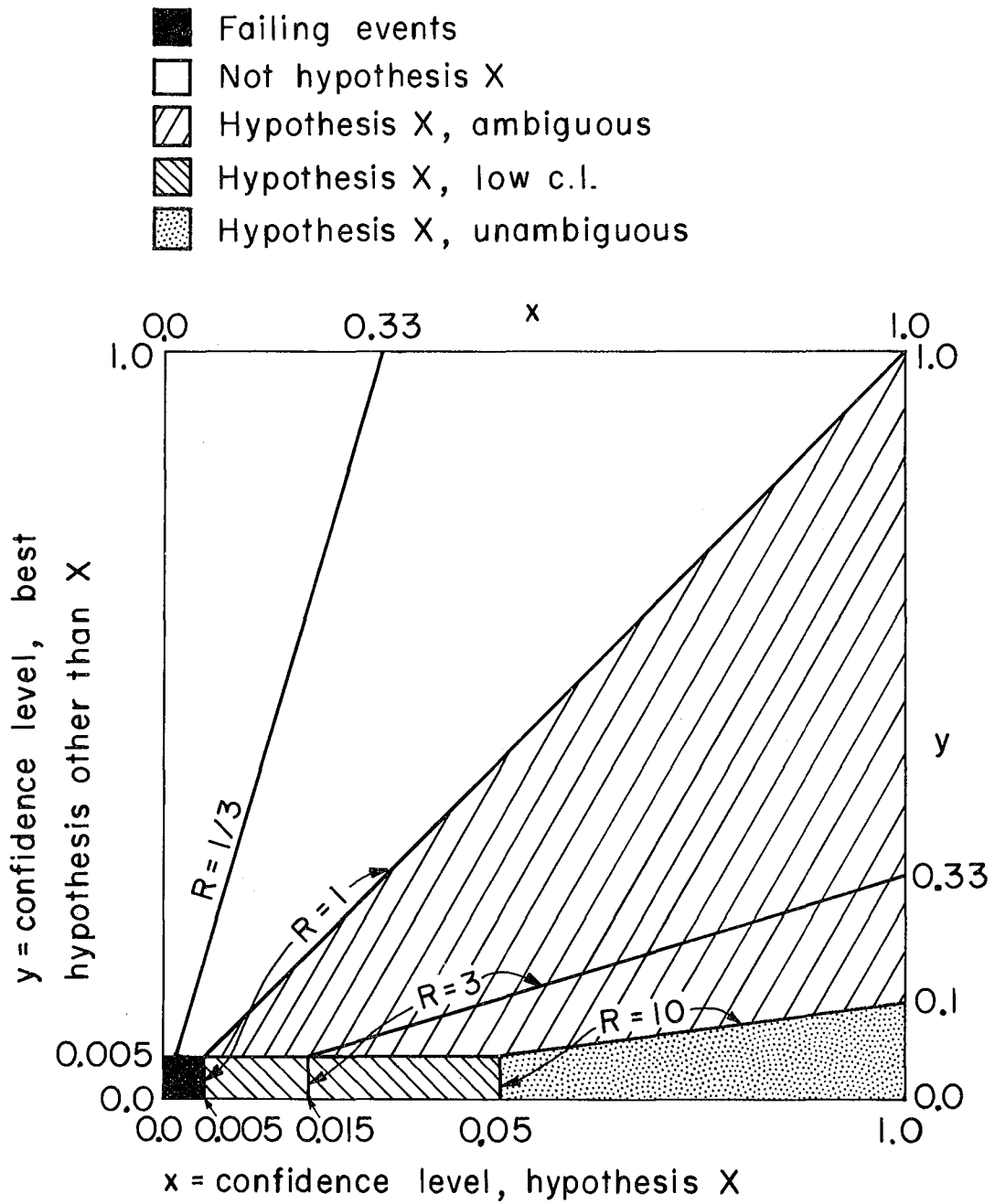
Low c.l.: greatest c.l. < 0.05 , and (second greatest c.l.) < 0.005 ;

Ambiguous: greatest c.l. $< 10 \times$ (second greatest c.l.), and (second greatest c.l.) ≥ 0.005 .

The classification of events is illustrated in Fig. IV-3, which corresponds to the scatter plot of Fig. IV-2.

We define an ambiguity ratio R as the lesser of x/y and $x/0.005$ (see Fig. IV-3).⁵² Events assigned to hypothesis X are those having $R > 1$; those having $R \geq 10$ are unambiguous by the definition above. Figure IV-1 indicates that few, if any, events having $R \geq 3$ are likely to be assigned to the wrong final-state hypothesis; accordingly we expect our unambiguous sample ($R \geq 10$) to be virtually free of wrongly identified final states.

In Tables IV-I, IV-II, and IV-III we tabulate the passing events (types 72, 74, and 12) in each of the defined classifications. We note



MUB 13870

Fig. IV-3

Table IV-I. Classification of passing type-72 events.

Classification	2nd best hyp. ^b	Best hypothesis ^b								Total A-E	Total A-H
		Ξ^- candidates					Non- Ξ^- candidates				
		A	B	C	D	E	F	G	H		
Ambiguous ($1 \leq R < 10$)	A	--	0	0 ^a	0	0 ^a	0	0	0	0	0
	B	2	--	21 ^a	2	2 ^a	0	0	0	27	27
	C	1 ^a	25 ^a	--	3 ^a	1	0	0	0	30	30
	D	1	2	13 ^a	--	1 ^a	0	0	0	17	17
	E	0 ^a	7 ^a	0	9 ^a	--	0	0	0	16	16
	F	0	0	0	0	0	--	1	0	0	1
	G	0	0	0	0	0	1	--	0	0	1
	H	0	0	0	0	0	1	0	--	0	1
	Total A-H	4	34	34	14	4	2	1	0	90	93
Low c.l. ($1 \leq R < 10$)		25	7	11	5	3	8	0	6	51	65
Unambiguous ($R \geq 10$)		1135	438	577	52	101	176	30	53	2303	2562
Total		1164	479	622	71	108	186	31	59	2444	2720

^aThese entries represent ambiguities remaining after application of available ionization information. About half cannot be resolved; the others have not yet been examined.

Hypothesis code	Eq.	Reaction
A	(IV-2)	$K^- + p \rightarrow \Xi^- + K^+$; $\Xi^- \rightarrow \Lambda + \pi^-$ (Λ seen)
B	(IV-3)	$\rightarrow \Xi^- + K^+ + \pi^0$; $\Xi^- \rightarrow \Lambda + \pi^-$ (Λ seen)
C	(IV-4)	$\rightarrow \Xi^- + K^0 + \pi^+$; $\Xi^- \rightarrow \Lambda + \pi^-$ (Λ seen, K^0 unseen)
D	(IV-5)	$\rightarrow \Xi^- + K^+ + \text{neutrals}$; $\Xi^- \rightarrow \Lambda + \pi^-$ (Λ seen)
E	(IV-6)	$\rightarrow \Xi^- + \pi^+ + \text{neutrals}$; $\Xi^- \rightarrow \Lambda + \pi^-$ (Λ seen)
F	(IV-10)	$\rightarrow \Xi^- + K^0 + \pi^+$; $\Xi^- \rightarrow \Lambda + \pi^-$ (K^0 seen, Λ unseen)
G	(IV-11)	$\rightarrow \Xi^- + K^0 + \pi^+ + \pi^0$; $\Xi^- \rightarrow \Lambda + \pi^-$ (K^0 seen, Λ unseen)
H	(IV-12)	$\rightarrow \Sigma^- + K^+ + \bar{K}^0$; $\Sigma^- \rightarrow n + \pi^-$ (K^0 seen)

Table IV-II. Classification of passing type-74 events.

Classification ^a	Total
Ambiguous ^b ($1 \leq R < 10$)	1
Low c.l. ($1 \leq R < 10$)	2
Unambiguous ($R \geq 10$)	78
Total	81

^aThe only hypothesis tested is $K^- + p \rightarrow \Xi^- + K^+ + \pi^+ + \pi^-$ (Eq. IV-7).

^bAmbiguous in identification of K^+ and π^+ .

Table IV-III. Classification of passing type-12 events.

Classification	Best hypothesis ^a		
	A	B	Total
Ambiguous ($1 \leq R < 10$)	0	0	0
Low c.l. ($1 \leq R < 10$)	8	0	8
Unambiguous ($R \geq 10$)	266	37	303
Total	274	37	311

^a Hypothesis code	Eq.	Reaction
A	(IV-8)	$K^- + p \rightarrow \Xi^- + K^0 + \pi^+$; $\Xi^- \rightarrow \Lambda + \pi^-$; Λ and K^0 seen
B	(IV-9)	$\rightarrow \Xi^- + K^0 + \pi^+ + \pi^0$; $\Xi^- \rightarrow \Lambda + \pi^-$; Λ and K^0 seen

that among 2720 passing type-72 events, there are no ambiguities whatever between hypotheses (A-E) and hypotheses (F-H). Because a Λ from Ξ^- decay is so readily distinguished from a K^0 at the production vertex, we judge that the Ξ^- candidates (involving a Ξ^- with visible Λ decay) contain negligible non- Ξ^- background. Final states produced by π^- contamination in the beam--for example, $\pi^- p \rightarrow \Sigma^- K^0 \pi^+$ or $\pi^- p \rightarrow p K^0 K^-$ (with K^- decay)--likewise involve a K^0 at the production vertex and are not easily mistaken for Ξ^- events with visible Λ decay.

In the analysis of $\Xi^*(1530)$ and $\Xi^*(1817)$ (Secs. VI and VII) we use only unambiguous events, in order to avoid including events assigned to incorrect final states. However, because our analysis of Ξ spin and decay parameters (Sec. V) is essentially independent of the final state in which the Ξ is formed, all Ξ^- candidates are used in that analysis. The following are (very approximate) conservative guesses of background in the Ξ^- samples selected:

$$\text{(Sec. V): } \frac{\text{non-}\Xi^- \text{ events}}{\Xi^- \text{ candidates}} \lesssim 0.1\%$$

$$\text{(Secs. VI, VII): } \frac{\text{wrongly assigned final states}}{\text{unambiguous } \Xi^- \text{ events}} \lesssim 5\%.$$

2. Ξ^0 Events

The only Ξ^0 events analyzed are those in which both the Ξ^0 and the Λ decay in the chamber, via

$$\Xi^0 \rightarrow \Lambda + \pi^0; \quad \Lambda \rightarrow p + \pi^- . \quad \text{(IV-13)}$$

We consider the following final states and event-type topologies:

Event-type 32 (two prongs with vee):

$$K^- + p \rightarrow \Xi^0 + K^+ + \pi^- \quad \text{(IV-14)}$$

Event-type 40 (zero prong with two vees):

$$K^- + p \rightarrow \Xi^0 + K^0; \quad K^0 \rightarrow \pi^+ + \pi^- \quad \text{(IV-15)}$$

Event-type 42 (two prongs with two vees):

$$K^- + p \rightarrow \Xi^0 + K^0 + \pi^+ + \pi^-; \quad K^0 \rightarrow \pi^+ + \pi^- . \quad \text{(IV-16)}$$

In the fitting of each of the hypotheses (IV-14) through (IV-16), a 1C fit was made at the Λ decay vertex, and a 3C fit at the K^0 decay vertex where a K^0 was observed. Then the Ξ^0 production and decay were fit simultaneously in a 3C two-vertex fit, under the requirement that the Ξ^0 and Λ momenta be coplanar with a line joining the Ξ^0 production vertex and the Λ decay vertex. [Due to limitations in PACKAGE, the coplanarity constraint was not applied in fitting examples of (IV-16); here the fit was 2C.] Both possible assignments were tested for the Λ and K^0 of (IV-16).

Each event having one of the three topologies listed above was also fit (in K-63 PACKAGE) to a number of other K^-p final-state hypotheses.⁴⁸ Events were classified as failing, Ξ^0 candidates, or non- Ξ^0 candidates exactly as were the Ξ^- events; only Ξ^0 candidates [greatest c.l. ≥ 0.005 and from one of the hypotheses (IV-14) through (IV-16)] were analyzed further. These were fit (by π -63 PACKAGE) to a number of π^-p final-state hypotheses,⁵³ and confidence levels were calculated as for K^-p hypotheses. The classification of Ξ^0 candidates as unambiguous, low c.l., and ambiguous, and the definition of the ambiguity ratio R, are exactly as for Ξ^- candidates, except that for Ξ^0 events, π^-p hypotheses as well as K^-p hypotheses are considered. We define as π hypotheses those Ξ^0 candidates having $R < 1$; i. e., those Ξ^0 candidates for which a π^-p hypothesis is preferred over the Ξ^0 hypothesis.

The selection criteria for Ξ^0 events were chosen after examination of confidence level plots similar to that of Fig. IV-2. Specifically, we sought a cutoff value of R that would reject most of the non- Ξ^0 background while retaining a sizeable fraction of the true Ξ^0 events. The above definition of unambiguous events corresponds to the choice $R \geq 10$, the value finally selected. For these events, the distribution of confidence levels (for the Ξ^0 hypothesis) is reasonably uniform from 0.05 (the minimum value) to 1.00.

In order to determine the effects of π^- contamination in the K-63 beam, we subjected a sample of π^- -produced events to the same analysis as the K-63 events. Some 3000 π -63 events (including events failing π -63 hypotheses) of types 32, 40, and 42, at incident π^- momenta from

2.1 to 3.1 BeV/c, were first fit by K-63 PACKAGE; then the K^-p confidence levels of all Ξ^0 candidates were compared with those obtained from π -63 PACKAGE.

In Figs. IV-4 through IV-8 we plot, for both K-63 and π -63 events, the number of events vs $\log_{10} R$, for each of the following event types and momentum intervals:⁵⁴

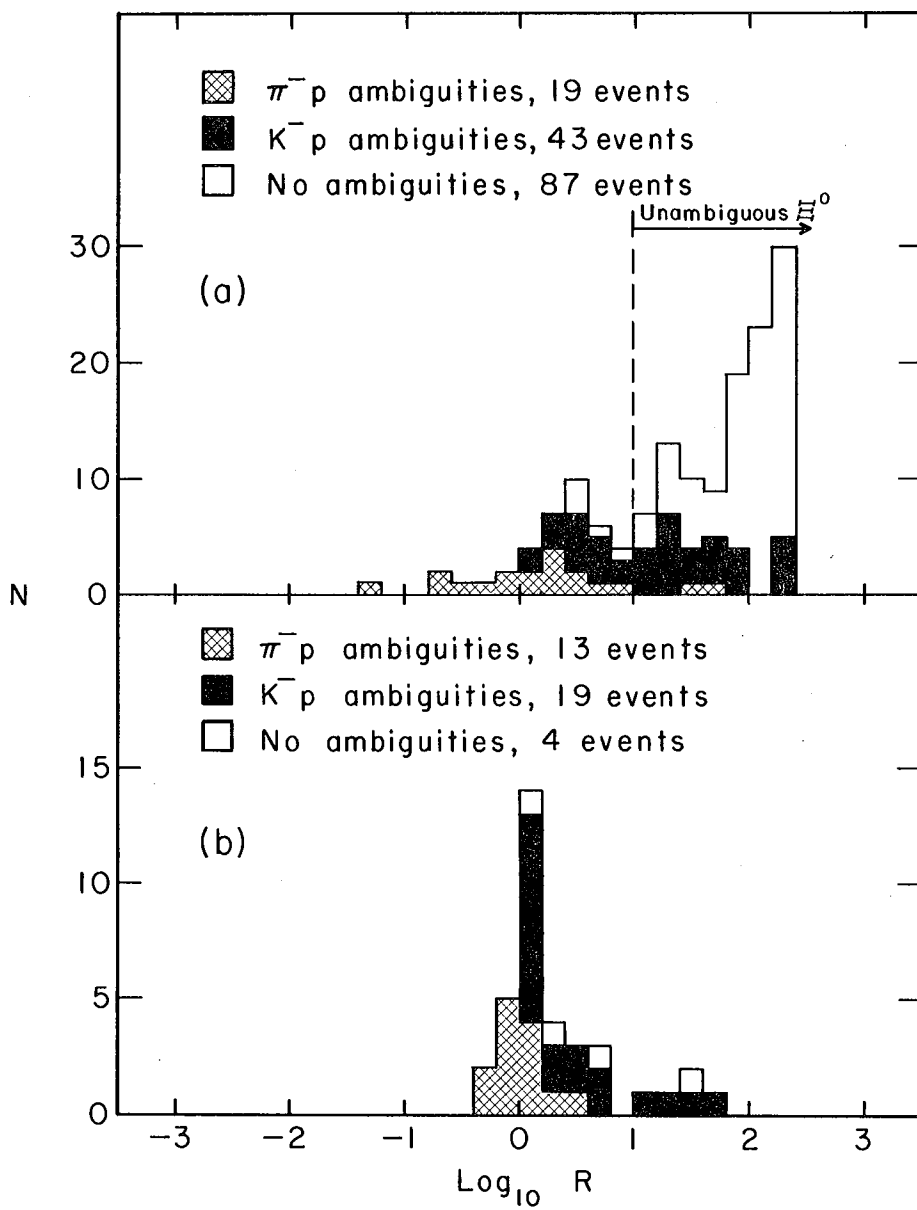
Fig.	Event type	K-63 momenta (BeV/c)	π -63 momenta (BeV/c)
IV-4	32($\Xi^0 K^+ \pi^-$)	1.7, 2.1	2.1
IV-5	32($\Xi^0 K^+ \pi^-$)	2.45 to 2.7	2.6, 3.1
IV-6	40($\Xi^0 K^0$)	1.7, 2.1	2.1
IV-7	40($\Xi^0 K^0$)	2.45 to 2.7	2.6, 3.1
IV-8	42($\Xi^0 K^0 \pi^+ \pi^-$)	2.45 to 2.7	2.6, 3.1

Only Ξ^0 candidates are plotted. The various shadings (i. e., π^-p ambiguities, K^-p ambiguities, and no ambiguities) indicate, regardless of the value of R , whether the best non- Ξ^0 hypothesis is a π^-p or a K^-p hypothesis, or whether only the Ξ^0 hypothesis has a c.l. ≥ 0.005 . With unambiguous, low c.l., ambiguous, and π hypotheses defined as described above, the Ξ^0 candidates are classified as follows:

<u>R</u>	<u>$x = \log_{10} R$</u>	<u>π^-p ambiguities</u>	<u>K^-p ambiguities</u>	<u>No ambiguities</u>
$R < 1$	$x < 0$	π hypotheses	—	—
$1 \leq R < 10$	$0 \leq x < 1$	ambiguous	ambiguous	low c.l.
$R \geq 10$	$x \geq 1$	unambiguous	unambiguous	unambiguous

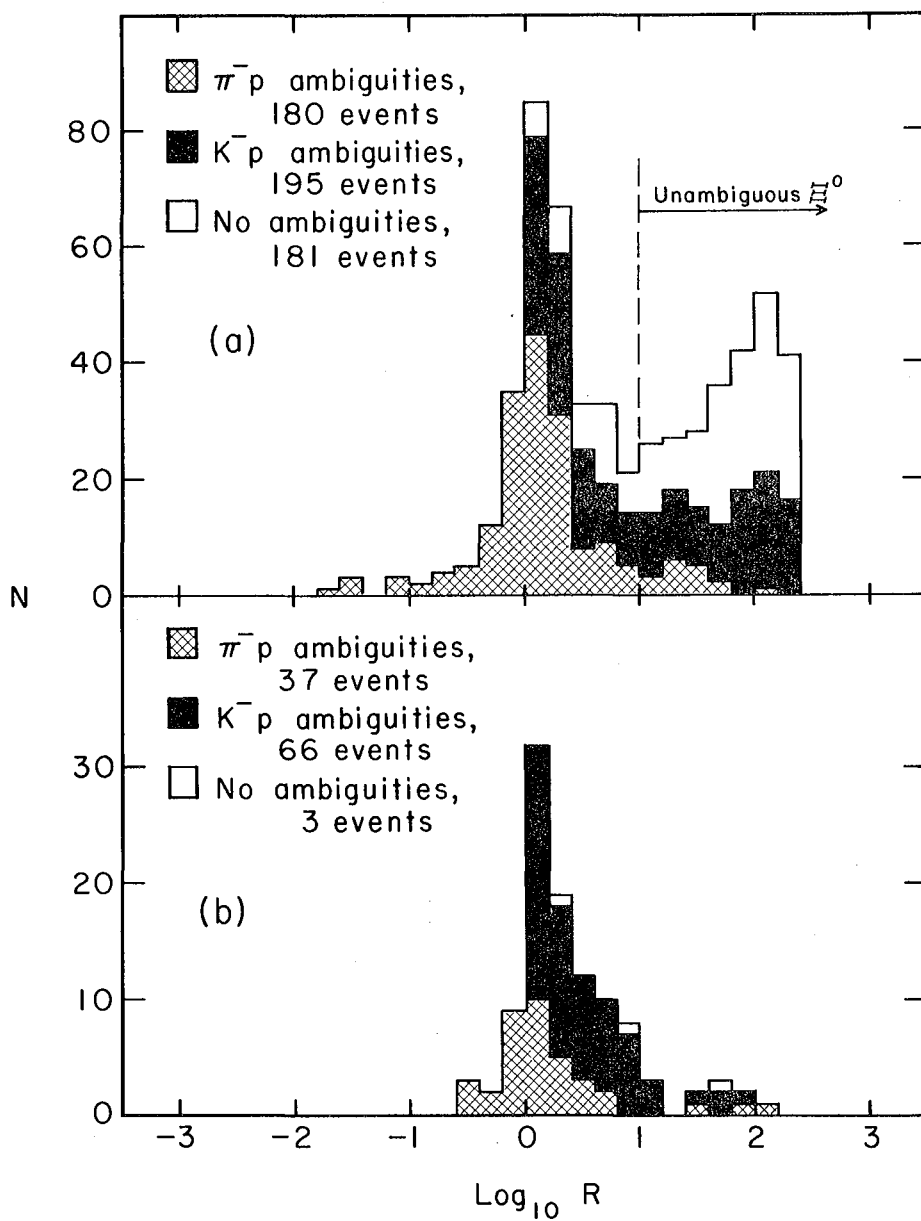
The nature of the ambiguities among K-63 and π -63 Ξ^0 candidates is illustrated in Table IV-IV.

It is seen from Figs. IV-4 through IV-8 and Table IV-IV that the criterion ($R \geq 10$) defining the unambiguous sample effectively removes most π^- -produced events. Knowing the effective path length of the π -63 sample, and the effective π^- path length (due to beam contamination) of the K-63 sample (see Appendix D), we may estimate the number of π^- -produced events remaining in the unambiguous K-63 Ξ^0 sample. The results of this analysis are presented in Table IV-V.



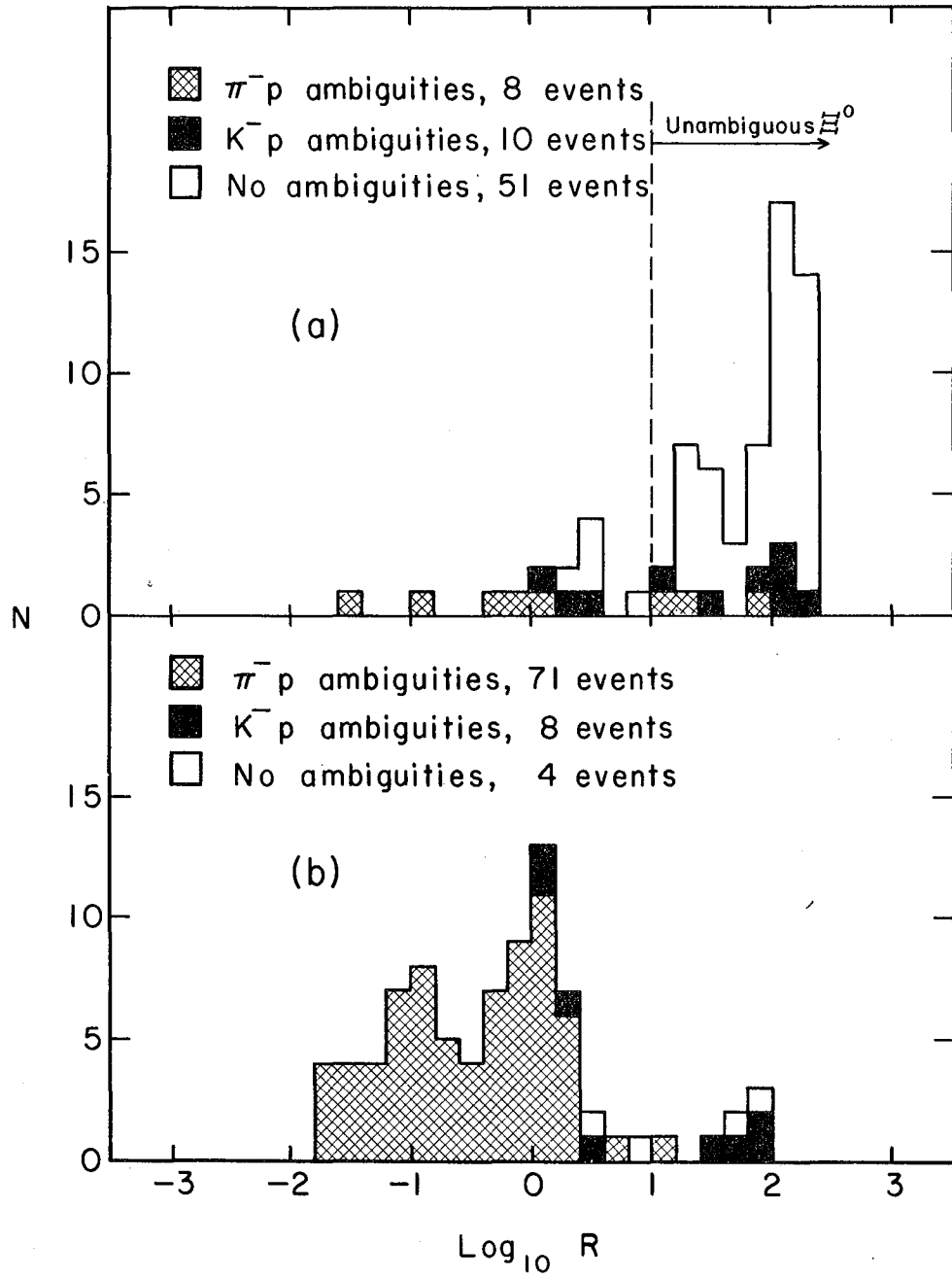
MU 37091

Fig. IV-4



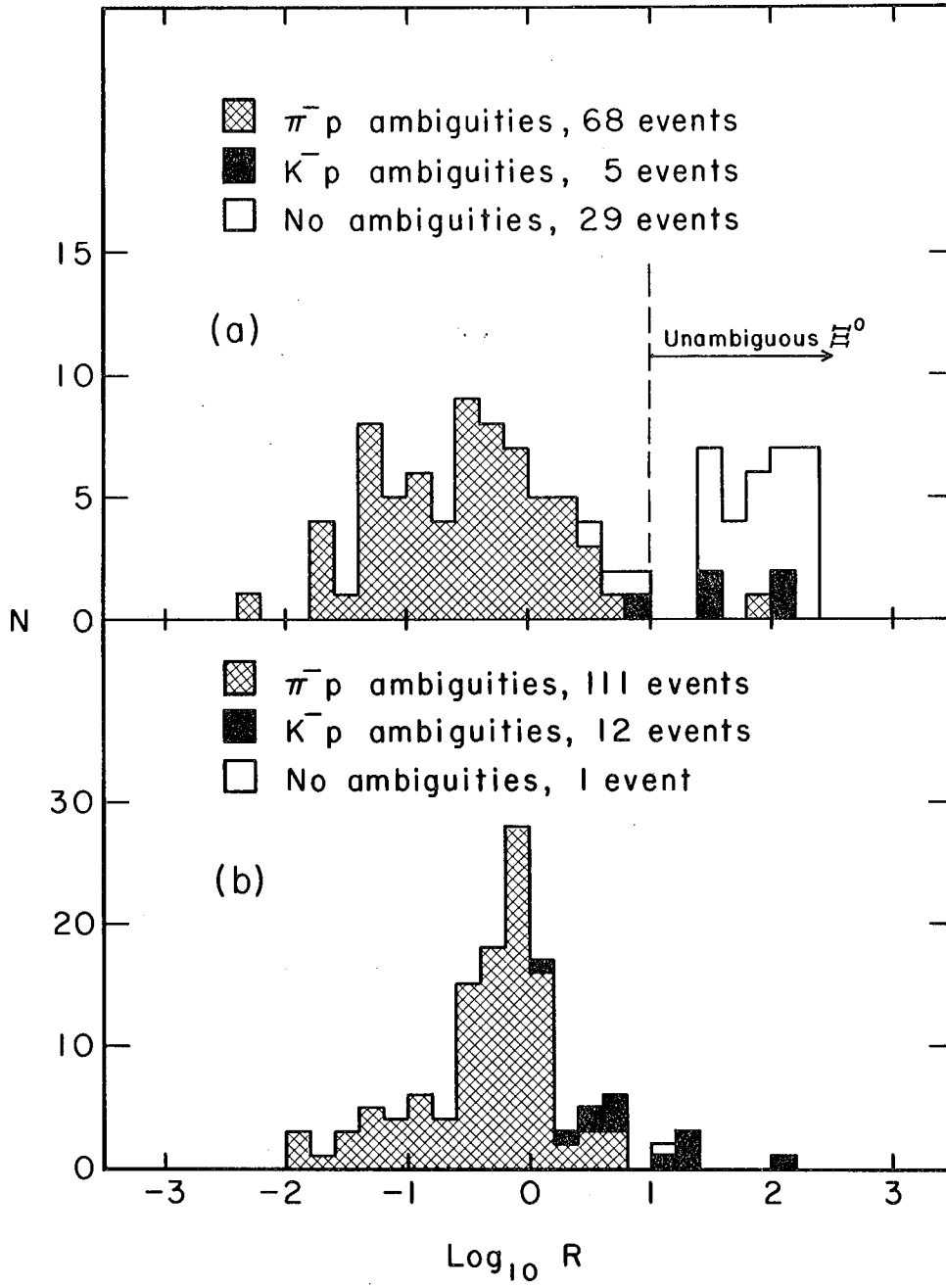
MU 37092

Fig. IV-5



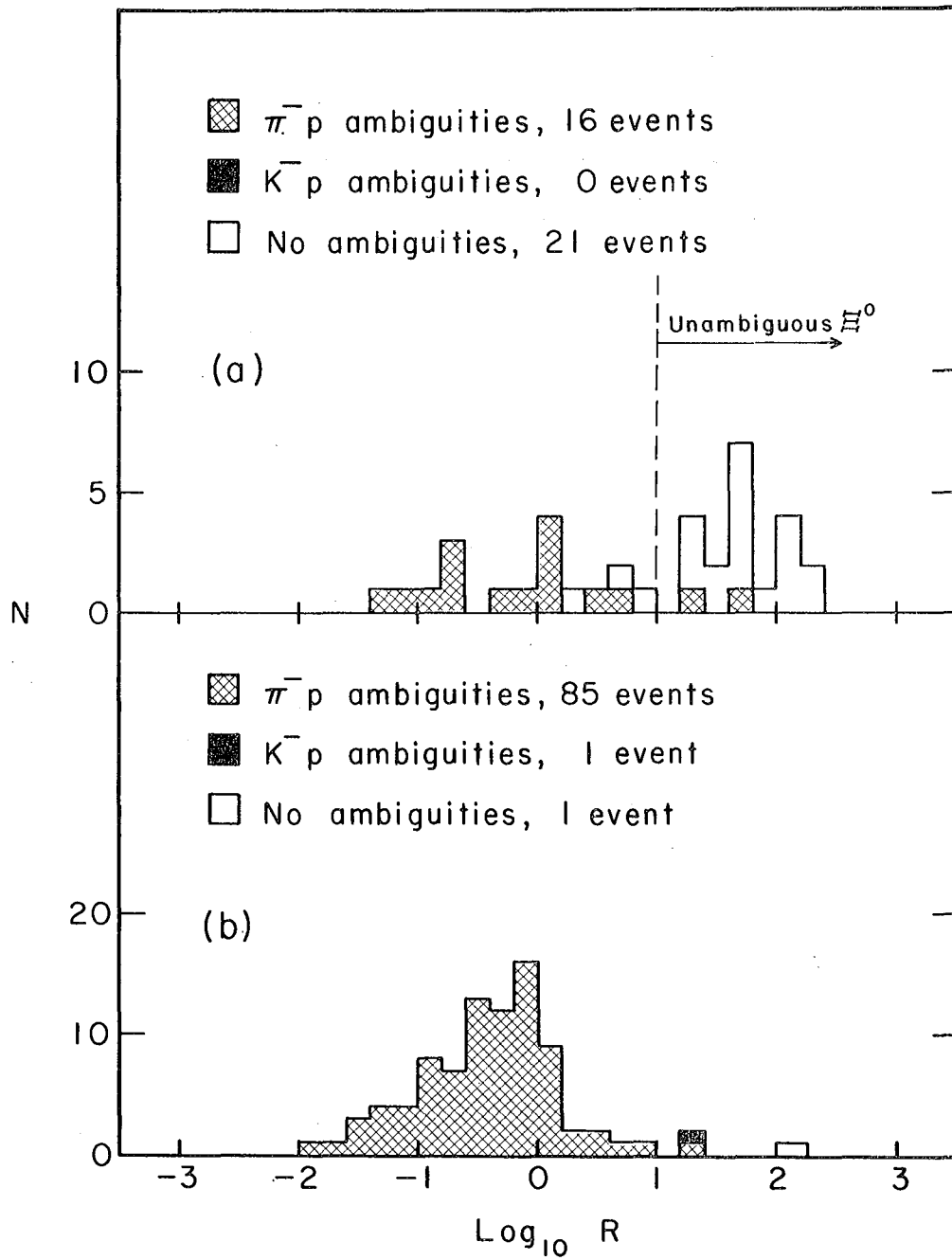
MU 37089

Fig. IV-6



MU 37090

Fig. IV-7



MU 37093

Fig. IV-8

Table IV-IV. Ambiguities among Ξ^0 candidates.

		Event type 32 $K^-p \rightarrow \Xi^0 K^+ \pi^-$ (Eq. IV-14)		Event type 40 $K^-p \rightarrow \Xi^0 K^0$ (Eq. IV-15)		Event type 42 $K^-p \rightarrow \Xi^0 K^0 \pi^+ \pi^-$ (Eq. IV-16)			
		K-63	π -63	K-63	π -63	K-63	π -63		
π hypotheses ($R < 1$)	$\pi^- p \rightarrow \Lambda K^+ \pi^-$	8	11	ΛK^0	21	58	$\Lambda K^0 \pi^+ \pi^-$	0	39
	$\rightarrow \Sigma^0 K^+ \pi^-$	15	8	$\Sigma^0 K^0$	29	61	$\Sigma^0 K^0 \pi^+ \pi^-$	4	18
	$\rightarrow \Lambda K^+ \pi^- \pi^0$	17	1	$\Lambda K^0 \pi^0$	6	17	$\Lambda K^0 \pi^+ \pi^- \pi^0$	4	10
	$\rightarrow \Lambda (K^0) \pi^+ \pi^-$ ^a	28	1	Other ^d	1	3	Other ^d	0	2
	\rightarrow Other ^d	4	0						
$(1 \leq R < 10)$ Ambiguous with:	$\pi^- p \rightarrow \Lambda K^+ \pi^-$	3	14	ΛK^0	2	17	$\Lambda K^0 \pi^+ \pi^-$	0	7
	$\rightarrow \Sigma^0 K^+ \pi^-$	22	9	$\Sigma^0 K^0$	8	20	$\Sigma^0 K^0 \pi^+ \pi^-$	2	5
	$\rightarrow \Lambda K^+ \pi^- \pi^0$	47	2	$\Lambda K^0 \pi^0$	3	6	$\Lambda K^0 \pi^+ \pi^- \pi^0$	4	3
	$\rightarrow \Lambda (K^0) \pi^+ \pi^-$ ^a	31	1	Other ^d	1	0	Other ^d	0	0
	\rightarrow Other ^d	5	0						
	$K^- p \rightarrow \Lambda \pi^+ \pi^-$	1	0	$\Lambda K^0 \bar{K}^0$	0	2	$\Lambda K^+ \bar{K}^0 \pi^-$	0	0
	$\rightarrow \Sigma^0 \pi^+ \pi^-$	0	4	$\Lambda K^0 + mm$ ^b	3	6	$\Lambda K^0 \bar{K}^- \pi^+$	0	0
$\rightarrow \Lambda \pi^+ \pi^- \pi^0$	15	24	$\Lambda K^0 + mm$ ^c	2	2				
$\rightarrow \Lambda \pi^+ \pi^- + mm$	42	9	Other ^e	0	0				
$\rightarrow \Lambda K^+ K^-$	7	0							
$\rightarrow \Lambda +$ other ^e	42	31							
$\rightarrow K^0$ hypotheses	7	6							
Totals:									
$R < 1$	π hypotheses	72	21		57	139		8	69
$1 \leq R < 10$	Ambig. with $\left\{ \begin{array}{l} \pi^- p \\ K^- p \end{array} \right\}$ hyp.	108	26		14	43		6	15
	Low c.l.	48	5		5	10		0	0
$R \geq 10$	Unambiguous	363	16		8	2		3	0
	Total Ξ^0 candidates	705	142		87	13		20	3
					171	207		37	87

^a Λ seen, K^0 unseen.

^b 1C Λ used in fit.

^c 3C Λ used in fit.

^d See Ref. 53 for a complete list of $\pi^- p$ hypotheses tested.

^e See Ref. 48 for a complete list of $K^- p$ hypotheses tested.

Table IV-V. Estimate of π^- -produced background in "unambiguous" K-63 Ξ^0 sample.

Eq.	Reaction	K-63 or π -63	Momentum (BeV/c)	Effective π^- path length ^a (events/ μ b)	"Unambiguous" Ξ^0 events	π^- -produced background in "unambiguous" K-63 Ξ^0 sample	
						Events	Percent
(IV-14)	$K^-p \rightarrow \Xi^0 K^+ \pi^-$	}K } π	1.7, 2.1	1.1 ± 0.8	111	1.0 ± 0.9	0.9 ± 0.8
			2.1	4.5 ± 0.3	4	--	--
(IV-14)	$K^-p \rightarrow \Xi^0 K^+ \pi^-$	}K } π	2.45-2.7	3.4 ± 1.0	271	6.7 ± 2.8	2.5 ± 1.1
			2.6, 3.1	5.6 ± 0.4	11	--	--
(IV-15)	$K^-p \rightarrow \Xi^0 K^0$	}K } π	1.7, 2.1	2.0 ± 1.2	56	3.6 ± 2.6	6 ± 5
			2.1	3.9 ± 0.3	7	--	--
(IV-15)	$K^-p \rightarrow \Xi^0 K^0$	}K } π	2.45-2.7	4.1 ± 1.3	32	2.7 ± 1.4	8 ± 5
			2.6, 3.1	9.3 ± 0.6	6	--	--
(IV-16)	$K^-p \rightarrow \Xi^0 K^0 \pi^+ \pi^-$	}K } π	2.45-2.7	4.1 ± 1.3	20	0.9 ± 0.6	5 ± 3
			2.6, 3.1	13.3 ± 0.9	3	--	--
	Combined	}K } π	1.7-2.7	--	490	15 ± 7	3.0 ± 1.4
			2.1-3.1	--	31	--	--

^aEffective path lengths were estimated similarly for K-63 and π -63 samples analyzed, as described in Appendix D. Path lengths refer to entire scanned volume of bubble chamber.

An accurate estimate of K^- -produced non- Ξ^0 background would involve a detailed analysis of Monte Carlo events, which we have not attempted. Nevertheless we find that among K-63 Ξ^0 candidates, ambiguities with π^-p hypotheses are as numerous as K^-p ambiguities, even though K^-p final states comprise the majority of K-63 events. We infer that Ξ^0 final states are more easily faked by π^-p than by K^-p final states, and that at least half of the non- Ξ^0 background in the unambiguous Ξ^0 sample is likely to be π^- -produced.

In our further analysis of Ξ^0 final states, we use only unambiguous events, which by a conservative estimate contain $6 \pm 3\%$ non- Ξ^0 background.

V. PROPERTIES OF THE Ξ^- AND Ξ^0 HYPERONS

In this chapter we consider only Ξ^- and Ξ^0 with visible Λ decay. In Table V-I we list the events analyzed according to momentum and final state. Much of the data (all K-72 data, and most of the K-63 $\Xi^- K^+$ events) has been previously analyzed.⁷⁻¹⁰ The K-63 events analyzed here are the Ξ^- candidates and unambiguous Ξ^0 described in Sec. IV; the selection of K-72 events is discussed in Refs. 7 and 8.

The analysis of Ξ^- and Ξ^0 in 2-, 3-, and 4-body final states (ΞK , $\Xi K\pi$, and $\Xi K\pi\pi$) is identical; in each case Ξ polarization parameters t_{LM} are expressed with reference to axes $\hat{Y}=\hat{K}$, $\hat{Z}=\hat{K}\times\hat{\Xi}$, $\hat{X}=\hat{Y}\times\hat{Z}$, defined in the production c.m. as in Fig. II-I. Polarization along other axes [for example, along the $\Xi^*(1530)$ production normal in 3- and 4-body final states] has not been investigated.

The Ξ spin is analyzed in Sec. V.A for a combined sample including both K-72 and K-63 events. Decay parameters are analyzed in Sec. V.B both for a combined sample and for K-72 and K-63 data separately. Decay distributions are presented in Sec. V.C., and scanning biases and other possible systematic errors are discussed in Appendix B.

A. Spin Analysis

1. Preliminary Considerations

The existence, in the observed Ξ decay distribution, of any non-zero t_{LM} having $L > 1$ would immediately establish the Ξ spin J to be greater than $1/2$. In Table V-II we present, for 15 subsamples of Ξ^- and Ξ^0 events, values of t_{LM} obtained from maximum-likelihood fits assuming $J = 3/2$, $L_{\max} = 3$, $a_{\Lambda} = 0.62$, $a_{\Xi^-} = a_{\Xi^0} = -0.40$, $\Phi_{\Xi^-} = \Phi_{\Xi^0} = 0$.^{39, 55} The Ξ^- data have been corrected for scanning biases, as explained in Appendix B. We compare values of $\ln \mathcal{L}$ from the $L_{\max} = 3$ fits (seven parameters per sample) with values obtained assuming $L_{\max} = 1$ (one parameter per sample). For the 15 samples, we observe an overall increase of 44.1 in $\ln \mathcal{L}$ as L_{\max} is increased from 1 to 3 (an increase of 45.0 is expected). We conclude that the spin- $1/2$ hypothesis is permitted, although not required, by the data.

Table V-I. Final states and momenta of Ξ^- and Ξ^0 events analyzed.

Exptl.	p (BeV/c)	Ξ^- event type									Ξ^0 event type			Ξ^- total	Ξ^0 total	Grand total
		72			12			74			40	32	42			
		Ξ^-K^+	$\Xi^-K^+\pi^0$	$\Xi^-K^0\pi^+$	$\Xi^-K^+\pi^+$ + neutrals	$\Xi^-K^+\pi^+$ + neutrals	$\Xi^-K^0\pi^+$	$\Xi^-K^0\pi^+\pi^0$	$\Xi^-K^+\pi^+\pi^-$	Ξ^0K^0	$\Xi^0K^+\pi^-$	$\Xi^0K^0\pi^+\pi^-$				
K-72	1.2	33	0	0	0	0	0	0	0	5	0	0	33	5	38	
K-72	1.3	74	0	0	0	0	0	0	7	0	0	74	7	81		
K-72	1.4	87	0	0	0	0	0	0	3	0	0	87	3	90		
K-72	1.5	470	6	10	0	0	3	0	63	18	0	489	81	570		
K-72	1.6	61	4	9	0	0	2	0	9	9	0	76	18	94		
K-72	1.7	105	8	20	0	0	10	0	19	26	0	143	45	188		
K-63	1.7	272	31	54	0	0	0	0	29	17	0	357	46	403		
K-63	2.1	342	105	173	1	6	94	0	27	94	0	725	121	846		
K-63	2.45	76	47	50	6	7	24	10	8	5	56	228	64	292		
K-63	2.55	103	66	85	15	24	26	6	11	25	5	342	41	383		
K-63	2.6	153	131	145	28	45	67	15	10	112	8	622	130	752		
K-63	2.7	76	49	54	13	24	22	6	6	78	4	255	88	343		
K-72 total		830	18	39	0	0	15	0	106	53	0	902	159	1061		
K-63 total		1022	429	561	63	106	233	37	88	382	20	2529	490	3019		
Grand total		1852	447	600	63	106	248	37	194	435	20	3431	649	4080		

Table V-II, Search for $J = 3/2$ moments in Ξ decay.

Expt.	Subsample		N	$w = f n \alpha^2$			$t_{LM} (\times 100)$						
	Final state	p(BeV/c)		$L_{\max} = 1$	$L_{\max} = 3$	Δw	t_{10}	t_{20}	Re t_{22}	Im t_{22}	t_{30}	Re t_{32}	Im t_{32}
1.	K-72	$\Xi^- K^+$	194	4.8	5.9	1.1	-35±14	2±7	5±5	1±5	-7±8	-3±6	-4±6
2.	K-72	$\Xi^- K^+$	470	3.8	6.4	2.6	0±10	5±5	2±3	-2±3	-3±6	3±4	-6±4
3.	K-72	$\Xi^- K^+$	166	6.5	8.5	2.0	40±17	-13±8	-2±5	0±5	7±9	2±7	-2±6
4.	K-63	$\Xi^- K^+$	272	7.4	14.0	3.6	27±12	-5±6	-7±4	-3±4	9±7	-4±5	-6±5
5.	K-63	$\Xi^- K^+$	342	4.9	8.7	3.8	17±11	-9±6	-4±4	-5±4	-7±6	-6±4	3±4
6.	K-63	$\Xi^- K^+$	179	6.9	9.1	2.2	55±15	4±7	4±5	-5±5	4±8	-9±6	-2±6
7.	K-63	$\Xi^- K^+$	229	7.7	10.1	2.4	47±14	4±7	3±5	2±5	12±8	8±5	-2±5
8.	K-72, K-63	$\Xi^- K^+ n^0$	154	1.6	5.2	3.6	4±17	0±8	-1±6	-5±6	15±9	-3±6	12±7
9.	K-63	$\Xi^- K^+ n^0$	304 ^a	2.2	3.9	1.7	-18±13	-7±6	2±4	3±4	-7±7	0±5	0±5
10.	K-72, K-63	$\Xi^- K^0 n^+$	367 ^a	11.5	15.1	3.6	-31±11	4±5	0±4	-8±4	4±6	-3±4	2±4
11.	K-63	$\Xi^- K^0 n^+$	473	8.0	14.3	6.3	-2±10	0±4	2±3	-6±3	-9±6	-6±4	7±4
12.	K-63	$\Xi^- K \pi \pi$	All	4.6	6.4	1.8	-27±13	3±6	1±5	-2±4	10±7	-3±5	-3±5
13.	K-72, K-63	$\Xi^0 K^0$	All	1.2	4.7	3.5	-21±14	1±7	-3±5	13±5	0±8	-3±6	-1±6
14.	K-72, K-63	$\Xi^0 K^+ n^-$	164	2.8	4.2	1.4	0±16	7±8	3±6	-1±6	6±9	4±6	5±6
15.	K-63	$\Xi^0 K^+ n^-$	274	3.9	8.4	4.5	2±12	1±6	3±4	4±4	1±7	0±5	14±5
		$\Xi^0 K^0 n^+ n^-$	All										
1-12	Ξ^- total		3431	69.9	104.6	34.7	2.6±3.6	-0.5±1.7	0.3±1.2	-3.0±1.2	0.6±2.0	-2.1±1.4	-0.1±1.4
13-15	Ξ^0 total		649	7.9	17.3	9.4	-5.3±8.1	2.5±3.9	1.0±2.7	5.6±2.7	1.9±4.7	0.3±3.2	7.2±3.2
1-15	Ξ^- and Ξ^0 , total		4080	77.8	121.9	44.1	1.3±3.3	0.0±1.6	0.5±1.1	-1.6±1.1	0.8±1.8	-1.7±1.3	1.0±1.3

^aSample No. 9 contains eight K-72 $\Xi^- K^0 n^+$.

The spin-3/2 hypothesis could be ruled out if one of the inequalities (II-17) or (II-19) were violated. Although the spin-3/2 density matrix constraint (II-19) is technically violated by three subsamples (3, 6, and 7), the effect is less than 1 standard deviation in each case. Violation of the spin-5/2 density matrix constraint (II-20) is only slightly more significant.

Hence, only the presence of the $(2J+1)$ factor in the transverse Λ polarization distribution (II-48c) or (II-50c) affords us a possibility of spin discrimination.

2. $(2J+1)$ Spin Factor

We have investigated the $(2J+1)$ spin factor using 3278 K-72 and K-63 Ξ^- events (only 96% of the events appearing in Table V-I were available at the time of this analysis). The data were arbitrarily divided into 47 approximately equal subsamples according to final state, momentum, and c.m. Ξ production angle (see Table V-III). No attempt was made to optimize the binning criteria. Also listed in Table V-III are seven Ξ^0 subsamples to be discussed in Sec. V.A.3.

Maximum-likelihood fits were performed to an assumed Ξ decay distribution of the form (II-54); variable parameters in the fits were a_Λ , a_{Ξ^-} , Φ_{Ξ^-} , and a value of t_{10} for each of the 47 subsamples. (The method of analysis is identical with that described in Ref. 7). Having found t_{20} , t_{22} , t_{30} , and t_{32} to be consistent with zero, we assumed $L_{\max} = 1$ (i. e., $t_{20} = t_{22} = t_{30} = t_{32} = 0$); the assumption does not bias our determination of $(2J+1)$. Fits were performed in three ways: (i) with no information regarding a_Λ or a_{Ξ^-} ; (ii) with a_Λ constrained to be 0.62 ± 0.07 , corresponding to the value of Cronin and Overseth;⁵⁶ (iii) with a_Λ constrained to be 0.62 ± 0.07 and $a_\Lambda a_{\Xi^-}$ constrained to be -0.321 ± 0.048 , a value roughly corresponding to the world average of spin-independent determinations of $a_\Lambda a_{\Xi^-}$, excluding Berkeley data. (These constraints were applied by including in the likelihood \mathcal{L} factors of the form $\exp[-\frac{1}{2}(a_\Lambda - 0.62)^2/(0.07)^2]$ and $\exp[-\frac{1}{2}(a_\Lambda a_{\Xi^-} + 0.321)^2/(0.048)^2]$.)

Table V-III. Subsamples used in Ξ spin analysis (K-72 and K-63 data combined).

Subsample		Events	Sub- samples	Events per subsample	$\hat{\Xi} \hat{K}$ cutoff points
Final state	p(BeV/c)				
$\Xi^- K^+$	1.2-1.4	194	3	65	0.69, 0.10
$\Xi^- K^+$	1.5	470	7	67	0.94, 0.78, 0.59, 0.29, -0.11, -0.51
$\Xi^- K^+$	1.6, 1.7	304	4	76	0.87, 0.65, -0.14
$\Xi^- K^+$	2.1	355	5	71	0.89, 0.76, 0.44, -0.44
$\Xi^- K^+$	2.45, 2.55	179	3	60	0.86, 0.26
$\Xi^- K^+$	2.6, 2.7	229	3	76	0.89, 0.50
$\Xi^- K^+ \pi^0$	1.5-2.1	147	2	73	0.43
$\Xi^- K^+ \pi^0$	2.45, 2.55	112	2	56	0.34
$\Xi^- K^+ \pi^0$	2.6, 2.7	180	2	90	0.43
$\Xi^- K^0 \pi^+$	1.5-2.1	350	5	70	0.69, 0.44, -0.02, -0.48
$\Xi^- K^0 \pi^+$	2.45, 2.55	186	3	62	0.70, 0.07
$\Xi^- K^0 \pi^+$	2.6, 2.7	288	4	72	0.78, 0.43, -0.17
$\Xi^- K^+ \pi \pi$	all	135	2	68	0.29
$\Xi^- K^0 \pi^+ \pi^0$	all	149	2	74	-0.05
Ξ^- sample, total		3278	47	70	--

$\Xi^0 K^0$	1.2-1.7 (K-72)	106	1	106	--
$\Xi^0 K^0$	1.7-2.7 (K-63)	88	1	88	--
$\Xi^0 K^+ \pi^-$	1.5-1.7	70	1	70	--
$\Xi^0 K^+ \pi^-$	2.1	94	1	94	--
$\Xi^0 K^+ \pi^-$	2.45, 2.55	81	1	81	--
$\Xi^0 K^+ \pi^-$	2.6	112	1	112	--
$\Xi^0 K^+ \pi^-$	2.7	78	1	98	--
$\Xi^0 K^0 \pi^+ \pi^-$	all	20			
Ξ^0 sample, total		649	7	93	--

In Fig. V-1 we illustrate the behavior of $w = \ln \mathcal{L}$ as a function of the assumed spin factor $(2J+1)$. From curve (ii) (a_Λ constrained to 0.62 ± 0.07 , a_{Ξ^-} free) we estimate $(2J+1) = 2.0^{+0.7}_{-0.4}$, corresponding to a Ξ spin $J = 1/2$. (At the likelihood maximum, $a_\Lambda = 0.65 \pm 0.05$, $a_{\Xi^-} = -0.41 \pm 0.04$, and $\Phi_{\Xi^-} = 13^\circ \pm 9^\circ$.) The $J = 1/2$ hypothesis is favored over $J = 3/2$ by $\approx (2 \times 3.0)^{1/2} = 2.45$ standard deviations; higher spin hypotheses are excluded by > 3 standard deviations. Violation of the spin-3/2 density matrix constraint in 16 subsamples causes a decrease of 7.03 in $w = \ln \mathcal{L}$ when the constraint is applied; however, the violation is not statistically significant. ⁵⁷

3. Analysis of Monte Carlo Events

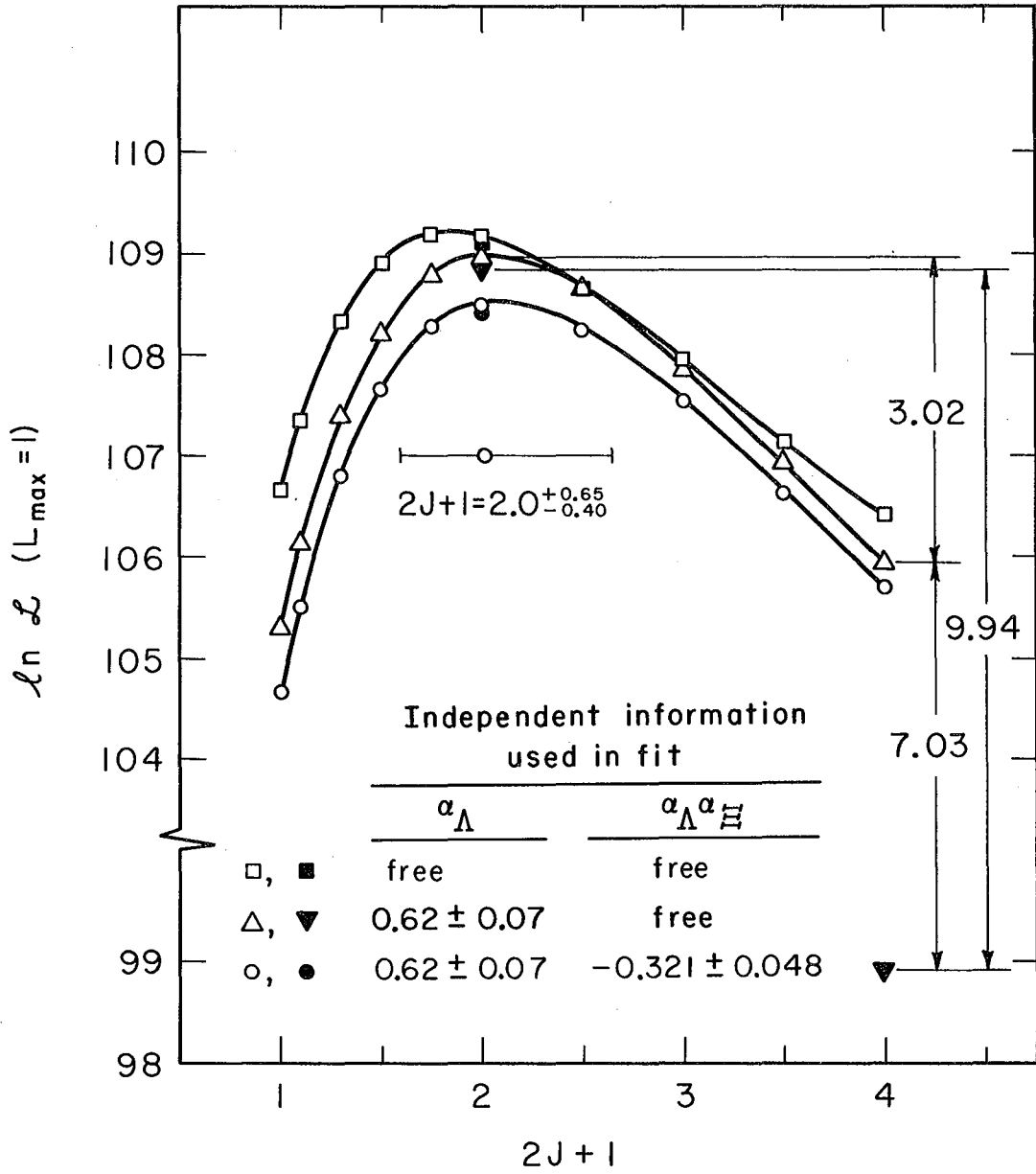
The conclusions of Sec. V.A.2 were checked by comparing experimental data with samples of computer-generated Monte Carlo events. For comparison with the 15 Ξ^- and Ξ^0 subsamples of Table V-II, we generated 75 Monte Carlo samples, having 272 events each, according to each of the following hypotheses:

- (a) $J = 1/2$, $a_\Lambda = 0.62$, $a_{\Xi^-} = -0.40$, $\Phi_{\Xi^-} = 0$, $t_{10} = 0$
(indistinguishable from $J = 3/2$ with $t_{10} = 0$);
- (b) $J = 1/2$, $a_\Lambda = 0.62$, $a_{\Xi^-} = -0.40$, $\Phi_{\Xi^-} = 0$, $t_{10} = t_{10}^{\max} = 0.57$;
- (c) $J = 3/2$, $a_\Lambda = 0.62$, $a_{\Xi^-} = -0.40$, $\Phi_{\Xi^-} = 0$, $t_{10} = t_{10}^{\max} = 0.43$.

For each sample, we performed two maximum-likelihood fits, assuming $a_\Lambda = 0.62$, $\Phi_{\Xi^-} = 0$, and $J = 1/2$ and $3/2$, respectively; a_{Ξ^-} and t_{10} were free parameters in the fits. In Figs. V-2 and V-3 we present distributions of $X \equiv \Delta \ln \mathcal{L} \equiv \ln \mathcal{L} (J = 1/2) - \ln \mathcal{L} (J = 3/2)$ for the experimental data and for the Monte Carlo samples. The curves plotted for the Monte Carlo distributions are estimates of $P(X, J)$, the probability of observing a value X if spin J is assumed. The form of $P(X, J)$ will now be discussed.

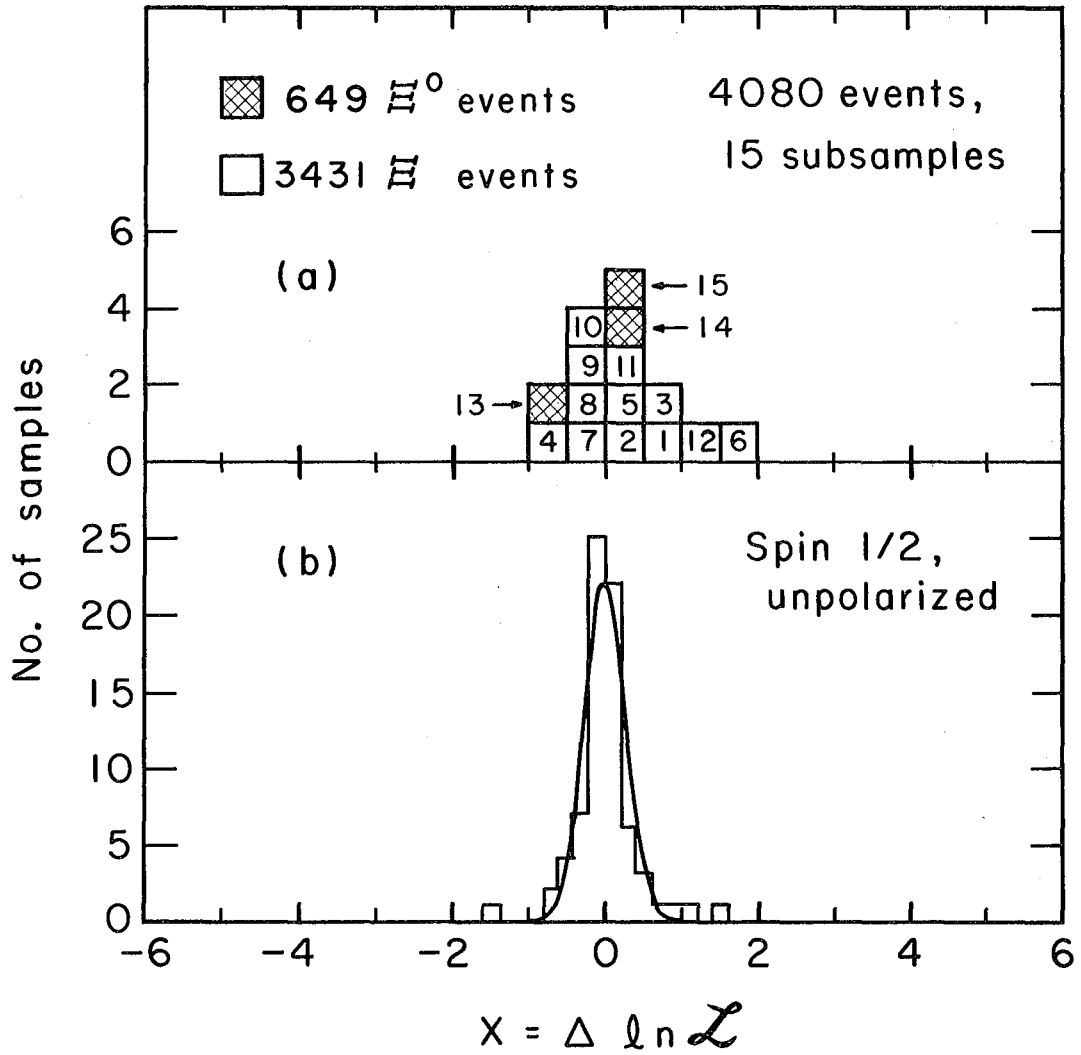
a. Form of $P(X, J)$ for a simplified model. Let us assume that the likelihood function $\mathcal{L}(J)$ for a given experiment is Gaussian in $(2J+1)$ and hence in J ; i. e.,

$$\mathcal{L}(J) \propto \exp\left[-\frac{1}{2} (J - J')^2 / \sigma_{J'}^2\right], \quad (\text{V-1})$$



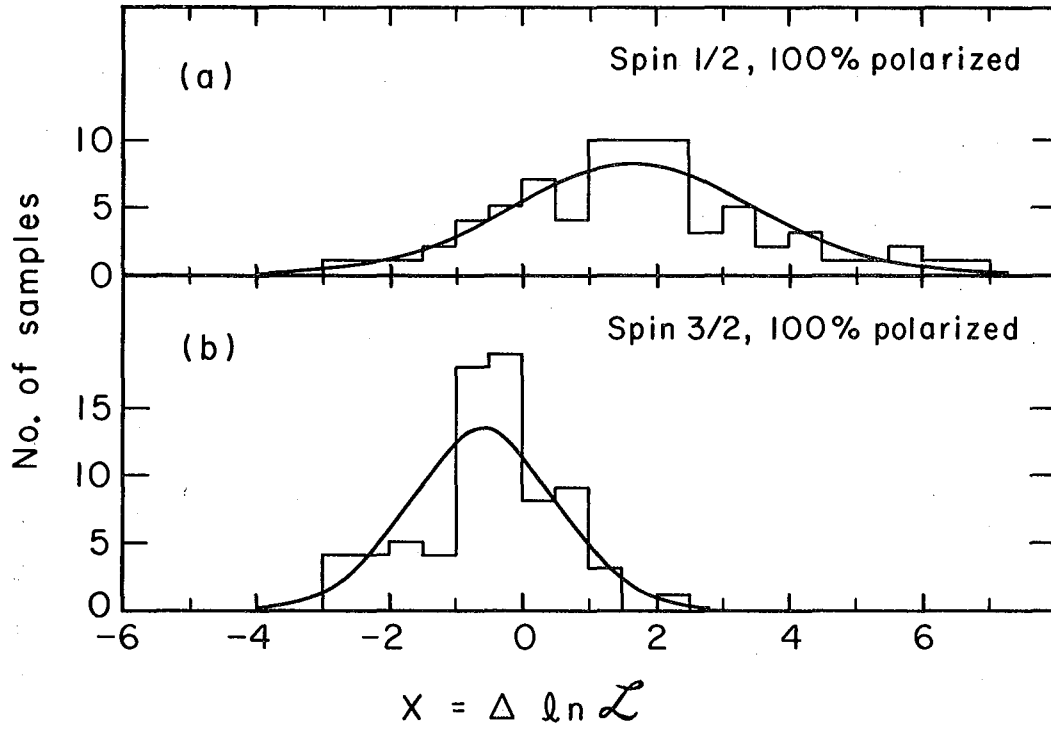
MU-36800

Fig. V-1



MUB-13653

Fig. V-2



MU-36863

Fig. V-3

where $J' \pm \sigma_{J'}$ is the best value of J for this experiment. Moreover, we assume the maximum-likelihood function to be an asymptotically unbiased and efficient estimator of the spin J ,⁵⁸ implying that individual determinations of J' are distributed according to

$$\frac{dN}{dJ'} \propto \exp\left[-\frac{1}{2} \frac{(J_{\text{actual}} - J')^2}{\sigma_{J'}^2}\right], \quad (\text{V-2})$$

where $\sigma_{J'} = \sigma_{J'}$. (We neglect variations in individual determinations of $\sigma_{J'}$.) For the assumed model, individual determinations of

$$X = \ln \mathcal{L}(1/2) - \ln \mathcal{L}(3/2) = \frac{1 - J'}{\sigma_{J'}} \quad (\text{V-3})$$

are distributed according to

$$P(X, J_{\text{actual}}) \propto \frac{dN}{dX} = \frac{dN}{dJ'} \cdot \frac{dJ'}{dX} \propto \exp\left[-\frac{1}{2} \frac{(X - \bar{X})^2}{\sigma_X^2}\right] \quad (\text{V-4})$$

where

$$\sigma_X = (\sigma_{J'})^{-1} \quad (\text{V-5})$$

and

$$\bar{X} = \frac{1 - J_{\text{actual}}}{\sigma_{J'}} = (\pm) \frac{1}{2\sigma_{J'}} = (\pm) \frac{1}{2} \sigma_X^2 \quad \text{for } J_{\text{actual}} = \begin{pmatrix} 1/2 \\ 3/2 \end{pmatrix}. \quad (\text{V-6})$$

Henceforth we shall use the symbol J to mean J_{actual} .

For a sample of N events having average polarization P_{Ξ} ,⁵⁸ a lower limit on σ_J (ignoring error correlations) is given by

$$\frac{1}{\sigma_J^2} \leq -N \int I(\hat{\Lambda}, \hat{p}) \frac{\partial^2 \ln I(\hat{\Lambda}, \hat{p})}{(\partial J)^2} d\Omega_{\Lambda} d\Omega_P \quad (\text{V-7a})$$

$$= N \int \frac{1}{I(\hat{\Lambda}, \hat{p})} \left[\frac{\partial I(\hat{\Lambda}, \hat{p})}{\partial J} \right]^2 d\Omega_{\Lambda} d\Omega_P \quad (\text{V-7b})$$

where $I(\hat{\Lambda}, \hat{p})$ is the (normalized) Ξ decay distribution (II-51). Evaluating the integral and assuming $J = 1/2$, $\alpha_{\Lambda} = 0.62$, $\alpha_{\Xi} = -0.40$, and $\Phi_{\Xi} = 0$, one finds⁵⁹

$$\frac{1}{\sigma_J^2} = \sigma_X^2 = 2\bar{X} \lesssim 0.08 NP_{\Xi}^2 \quad (V-8)$$

If correlations between J and other parameters are considered, the constant factor decreases, but $\frac{1}{\sigma_J^2}$ remains approximately proportional to NP_{Ξ}^2 . If measurements of P_{Ξ} have a statistical uncertainty $\sigma(P_{\Xi})$, we expect σ_X and \bar{X} to depend upon rms and average values of P_{Ξ} , respectively, i. e.,

$$\sigma_X^2 \approx CN \langle P_{\Xi}^2 \rangle \quad (V-9)$$

$$\bar{X} \approx \frac{1}{2} CN \langle P_{\Xi}^2 - \sigma^2(P_{\Xi}) \rangle \approx \frac{1}{2} CN \langle P_{\Xi} \rangle^2, \quad (V-10)$$

where C is a constant to be determined, and $\langle \rangle$ denotes an expectation value. We may generalize the result to include the case $J = 3/2$ as well as $J = 1/2$ (for $J = 1/2$, $P_{\Xi} = \sqrt{3} t_{10}$):

$J = 1/2$	$J = 3/2$
$\sigma_X^2 \approx C_{1/2} N \langle t_{10}^2 \rangle$	$\sigma_X^2 \approx C_{3/2} N \langle t_{10}^2 \rangle$
$\bar{X} \approx + 1/2 C_{1/2} N \langle t_{10} \rangle^2$	$\bar{X} = - \frac{1}{2} C_{3/2} N \langle t_{10} \rangle^2$

The constants $C_{1/2}$ and $C_{3/2}$ may be determined from analysis of Monte Carlo events, by performing fits under the assumptions $J = 1/2$ and $3/2$, respectively.

b. Calculation of Ξ spin probabilities. In Table V-IV we present observed values of σ_X , \bar{X} , $\langle t_{10}^2 \rangle$, and $\langle t_{10} \rangle^2 = \langle t_{10}^2 - (\delta t_{10})^2 \rangle$ for the Monte Carlo distributions of Figs. V-2(b) and V-3. The observed distributions $P(X, J)$ are correctly predicted by our simplified model, with $C_{1/2} = 0.037 \pm 0.005$ and $C_{3/2} = 0.021 \pm 0.005$.

Table V-IV. Determination of $C_{1/2}$ and $C_{3/2}$ from analysis of Monte Carlo events.

J	t_{10} assumed	σ_X	\bar{X}	$\langle t_{10}^2 \rangle$	$\langle t_{10} \rangle^2$	$\frac{\sigma_X^2}{N\langle t_{10}^2 \rangle}$	$\frac{ 2\bar{X} }{N\langle t_{10} \rangle^2}$
1/2	0	0.27	0.00	0.0081	0	0.033 ^a	--
1/2	0.57	1.93	1.66	0.330	0.325	0.041 ^a	0.037 ^a
3/2	0	0.27	0.00	0.0169	0	0.016 ^a	--
3/2	0.43	1.07	-0.67	0.198	0.184	0.021 ^a	0.027 ^a

^aBest values are $C_{1/2} = 0.037 \pm 0.005$, $C_{3/2} = 0.021 \pm 0.005$.

Given the expectation values $\langle t_{10}^2 \rangle$ and $\langle t_{10} \rangle^2$ for each of the 15 Ξ^- and Ξ^0 subsamples of Table V-II and Fig. V-2(a), one could, in principle, calculate the spin-1/2 and spin-3/2 probability for each subsample. The overall probability would then be the product of the individual probabilities. However, for individual subsamples the quantities $\langle t_{10}^2 \rangle$ and $\langle t_{10} \rangle^2$ have large errors. A more reliable estimate of spin probabilities is obtained by summing the quantities X from all 15 subsamples and calculating the expected distribution of the resulting sum. We re-define $X = \sum_{k=1}^{15} X_k$, where X_k is the value of X for subsample k . Under our previous assumption that each X_k is distributed according to

$$P(X_k, J) \propto \exp\left[-\frac{1}{2} (X_k - \bar{X}_k)^2 / \sigma_{X_k}^2\right], \quad (V-11)$$

the sum X is distributed according to

$$P(X, J) \propto \exp\left[-\frac{1}{2} (X - \bar{X})^2 / \sigma_X^2\right], \quad (V-12)$$

where

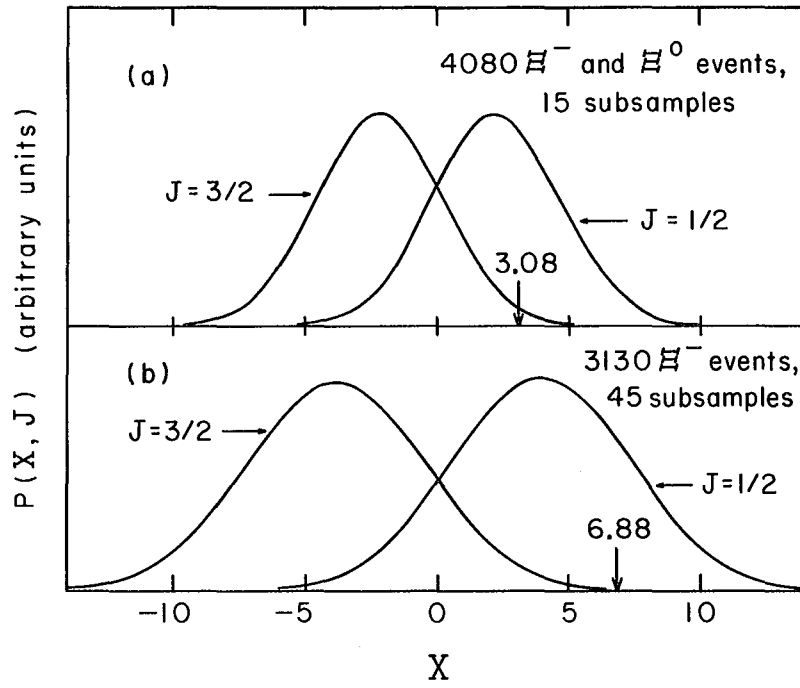
$$\bar{X} = \sum_{k=1}^{15} \bar{X}_k = (-)^{J-1/2} \frac{C_J}{2} \sum_{k=1}^{15} N_k \langle t_{10} \rangle_k^2 \quad (V-13)$$

and

$$\sigma_X^2 = \sum_{k=1}^{15} \sigma_{X_k}^2 = C_J \sum_{k=1}^{15} N_k \langle t_{10}^2 \rangle_k. \quad (V-14)$$

We evaluate the quantities $\sum_{k=1}^{15} N_k \langle t_{10} \rangle_k^2$ and $\sum_{k=1}^{15} N_k \langle t_{10}^2 \rangle_k$ as $\sum_{k=1}^{15} N_k (t_{10} - (\delta t_{10}))^2_k$ and $\sum_{k=1}^{15} N_k (t_{10}^2)_k$, respectively, where $(t_{10})_k \pm (\delta t_{10})_k$ is the measured value of t_{10} for subsample k .

In Fig. V-4 we compare the observed value $X_{\text{obs}} = 3.08$ with the calculated distributions $P(X, 1/2)$ and $P(X, 3/2)$. Parameters of the calculated curves appear in Table V-V. For the 4080-event combined



MU-36864

Fig. V-4

Ξ^- and Ξ^0 sample (see Table V-II), we estimate the relative (spin-3/2)/(spin-1/2) probability as

$$\frac{P(X_{\text{obs}}, 3/2)}{P(X_{\text{obs}}, 1/2)} = \frac{P(3.08, 3/2)}{P(3.08, 1/2)} \approx 0.10. \quad (\text{V-15})$$

The probability $P(X \geq X_{\text{obs}}) = P(X \geq 3.08)$ of observing $X \geq 3.08$, if the spin is really 3/2 (1/2), is 0.015 (0.35).

If X_k and $\sigma_{X_k}^2$ are proportional to N_k , as predicted by our simplified model, then the analysis of this section may be extended to the 3278-event Ξ^- sample of Table V-III. For this sample,

$$\frac{P(X_{\text{obs}}, 3/2)}{P(X_{\text{obs}}, 1/2)} = \frac{P(6.88, 3/2)}{P(6.88, 1/2)} \approx 0.01, \quad (\text{V-16})$$

and $P(X \geq X_{\text{obs}}) = P(X \geq 6.88) = 0.0008$ (0.16) for $J = 3/2$ (1/2).⁶⁰ [The estimate of $P(X_{\text{obs}}, 3/2)/P(X_{\text{obs}}, 1/2) \approx 0.01$ is to be compared with the value $e^{-3.02} = 0.05$ obtained in the analysis of Sec. V.A.2.]

Inclusion of 649 Ξ^0 events in seven subsamples (defined in Table V-III) reduces the spin-3/2 probability still further. (See Table V-V and Fig. V-5.)

The conclusions of the Ξ spin analysis are not substantially affected by scanning biases or other systematic errors. (See Appendix B.)

c. Validity of assumed model. The spin analysis of Sec. V.A.3 is open to question as a result of the following assumptions:

(i) Assumed X-dependence of $P(X, J)$: The observed Monte Carlo distributions are consistent with the predictions of our assumed model, that

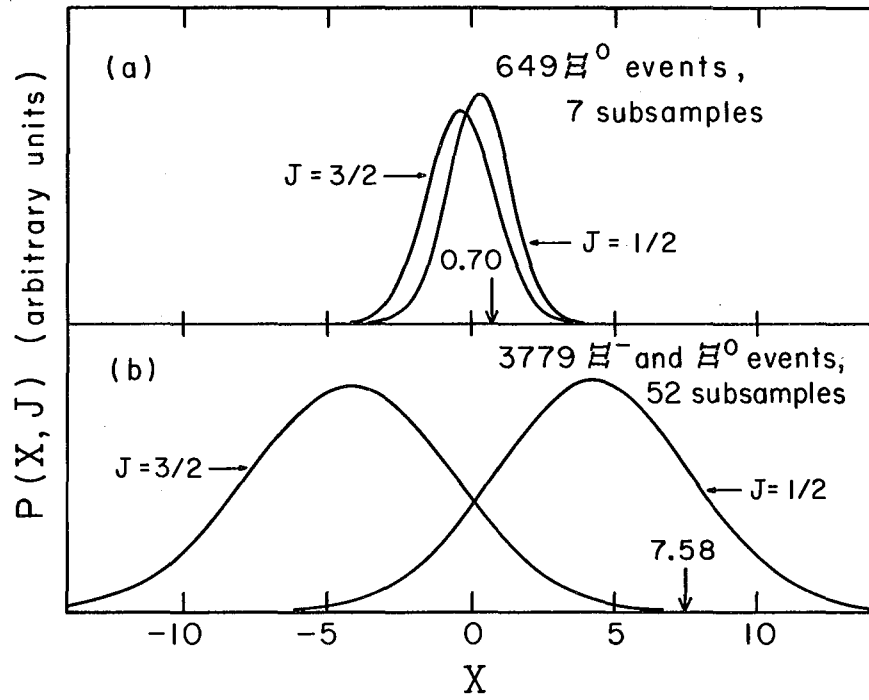
$$P(X, J) \propto \exp\left[-\frac{1}{2}(X-\bar{X})^2/\sigma_X^2\right] \quad (\text{V-17})$$

where

$$\bar{X} = (\pm) \frac{1}{2} \sigma_X^2 \quad \text{for } J = \begin{pmatrix} 1/2 \\ 3/2 \end{pmatrix} \quad (\text{V-18})$$

(if measurement errors are neglected). The model assumes that $\mathcal{L}(J)$ and dN/dJ are Gaussian in J , which is not the case in Fig. V-1.

A rough calculation based on the observed form of $\mathcal{L}(J)$ yields values



MU-36865

Fig. V-5

Table V-V. Estimates of Ξ spin probabilities.

		Sample			
		Ξ^-, Ξ^0	Ξ^-	Ξ^0	Ξ^-, Ξ^0
No. of events		4080	3130 ^a	649	3779 ^a
No. of samples		15	45 ^a	7	52 ^a
X_{obs}		3.08	6.88	0.70	7.58
Spin probabilities and related quantities					
J = 1/2 hypothesis	$\langle t_{10} \rangle^2$ ^b	0.029	0.064	0.023	0.057
		± 0.009	± 0.015	± 0.025	± 0.013
	$\langle t_{10}^2 \rangle$ ^c	0.037	0.091	0.046	0.083
		± 0.009	± 0.015	± 0.025	± 0.013
	\bar{X}	2.19	3.70	0.28	3.99
	σ_X	2.37	3.25	1.05	3.41
	Std. devs. ^d	0.38	0.98	0.40	1.05
	$P(X \geq X_{\text{obs}})$	0.35	0.16	0.34	0.15
J = 3/2 hypothesis	$\langle t_{10} \rangle^2$ ^b	0.047	0.108	0.047	0.098
		± 0.018	± 0.029	± 0.051	± 0.030
	$\langle t_{10}^2 \rangle$ ^c	0.065	0.166	0.095	0.154
		± 0.018	± 0.029	± 0.051	± 0.030
	\bar{X}	-2.01	-3.55	-0.32	-3.89
	σ_X	2.36	3.31	1.14	3.50
	Std. devs. ^d	2.16	3.15	0.89	3.28
	$P(X \geq X_{\text{obs}})$	0.015	0.0008	0.19	0.0005
$P(X_{\text{obs}}, 3/2)/P(X_{\text{obs}}, 1/2)$		0.10	0.01	0.70	0.007

^aSee Ref. 60.

$${}^b \langle t_{10} \rangle^2 \equiv \frac{1}{N} \sum_k N_k [t_{10}^2 - (\delta t_{10})^2]_k.$$

$${}^c \langle t_{10}^2 \rangle \equiv \frac{1}{N} \sum_k N_k (t_{10}^2)_k.$$

$${}^d \text{Std. devs.} = (X_{\text{obs}} - \bar{X})/\sigma_X.$$

of $|\bar{X}|^{1/2}$ and σ_X about half as large as expected (i. e.,

$|2\bar{X}|^{1/2} \approx \sigma_X \approx \frac{1}{2\sigma_J}$); however, the relations (V-17) and (V-18) are still approximately valid. A more sensitive check would require analysis of more Monte Carlo events.

(ii) Assumed P_{Ξ} -dependence of \bar{X} and σ_X : The assumed proportionality between P_{Ξ}^2 , \bar{X} , and σ_X^2 is verified within $\approx 25\%$ from the observed Monte Carlo distributions. As a visual check on the P_{Ξ} -dependence of \bar{X} and σ_X , we present in Fig. V-6 a scatter plot of X vs $|t_{10}| = |\bar{P}_{\Xi}| / \sqrt{3}$ for the 45 Ξ^- subsamples and 7 Ξ^0 subsamples of Table V-III.⁶⁰ The data are consistent with the $J = 1/2$ hypothesis.

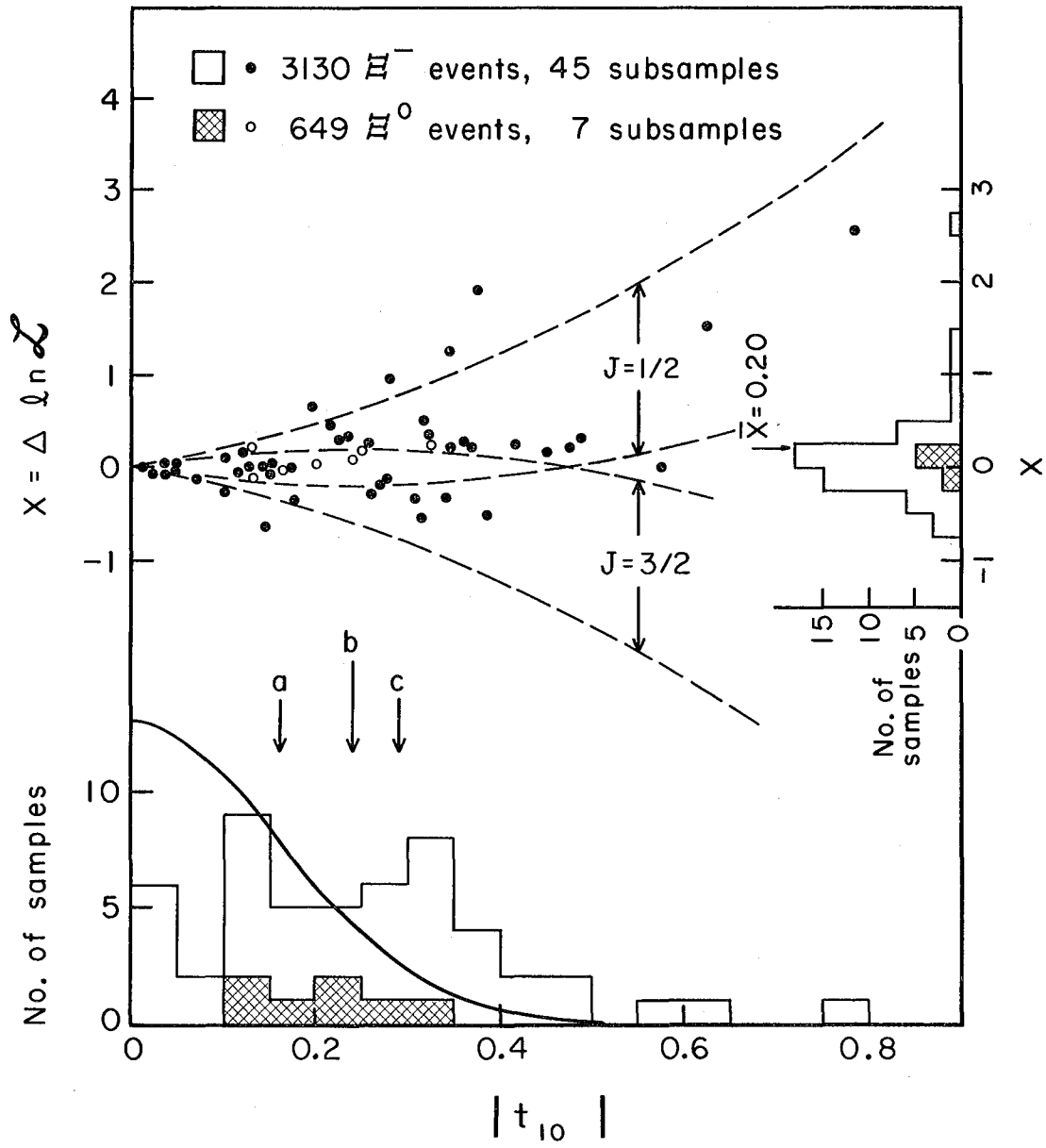
(iii) Uncertainty in C_J , $\langle t_{10} \rangle^2$ and $\langle t_{10}^2 \rangle$: Provided the relations (V-17) and (V-18) are approximately satisfied, the spin analysis is not sensitive to calculated values of C_J , $\langle t_{10} \rangle^2$, and $\langle t_{10}^2 \rangle$.

Allowing for $\approx 25\%$ error in C_J and for estimated statistical errors in $\langle t_{10} \rangle^2$ and $\langle t_{10}^2 \rangle$ (see Table V-V), we find that $[(X_{\text{obs}} - \bar{X})/\sigma_X]$ does not vary by more than ≈ 0.2 standard deviations; this value corresponds to $\leq 50\%$ variation in estimated spin probabilities $P(X \geq X_{\text{obs}})$, and to $\leq 10\%$ variation in the ratio $P(X_{\text{obs}}, 3/2)/P(X_{\text{obs}}, 1/2)$.

(iv) Assumed N-dependence of \bar{X} and σ_X : The assumed N-dependence of \bar{X} and σ_X seems reasonable, simply because $X = \ln \mathcal{L}(1/2) - \ln \mathcal{L}(3/2)$ is proportional to N. Even if the assumed N-dependence is not correct, the conclusions drawn from the 4080-event combined Ξ^- and Ξ^0 sample of Table V-II are not affected (because the Ξ samples and the Monte Carlo samples contain the same average number of events).

4. Discussion

Our conclusion that the Ξ has spin $1/2$ is in agreement with the prediction of SU(3) and with the findings of previous investigations. A maximum-likelihood analysis identical with that of Sec. V.A.2, performed on 828 K-72 $\Xi^- K^+$ events alone, yields a value $X = \ln \mathcal{L}(1/2) - \ln \mathcal{L}(3/2) = 2.60$, favoring the spin- $1/2$ hypothesis by 2.3 standard deviations.⁷ (Our analysis of 3278 events yields only slightly better spin discrimination (2.45 s. d.), partly because K-63 events are not strongly polarized and



MU-36866

Fig. V-6

partly because we have not optimized the binning criteria, as was done in Ref. 7.

In an alternative approach, one may calculate directly the factor $(2J+1)$ as a ratio of odd-L moments of the transverse and longitudinal Λ polarization distributions.^{7, 9, 21, 61} In the notation of Ref. 61, if only moments proportional to t_{10} are considered,

$$(2J+1) = \frac{[\langle \hat{p} \cdot \hat{n} \times \hat{\Lambda} \rangle^2 + \langle \hat{p} \cdot \hat{\Lambda} \times (\hat{n} \times \hat{\Lambda}) \rangle^2]^{1/2}}{(1 - \alpha_{\Xi}^2)^{1/2} \langle (\hat{p} \cdot \hat{\Lambda})(\hat{n} \cdot \hat{\Lambda}) \rangle} \quad (V-19)$$

For 356 Ξ^- events, Carmony et al.⁶¹ obtain a value $(2J+1) = 1.53$, assuming $\alpha_{\Xi^-} = -0.48$. They presumably calculate an expected distribution in $(2J+1)$ by assuming the numerator and denominator of Eq. (V-19) to be normally distributed quantities,⁶² thereby obtaining an exclusion of the spin-3/2 hypothesis by 3.1 standard deviations. (Button-Shafer has pointed out that the assumption is not valid, as neither term in the numerator of Eq. (V-19) is negligible in UCLA data.)

For 749 Ξ^- events of the K-72 experiment, Button-Shafer obtains values of $(2J+1) = 2.86$ and 2.18, assuming $\alpha_{\Xi^-} = -0.48$ and -0.34 , respectively.^{7, 9} Here the expected distribution is calculated as the ratio of two normally distributed quantities,⁶² by ignoring the $\langle \hat{p} \cdot \hat{n} \times \hat{\Lambda} \rangle$ term (proportional to β_{Ξ}) and correcting for the error thus introduced. The resulting confidence levels, with α_{Ξ^-} assumed to be -0.48 (-0.34), are 0.22 (0.42) for $J = 1/2$, 0.15 (0.015) for $J = 3/2$, and 0.003 (0.0002) for $J = 5/2$.

B. Decay Parameters

1. Maximum-Likelihood Analysis

In our analysis of Ξ decay parameters, we consider the 902 K-72 Ξ^- , 2529 K-63 Ξ^- , 159 K-72 Ξ^0 , and 490 K-63 Ξ^0 appearing in Table V-I. The data are divided into 53 subsamples, defined in Table V-VI.

In Tables V-VII and V-VIII we present values of Ξ decay parameters obtained from maximum-likelihood analysis. Results appearing in Tables V-VII and V-VIII are for Ξ^- and Ξ^0 data treated separately and together, respectively. With the exception of values quoted for $a_{\Lambda} a_{\Xi^-}$ and $a_{\Lambda} a_{\Xi^0}$ (which are spin-independent), all results were obtained under the assumption $J_{\Xi} = 1/2$. For combined K-72 and K-63 data, our best estimates of decay parameters are the boxed values appearing in Table V-VIII.

Quoted results were obtained as follows:

a. Ξ^- and Ξ^0 analyzed separately (Table V-VII). The method of analysis is identical to that previously applied to K-72 data.⁷ The sample described in Ref. 7 contains additional events not in our K-72 sample, but polarization information from 3-body final states was not used. The previously published K-72 results are included in Table V-VII for comparison with our values.

Estimates of $a_{\Lambda} a_{\Xi}$ were obtained from fits to a decay distribution of the form $1 + a_{\Lambda} a_{\Xi} (\hat{p} \cdot \hat{\Lambda})$; these estimates are independent of both the spin and the way in which subsamples are defined. Estimates of a_{Λ} , a_{Ξ} , and Φ_{Ξ} were obtained from maximum-likelihood fits under the assumption $J = 1/2$; variable parameters in the fits were a_{Λ} , a_{Ξ} , Φ_{Ξ} and the polarization of each subsample. Fits to the Ξ^- data were performed (as indicated) both with a_{Λ} free, and with a_{Λ} constrained (by a factor $\exp[-\frac{1}{2} (a_{\Lambda} - 0.62)^2 / (0.07)^2]$ in the likelihood) to be 0.62 ± 0.07 .⁵⁶ The Ξ^0 data could not be fit unless the constraint was applied.

Quoted errors on a_{Λ} , a_{Ξ} , and Φ_{Ξ} were obtained from the error matrix G, calculated as the negative of the inverse of the second derivative matrix of $w = \ln \mathcal{L}$. If $a_1, a_2 \dots$ etc. are variable parameters

Table V-VI. Subsamples used in Ξ decay parameter analysis (K-72 and K-63 data separated).

Expt.	Subsample Final state	p(BeV/c)	Events	Sub- samples	Events per subsample	$\hat{\Xi} \cdot \hat{K}$ cutoff points
K-72	$\Xi^- K^+$	1.2-1.4	194	3	65	0.69, 0.10
K-72	$\Xi^- K^+$	1.5	470	7	67	0.90, 0.78, 0.59
K-72	$\Xi^- K^+$	1.6, 1.7	166	2	83	0.66
{K-72	$\Xi^- K^+ \pi^0$	All	18	1	72	--
K-72	$\Xi^- K^0 \pi^+$	All	54			
K-72	Ξ^- sample, total		902	13	69	--
K-63	$\Xi^- K^+$	1.7	272	4	68	0.88, 0.70, -0.07
K-63	$\Xi^- K^+$	2.1	342	5	68	0.90, 0.75, 0.45, -0.43
K-63	$\Xi^- K^+$	2.45, 2.55	179	2	89	0.73
K-63	$\Xi^- K^+$	2.6, 2.7	229	3	76	0.89, 0.50
K-63	$\Xi^- K^+ \pi^0$	1.7, 2.1	136	2	68	0.43
K-63	$\Xi^- K^+ \pi^0$	2.45, 2.55	113	2	56	a
K-63	$\Xi^- K^+ \pi^0$	2.6, 2.7	180	2	90	0.43
K-63	$\Xi^- K^0 \pi^+$	1.7, 2.1	321	4	80	0.58, 0.20, -0.36
K-63	$\Xi^- K^0 \pi^+$	2.45, 2.55	185	3	62	0.70, 0.07
K-63	$\Xi^- K^0 \pi^+$	2.6, 2.7	288	4	72	0.78, 0.43, -0.17
K-63	$\Xi^- K \pi \pi$	All	115	1	115	--
{K-63	$\Xi^- K^+ + \text{neutrals}$	All	169	2	85	0.04
K-63	$\Xi^- \pi^+ + \text{neutrals}$	All				
K-63	Ξ^- sample, total		2529	34	75	--
K-72	Ξ^0 sample, total		159	1	159	--
K-63	$\Xi^0 K^0$	All	88	1	88	--
K-63	$\Xi^0 K^+ \pi^-$	1.7, 2.1	111	1	111	--
K-63	$\Xi^0 K^+ \pi^-$	2.45, 2.55	81	1	81	--
K-63	$\Xi^0 K^+ \pi^-$	2.6	112	1	112	--
{K-63	$\Xi^0 K^+ \pi^-$	2.7	78	1	98	--
K-63	$\Xi^0 K^0 \pi^+ \pi^-$	All	20			
K-63	Ξ^0 sample, total		490	5	98	--

^a Both subsamples contain events from $\hat{\Xi} \cdot \hat{K} = -1$ to $+1$.

Table V-VII. Decay parameters, Ξ^- and Ξ^0 data analyzed separately.

Independent a_Λ information used in fit	Fitted parameters							Correlation matrix			
	Sample	Events	$a_\Lambda^{a_\Xi}$	Subsamples	$\ln \mathcal{L}$	a_Λ	a_Ξ	Φ_Ξ (deg)	$(a_\Lambda^{a_\Xi})$	$(a_\Lambda^{\Phi_\Xi})$	$(a_\Xi^{\Phi_\Xi})$
a_Λ free	K-63 Ξ^-	2529	-0.262±0.033	34	68.95	0.743±0.122	-0.344±0.063	10.1±11.4	0.789	-0.027	-0.018
	K-72 Ξ^-	902	-0.281±0.055	13	41.16	0.685±0.107	-0.426±0.067	9.7±14.1	0.295	0.008	-0.020
	Combined Ξ^- ^a	3431	-0.267±0.028	47	109.70	0.698±0.069	-0.381±0.045	10.0± 8.9	0.653	-0.026	-0.025
	K-72 Ξ^- ^a	1004 ^b	--	12	38.74	0.682±0.104	-0.362±0.058	0.3±10.6	0.295	0.027	0.015
$a_\Lambda = 0.62 \pm 0.07$	K-63 Ξ^-	2529	-0.262±0.033	34	68.53	0.656±0.055	-0.375±0.051	9.8±11.6	0.404	-0.018	-0.015
	K-72 Ξ^-	902	-0.281±0.055	13	41.02	0.641±0.057	-0.432±0.066	9.8±14.3	0.099	0.040	-0.018
	Combined Ξ^- ^a	3431	-0.267±0.028	47	109.41	0.657±0.047	-0.394±0.041	9.9± 9.0	0.383	-0.013	-0.019
	K-72 Ξ^- ^a	1004 ^b	--	12	38.65	0.641±0.056	-0.368±0.057	0.5±10.7	0.096	0.044	0.007
	K-63 Ξ^0	490	-0.269±0.076	5	10.75	0.600±0.067	-0.489±0.124	107±39	0.345	-0.013	-0.041
	K-72 Ξ^0	159	-0.183±0.139	1	3.73	0.628±0.070	-0.116±0.193	- 1±28	-0.165	0.018	-0.091
	K-72 Ξ^0	159	-0.183±0.139	1	2.43 ^c	0.618±0.069	-0.281±0.205	177±32	0.106	0.003	-0.049
	Combined Ξ^0 ^a	649	-0.249±0.067	6	12.11	0.599±0.068	-0.444±0.114	151±36 ^d	0.384	-0.064	-0.144
K-72 Ξ^0 ^a	206 ^c	--	1	5.01	0.627±0.07	-0.149±0.154	- 3±23	-0.058	0.003	-0.064	

^a Previously published results, included for comparison with our K-72 sample (see Ref. 7).

^b Includes 176 events providing information only on $a_\Lambda^{a_\Xi}$.

^c Includes 60 events providing information only on $a_\Lambda^{a_\Xi^0}$.

^d Likelihood function extremely non-Gaussian in Φ_Ξ^0 (see Fig. V-7 and text).

^e Secondary K-72 Ξ^0 solution, less likely by ≈1.6 standard deviations.

Table V-VIII. Decay parameters, Ξ^- and Ξ^0 data combined.

Independent a_Λ information used in fit	Sample	Events	$\ln \chi^2$	Fitted parameters				Correlation matrix ^b			
				a_Λ	a_{Ξ^-}	a_{Ξ^0}	Φ_{Ξ^-} (deg)	Φ_{Ξ^0} (deg)	$(a_\Lambda a_{\Xi^-})$	$(a_\Lambda a_{\Xi^0})$	$(a_{\Xi^-} a_{\Xi^0})$
a_Λ free	K-63	3019	79.24	0.682 ± 0.102	-0.366 ± 0.059	-0.438 ± 0.124	9.9 \pm 11.5	108 \pm 38	0.63	0.50	0.32
	K-72	1061	45.02	0.708 ± 0.110	-0.424 ± 0.068	-0.447 ± 0.179	9.7 \pm 14.0	-1 \pm 28	0.36	-0.15	-0.06
	K-72	1061	43.56 ^a	0.679 ± 0.105	-0.427 ± 0.067	-0.264 ± 0.195	9.7 \pm 14.2	177 \pm 32	0.28	0.18	0.05
	Combined	4080	121.45	0.673 ± 0.072	-0.389 ± 0.044	-0.398 ± 0.106	9.9 \pm 8.9	154 \pm 34 ^c	0.51	0.41	0.21
$a_\Lambda = 0.62 \pm 0.07$	K-63	3019	79.10	0.642 ± 0.055	-0.380 ± 0.052	-0.463 ± 0.116	9.8 \pm 11.6	107 \pm 38	0.38	0.30	0.11
	K-72	1061	44.79	0.647 ± 0.057	-0.432 ± 0.065	-0.424 ± 0.189	9.8 \pm 14.3	-1 \pm 28	0.11	-0.12	-0.01
	K-72	1061	43.44 ^a	0.639 ± 0.057	-0.433 ± 0.066	-0.275 ± 0.200	9.8 \pm 14.3	177 \pm 32	0.09	0.09	0.01
	Combined	4080	121.31	0.647 ± 0.048	-0.398 ± 0.041	-0.443 ± 0.104	9.8 \pm 9.0	153 \pm 35 ^c	0.34	0.28	0.10

^aSecondary K-72 Ξ^0 solution, less likely by ≈ 1.6 standard deviations.

^bCorrelation coefficients not listed ($a_\Lambda \Phi_{\Xi^-}$, $a_{\Xi^-} \Phi_{\Xi^-}$, etc.) are all ≤ 0.1 .

^cLikelihood function extremely non-Gaussian in Φ_{Ξ^0} (see Fig. V-7 and text).

in the maximum-likelihood fit, the error δa_i of a parameter a_i is given by

$$(\delta a_i)^2 = G_{ii} \quad (V-20)$$

where

$$(G^{-1})_{jk} = - \frac{\partial^2 w}{\partial a_j \partial a_k} \quad (V-21)$$

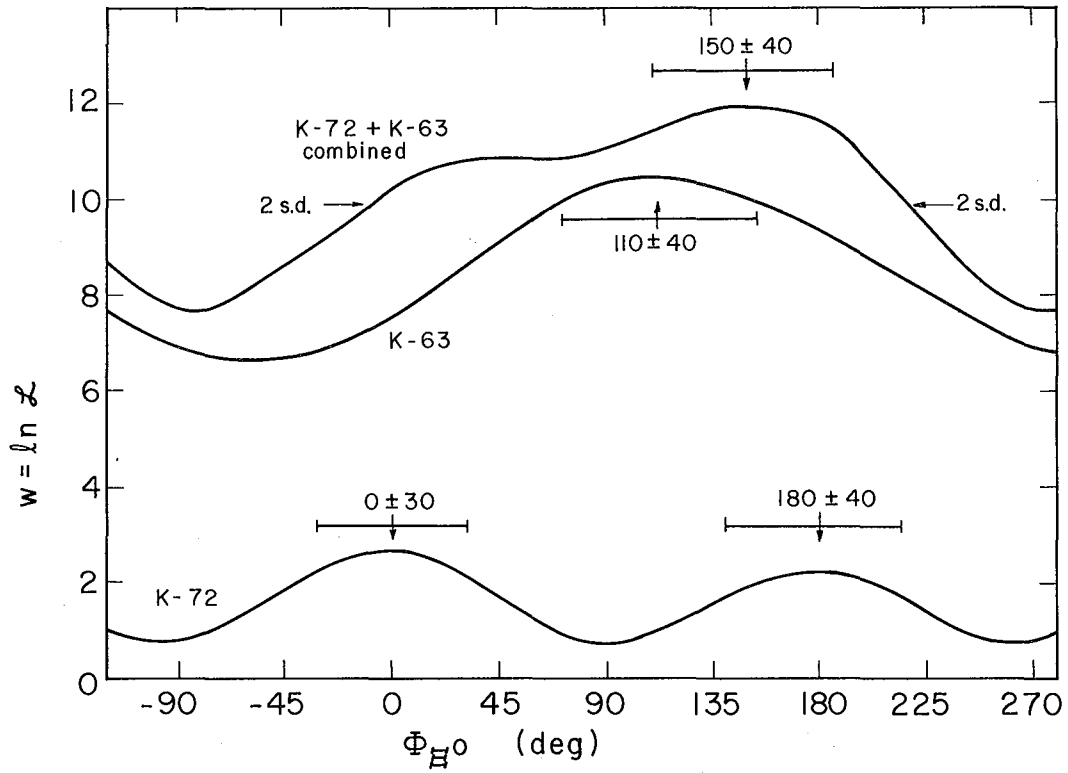
The correlation coefficients listed are off-diagonal elements of the normalized error matrix $C_{jk} = G_{jk} \cdot (G_{jj} G_{kk})^{-1/2}$. We note that Φ_{Ξ} is virtually uncorrelated with a_{Λ} or a_{Ξ} . A study of Monte Carlo events (see Appendix E) demonstrates that the calculated errors δa_i correspond to the rms deviation of independent measurements of a_i , i. e.,

$$(\delta a_i)^2 = \langle (a_i - \langle a_i \rangle)^2 \rangle = \langle a_i^2 \rangle - \langle a_i \rangle^2 \quad (V-22)$$

The 159-event K-72 Ξ^0 sample yields a best value $\Phi_{\Xi^0} = -1^\circ \pm 28^\circ$ and a secondary solution $\Phi_{\Xi^0} = 177^\circ \pm 32^\circ$ (less likely by ≈ 1.6 standard deviations). (Two maxima are also observed for the 206-event K-72 Ξ^0 sample of Ref. 7, although there the solution near 180° is more strongly excluded than for our sample.) Because of the cyclic nature of Φ_{Ξ^0} , best values from K-63 and K-72 data cannot be averaged in a simple fashion. In Fig. V-7 we present a plot of $w = \ln \mathcal{L}$ as a function of assumed Φ_{Ξ^0} , for the 159-event K-72 Ξ^0 sample, for the 490-event K-63 Ξ^0 sample, and for the combined data. In these fits we assume $J = 1/2$, $a_{\Lambda} = 0.62$, and $a_{\Xi^0} = -0.40$; the polarization of each subsample is allowed to vary as a free parameter.

b. Ξ^- and Ξ^0 analyzed together (Table V-VIII). Because different values of a_{Λ} are obtained in separate fits to Ξ^- and Ξ^0 data, values of Ξ^- and Ξ^0 decay parameters (particularly a_{Ξ^-} and a_{Ξ^0}) in Table V-VII should not be compared directly. Peter Berge is presently (8/66) constructing a program that will fit Ξ^- and Ξ^0 data simultaneously with a single value of a_{Λ} , allowing a_{Ξ^-} , a_{Ξ^0} , Φ_{Ξ^-} , and Φ_{Ξ^0} to vary independently.

The results appearing in Table V-VIII simulate the results of such a program.



MUB-13871

Fig. V-7

In actual practice we have fit the Ξ^- and Ξ^0 data separately for various assumed values of a_Λ , and then selected that value which maximizes the likelihood for the combined data. Errors quoted in Table V-VIII take into account the correlation of a_{Ξ^-} and Φ_{Ξ^-} with a_Λ . The correlation coefficients listed were obtained from the relations

$$C(a_\Lambda a_{\Xi^-,0}) = \frac{\delta a_\Lambda}{\delta a_{\Xi^-,0}} \cdot \left(\frac{\partial a_{\Xi^-,0}}{\partial a_\Lambda} \right) \quad (V-23)$$

$$C(a_{\Xi^-} a_{\Xi^0}) = C(a_\Lambda a_{\Xi^-}) \cdot C(a_\Lambda a_{\Xi^0}), \quad (V-24)$$

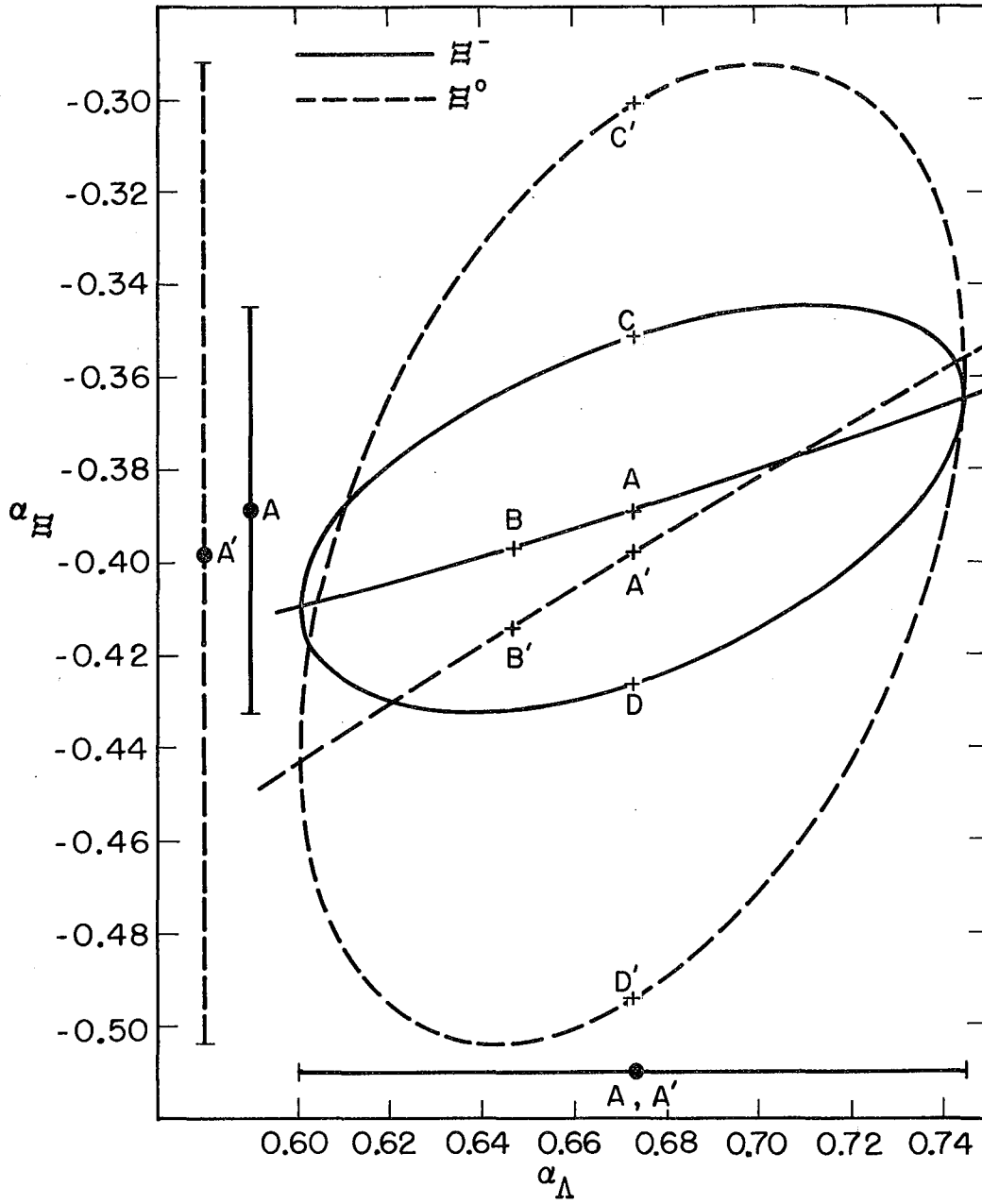
where δa_Λ , δa_{Ξ^-} , and δa_{Ξ^0} are quoted errors, and where $(\partial a_{\Xi^-,0} / \partial a_\Lambda)$ describes the variation of a_{Ξ^-} or a_{Ξ^0} as a function of a_Λ when all other parameters are allowed to vary freely.

In Fig. V-8 we illustrate the correlation between a_Λ and $a_{\Xi^-,0}$ for the combined K-72 and K-63 data. (See figure caption for a detailed discussion.) The overlap of the Ξ^- and Ξ^0 error ellipses indicates that the data are consistent with equality of a_{Ξ^-} and a_{Ξ^0} , as predicted by the $|\Delta I| = 1/2$ rule.

2. Discussion

The values of Ξ decay parameters reported in Tables V-VII and V-VIII are in agreement with previously published results obtained from K-72 data and from K-63 $\Xi^- K^+$ data.⁷⁻¹⁰ The slight discrepancies observed are due to differences in the samples analyzed, in binning criteria, and in values assumed for a_Λ .

In Table V-IX and Fig. V-9 we compare values listed in Table V-VIII (with a_Λ constraint applied) with values previously reported in other experiments,^{7,61,63-65} and we list approximate world averages of a_{Ξ^-} , a_{Ξ^0} , and Φ_{Ξ^-} . Because different assumed values of a_Λ were used in various experiments, and because a_Λ and a_{Ξ^-} are highly correlated, values of a_{Ξ^-} and a_{Ξ^0} were not averaged directly. For non-Berkeley



MUB13872

Fig. V-8

Table V-IX. Decay parameters, comparison of experimental results.

Lab	Events		$\alpha_{\Lambda} \alpha_{\Xi^-}$	$\alpha_{\Lambda} \alpha_{\Xi^0}$	Fitted or assumed value of α_{Λ}	α_{Ξ^-}	α_{Ξ^0}	Φ_{Ξ^-} (deg)	Φ_{Ξ^0} (deg)
	Ξ^-	Ξ^0							
LRL(K-72) ^a	1004	206	--	--	0.641±0.056 0.627±0.070	-0.368 ±0.057	-0.149 ±0.154	0.5±10.7	-3±23 ^g
LRL(K-63) ^b	2529	490	-0.262 ±0.033	-0.269 ±0.076	0.642 ±0.055	-0.380 ±0.052	-0.463 ±0.116	9.8±11.6	107±38

LRL combined ^b	3431	649	-0.267 ±0.028	-0.249 ±0.067	0.647 ±0.048	-0.398 ±0.041	-0.413 ±0.104	9.8±9.0	i
BNL+S ^c	700	46	-0.34 ±0.09	-0.12 ±0.23	0.62 ±0.07	-0.47 ±0.12	-0.20 ^h ±0.37	0±20	--
EP+ ^d	517	25	-0.27 ±0.07	-0.3 ±0.4	0.62 ±0.07	-0.44 ±0.11	-0.5 ^h ±0.4	-16±37	--
UCLA ^e	356	54	-0.41 ±0.10	--	0.62 ±0.07	-0.62 ±0.12	--	54±25	--
CERN ^f	62	4	-0.35 ±0.18	--	0.61	-0.73 ±0.21	--	45±30	--
Average ^j	5066	777	-0.283 ±0.024	-0.240 ±0.064	0.647 ±0.048	-0.419 ±0.037	-0.397 ±0.099	13.4±7.4	i

^a See Ref. 7.

^b See Table V-VIII, bottom (with α_{Λ} constraint applied).

^c (Brookhaven National Laboratory and Syracuse University). See Ref. 63.

^d (Ecole Polytechnique and others). See Ref. 64.

^e See Ref. 61.

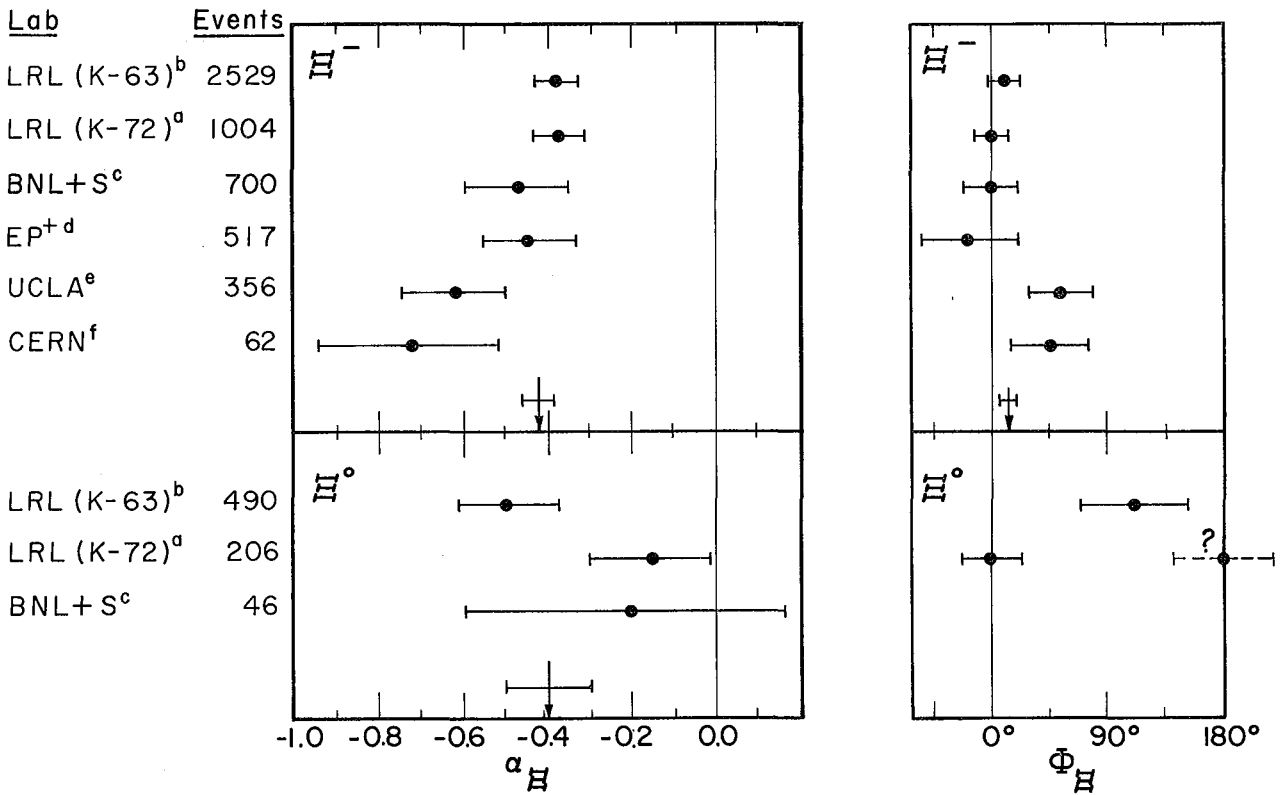
^f See Ref. 65.

^g A secondary solution is observed with $\Phi_{\Xi^0} \approx 180$ deg.

^h α_{Ξ^0} estimated directly from $\alpha_{\Lambda} \alpha_{\Xi^0}$.

ⁱ Likelihood function for combined Berkeley data extremely non-Gaussian in Φ_{Ξ^0} (see Fig. V-7 and text).

^j Only entries below dashed line are included in average. See text regarding average values of α_{Ξ^-} and α_{Ξ^0} .



MUB-12253

Fig. V-9

data, we calculated $a_{\Lambda} a_{\Xi^-} = -0.325 \pm 0.047$ and $a_{\Lambda} a_{\Xi^0} = -0.16 \pm 0.20$; then assuming $a_{\Lambda} = 0.647 \pm 0.048$, we obtained values $a_{\Xi^-} = -0.502 \pm 0.082$ and $a_{\Xi^0} = -0.25 \pm 0.31$, which were averaged with Berkeley values to obtain the world averages listed.

In the following discussion we assume the Ξ spin to be $1/2$ (see Sec. V.A). The $|\Delta I| = 1/2$ prediction, that the Ξ^- and Ξ^0 decay amplitudes are proportional [i. e., $S(\Xi^-) = \sqrt{2} S(\Xi^0)$ and $P(\Xi^-) = \sqrt{2} P(\Xi^0)$], and thus that the decay parameters are equal, is satisfied within experimental error. The nonzero value of a_{Ξ^-} (and a_{Ξ^0}) shows that both S- and P-wave amplitudes contribute to the decay, and the positive value of $\gamma_{\Xi^-} = \sqrt{1 - a_{\Xi^-}^2} \cos \Phi_{\Xi^-}$ shows that the S-wave (parity-nonconserving) amplitude dominates. For Ξ^0 decay, solutions having $\gamma_{\Xi^0} < 0$ cannot be excluded.

The phase difference of S and P amplitudes, calculated from the Berkeley values $a_{\Xi^-} = -0.40 \pm 0.04$, $\Phi_{\Xi^-} = 10^\circ \pm 9^\circ$, is⁶⁶

$$(\Delta_P - \Delta_S) = \tan^{-1}(\beta_{\Xi^-} / a_{\Xi^-}) = 157^\circ \text{ to } 21^\circ \text{ to } -25^\circ. \quad \text{In the absence of final-state}$$

interactions, T invariance in the decay transition requires $(\Delta_P - \Delta_S) = 0$ or π , whereas C invariance requires $(\Delta_P - \Delta_S) = \pm \pi/2$.⁶⁷ It appears that the hypothesis of T invariance is favored by the data.

Under the assumptions of SU(3) symmetry, octet dominance, and invariance under R (i. e., inversion through the origin $I_z = 0$, $Y = 0$), Lee⁶⁸ has predicted a triangular relationship among the non-leptonic covariant decay amplitudes for the processes

$$\Xi^- : \Xi^- \rightarrow \Lambda + \pi^- \quad (V-25)$$

$$\Lambda^0 : \Lambda^0 \rightarrow p + \pi^- \quad (V-26)$$

and

$$\Sigma_0^+ : \Sigma^+ \rightarrow p + \pi^0. \quad (V-27)$$

According to Lee, both the S-wave (parity-nonconserving) and P-wave (parity-conserving) amplitudes satisfy the relationship

$$2 \Xi_-^- - \Lambda_-^0 = \sqrt{3} \Sigma_0^+ . \quad (\text{V-28})$$

The same relationship (for either parity-nonconserving or parity-conserving amplitudes, or both) has been derived by other authors under different assumptions.⁶⁹

Furthermore, the $|\Delta I| = 1/2$ rule predicts a triangle relation

$$\Sigma_0^+ = \frac{1}{\sqrt{2}} [\Sigma_-^- - \Sigma_+^+] \quad (\text{V-29})$$

between amplitudes for the processes

$$\Sigma_0^+ : \Sigma^+ \rightarrow p + \pi^0 \quad (\text{V-27})$$

$$\Sigma_+^+ : \Sigma^+ \rightarrow n + \pi^+ \quad (\text{V-30})$$

$$\Sigma_-^- : \Sigma^- \rightarrow n + \pi^- , \quad (\text{V-31})$$

so that the Lee triangle prediction and the $|\Delta I| = 1/2$ rule together require

$$\frac{1}{\sqrt{3}} [2 \Xi_-^- - \Lambda_-^0] = \frac{1}{\sqrt{2}} [\Sigma_-^- - \Sigma_+^+] . \quad (\text{V-32})$$

In Eqs. (V-28), (V-29), and (V-32), the covariant S- and P-wave amplitudes (denoted by A and B, respectively) are related to the partial decay rate w by

$$w = \frac{q}{8\pi M^2} \left\{ |A|^2 [(M+m)^2 - \mu^2] + |B|^2 [(M-m)^2 - \mu^2] \right\} , \quad (\text{V-33})$$

where M, m, and μ are the rest masses of the parent baryon, the decay baryon, and the decay pion, respectively, and q is the pion momentum in the rest frame of the parent baryon. In terms of the phenomenological decay amplitudes a and b appearing in Eq. (II-39), A and B are given by

$$\left(\frac{B}{A} \right)^2 = \left(\frac{b}{a} \right)^2 \cdot \frac{(M+m)^2 - \mu^2}{(M-m)^2 - \mu^2} . \quad (\text{V-34})$$

A recent determination of the Σ decay parameters $a(\Sigma_0^+)$, $a(\Sigma_+^+)$, and $a(\Sigma_-^-)$ has demonstrated that (V-29) is well satisfied,⁷⁰ and also permits a more accurate test of Eqs. (V-28) and (V-32) than was previously possible.^{7,71} In Table V-X we present covariant amplitudes A and B for the processes (V-25), (V-26), (V-27), (V-30), and (V-31), calculated under the assumption that A and B are relatively real.⁷² Only the relative signs of A and B are experimentally observable; a further ambiguity exists in the case of the Σ_0^+ and Σ_-^- decays (V-27) and (V-31), where the sign of γ has not been determined. A recent experiment has shown that $\gamma < 0$ for Σ_+^+ decay (V-30).⁷³ In Table V-X, world average values of lifetimes, branching fractions, and decay parameters are used.⁷⁴

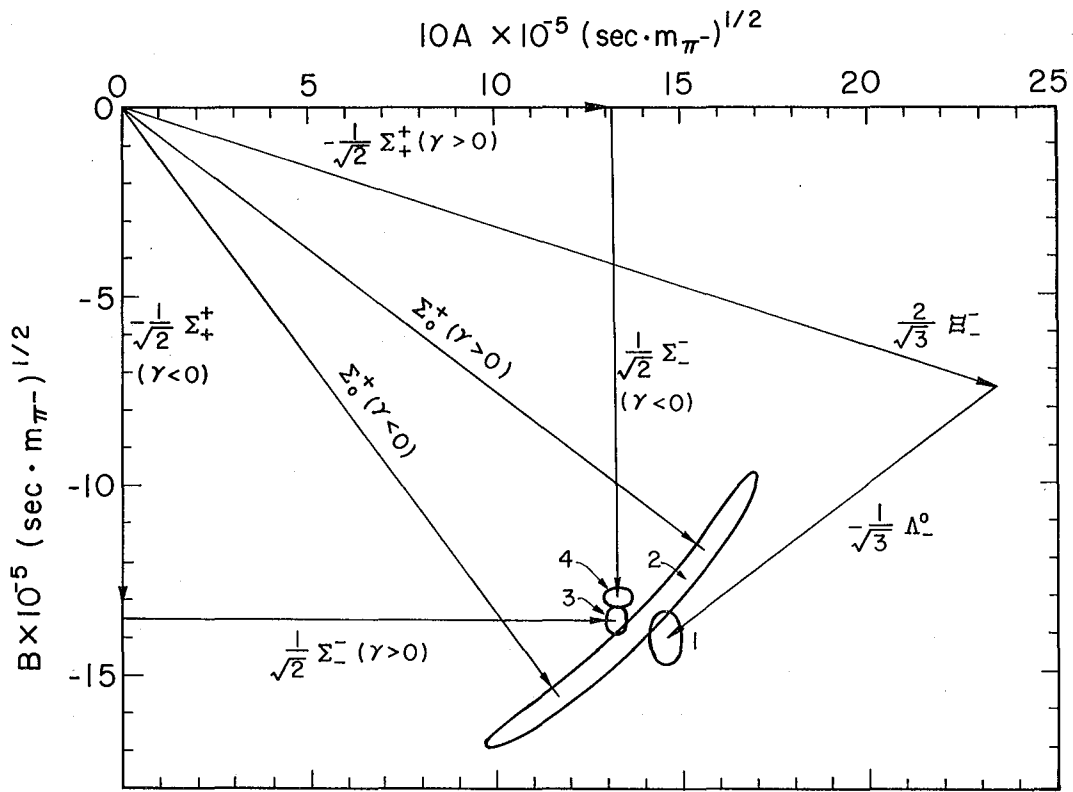
The consistency of the data with Eqs. (V-28), (V-29), and (V-32) is illustrated in Fig. V-10. In plotting the error ellipse for $\frac{1}{\sqrt{3}} (2 \Xi_-^- - \Lambda_-^0)$, we have taken into account the correlation between a_Λ and $a_{\Xi_-^-}$. We conclude that Eqs. (V-28) and (V-29) are well satisfied by the experimental data; Eq. (V-32) is less well satisfied.

A veritable flood of predictions concerning non-leptonic hyperon decay has resulted from the advent of SU(6) and higher symmetry schemes. (As of August 1966, at least 70 papers containing specific predictions regarding decay amplitudes have appeared in the literature. Most of these deal with the Lee SU(3) triangle prediction and the reasons for its apparent validity.) The theoretical situation is far too complex to discuss here, and the reader is referred to a recent review article by Pais.⁷⁵ Predictions of various theoretical models may be readily checked with the aid of Table V-X.

Table V-X. Non-leptonic hyperon decay amplitudes.

Decay	τ $\times 10^{10} \text{ sec}^{-1}$	Branching fraction	α	A $\times 10^{-5} (\text{sec} \cdot m_{\pi^-})^{1/2}$	B	(A, B) Correlation coefficient
$\Xi^- (\Xi^- \rightarrow \Lambda + \pi^-)$	1.75 ± 0.05	1.00	-0.381 ± 0.037	2.025 ± 0.029	-6.46 ± 0.66	0.136
$\Lambda^0 (\Lambda \rightarrow p + \pi^-)$	2.53 ± 0.05	0.663 ± 0.044	0.690 ± 0.048	1.528 ± 0.030	11.48 ± 0.97	-0.532
$\Sigma_0^+ (\Sigma^+ \rightarrow p + \pi^0)$ $\left\{ \begin{array}{l} \gamma > 0 \\ \gamma < 0 \end{array} \right\}$	0.810 ± 0.013	0.528 ± 0.015	-0.960 ± 0.067	$\left\{ \begin{array}{l} 1.558 \pm 0.142 \\ 1.168 \pm 0.187 \end{array} \right\}$	$\left\{ \begin{array}{l} -11.71 \pm 1.88 \\ -15.61 \pm 1.42 \end{array} \right\}$	-0.959
$\Sigma_+^+ (\Sigma^+ \rightarrow n + \pi^+)$ $\left\{ \begin{array}{l} \gamma > 0^a \\ \gamma < 0 \end{array} \right\}$	0.810 ± 0.013	0.472 ± 0.015	-0.006 ± 0.043	$\left\{ \begin{array}{l} -1.861 \pm 0.034 \\ -0.005 \pm 0.040 \end{array} \right\}$	$\left\{ \begin{array}{l} 0.05 \pm 0.41 \\ 19.08 \pm 0.35 \end{array} \right\}$	-0.001
$\Sigma_-^- (\Sigma^- \rightarrow n + \pi^-)$ $\left\{ \begin{array}{l} \gamma > 0 \\ \gamma < 0 \end{array} \right\}$	1.654 ± 0.031	1.00	-0.017 ± 0.042	$\left\{ \begin{array}{l} 1.863 \pm 0.017 \\ 0.015 \pm 0.039 \end{array} \right\}$	$\left\{ \begin{array}{l} -0.15 \pm 0.39 \\ -18.34 \pm 0.17 \end{array} \right\}$	-0.016
$\frac{1}{\sqrt{3}} (2\Xi_-^- - \Lambda^0)$	--	--	--	1.455 ± 0.040	-44.09 ± 0.70	0.004
$\frac{1}{\sqrt{2}} (\Sigma_-^- - \Sigma_+^+)$ $\left\{ \begin{array}{l} \gamma(\Sigma_-^-) > 0, \gamma(\Sigma_+^+) < 0 \\ \gamma(\Sigma_-^-) < 0, \gamma(\Sigma_+^+) > 0^a \end{array} \right\}$	--	--	--	$\left\{ \begin{array}{l} 1.321 \pm 0.031 \\ 1.327 \pm 0.037 \end{array} \right\}$	$\left\{ \begin{array}{l} -13.60 \pm 0.37 \\ -13.01 \pm 0.31 \end{array} \right\}$	$\left\{ \begin{array}{l} 0.005 \\ 0.005 \end{array} \right\}$

^aThis solution is inconsistent with recent evidence that $\gamma(\Sigma_+^+) < 0$. See Ref. 73.



MUB13873

Fig. V-10

C. Decay Distributions

As a visual check on the results already presented, we display certain angular correlations in the observed Ξ^- and Ξ^0 decay distributions.

In Fig. V-11 we present distributions of $(\hat{p} \cdot \hat{\Lambda})$ for 4080 Ξ^- and Ξ^0 events (Table V-I), which should be proportional to $1 + a_{\Lambda} a_{\Xi} (\hat{p} \cdot \hat{\Lambda})$ regardless of the Ξ polarization and for any Ξ spin J . The observed distributions agree with the expected distributions, which are plotted for $a_{\Lambda} a_{\Xi^-} = -0.27$ and $a_{\Lambda} a_{\Xi^0} = -0.25$, the values listed in Table V-VII.

In Figs. V-12 through V-15 we present distributions of the four quantities N (no. of events), $\sum_{i=1}^N (\hat{p} \cdot \hat{\Lambda})_i$, $\sum_{i=1}^N (\hat{p} \cdot \hat{y})_i$, and $\sum_{i=1}^N (\hat{p} \cdot \hat{x})_i$ as a function of $(\hat{\Lambda} \cdot \hat{n}) = \cos \theta$. In Figs. V-12 through V-15 appear, respectively, distributions from (i) the 4080 Ξ^- and Ξ^0 events listed in Table V-I; (ii) the 649 Ξ^0 events alone; (iii) a 4080-event Monte Carlo sample generated under the assumption that $J = 1/2$, $a_{\Lambda} = 0.62$, $a_{\Xi} = -0.40$, $\Phi_{\Xi} = 0$, and $t_{10} = t_{10}^{\max} = 0.57$; (iv) a similar Monte Carlo sample having $J = 3/2$, and $t_{10} = t_{10}^{\max} = 0.43$.

The observed distributions in Figs. V-12 through V-14 agree with the expected distributions for $J = 1/2$, namely

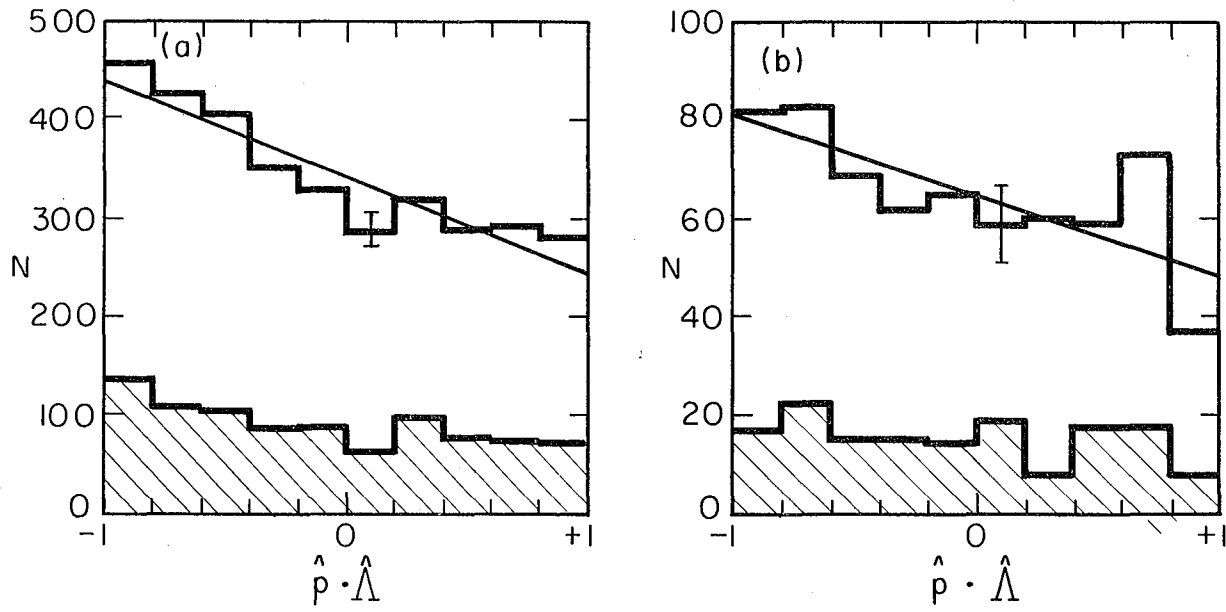
$$4\pi \frac{N}{10} I(\theta) = \frac{N}{10} [1 + a_{\Xi} P_{\Xi} \cos \theta] \quad (\text{V-35a})$$

$$4\pi \frac{N}{10} \frac{a_{\Lambda}}{3} I \vec{P}_{\Lambda} \cdot \hat{\Lambda} = \frac{N}{10} \frac{a_{\Lambda}}{3} [a_{\Xi} + P_{\Xi} \cos \theta] \quad (\text{V-35b})$$

$$4\pi \frac{N}{10} \frac{a_{\Lambda}}{3} I \vec{P}_{\Lambda} \cdot \hat{y} = \frac{N}{10} \frac{a_{\Lambda}}{3} [\beta_{\Xi} P_{\Xi} \sin \theta] \quad (\text{V-35c})$$

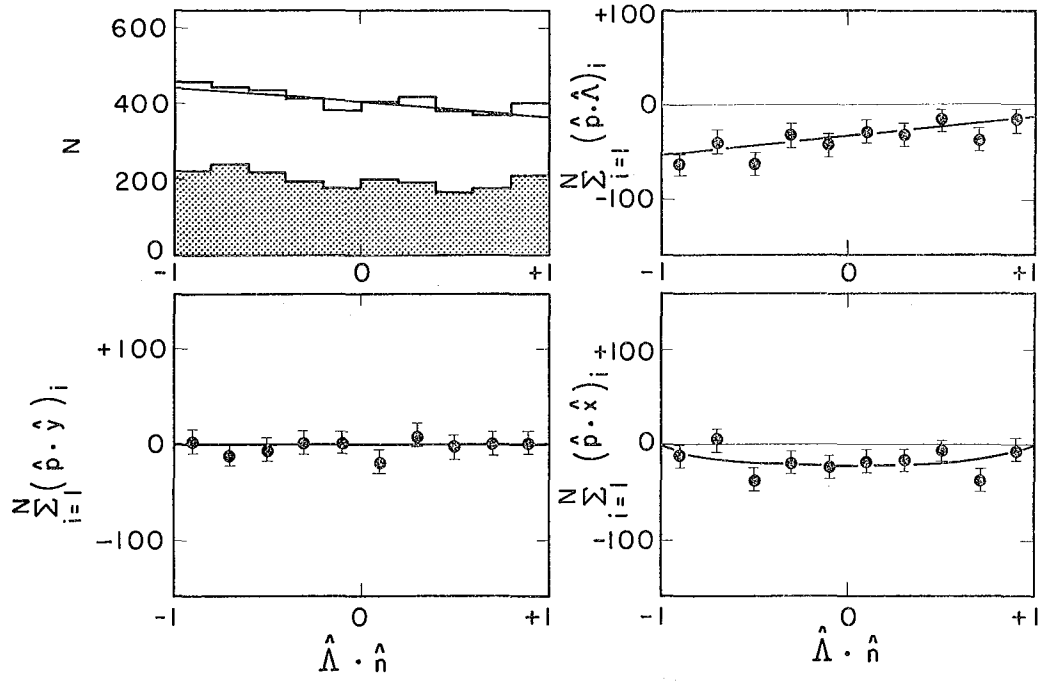
$$4\pi \frac{N}{10} \frac{a_{\Lambda}}{3} I \vec{P}_{\Lambda} \cdot \hat{x} = \frac{N}{10} \frac{a_{\Lambda}}{3} [-\gamma_{\Xi} P_{\Xi} \sin \theta]. \quad (\text{V-35d})$$

Similarly, the observed distributions in Fig. V-15 agree with those expected for $J = 3/2$. Parameters corresponding to the plotted curves are specified in the figure captions.



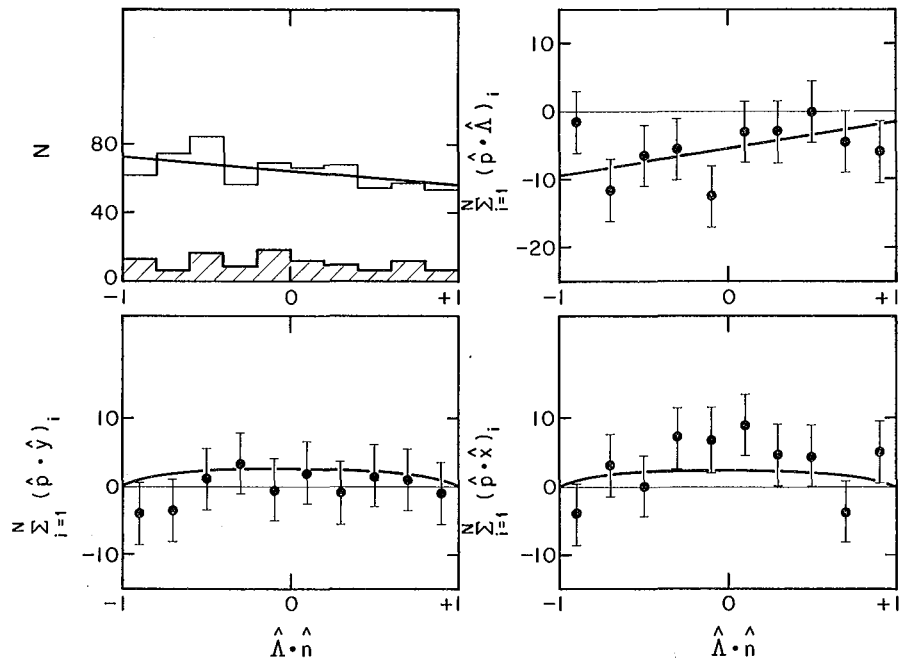
MUB-9195

Fig. V-11



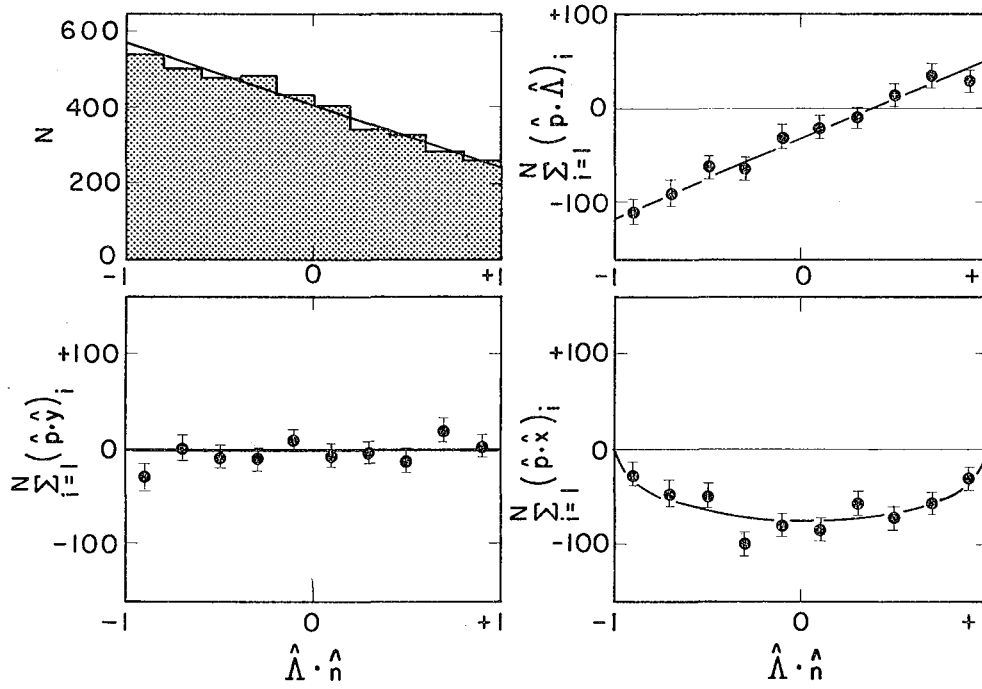
MU-36794

Fig. V-12



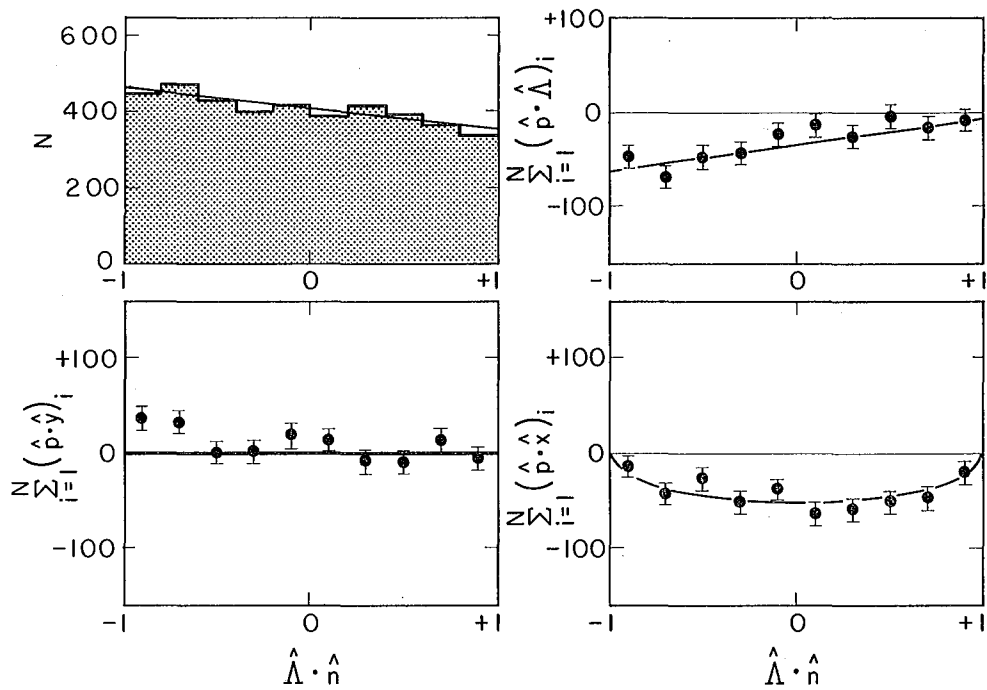
MU-36855

Fig. V-13



MU-36795

Fig. V-14



MU-36796

Fig. V-15

VI. PROPERTIES OF $\Xi^*(1530)$

The $\Xi^*(1530)$ has been discussed by a number of authors.^{7, 11-14, 63, 76, 77} Best estimates of its mass and width are $m_0 = 1529.7 \pm 0.9$ MeV, $\Gamma = 7.5 \pm 1.7$ MeV; the $I = 1/2$ assignment has been confirmed.¹⁷ Several experiments have shown the spin to be $\geq 3/2$;^{13, 63, 76} using a portion of the data analyzed in this report, Button-Shafer et al.¹³ have ruled out the $D_{3/2}$ parity assignment. Although spin hypotheses $J > 3/2$ have not been ruled out experimentally, the $\Xi^*(1530)$ is generally believed to be the $I = 1/2$ member of an SU(3) $3/2^+$ decuplet containing $N^*(1238)$, $Y_1^*(1385)$, $\Xi^*(1530)$, and $\Omega(1675)$. In this section we measure the $\Xi^*(1530)$ electromagnetic mass difference, and we investigate the $\Xi^*(1530)$ spin and parity, using a data sample larger than that analyzed in Ref. 13.

A. Final States Analyzed

In the K-63 experiment, at incident K^- lab momenta of 1.7 to 2.7 BeV/c, we observe $\Xi^*(1530)$ in the following states:

$\Xi K \pi$ final states:

$$K^- + p \rightarrow \Xi^- + K^0 + \pi^+ \quad (\Xi^{*0}) \quad (\text{VI-1})$$

$$\rightarrow \Xi^- + K^+ + \pi^0 \quad (\Xi^{*-}) \quad (\text{VI-2})$$

$$\rightarrow \Xi^0 + K^+ + \pi^- \quad (\Xi^{*-}) \quad (\text{VI-3})$$

$\Xi K \pi \pi$ final states:

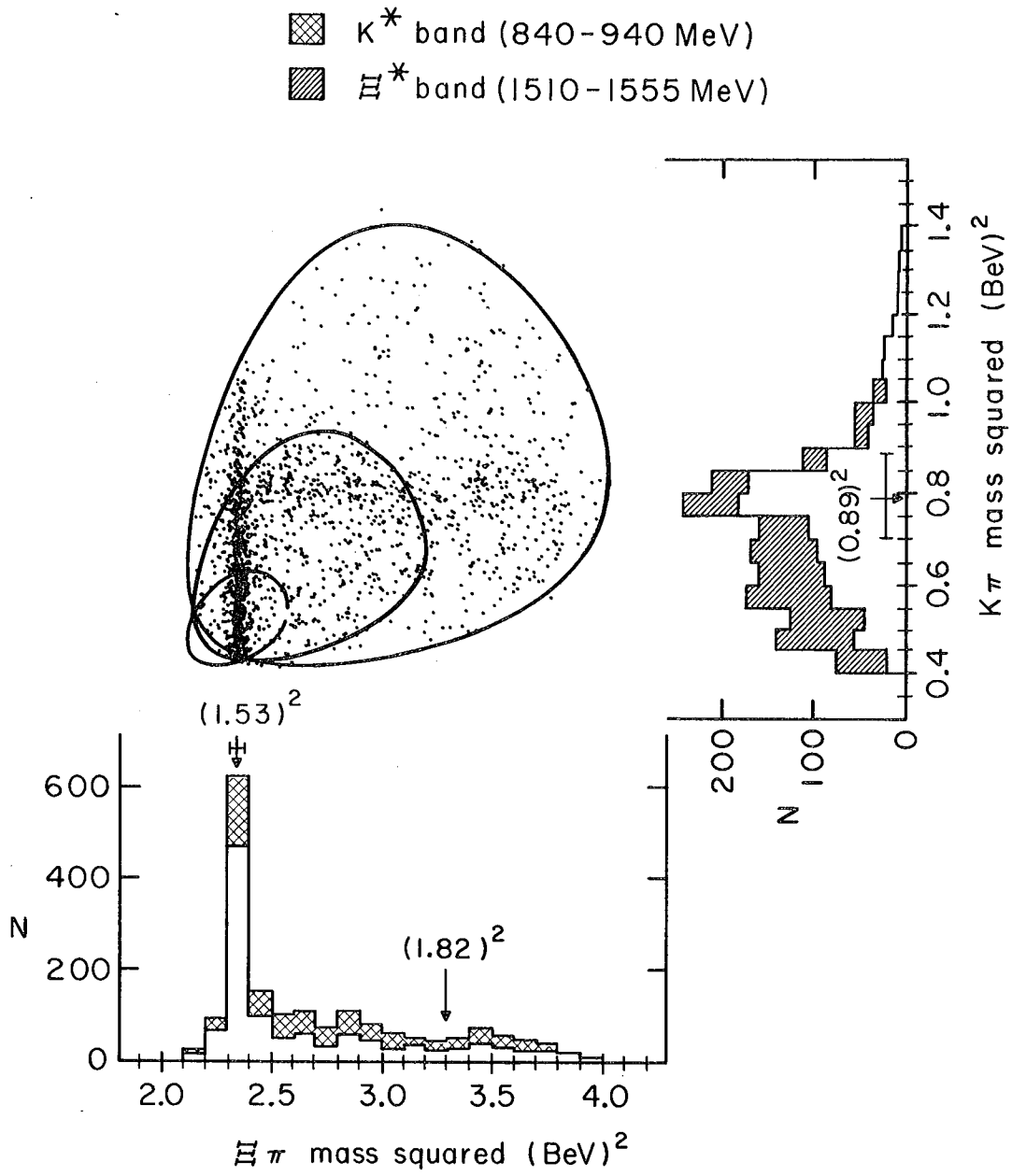
$$K^- + p \rightarrow \Xi^- + K^+ + \pi^+ + \pi^- \quad (\Xi^{*0}) \quad (\text{VI-4})$$

$$\rightarrow \Xi^- + K^0 + \pi^+ + \pi^0 \quad (\Xi^{*0} \text{ and } \Xi^{*-}) \quad (\text{IV-5})$$

$$\rightarrow \Xi^0 + K^0 + \pi^+ + \pi^- \quad (\Xi^{*-}) \quad (\text{VI-6})$$

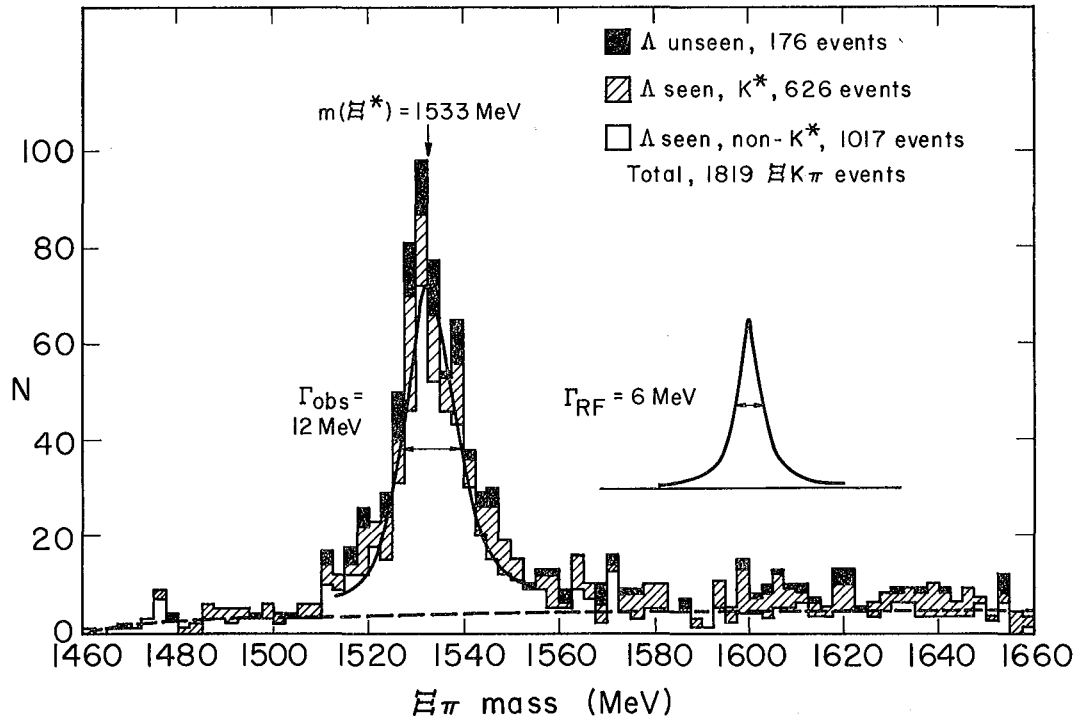
1. $\Xi K \pi$ Final States

In Fig. VI-1 we present a Dalitz plot for 1819 unambiguous $\Xi K \pi$ final states, including 1024 $\Xi^- K^0 \pi^+$, 435 $\Xi^- K^+ \pi^0$, and 363 $\Xi^0 K^+ \pi^-$.⁷⁸ (Of the 1024 $\Xi^- K^0 \pi^+$ events, 176 lack visible Λ decay and are not analyzed further.) Approximately 60% of the events are at 2.45 to 2.7 BeV/c, 30% at 2.1 BeV/c, and 10% at 1.7 BeV/c. Both $\Xi^*(1530)$ and $K^*(890)$ are apparent in all three final states. It is difficult to say that any κ at $m^2 = (0.725 \text{ BeV})^2 = 0.53 (\text{BeV})^2$ exists in



MU-37094

Fig. VI-1



MUB13874

Fig. VI-2

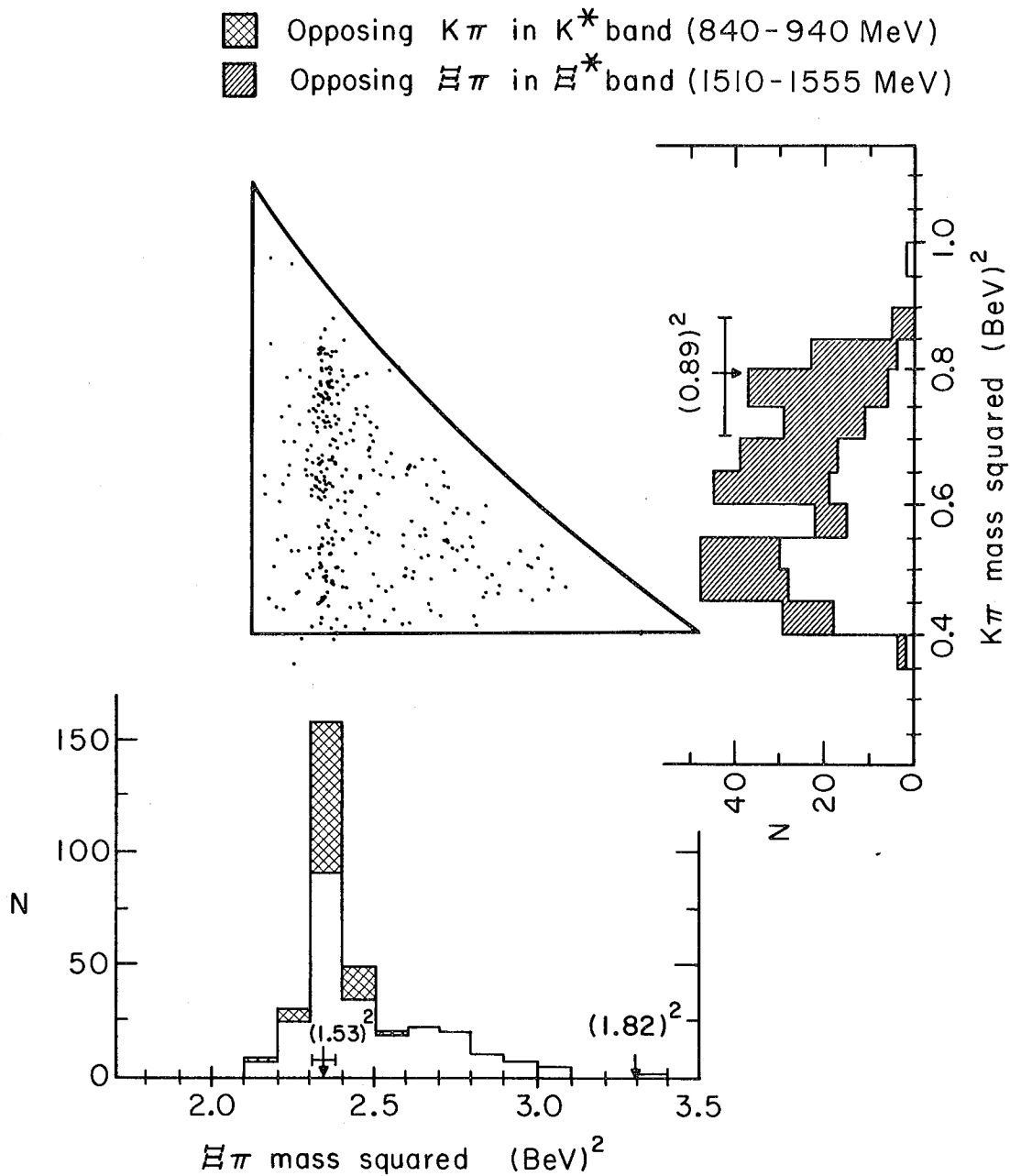
our data. We do not see $\Xi^*(1817)$; the slight $\Xi\pi$ enhancement around $(1.86 \text{ BeV})^2 = 3.45 (\text{BeV})^2$ is believed to be $\Xi^*(1933)$, shifted due to limited phase space. A slight enhancement around $(1.7 \text{ BeV})^2 = 2.9 (\text{BeV})^2$, pointed out by Smith and Lindsey,¹⁴ shows up more clearly in $\Lambda K\bar{K}$ final states.

The $\Xi\pi$ mass distribution in the $\Xi^*(1530)$ region is shown more clearly in Fig. VI-2. For the 1017 non- K^* events analyzed further (unshaded), we estimate $N(\Xi^*)/N \approx 475/1017 \approx 47 \pm 5\%$, $m_0 \approx 1533 \pm 3 \text{ MeV}$, and Γ_{obs} (observed width) $\approx 12 \pm 3 \text{ MeV}$.⁷⁹ The data are adequately fit by a P-wave resonance having Γ_0 (true width) $\approx 7 \text{ MeV}$, folded with the experimental resolution function (illustrated).⁸⁰

2. $\Xi K\pi\pi$ Final States

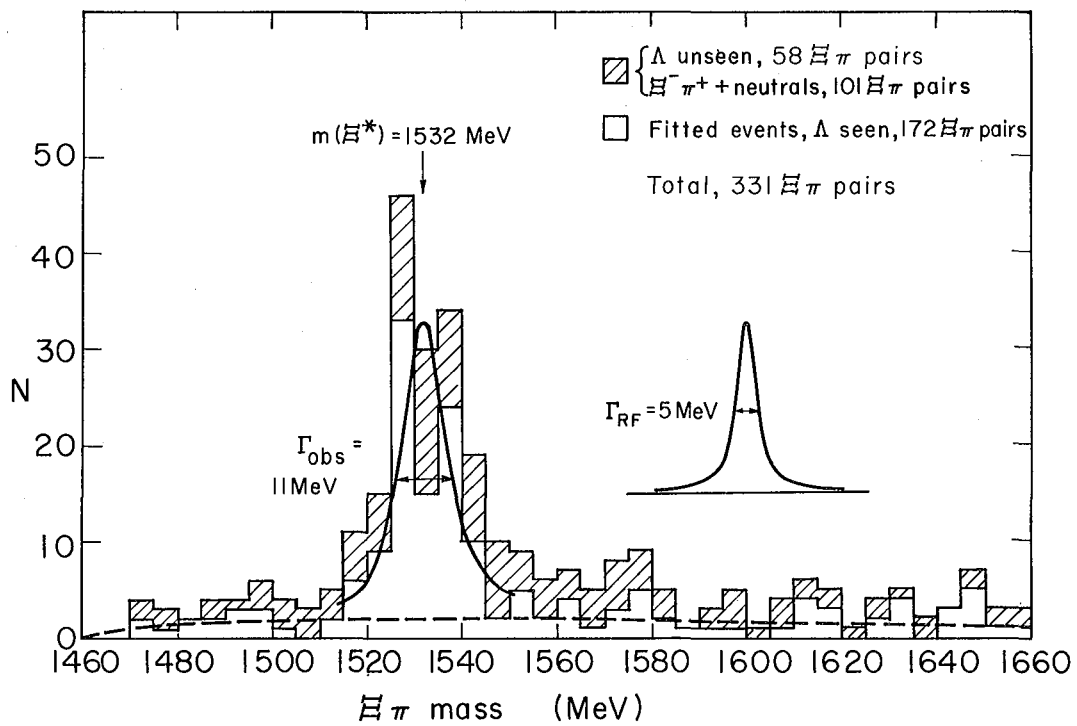
Figure VI-3 is a mass-squared plot for 265 unambiguous $\Xi K\pi\pi$ final states, including 78 $\Xi^- K^+ \pi^+ \pi^-$, 66 $\Xi^- K^0 \pi^+ \pi^0$, 101 $\Xi^- \pi^+$ + neutrals, and 20 $\Xi^0 K^0 \pi^+ \pi^-$.⁷⁸ (The 101 $\Xi^- \pi^+$ + neutrals, and 29 $\Xi^- K^0 \pi^+ \pi^0$ which lack visible Λ decay, are not analyzed further.) All but six of the events are at 2.45 to 2.7 BeV/c.

The $\Xi^*(1530)$ is clearly seen; about half of the Ξ^* are produced via $K^- + p \rightarrow \Xi^* + K^*$. The $\Xi\pi$ mass distribution is shown in greater detail in Fig. VI-4. For the 172 $\Xi\pi$ pairs analyzed further (unshaded), we estimate $N(\Xi^*)/N \approx 100/172 \approx 58 \pm 10\%$, $m_0 \approx 1532 \pm 4 \text{ MeV}$, and $\Gamma_{\text{obs}} \approx 11 \pm 5 \text{ MeV}$. The mass and width are consistent with those observed in $\Xi K\pi$ final states.



MU 37095

Fig. VI-3



MUB 13875

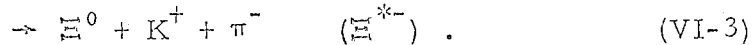
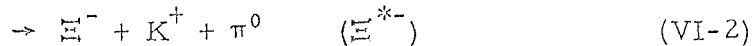
Fig. VI-4

B. Electromagnetic Mass Difference

The Ξ^* (1530) electromagnetic mass difference has been discussed in a number of recent theoretical papers.⁸¹⁻⁹⁰ Previous measurements have been reported by Pjerrou et al.⁷⁷ and by London et al.;⁶³ in our analysis we follow closely the methods adopted by Pjerrou et al.⁷⁷

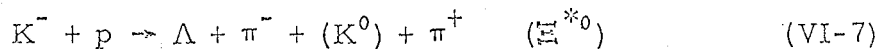
1. Selection and Fitting of Events

In principle, measurements of $m(\Xi^{*-})$ or $m(\Xi^{*0})$ may be made from data in any of the final states (VI-1) through (VI-6). Because our data in $\Xi K\pi\pi$ final states are statistically limited, we restrict our discussion to the $\Xi K\pi$ final states (VI-1) through (VI-3):



Due to the different topologies of the reactions involved, special fitting procedures are required if systematic errors are to be avoided.

As Pjerrou et al. have done,⁷⁷ events containing Ξ^- or Ξ^0 with visible Λ decay were fitted similarly, by disregarding the Ξ and by considering the Λ and π from Ξ decay as end products of the production reaction:



(The Λ and π^- from Ξ^- decay were first rotated backward in azimuth by the turning angle of the Ξ^- in the magnetic field.) After the Λ momentum had been obtained from a 1C fit at the Λ decay vertex, each event was fitted to one of the 1C hypotheses (VI-7) through (VI-9) (the missing particle in each case is indicated by parentheses). In reaction (VI-7) the K^0 was omitted from the fit even if it was observed

We have analyzed only unambiguous Ξ^- and Ξ^0 events with visible Λ decay, selected as described in Sec. IV. In the fits used to select events, we assumed $m(\Xi^0) = 1314.3$ MeV and $m(\Xi^-) = 1320.8$ MeV, corresponding to world average values.^{17, 91} A total of 1156 unambiguous

events were fit to the 1C hypotheses (VI-7) through (VI-9), of which 1133 (including 700 outside the K^* region) yielded acceptable fits (c.l. ≥ 0.005). In order to avoid possible K^* interference effects, we discarded events having $840 \text{ MeV} \leq m(K\pi) \leq 940 \text{ MeV}$. The events analyzed are listed by momentum and final state in Table VI-I. In Fig. VI-5 we present $\Lambda\pi\pi$ effective-mass distributions for the non- K^* events fit according to the 1C hypotheses (VI-7) through (VI-9).

2. Determination of Ξ^* Masses and Mass Difference

The Ξ^{*-} and Ξ^{*0} masses were obtained by fitting the distributions of Fig. VI-5 with a maximum-likelihood program, SUPER FIT, written by Friedman, Siegel, and Ross.⁹² In this program, the assumed $\Lambda\pi\pi$ ($\Xi\pi$) effective-mass distribution is of the form

$$\frac{dN}{dw} \propto (\text{phase space}) + (\text{phase space}) \times C_R \times \psi_R(w), \quad (\text{VI-10})$$

where C_R specifies the relative amounts of resonance and nonresonant background, and the Ξ^* resonance function $\psi_R(w)$ is that given by Jackson:⁹³

$$\psi_R(w) \propto \frac{w}{q} \frac{\Gamma(w)}{(w^2 - w_0^2)^2 + w_0^2 \Gamma^2(w)}. \quad (\text{VI-11})$$

Here w is the $\Xi\pi$ effective mass, w_0 is the resonant mass, and $q = q(w)$ is the Ξ momentum in the $\Xi\pi$ rest frame. The energy-dependent width $\Gamma(w)$ is given by

$$\Gamma(w) = \Gamma_0 \left(\frac{q}{q_0} \right)^3 B_1(q), \quad (\text{VI-12})$$

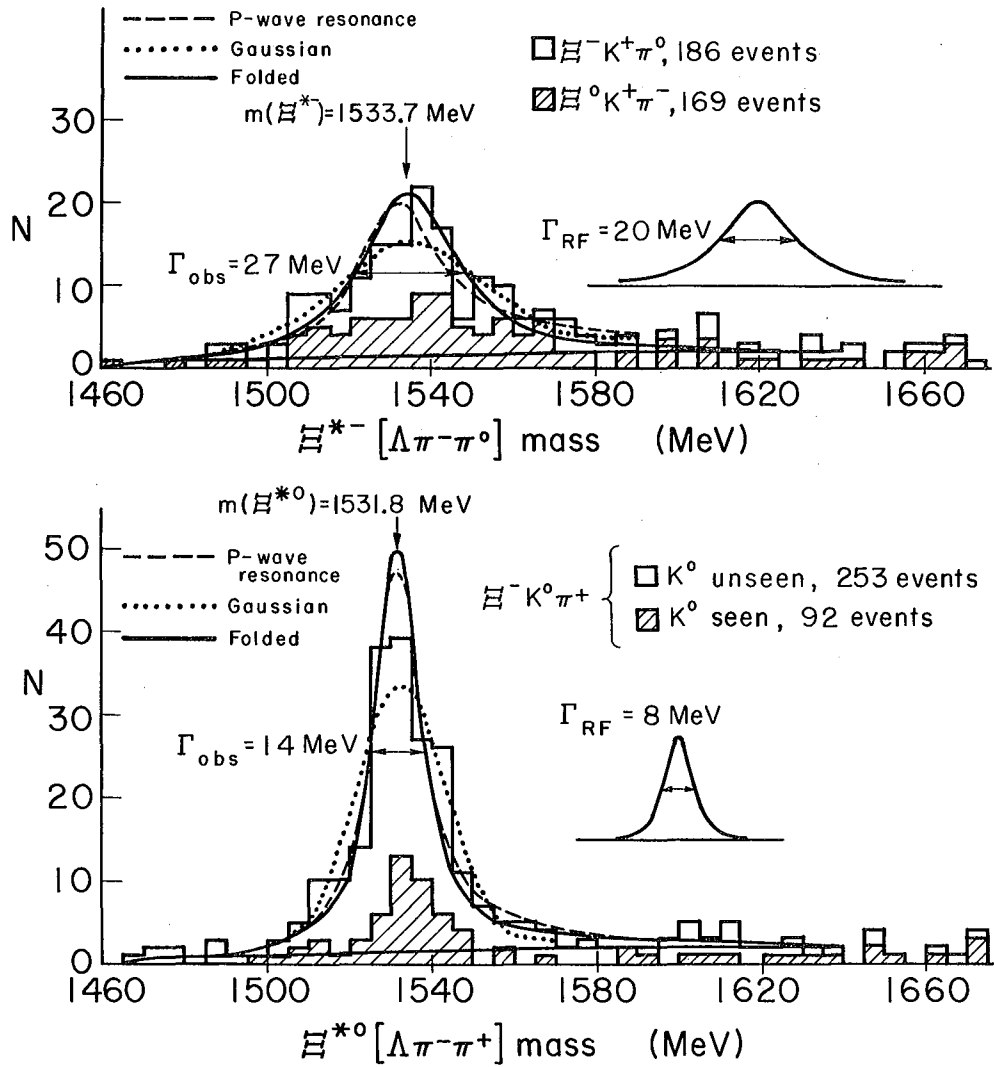
where $\Gamma_0 \equiv \Gamma(w_0)$ and $q_0 \equiv q(w_0)$. The function $B_1(q)$ is a P-wave angular-momentum barrier factor, given by⁹⁴

$$B_1(q) = \frac{1 + (q_0 R)^2}{1 + (q R)^2}, \quad (\text{VI-13})$$

where $R \equiv (2m_\pi)^{-1}$ is a characteristic radius of interaction. The form of $\psi_R(w)$ is insensitive to the value assumed for R .

Table VI-I. Events used in Ξ^* (1530) mass-difference analysis.
 Entries are of the form $N(\text{non-}K^*)/N_{\text{tot}}$. Events used in the
 mass-difference analysis are the 700 non- K^* events
 fitted according to Eqs. (VI-7)-(VI-9).

Final state	Usual fits (VI-I)-(VI-3)				1C fits (VI-7)- (VI-9)
	Momentum (BeV/c)				Total
	1.7	2.1	2.45-2.7	Total	
$\Xi^- K^0 \pi^+ \left\{ \begin{array}{l} K^0 \text{ seen} \\ \text{unseen} \end{array} \right\}$	0/0	46/67	47/96	93/163	92/157
	23/23	104/157	130/227	257/407	253/397
$\Xi^- K^+ \pi^0$	15/15	57/92	112/196	184/303	186/296
$\Xi^0 K^+ \pi^-$	11/11	45/76	114/196	170/283	169/283
Total Ξ^{*0}	23/23	150/224	177/323	350/570	345/554
Total Ξ^{*-}	26/26	102/168	226/392	354/586	355/579
Grand Total	49/49	252/392	403/715	704/1156	700/1133



MUB13656

Fig. VI-5

The assumed function $\phi_R(w)$ describes the observed distribution correctly only if $\Gamma_{RF} \ll \Gamma_0$ (where Γ_{RF} is the width of the experimental resolution function). Alternatively, if the resolution function is Gaussian and $\Gamma_{RF} \gg \Gamma_0$, $\phi_R(w)$ may be approximated by the Gaussian form

$$\phi_R(w) \propto \exp\left[-\frac{1}{2}(w-w_0)^2/\sigma^2\right]. \quad (\text{VI-14})$$

The Ξ^* (1530) resonance represents an intermediate case, with $\Gamma_{RF} \approx \Gamma_0$ for Ξ^{*0} , and $\Gamma_{RF} \approx 3\Gamma_0$ for Ξ^{*-} . We have fit the observed distributions assuming the two limiting cases (VI-11) and (VI-14); free parameters in the fits were $N(\Xi^*)/N$ (fraction of events contributing to the resonance), the resonant mass $m(\Xi^*) \equiv w_0$, and a width parameter Γ' ($= \Gamma_0$ or 2.35σ). Then $N(\Xi^*)/N$, w_0 , and Γ_{obs} were estimated with the assumption of a resonance having $\Gamma_0 \approx 7$ MeV, folded with the experimental resolution function. Data from the fits are presented in Table VI-II, and the corresponding theoretical curves are plotted in Fig. VI-5. After considering possible systematic errors (see Sec. VI.B.3), we estimate $\Delta m \equiv m(\Xi^{*-}) - m(\Xi^{*0})$ to be 2.0 ± 3.2 MeV. We compare this result with previously reported values of 5.7 ± 3.0 MeV⁷⁷ and 7.0 ± 4.0 MeV.⁶³

3. Possible Systematic Errors

We consider possible systematic errors due to the following effects:

- a. Uncertainty regarding form of $\phi_R(w)$. For the 345-event Ξ^{*0} sample and the 355-event Ξ^{*-} sample, we observe variation of the order of 0.5 MeV in w_0 as the assumed resonance function $\phi_R(w)$ is varied between the two limiting cases (VI-11) and (VI-14). (For the $\Xi^-\pi^0$ and $\Xi^0\pi^-$ samples considered separately, variation of the order of 1 to 2 MeV is observed, but the effect cancels out in the combined Ξ^{*-} sample.) Although the effect is small compared with statistical errors, we conservatively increase the estimated errors on $m(\Xi^{*0})$ and $m(\Xi^{*-})$ by 0.5 MeV. (See Table VI-II.)

Table VI-II. Resonance parameters of Ξ^{*0} and Ξ^{*-} .

Ξ^{*0} or Ξ^{*-}	Final state	N	Fit	$N(\Xi^*)/N$	$m(\Xi^*) \equiv w_0$ (MeV)	Γ' (MeV)
(0)	$\Xi^- K^0 \pi^+$	345	(a)	0.56 ± 0.04	1531.6 ± 0.8	14.7 ± 1.8
			(b)	0.48 ± 0.03	1532.1 ± 1.0	25.4 ± 2.8
			(c)	0.5 ± 0.1	1531.8 ± 1.4^d	14 ± 3
(-)	$\Xi^- K^+ \pi^0$	186	(a)	0.29 ± 0.05	1532.2 ± 2.4	18.0 ± 4.3
			(b)	0.26 ± 0.04	1529.8 ± 3.1	33.8 ± 8.0
(-)	$\Xi^0 K^+ \pi^-$	169	(a)	0.38 ± 0.06	1536.9 ± 3.9	32.3 ± 11.3
			(b)	0.32 ± 0.05	1537.7 ± 3.4	42.8 ± 4.7
(-)	$\Xi^- K^+ \pi^0, \Xi^0 K^+ \pi^-$ combined	355	(a)	0.33 ± 0.04	1533.7 ± 2.2	24.9 ± 6.1
			(b)	0.29 ± 0.03	1533.7 ± 2.4	40.5 ± 4.5
			(c)	0.3 ± 0.1	1533.7 ± 2.9^d	27 ± 10
	$\Delta m = m(\Xi^{*-}) - m(\Xi^{*0})$		(a)	--	2.4 ± 2.5	--
			(b)	--	1.6 ± 2.6	--
			(c)	--	2.0 ± 3.2^e	--

^aFit assuming $\Gamma_{RF} = 0$ (Eq. VI-14); $\Gamma' \equiv \Gamma_0$.

^bFit assuming $\Gamma_0 = 0$, Gaussian resolution function (Eq. VI-14); $\Gamma' \equiv \Gamma_{RF} = 2.35 \sigma$.

^cEstimate assuming $\Gamma_0 \approx 7$ MeV, folded with experimental resolution function; $\Gamma' \equiv \Gamma_{obs}$.

^dError on w_0 increased by 0.5 MeV due to uncertainty in form of $\phi_R(w)$.
(See Sec. VI. C. 3a.)

^eEstimate of Δm increased by 0.1 MeV due to removal of K^* band. (See Sec. VI. C. 3b.)

b. Assumed form of phase space. The phase space calculated by SUPER FIT is not corrected for effects due to removal of the K^* band (840 to 940 MeV). The error in w_0 may be roughly estimated by assuming a Gaussian resonance having $\sigma = \Gamma_{\text{obs}}/2.35$ and by assuming phase space to be linear in the vicinity of w_0 . If true and assumed phase space are proportional to $[1 + C(w-w_0)]$ and $[1 + C'(w-w_0)]$, respectively, the error in w_0 is approximately $(C-C') \cdot \sigma^2 = 0.18 (C-C') \cdot \Gamma_{\text{obs}}^2$. For the Ξ^{*0} and Ξ^{*-} resonances, we estimate

	$C(\text{MeV}^{-1})$	$C'(\text{MeV}^{-1})$	$\Gamma_{\text{obs}}(\text{MeV})$	Error in $w_0(\text{MeV})$
Ξ^{*0} :	0.0021	0.0044	14	-0.08
Ξ^{*-} :	0.0033	0.0045	27	-0.16

Accordingly we correct our estimate of Δm by +0.1 MeV. (See Table VI-II.)

c. Discrepancies in 1C fits. Pjerrou et al. have pointed out that the 1C fits used in fitting the various final states are not quite identical; i. e., in the three reactions (VI-7) through (VI-9), the missing particle is respectively the K , the pion not from Ξ decay, and the pion from Ξ decay.⁷⁷ The effect of these differences may be checked to some extent for the 93 $\Xi^- K^0 \pi^+$ events having visible K^0 decay, by performing all possible 1C fits, omitting in turn each of the observed particles (including the rotated π^- from Ξ^- decay). In Table VI-III we list values of w_0 obtained by fitting each of the resulting $\Lambda \pi \pi$ effective-mass distributions in the usual fashion. The limited data available allow us to detect systematic shifts in Δm of the order of 3 MeV. Effects this large are not observed, so we make no additional correction to our estimate of Δm .⁹⁵

d. Assumed masses. The only masses entering into the 1C fits are those of Λ , K , and π . All of these are known to within 0.3 MeV; variations of this order in the assumed masses cannot produce significantly larger variations in Δm . The assumed Ξ^- and Ξ^0 masses do not enter into the 1C fits, but enter only (a) in the selection of

Table VI-III. Analysis of 93 $\Xi^- K^0 \pi^+$ events with visible K^0 decay.

<u>1C hypothesis^a</u>	<u>Events fitting 1C hypothesis</u>	<u>w_0^b (MeV)</u>	<u>Analogous 1C fit in mass-difference analysis^a</u>
$\Lambda \pi^- (K^0) \pi^+$	92	1533.6 ± 1.7	$\Lambda \pi^- (K^0) \pi^+$ (VI-7)
$\Lambda \pi^- K^0 (\pi^+)$	88	1533.6 ± 2.6	$\Lambda \pi^- K^+ (\pi^0)$ (VI-8)
$\Lambda (\pi^-) K^0 \pi^+$	91	1535.3 ± 2.1	$\Lambda (\pi^0) K^+ \pi^-$ (VI-9)

^aParticle omitted from 1C fit is indicated by parentheses.

^bFits assume zero-width resolution function, as in Eq. (VI-11).

events; (b) in the calculation of the Ξ^- turning angle (the angle through which the Λ and π^- must be rotated before fitting);⁹⁶ and (c) in the calculation of three-body phase space, for the fitting of the $\Lambda\pi\pi$ effective-mass distributions.

As Pjerrou et al. have done, we too have repeated the entire mass-difference analysis, assuming slightly different values for $m(\Xi^-)$ and $m(\Xi^0)$. The dependence of $m(\Xi^*) \equiv w_0$ upon the assumed masses is illustrated by triangles in the top half of Fig. VI-6. From (a), (d), and (e), we estimate the following partial derivatives:

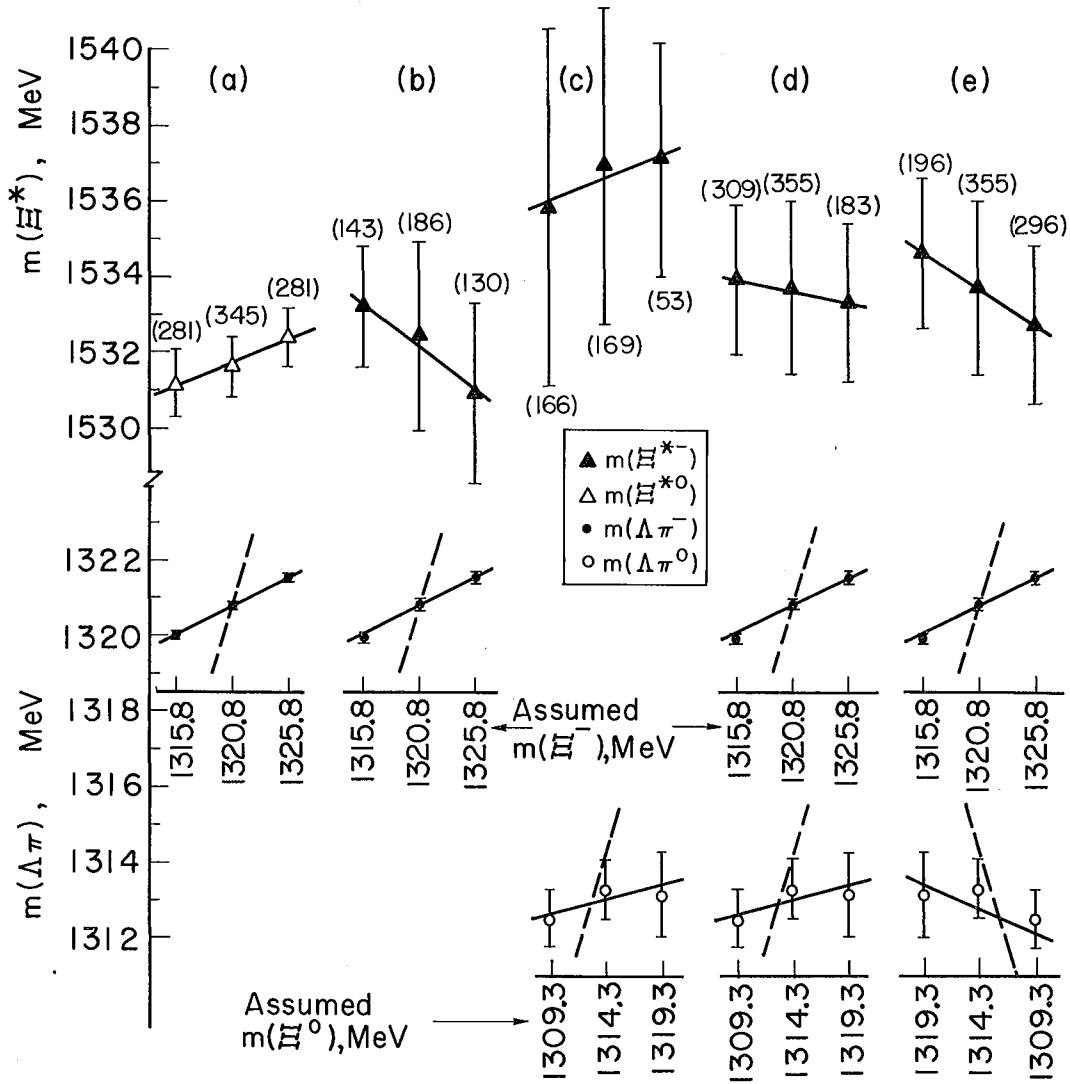
$$\frac{\partial m(\Xi^{*-})}{\partial m(\Xi^-)} \approx -0.15, \quad \frac{\partial m(\Xi^{*-})}{\partial m(\Xi^0)} \approx 0.04;$$

$$\frac{\partial m(\Xi^{*0})}{\partial m(\Xi^-)} \approx 0.12, \quad \frac{\partial m(\Xi^{*0})}{\partial m(\Xi^0)} = 0;$$

$$\frac{\partial (\Delta m)}{\partial m(\Xi^-)} \approx -0.27, \quad \frac{\partial (\Delta m)}{\partial m(\Xi^0)} \approx 0.04.$$

World average values of $m(\Xi^-)$ and $m(\Xi^0)$ are 1320.8 ± 0.2 MeV and 1314.3 ± 1.0 MeV, respectively.¹⁷ Variations (in the assumed Ξ masses) comparable with experimental errors cannot produce variations greater than ≈ 0.1 MeV in Δm .

In the lower half of Fig. VI-6 (circles) we have plotted weighted averages of $\Lambda\pi^-$ and $\Lambda\pi^0$ effective masses $m(\Lambda\pi)$ obtained from the 1C fits, as functions of assumed $m(\Xi^-)$ and $m(\Xi^0)$. The $\Lambda\pi$ effective masses thus calculated agree with the assumed Ξ masses, and are not sensitive to them. We estimate $\partial m(\Lambda\pi)/\partial m(\Xi) \approx 0.15, 0.16,$ and 0.08 for $\Xi^- K^0 \pi^+$, $\Xi^- K^+ \pi^0$, and $\Xi^0 K^+ \pi^-$ events, respectively. After a priori errors have been multiplied by an appropriate scaling factor of 1.15 (to yield correct χ^2 distributions), the $\Lambda\pi$ effective-mass distributions agree with the corresponding resolution functions. This consistency check provides evidence that the sample analyzed contains little non- Ξ background, and that systematic errors are not introduced in the 1C fits.



MUB-13654

Fig. VI-6

4. Discussion

Two well-established supermultiplets in the SU(3) unitary symmetry scheme are the spin-1/2 baryon octet (containing N, Λ , Σ , and Ξ), and the spin-3/2 decuplet [containing $N^*(1238)$, $Y_1^*(1385)$, $\Xi^*(1530)$, and $\Omega(1675)$]. In each case, the mass splitting between isomultiplets, due to a medium-strong symmetry-breaking interaction, is accurately described by the Gell-Mann-Okubo mass formula.^{3, 97} In the limit where SU(3) symmetry is violated only by the electromagnetic interaction, the e.m. mass splittings within isomultiplets are related as follows:^{81, 98}

Spin-1/2 octet:

$$m(\Xi^-) - m(\Xi^0) = m(\Sigma^-) - m(\Sigma^+) + m(p) - m(n) \quad (\text{VI-15})$$

Spin-3/2 decuplet:

$$m = m_0 + m_1 Q + m_2 Q^2, \quad (\text{VI-16})$$

where $Q = \text{charge}$, and m_0, m_1, m_2 are constants.

In the SU(6) symmetry scheme, the spin-1/2 octet and the spin-3/2 decuplet are incorporated into a 56-dimensional representation. In the limit where SU(6) symmetry is violated only by electromagnetism, the following relations hold, in addition to (VI-15) and (VI-16):⁸²

$$m(N^{*0}) - m(N^{*+}) = m(n) - m(p) \quad (\text{VI-17})$$

$$m(N^{*-}) - m(N^{*0}) = m(n) - m(p) + m(\Sigma^-) + m(\Sigma^+) - 2m(\Sigma^0). \quad (\text{VI-18})$$

By considering the effects of only the charge operator to second order, Sakita obtains an additional restriction:^{83, 99}

$$m(n) - m(p) = m(\Sigma^0) - m(\Sigma^+). \quad (\text{VI-19})$$

In Fig. VI-7(a) we illustrate the various SU(3) and SU(6) predictions in terms of a minimum number of free parameters.

Spin - 1/2 octet	Spin - 3/2 decuplet
(a)	
$N \begin{matrix} + \\ \bullet \end{matrix} (b) \begin{matrix} 0 \\ \bullet \end{matrix}$	$N^{*++} \begin{matrix} + \\ \bullet \end{matrix} (2b' - a') \begin{matrix} + \\ \bullet \end{matrix} (b') \begin{matrix} 0 \\ \bullet \end{matrix} (a') \begin{matrix} - \\ \bullet \end{matrix}$
$\Sigma \begin{matrix} + \\ \bullet \end{matrix} (b + \frac{c}{2}) \begin{matrix} 0 \\ \bullet \end{matrix} (a + \frac{c}{2}) \begin{matrix} - \\ \bullet \end{matrix}$	$Y^{*+} \begin{matrix} + \\ \bullet \end{matrix} (b') \begin{matrix} 0 \\ \bullet \end{matrix} (a') \begin{matrix} - \\ \bullet \end{matrix}$
$\Xi \begin{matrix} 0 \\ \bullet \end{matrix} (a + c) \begin{matrix} - \\ \bullet \end{matrix}$	$\Xi^{*0} \begin{matrix} 0 \\ \bullet \end{matrix} (a') \begin{matrix} - \\ \bullet \end{matrix}$
(b)	
$N \begin{matrix} + \\ \bullet \end{matrix} (b'') \begin{matrix} 0 \\ \bullet \end{matrix}$	$N^{*++} \begin{matrix} + \\ \bullet \end{matrix} (2b'' - a'') \begin{matrix} + \\ \bullet \end{matrix} (b'') \begin{matrix} 0 \\ \bullet \end{matrix} (a'') \begin{matrix} - \\ \bullet \end{matrix}$
$\Sigma \begin{matrix} + \\ \bullet \end{matrix} (b'' + \frac{c''}{2}) \begin{matrix} 0 \\ \bullet \end{matrix} (a'' + \frac{c''}{2}) \begin{matrix} - \\ \bullet \end{matrix}$	$Y^{*+} \begin{matrix} + \\ \bullet \end{matrix} (b'' + \frac{c''}{2}) \begin{matrix} 0 \\ \bullet \end{matrix} (a'' + \frac{c''}{2} - d'') \begin{matrix} - \\ \bullet \end{matrix}$
$\Xi \begin{matrix} 0 \\ \bullet \end{matrix} (a'' + c'') \begin{matrix} - \\ \bullet \end{matrix}$	$\Xi^{*0} \begin{matrix} 0 \\ \bullet \end{matrix} (a'' + c'' - d'') \begin{matrix} - \\ \bullet \end{matrix}$
(c)	
$N \begin{matrix} + \\ \bullet \end{matrix} \begin{pmatrix} 1.00x \\ -1.4 \\ +0 \end{pmatrix} \begin{matrix} 0 \\ \bullet \end{matrix}$	$N^{*++} \begin{matrix} + \\ \bullet \end{matrix} \begin{pmatrix} 1.12x \\ -3.19 \\ -4.18 \end{pmatrix} \begin{matrix} + \\ \bullet \end{matrix} \begin{pmatrix} 1.12x \\ +0 \\ -1.40 \end{pmatrix} \begin{matrix} 0 \\ \bullet \end{matrix} \begin{pmatrix} 1.12x \\ +3.19 \\ +1.40 \end{pmatrix} \begin{matrix} - \\ \bullet \end{matrix}$
$\Sigma \begin{matrix} + \\ \bullet \end{matrix} \begin{pmatrix} 1.45x \\ -0.1 \\ +1.03 \end{pmatrix} \begin{matrix} 0 \\ \bullet \end{matrix} \begin{pmatrix} 1.45x \\ +1.9 \\ +0.35 \end{pmatrix} \begin{matrix} - \\ \bullet \end{matrix}$	$Y^{*+} \begin{matrix} + \\ \bullet \end{matrix} \begin{pmatrix} 1.12x \\ -0.22 \\ -1.40 \end{pmatrix} \begin{matrix} 0 \\ \bullet \end{matrix} \begin{pmatrix} 1.12x \\ +3.26 \\ +1.40 \end{pmatrix} \begin{matrix} - \\ \bullet \end{matrix}$
$\Xi \begin{matrix} 0 \\ \bullet \end{matrix} \begin{pmatrix} 1.90x \\ +1.6 \\ +1.30 \end{pmatrix} \begin{matrix} - \\ \bullet \end{matrix}$	$\Xi^{*0} \begin{matrix} 0 \\ \bullet \end{matrix} \begin{pmatrix} 1.12x \\ +3.33 \\ +1.41 \end{pmatrix} \begin{matrix} - \\ \bullet \end{matrix}$

MUB-13877

Fig. VI-7

Other relationships have been obtained by considering the members of the octet and decuplet as bound states of quarks. The predictions of two proposed models (Rubinstein, Ref. 84) (which differ in assumptions regarding the spin- and isospin-dependence of forces between quarks) are illustrated in Fig. VI-7(b).

By assuming that the symmetry-breaking interaction is dominated by "tadpole" diagrams resulting from the existence of an octet of scalar particles, Coleman and Glashow⁸⁵ predict equal-mass e. m. splitting within the spin-3/2 decuplet, i. e.,

$$m = m_0 + m_1 Q, \quad (\text{VI-20})$$

where Q is charge, and where

$$m_1 \approx \frac{m(N^*) - m(Y^*)}{m(N) - m(\Xi)} \quad [m(\Sigma^+) - m(\Sigma^-)] \approx -3 \text{ MeV}. \quad (\text{VI-21})$$

The major non-tadpole contributions, which disrupt the equal-spacing pattern, have been estimated by Socolow;⁸⁶ the predictions of the corrected tadpole model are illustrated in Fig. VI-7(c). Dashen and Frautschi have derived the equal-mass-splitting rule from the bootstrap theory of octet enhancement.⁸⁷ Here again, higher order effects disrupt the equal-mass spacing pattern.

Finally, Kumar⁸⁸ has calculated the Ξ^* (1530) mass difference $\Delta m = m(\Xi^{*-}) - m(\Xi^{*0})$ to be 3.87 MeV, using an S-matrix method suggested by Dashen and Frautschi¹⁰⁰ and assuming the Ξ^* to be a bound state of \bar{K} and Λ . Gilman⁸⁹ is pursuing similar investigations but has not yet published an estimate of $\Delta m(\Xi^*)$.

To date, the following e. m. mass differences (in MeV) have been reported:¹⁰¹

Spin-1/2 octet:

$m(n) - m(p):$	1.2933 ± 0.0001	(Rosenfeld)	
$m(\Sigma^-) - m(\Sigma^+):$	7.90 ± 0.09	(Rosenfeld)	} average 7.90 ± 0.07
	7.89 ± 0.12	(Schmidt)	
$m(\Sigma^-) - m(\Sigma^0):$	4.86 ± 0.07	(Rosenfeld)	} average 4.89 ± 0.06
	4.99 ± 0.12	(Schmidt)	
$m(\Xi^-) - m(\Xi^0):$	6.5 ± 1.0	(Rosenfeld)	

Spin-3/2 decuplet:

$m(N^{*0}) - m(N^{*++}):$	0.45 ± 0.85	(Olsson)	
$m(N^{*-}) - m(N^{*++}):$	7.9 ± 6.8	(Gidal)	
$m(Y^{*-}) - m(Y^{*+}):$	17 ± 7	(Cooper)	} average 3.3 ± 1.2
	4.3 ± 2.2	(Huwe)	
	2.0 ± 1.5	(Armenteros)	
	11 ± 9	(London)	
$m(\Xi^{*-}) - m(\Xi^{*0}):$	5.7 ± 3.0	(Pjerrou)	} average 6.2 ± 2.4
	7.0 ± 4.0	(London)	
	2.0 ± 3.2	(this experiment)	
			} avg. 4.7 ± 1.9

The experimental data are in good agreement with the prediction of Kumar,⁸⁸ that $\Delta m(\Xi^*) = m(\Xi^{*-}) - m(\Xi^{*0}) = 3.87$ MeV. For the theoretical models relating $\Delta m(\Xi^*)$ to other mass differences, predicted values of $\Delta m(\Xi^*)$ may be obtained by performing fits to available data excluding Ξ^* data; the results of these fits are presented in Table VI-IV. The two-parameter SU(6) model⁸³ and the corrected tadpole model⁸⁶ do not describe the observed octet mass differences within experimental errors; here, in estimating $\Delta m(\Xi^*)$, we have allowed for ≈ 0.5 -MeV uncertainty in theoretical mass predictions.

In Fig. VI-8 we illustrate the agreement of the observed decuplet mass differences with the predictions of SU(3).

Table VI-IV. Comparison of predicted and observed e. m. mass splittings.

Hypothesis	$\chi^2(\text{NC})^g$		Fitted parameters (MeV)		Correlation coefficients		$\Delta m(\Xi^*)$ predicted (MeV)
	No Ξ^*	With Ξ^*	No Ξ^*	With Ξ^*	No Ξ^*	With Ξ^*	No Ξ^*
1. SU(3) octet ^a	0.01 (1C)		a =	3.17 ± 0.14	(a, c) =	-0.94	--
			b =	1.2933			
			c =	3.44 ± 0.18			
2. SU(3) decuplet ^b	0.55 (1C)	1.70 (2C)	a' =	2.44 ± 0.92	(a', b') =	0.66	2.44 ± 0.92
			b' =	0.98 ± 0.36		0.62	
				1.09 ± 0.35			
3. SU(6) ^c	1.40 (4C)	2.04 (5C)	a =	3.17 ± 0.14	(a, c) =	-0.94	3.17 ± 0.14
			b =	1.2933			
			c =	3.44 ± 0.18			
4. Restricted SU(6) ^d	h (5C)	h (6C)	a =	5.28 ± 0.31	(a, b) =	-0.10	5.28 ± 0.31
			b =	1.80 ± 0.24			
5. Quark model ^e	0.45 (3C)	1.89 (4C)	a'' =	3.18 ± 0.14	(a'', c'') =	-0.94	2.00 ± 1.20
			b'' =	1.2933	(a'', d'') =	-0.03	
			c'' =	3.42 ± 0.18	(c'', d'') =	0.04	
			d'' =	4.60 ± 1.20			
				3.83 ± 1.02			
6. Restricted quark model ^e	15.1 (4C)	16.1 (5C)	a'' =	3.20 ± 0.14	(a'', c'') =	-0.94	6.59 ± 0.07
			b'' =	1.2933			
			c'' =	3.39 ± 0.18			
7. Tadpole (i) ^{f, j}	h (6C)	h (7C)	x =	2.46 ± 0.13			2.76 ± 0.15
8. Tadpole (ii)	h (6C)	h (7C)	x =	2.02 ± 0.13			5.59 ± 0.15
9. Tadpole (iii)	h (6C)	h (7C)	x =	1.89 ± 0.13			6.86 ± 0.15

^aSee Ref. 98.

^bSee Ref. 81.

^cSee Ref. 82.

^dSee Ref. 83.

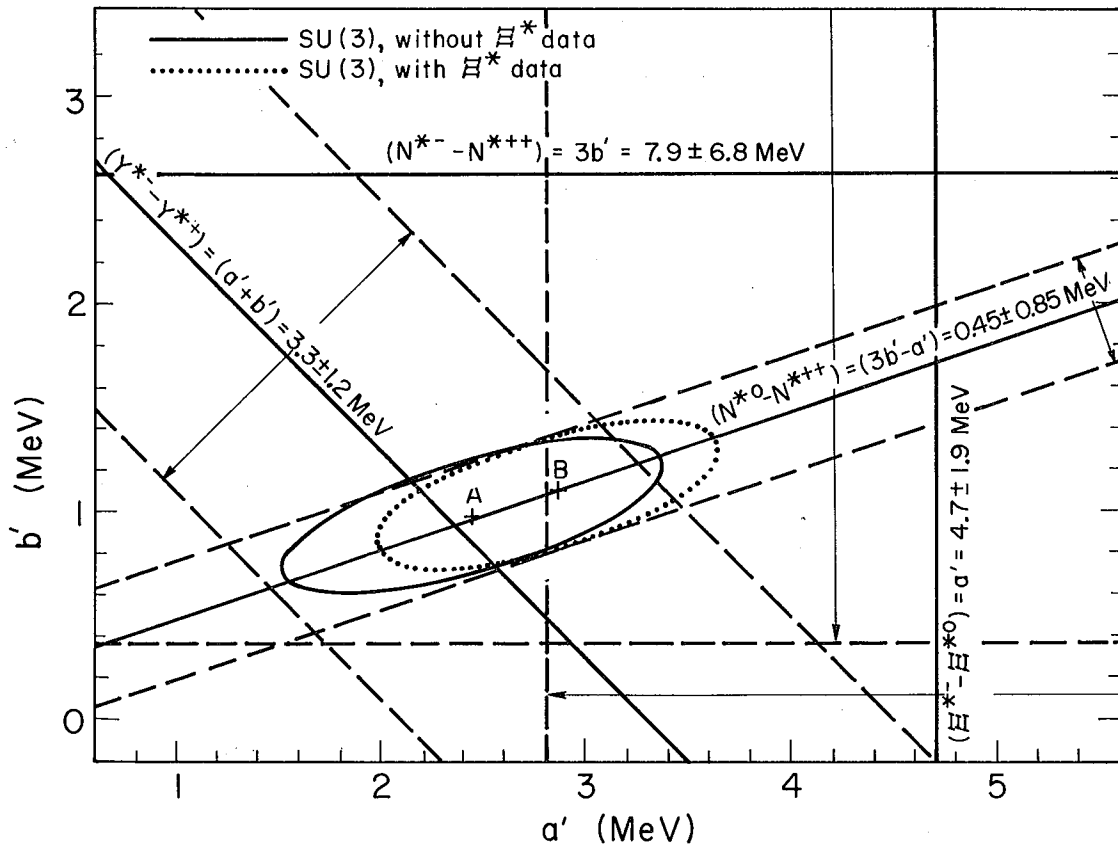
^eSee Ref. 84.

^fSee Refs. 85, 86.

^g $\chi^2(\text{NC})$ is a chi-squared for N degrees of freedom.

^hBaryon octet cannot be fitted within experimental errors ($\chi^2 > 300$). Quoted parameters are best values if one assumes 0.5 MeV uncertainty in theoretical mass predictions.

^j(i) = tadpole term alone; (ii) = (i) + correction due to spin-1/2 octet; (iii) = (i) + (ii) + correction due to spin-3/2 decuplet.

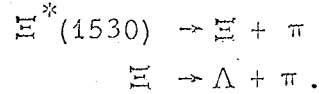


MUB-13876

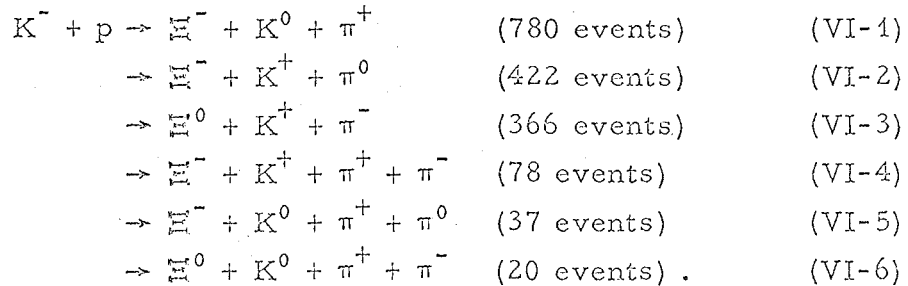
Fig. VI-8

C. Spin and Parity

Using the Byers-Fenster formalism, one may determine the spin and parity of $\Xi^*(1530)$ decaying via



In our analysis we fit the observed decay distribution to a distribution function analogous to (II-51), assuming spin 1/2 for the Ξ and disregarding the direction of the proton from Λ decay. We analyze only those K-63 events which have visible Λ decay and which unambiguously fit one of the following hypotheses:



(A sample containing essentially the events of type (VI-4) and (VI-6) has been analyzed previously.)¹³

In the present analysis we selected $\Xi\pi$ combinations (having $I_z = \pm 1/2$) in the range 1510 to 1555 MeV, corresponding to $\approx 4 \Gamma_{\text{obs}}$.¹⁰² In $\Xi^- K^0 \pi^+ \pi^0$ events containing two $\Xi^*(1530)$, only the Ξ^* nearer 1530 MeV was analyzed. In order to avoid possible K^* interference effects in $\Xi K\pi$ events, we required $(\hat{\Xi} \cdot \hat{\Xi}^*) \geq 0$ (where $\hat{\Xi}$ is the direction of the Ξ in the Ξ^* rest frame, and $\hat{\Xi}^*$ is the direction of transformation into that frame). All events in the $K^*(890)$ band were thus removed without distorting the Ξ^* decay distribution.¹⁰³ In the $\Xi^- K^0 \pi^+ \pi^0$ sample, which is the only $\Xi K\pi\pi$ final state where K^* interference can occur, there were no events having both a Ξ^* and an interfering K^* .

The remaining events were divided into four subsamples (159 $\Xi^- K^0 \pi^+$, 39 $\Xi^- K^+ \pi^0$, 53 $\Xi^0 K^+ \pi^-$, and 96 $\Xi K\pi\pi$). Each subsample was fit independently to various Ξ^* spin and parity hypotheses J^P ,

with spin $1/2$ assumed for the Ξ , and with $a_{\Xi^-} = a_{\Xi^0} = -0.4$. Fits were performed with the assumptions of $L_{\max} = 1$ (one parameter per sample) and $L_{\max} = 3$ (seven parameters per sample). The choice $\gamma = \pm 1$ is appropriate for the sequence $J^P = 1/2^+, 3/2^\pm, 5/2^+$, etc. Values of the t_{LM} and of $w = \ln \mathcal{L}$ are presented in Fig. VI-9 and Table VI-V. Axes used in defining the t_{LM} are $\vec{Z} = \hat{K} \times \hat{\Xi}^*$, $\hat{Y} = \hat{\Xi}^*$, and $\hat{X} = \hat{Y} \times \hat{Z}$.

Fits with $L_{\max} = 1, 3$, and 5 (1, 7, and 17 parameters respectively) were performed for the combined sample of 347 events; the results of these fits are presented in Table VI-VI. Due to the large number of parameters, fits with $L_{\max} = 5$ were not possible for the smaller subsamples.

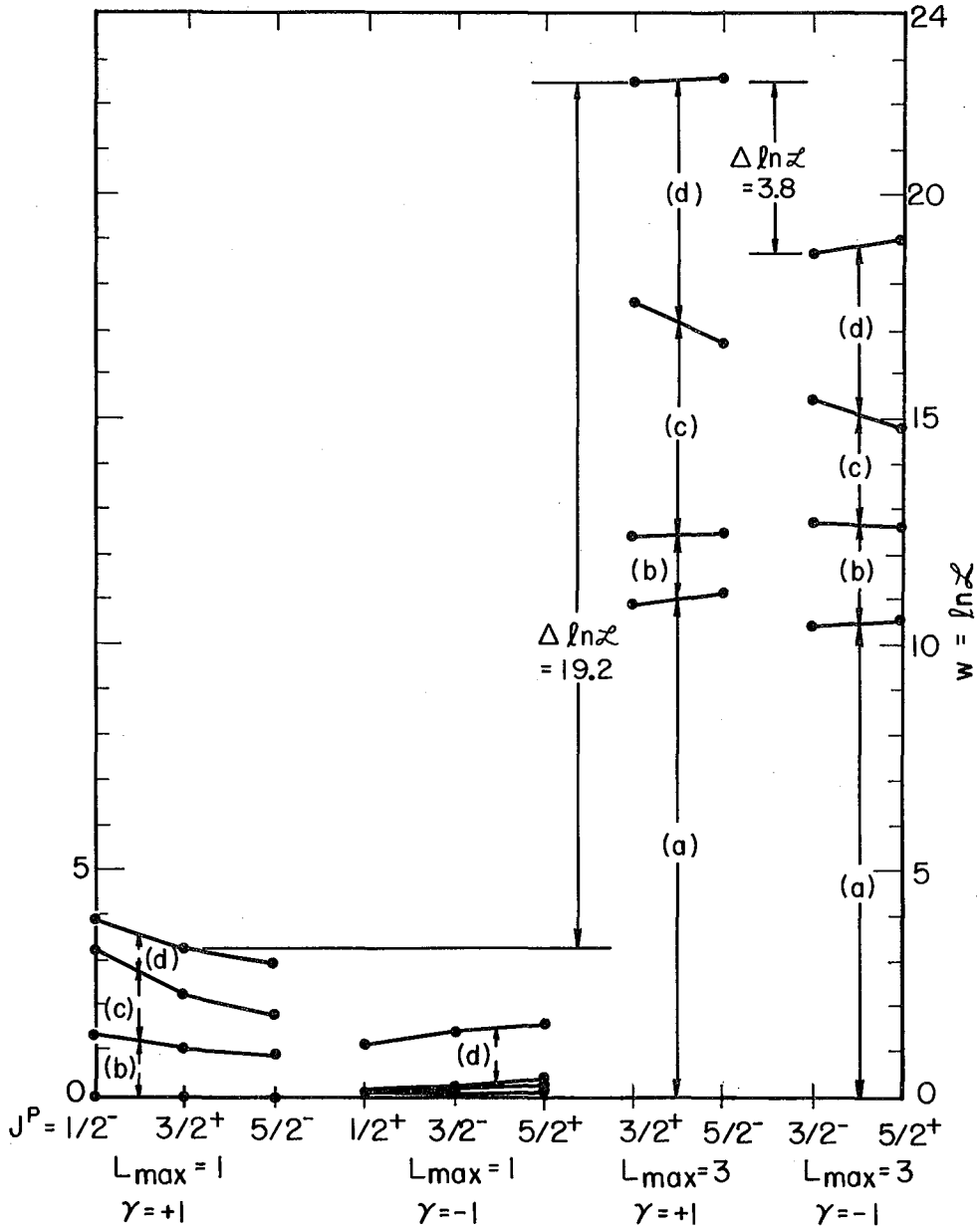
We may draw the following conclusions regarding the spin and parity of Ξ^* (1530):

(a) Spin $\geq 3/2$ is favored by the data. (Refer to Fig. VI-9) As L_{\max} is increased from 1 to 3 (for $J^P = 3/2^+$), $\ln \mathcal{L}$ is increased by 19.2, corresponding to a χ^2 of 38.4 for 24 degrees of freedom. The $J = 1/2$ (i. e., $L_{\max} = 1$) hypothesis is roughly 3.5% as likely as the $J = 3/2$ (i. e., $L_{\max} = 3$) hypothesis.

(b) The hypothesis $J^P = 3/2^+$ is favored over $3/2^-$ by $\approx (2 \times 3.8)^{1/2} = 2.8$ standard deviations. (Refer to Table VI-V.)

(c) Spin $\geq 5/2$ is slightly favored but not required by the data. (Refer to Table VI-VI.) As L_{\max} is increased from 3 to 5 (for $J^P = 5/2^+$), $\ln \mathcal{L}$ is increased by 8.3, corresponding to a χ^2 of 16.6 for 10 degrees of freedom. The $J = 3/2$ (i. e., $L_{\max} = 3$) hypothesis is roughly 8% as likely as the $J = 5/2$ (i. e., $L_{\max} = 5$) hypothesis. [If the Ξ^* (1530) spin is $5/2$, the hypothesis $J^P = 5/2^+$ is favored over $5/2^-$ by ≈ 2.4 standard deviations.]

For the 251 Ξ^* from $\Xi K\pi$ final states, which have not been analyzed previously, the $J = 1/2$ hypothesis is roughly 3 or 4% as likely ($\chi^2_{18C} = 30.8$) as the $J = 3/2$ hypothesis. The hypothesis $J^P = 3/2^+$ is favored over $3/2^-$ by ≈ 2.1 standard deviations. We compare these new results with those reported in recent experiments:



MUB-13655

Fig. VI-9

Table VI-V. Values of $w = \ell n \chi^2$ and $t_{LM} (\times 100)$ for $\Xi^*(1530)$ subsamples (a)-(d).

J^P		Sample				Total, (a)-(d)
		(a)	(b)	(c)	(d)	
		$\Xi^- K^0 \pi^+$	$\Xi^- K^+ \pi^0$	$\Xi^0 K^+ \pi^-$	$\Xi K \pi \pi$	
	$N(\Xi^*) =$	159	39	53	96	347
$1/2^-$	$\ell n \chi^2 =$	0.00	1.43	1.86	0.68	3.97
	$t_{10} =$	0 ± 20	-67 ± 36	64 ± 31	-31 ± 26	
$1/2^+$	$\ell n \chi^2 =$	0.18	0.00	0.02	0.95	1.15
	$t_{10} =$	12 ± 20	-2 ± 38	6 ± 30	36 ± 26	
$3/2^+$	$\ell n \chi^2 =$	10.88	1.55	5.15	4.91	22.49
	$t_{10} =$	8 ± 24	-91 ± 57	67 ± 41	-43 ± 34	
	$t_{20} =$	25 ± 8	-5 ± 16	1 ± 14	7 ± 9	
	$\text{Ret}_{22} =$	1 ± 5	-9 ± 11	-1 ± 10	4 ± 7	
	$\text{Imt}_{22} =$	13 ± 5	3 ± 15	11 ± 9	6 ± 8	
	$t_{30} =$	14 ± 17	-24 ± 34	75 ± 31	29 ± 18	
	$\text{Ret}_{32} =$	24 ± 12	-10 ± 27	25 ± 22	-14 ± 16	
	$\text{Imt}_{32} =$	-10 ± 11	-4 ± 31	17 ± 20	28 ± 16	
$3/2^-$	$\ell n \chi^2 =$	10.35	2.33	2.70	3.31	18.69
	$t_{10} =$	18 ± 24	46 ± 54	-28 ± 39	46 ± 33	
	$t_{20} =$	-25 ± 8	-4 ± 17	3 ± 15	7 ± 9	
	$\text{Ret}_{22} =$	3 ± 5	-6 ± 11	5 ± 11	5 ± 7	
	$\text{Imt}_{22} =$	11 ± 5	2 ± 15	8 ± 9	6 ± 8	
	$t_{30} =$	-28 ± 17	-33 ± 37	-2 ± 34	-18 ± 19	
	$\text{Ret}_{32} =$	-8 ± 11	8 ± 26	28 ± 24	10 ± 16	
	$\text{Imt}_{32} =$	-10 ± 11	56 ± 28	46 ± 25	-16 ± 16	

Table VI-VI. Values of $w = \ln \mathcal{L}$ and $t_{LM} (\times 100)$ for combined $\Xi^*(1530)$ sample.

	$J^P = 1/2^-, 3/2^+, 5/2^- (\gamma = +1)$			$J^P = 1/2^+, 3/2^-, 5/2^+ (\gamma = -1)$		
	$L_{\max} = 1$	$L_{\max} = 3$	$L_{\max} = 5$	$L_{\max} = 1$	$L_{\max} = 3$	$L_{\max} = 5$
$\ln \mathcal{L} (J = 1/2)$	0.07 ^a	--	--	0.67 ^a	--	--
$\ln \mathcal{L} (J = 3/2)$	0.24	7.78 ^a	--	0.65	6.86 ^a	--
$\ln \mathcal{L} (J = 5/2)$	0.32	8.27	12.83 ^a	0.61	7.28	15.63 ^a
t_{10}	-5 ± 14	-13 ± 17	-12 ± 17	15 ± 13	19 ± 17	17 ± 17
t_{20}		-10 ± 5	-11 ± 5		-11 ± 5	-9 ± 5
Ret ₂₂		3 ± 3	4 ± 4		3 ± 3	3 ± 4
Imt ₂₂		9 ± 4	8 ± 3		9 ± 4	9 ± 3
t_{30}		20 ± 11	35 ± 16		-19 ± 11	-32 ± 16
Ret ₃₂		12 ± 8	15 ± 12		2 ± 8	-5 ± 12
Imt ₃₂		5 ± 8	10 ± 11		-2 ± 8	-2 ± 11
t_{40}			3 ± 6			2 ± 6
Ret ₄₂			-7 ± 4			-7 ± 4
Imt ₄₂			1 ± 4			1 ± 4
Ret ₄₄			7 ± 4			6 ± 4
Imt ₄₄			2 ± 4			1 ± 4
t_{50}			2 ± 10			-6 ± 10
Ret ₅₂			5 ± 8			-2 ± 7
Imt ₅₂			3 ± 6			-19 ± 6
Ret ₅₄			-9 ± 7			0 ± 7
Imt ₅₄			1 ± 7			-9 ± 7

^aValue of $\ln \mathcal{L}$ corresponding to t_{LM} listed.

Using 77 Ξ^* produced in $\Xi^- K^+ \pi^+ \pi^-$ and $\Xi^0 K^0 \pi^+ \pi^-$ final states by $K^- + p$ at 2.45-2.7 BeV/c (Berkeley K-63 data), Button-Shafer¹³ finds $J \geq 3/2$ (for the $J = 1/2$ hypothesis, $\chi^2_{48C} = 449$); $J = 5/2$ is not required by the data. The $3/2^+$ and $3/2^-$ hypotheses have confidence levels of 0.75 ($\chi^2_{8C} = 5.0$) and 0.005 ($\chi^2_{8C} = 21.5$), respectively.¹⁰⁴ (If $J = 5/2$, the hypothesis $J^P = 5/2^-$ is preferred over $5/2^+$.)

Using 80 Ξ^{*0} produced in $\Xi^- K^0 \pi^+$ final states by $K^- + p$ at 1.8 and 1.95 BeV/c (UCLA), Schlein et al.⁷⁶ find $J \geq 3/2$ (for the $J = 1/2$ hypothesis, $\chi^2_{24C} = 47$); $J = 5/2$ is not required by the data. The $3/2^+$ and $3/2^-$ hypotheses have confidence levels of 0.83 ($\chi^2_{4C} = 1.5$) and 0.035 ($\chi^2_{4C} = 10.3$), respectively.¹⁰⁴ (If $J = 5/2$, the hypothesis $J^P = 5/2^-$ is preferred over $5/2^+$.)

Using 132 Ξ^* produced in $\Xi K \pi$ final states by $K^- + p$ at 2.24 BeV/c (Brookhaven), London et al.⁶³ find that the $J = 1/2$ hypothesis is discriminated against with a confidence level of $\approx 1\%$. They did not investigate parity.

Using 108 Ξ^* produced in $\Xi K \pi$ final states by $K^- + p$ at 1.5 to 1.7 BeV/c (Berkeley K-72 data), Berge et al.⁷ find very slight evidence favoring $J \geq 3/2$ (c.l. of $J = 1/2$ hypothesis $\approx 12\%$), but results are inconclusive.

Experimental results to date are consistent with the assignment of the $\Xi^*(1530)$ to an SU(3) $3/2^+$ decuplet containing $N^*(1238)$, $Y_1^*(1385)$, $\Xi^*(1530)$, and $\Omega(1675)$. At present, however, the possibility of higher spin for $\Xi^*(1530)$ cannot be excluded.

VII. PROPERTIES OF $\Xi^*(1817)$

The existence of $\Xi^*(1817 \text{ MeV})$ has been established in a number of recent experiments.^{11, 12, 14-16} The state is most clearly seen as ΛK^- and $\Lambda \bar{K}^0$ in the reactions $K^- + p \rightarrow \Lambda + K^{+,0} + \bar{K}^{-,0}$; these observations are sufficient to establish the $S = -2$, $I = 1/2$ assignment. Estimates of the Ξ^* mass and width, as obtained from $\Lambda \bar{K}$ mass distributions, are $m = 1817 \pm 7 \text{ MeV}$, $\Gamma = 30 \pm 7 \text{ MeV}$ (Berkeley),¹⁴ and $m = 1814 \pm 4 \text{ MeV}$, $\Gamma = 12 \pm 4 \text{ MeV}$ (Paris-Saclay-Amsterdam).¹⁵

The $\Xi^*(1817)$ is also observed as $\Xi^*(1530) + \pi$ and $\Xi\pi\pi$, in $\Xi K\pi\pi$ final states; the intensity of this effect is $\approx 25\%$ that of $\Lambda \bar{K}$.¹⁴ Observed branching ratios in the production and decay of $\Xi^*(1817)$ confirm the isospin assignment of $1/2$.

A broad enhancement in the region 1825 to 1950 MeV, which was originally interpreted as an alternate decay mode of $\Xi^*(1817)$, was reported in $\Xi\pi$ mass distributions from $\Xi K\pi$ final states;^{11, 12} the apparent broadening and upward shift of the peak was not understood. Later the Paris-Saclay-Amsterdam group reported the existence of a possible new Ξ^* resonance (in $\Xi^- K^0 \pi^+$ final states) having mass $m = 1933 \pm 16 \text{ MeV}$ and width $\Gamma = 140 \pm 35 \text{ MeV}$.¹⁵ A rough fit to the $\Xi\pi$ mass distributions in the Berkeley data indicates that the broad enhancement around 1900 MeV in the $\Xi\pi$ distributions may be entirely due to $\Xi^*(1933)$, attenuated by phase space.¹⁴

Finally, there is evidence in K-63 data for an $S = -2$, $I = 1/2$ enhancement around 1705 MeV in $\Xi^- \pi^0$ and $\Lambda \bar{K}^{0,-}$ mass distributions from $\Xi^- K^+ \pi^0$ and $\Lambda K \bar{K}$ final states.^{12, 14} At present the data are too limited for conclusions to be drawn regarding the spin and parity of $\Xi^*(1705)$.

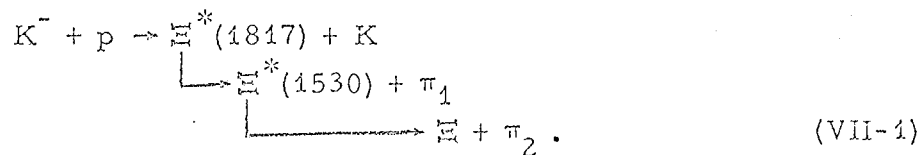
A. Analysis of $\Xi^*(1817) \rightarrow \Xi^*(1530) + \pi$

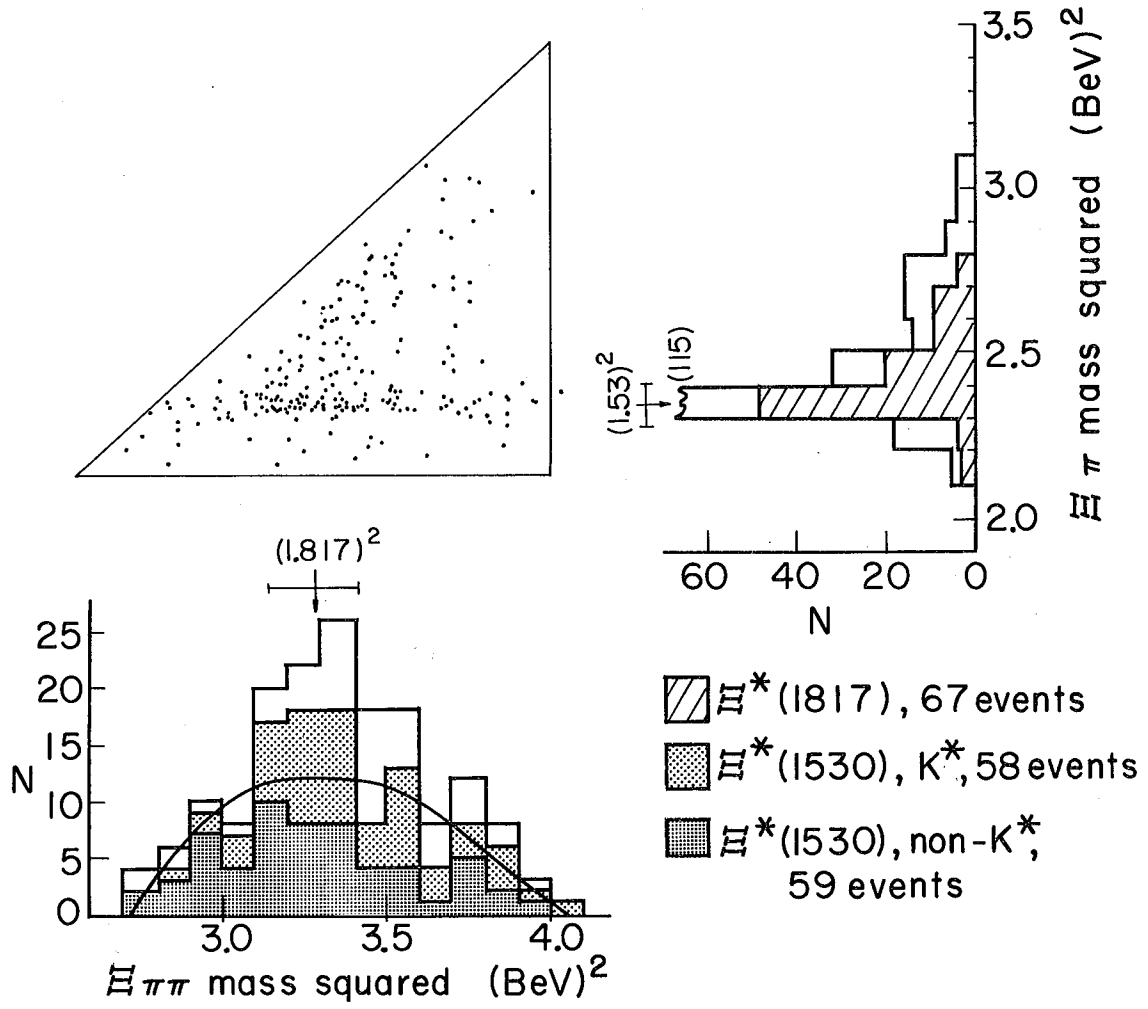
In this section we investigate the spin and parity of $\Xi^*(1817)$, using a cleaner sample of $\Xi^0 K^0 \pi^+ \pi^-$ events than that studied previously, and utilizing two spin tests proposed by Button-Shafer.²² (One of these has been previously applied.)¹¹ The scarcity of data prevents the use of more elaborate tests.

In Fig. VII-1 we present a plot of $\Xi\pi$ mass squared vs $\Xi\pi\pi$ mass squared for 164 $\Xi K\pi\pi$ events from the K-63 experiment. Six events are at 2.1 BeV/c, and the remainder are from 2.45 to 2.7 BeV/c. Plotted are 135 unambiguous events (78 $\Xi^- K^+ \pi^+ \pi^-$, 20 $\Xi^0 K^0 \pi^+ \pi^-$, and 37 $\Xi^- K^0 \pi^+ \pi^0$) with visible lambda decay, plus 29 $\Xi^- K^0 \pi^+ \pi^0$ events without visible lambda decay. Only the 135 unambiguous events are further analyzed. Events designated $\Xi^*(1817)$ have $\Xi\pi\pi$ effective masses between 1775 and 1850 MeV, corresponding to an interval of $\approx 2 \times \Gamma_{\text{obs}}$. Events designated $\Xi^*(1530)$ have at least one $\Xi\pi$ pair with $I_z = \pm 1/2$ and $[1510 \text{ MeV} \leq m(\Xi\pi) \leq 1550 \text{ MeV}]$; events designated K^* have at least one $K\pi$ pair with $I_z = \pm 1/2$ and $[840 \text{ MeV} \leq m(K\pi) \leq 940 \text{ MeV}]$. Of the events designated as both $\Xi^*(1817)$ and $\Xi^*(1530)$, about half are due to non-resonant background.

Using the extended Byers-Fenster formalism for hyperon decay into a spin-3/2 fermion plus a spin-zero boson (see Sec. II.A.4.b and Ref. 22), and assuming the $\Xi^*(1530)$ to have spin 3/2, we examine the spin and parity [relative to $\Xi^*(1530)$] of $\Xi^*(1817)$ decaying via $\Xi^*(1817) \rightarrow \Xi^*(1530) + \pi$. The sample analyzed contains 41 unambiguous $\Xi K\pi\pi$ events (23 $\Xi^- K^+ \pi^+ \pi^-$, 13 $\Xi^- K^0 \pi^+ \pi^0$, and 5 $\Xi^0 K^0 \pi^+ \pi^-$) having both a $\Xi^*(1817)$ and a $\Xi^*(1530)$. Of the 13 $\Xi^- K^0 \pi^+ \pi^0$ events, 6 contain a $\Xi^{*0}(1530)$ and 7 contain a $\Xi^{*-}(1530)$; none contains both.

Let us designate as π_2 and π_1 the pions included and not included, respectively, in the $\Xi^*(1530)$; i. e.,





MUB-13657

Fig. VII-1

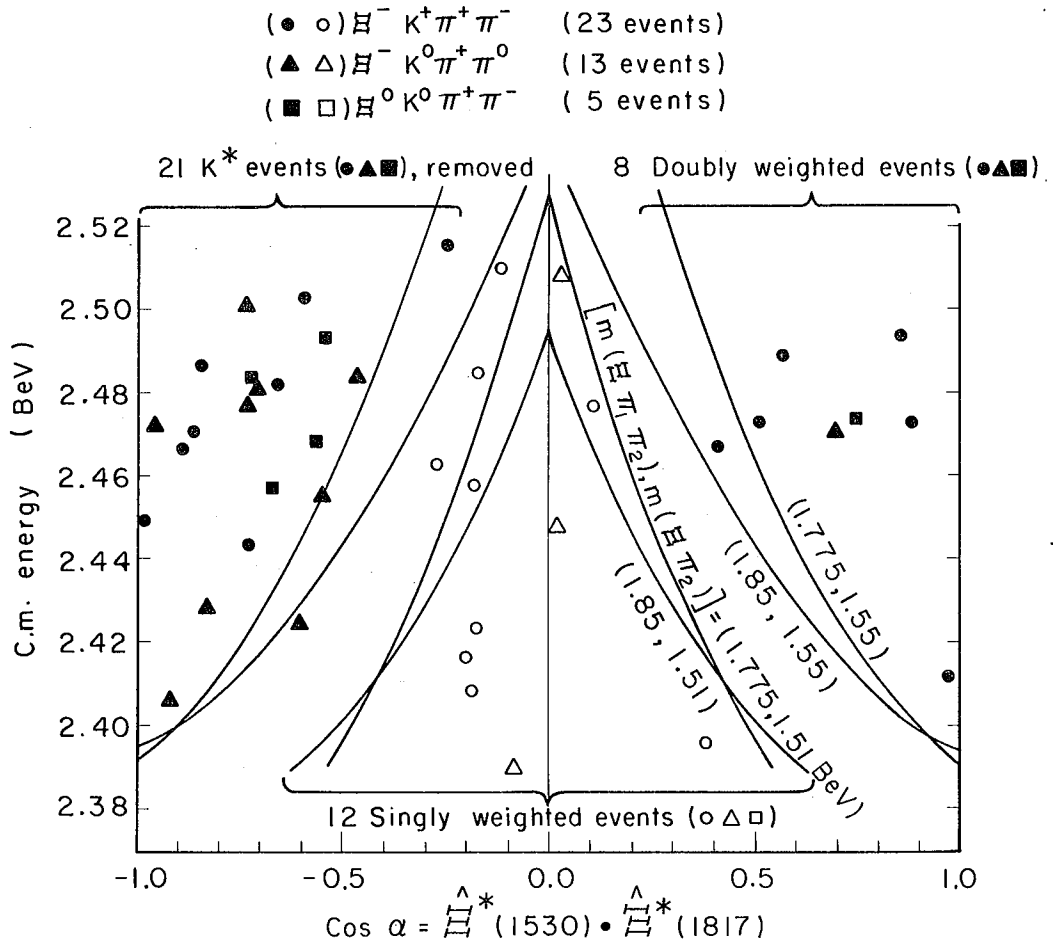
In the $\Xi^- K^0 \pi^+ \pi^0$ final state, either $K\pi_1$ or $K\pi_2$ may form a K^* , whereas in the $\Xi^- K^+ \pi^+ \pi^-$ and $\Xi^0 K^0 \pi^+ \pi^-$ final states, only $K\pi_1$ may form a K^* .

From the 41-event sample, in order to avoid interference effects between $\Xi^*(1817)$ and $K^*(890)$, we removed 21 events having $m(K\pi_1) > 840$ MeV. The 20 events remaining include 15 $\Xi^- K^+ \pi^+ \pi^-$, 4 $\Xi^- K^0 \pi^+ \pi^0$, and 1 $\Xi^0 K^0 \pi^+ \pi^-$. None of the 4 $\Xi^- K^0 \pi^+ \pi^0$ events remaining has a $K\pi_2$ effective mass in the K^* region.

In order that the angular distributions of interest be undistorted by the removal of K^* events, we assigned double weight to certain non- K^* events, selected as follows. For an event of type (VII-1), the K^* cutoff criterion $m(K\pi_1) > 840$ MeV may be re-expressed as a cutoff in $\cos \alpha \equiv \hat{\Xi}^*(1530) \cdot \hat{\Xi}^*(1817)$, where the cutoff point in $\cos \alpha$ depends upon the c.m. energy of the $K\bar{p}$ system and upon the effective masses $m(\Xi\pi_1\pi_2)$ and $m(\Xi\pi_2)$ for the particular event. The curves plotted in the left half of Fig. VII-2 represent, as a function of c.m. energy, the value of $\cos \alpha$ corresponding to $m(K\pi_1) = 840$ MeV for events having both a $\Xi^*(1817)$ and a $\Xi^*(1530)$. In the right half of Fig. VII-2 the same curves appear, reflected about the line $\cos \alpha = 0$. For each event we imagine a single curve (and its reflection) corresponding to the particular values of $m(\Xi\pi_1\pi_2)$ and $m(\Xi\pi_2)$ for that event. Each K^* event falls to the left of the left-hand curve and is discarded; in order to correct for the events lost, each event falling to the right of the reflected curve (on the right-hand side) is assigned double weight in the analysis to follow. In effect, some events having $\cos \alpha < 0$ are replaced by other events having $\cos \alpha > 0$. The removal-and-replacement procedure does not systematically bias either of the two experimental distributions of interest in the following analysis.

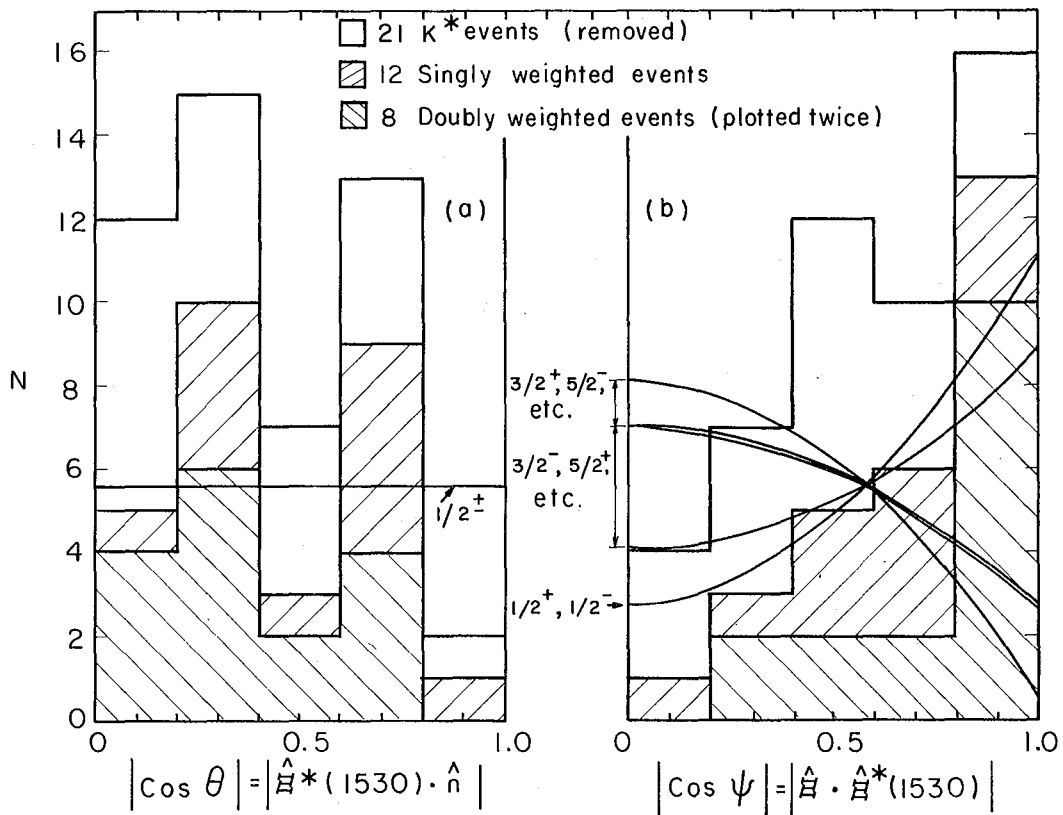
In Fig. VII-3(a) we plot the distribution of $|\cos \theta| \equiv |\hat{\Xi}^*(1530) \cdot \hat{n}|$, where $\vec{n} = \vec{K} \times \hat{\Xi}^*(1817)$ is the $\Xi^*(1817)$ production normal. Assuming $I(\theta)$ to be of the form $1 + a_2 P_2(\cos \theta)$, we calculate the coefficient a_2 as

$$a_2 = 5 \langle P_2 \rangle = \frac{5}{N} \sum_{i=1}^{N'} P_2(\cos \theta_i) \quad (\text{VII-2})$$



MUB 13878

Fig. VII-2



MUB13879

Fig. VII-3

with an experimental error

$$\delta a_2 = 5 \delta \langle P_2 \rangle = \left(\frac{5}{N} \right)^{1/2} \left[1 + \frac{2}{7} a_2 - \frac{1}{5} a_2^2 \right]^{1/2}. \quad (\text{VII-3})$$

Here $N (= 20)$ is the actual number of events, and $N' (= 28)$ is the number with doubly weighted events counted twice. For the non- K^* events of Fig. VII-3 we obtain $a_2 = 0.6 \pm 0.5$, consistent with isotropy and with the $J = 1/2$ assignment. We cannot rule out higher spin hypotheses. Background events lying outside the $\Xi^*(1817)$ region (1775 to 1850 MeV), but otherwise selected just as the $\Xi^*(1817)$ events, also yield an $I(\theta)$ distribution consistent with isotropy.

In Fig. VII-3(b) we plot the distribution of $|\cos \psi| \equiv |\hat{\Xi} \cdot \hat{\Xi}^*(1530)|$, i.e., the decay angle of $\Xi^*(1530)$ relative to its line of flight. The expected distribution is of the form $\mathcal{D}(\psi) \propto 1 + a_2 P_2(\cos \psi)$ for any value of the $\Xi^*(1817)$ spin J . For a pure sample of $\Xi^*(1817)$ decaying via $\Xi^*(1817) \rightarrow \Xi^*(1530) + \pi$, predicted values of the coefficient a_2 are as follows (see Sec. II.A.4.b):¹⁰⁵

J^P	Partial wave ℓ	a_2 predicted
$1/2^+$	1	1.0
$1/2^-$	2	
$3/2^-$	0, 2	≈ -0.5 to $+0.5$
$5/2^+$	1, 3	
$7/2^-$	2, 4	
etc.	etc.	
$3/2^+$	1, 3	≈ -0.9 to -0.5
$5/2^-$	2, 4	
$7/2^+$	3, 5	
etc.	etc.	

The observed value is 1.4 ± 0.5 , which favors the hypotheses $J^P = 1/2^\pm$ and $J^P = 3/2^-, 5/2^+, 7/2^-, \text{etc.}$ over $J^P = 3/2^+, 5/2^-, 7/2^+, \text{etc.}$

The hypotheses $1/2^-$, $1/2^+$, and $3/2^-$ correspond respectively to $\ell = 0, 1$, and 2 for $\Xi^*(1817) \rightarrow \Lambda + \bar{K}$ and (if higher waves are ignored) to $\ell = 2, 1$, and 0 for $\Xi^*(1817) \rightarrow \Xi^*(1530) + \pi$.

Background events outside the $\Xi^*(1817)$ region yield a value $a_2 = 0.2 \pm 0.4$, indicating that the observed anisotropy may indeed be associated with $\Xi^*(1817)$. However, because the $\Xi^*(1817)$ sample contains $\geq 50\%$ background, we cannot ignore the possibility that the anisotropy may be due to $\Xi^*(1817)$ interference with non-resonant background. In conclusion, our analysis does not permit us to rule out conclusively any J^P hypothesis for $\Xi^*(1817)$.

B. Discussion

There is no evidence for a Ξ^* resonance near 1600 MeV, which has been suggested as the missing member of a $3/2^-$ unitary octet containing $N_{1/2}^*(1518)$, $Y_0^*(1520)$, and $Y_1^*(1660)$. However, if a phenomenon analogous to ω - ϕ mixing in the pseudoscalar octet occurs, the $\Xi^*(1817)$ could be incorporated in the SU(3) symmetry scheme as a member of a $3/2^-$ nonet.

In another approach, Corben has recently devised a symmetry scheme based on the relativistic quantum theory of the symmetric top, in which the simplest choices of certain quantum numbers lead to a correct description of J, I, I_z, S , and P (or G) for every known strongly interacting meson or baryon state.¹⁰⁶ In this scheme, $\Xi^*(1817)$ is tentatively assigned [along with $Y_1^*(1765)$] to a multiplet having $J^P = 5/2^-$.

Our results from the analysis of $\Xi^*(1817) \rightarrow \Xi^*(1530) + \pi$ are consistent with those obtained in previous investigations. In an earlier analysis¹¹ of essentially the same data, the distribution appearing in Fig. VII-3(a) was found to be consistent with isotropy. In the same analysis, the observed branching ratios of $\Xi^*(1817)$ into $\Xi^*(1530) + \pi$, $\Lambda + \bar{K}$, and $\Xi + \pi$ were cited as evidence possibly favoring the $J^P = 3/2^-$ and $5/2^+$ hypotheses. (More recent information regarding branching ratios renders the same test somewhat less conclusive than it was considered earlier.)

In Ref. 12 Button-Shafer performed a Byers-Fenster moment analysis of $\Xi^*(1817)$ (in $K\bar{K}$ final states) decaying into $\Lambda + \bar{K}$. [We disregard a similar analysis of $\Xi^*(1817) \rightarrow \Xi + \pi$, as it is now believed that the $\Xi\pi$ enhancement near 1817 MeV may be entirely due to $\Xi^*(1933)$.]¹⁴ The analysis of $\Xi^*(1817)$ in $\Lambda K\bar{K}$ final states is complicated by the presence of interfering $\phi(1020)$ and (in $\Lambda K^0 \bar{K}^0$ final states) by the impossibility of distinguishing K^0 from \bar{K}^0 . After removal of events in the $\phi(1020)$ region, 71 events in the region $[1775 \text{ MeV} \leq m(\Lambda\bar{K}) \leq 1850 \text{ MeV}]$ were found to require spin $> 1/2$, with the hypothesis $J^P = 3/2^-$ slightly preferred over $3/2^+$. However, strong conclusions could not be drawn; i. e. "background events outside the $\Xi^*(1820)$ region also require a 'spin' greater than $1/2$, but perhaps not so firmly as do the resonant events," and "the evidence (for $J^P = 3/2^-$ over $3/2^+$) is exceedingly weak because of large background in the $\Xi^*(1820)$ decay channels."¹²

We have attempted a maximum-likelihood analysis of a somewhat larger $\Lambda K\bar{K}$ data sample than that analyzed earlier. Here we removed events containing $\phi(1020)$ by requiring $(\hat{\Lambda} \cdot \hat{\Xi}^*(1817)) \leq 0$, whereas in the previous analysis (due to statistical limitations) only events in a narrow ϕ band were removed. For 59 events in the region $[1787 \text{ MeV} \leq m(\Lambda\bar{K}) \leq 1847 \text{ MeV}]$ we obtain values of $w = \ln \mathcal{L} = 0.00, 1.01, 3.36, \text{ and } 3.66$ for $J^P = 1/2^-, 1/2^+, 3/2^+, \text{ and } 3/2^-$, respectively. An increase of 3.0 is to be expected as J is increased from $1/2$ to $3/2$, simply from the addition of six extra parameters, so that our analysis of $\Xi^*(1817) \rightarrow \Lambda + \bar{K}$ provides no spin or parity discrimination whatever. [Comparable results are obtained for background events outside the $\Xi^*(1817)$ region.]

In contrast with the earlier analysis "requiring" spin $> 1/2$, the recent analysis indicates that the spin as well as the parity of $\Xi^*(1817)$ is still an open question. [The recent analysis does not favor spin $1/2$; however, the way in which $\phi(1020)$ were removed in the earlier analysis could have produced anomalously high χ^2 values for the $J = 1/2$ hypothesis.] The $\Xi^*(1817)$ will be studied further as more data become available.

ACKNOWLEDGMENTS

I am grateful to my advisor, Dr. Janice Button-Shafer, for her interest and concern in my work, and for an unusually generous share of her time and attention. In addition, she played a central role in the design of the K-63 beam, and she is largely responsible for the data at my disposal.

I have particularly enjoyed my association with Dr. Arthur Rosenfeld, who has provided continuous support and encouragement. Dr. Peter Berge has furnished me with useful computer programs and much helpful advice. Members of the Technical Information Division staff, particularly Mrs. Ruth Gross, have assisted greatly in preparing the manuscript. Special thanks are due to Dr. Joseph Murray, who supervised the beam design and construction. The Bevatron and bubble chamber crews, and Thelonus Bonk, have provided indispensable services. I wish to thank my wife for countless hours of typing and proofreading, and for great patience.

Dr. Luis Alvarez, through rare ability and persistent effort, has created surroundings in which my graduate career has been both pleasurable and rewarding.

This work was performed under the auspices of the U. S. Atomic Energy Commission.

APPENDICES

A. Current Status of K-63 Data Analysis

The K-63 data analyzed in this report are those which were available September 1965 on the following data-summary tapes:

- 1.7 BeV/c: 814*14, 821*11, 831*6
- 2.1 BeV/c: 513*28, 525*15, 531*11, 544*4
- 2.45 BeV/c: 114*34, 125*45, 132*27
- 2.55 BeV/c: 415*30, 423*8
- 2.6 BeV/c: 311*61, 317*12, 324*39, 333*28, 339*4, 344*19, 351*6
- 2.7 BeV/c: 214*59, 232*12, 234*8, 253*8 .

Approximately 200 type-72 events were updated with additional ionization information not contained on the tapes listed.¹⁰⁷ In our analysis of the Ξ^* (1530) e. m. mass difference, only $\approx 70\%$ of the events could be used, namely those available on master PANAL tapes as of September 1965.

In Table A-I we tabulate events observed at each momentum (from first scan tallies) and events passing the selection criteria of Sec. IV. From these data one may estimate the total number of Ξ events expected in the K-63 experiment. For example, type-40 events at 1.7 BeV/c should yield approximately

$$29 \times \frac{41}{34} \times \frac{159}{134} = 42$$

unambiguous $\Xi^0 K^0$ events (by the criteria of Sec. IV), when all events have been measured, and when all Ξ^0 candidates have been processed in π -63 PACKAGE. Similarly, we have estimated the numbers of events expected to survive the additional selection criteria (K^* and Ξ^* mass limits, etc.) of Secs. VI and VII.

In Table A-II we estimate the total K-63 data available for the analysis of Ξ decay parameters, Ξ^* (1530) e. m. mass difference, etc., assuming that all selection criteria remain unchanged. Because few events have yet been measured more than once, we cannot estimate how many presently failing events will pass on subsequent measurements. Hence the estimates of total K-63 events in Table A-II are lower limits, being based on currently observed ratios of (passing events)/(events measured).

Table A-I. Status of K-63 data analysis, September 1965.

	Momentum (BeV/c)	Event type					
		72	74	12	32	40	42
Events observed	1.7	555	2	37	17 400	159	23
	2.1 ^a	769	15	135	28 300	315	41
	2.45	291	15	40	8 900	163	40
	2.55	486	35	50	17 400	299	79
	2.6	834	70	104	29 900	500	121
	2.7	479	40	31	45 500	446	132
	Total	3414	177	397	117 400	1852	436
Events measured	1.7	478	1	13	12 800	134	17
	2.1	789	17	119	17 600	311	44
	2.45	267	15	38	8 300	137	31
	2.55	463	31	48	10 000	287	69
	2.6	731	55	101	26 700	451	96
	2.7	403	28	29	14 000	365	96
	Total	3131	147	348	89 400	1685	353
Events passing any hypothesis	1.7	403	0	9	8 600	65	0
	2.1	696	4	94	13 800	193	0
	2.45	203	8	34	7 400	81	6
	2.55	327	17	32	6 800	185	12
	2.6	588	38	83	19 900	312	23
	2.7	259	11	28	11 700	227	21
	Total	2476	78	280	68 200	1063	62
Ξ candidates	1.7	387	0	9	29	41	0
	2.1	634	4	94	197	38	0
	2.45	186	8	34	87	10	5
	2.55	293	17	32	143	34	9
	2.6	504	38	83	348	36	13
	2.7	216	11	28	199	44	12
	Total	2220	78	280	1 003	203	39
Ξ candidates processed in π-63 PACKAGE	1.7				22	34	0
	2.1				128	37	0
	2.45				86	10	5
	2.55				49	26	8
	2.6				254	27	13
	2.7				188	40	11
	Total				727	174	37
Unambiguous events	1.7	354	0	9	17	29	0
	2.1	578	4	89	94	27	0
	2.45	157	7	32	56	5	3
	2.55	253	15	31	25	11	5
	2.6	409	35	73	112	10	8
	2.7	172	11	26	78	6	4
	Total	1923	72	260	382	88	20

^aSome events measured at 2.1 BeV/c do not appear on first scan tally.

Table A-II. Percentage of K-63 data analyzed.

	Total K-63 events ^a (estimate)	Events analyzed	Approximate percentage of K-63 data analyzed
Ξ^- spin and decay parameters	2800	2529	90
Ξ^0 decay parameters	850	490	60
$\Xi^*(1530)$ spin and parity	3-body	251	75
	4-body	96	85
	Total	347	80
$\Xi^*(1530)$ e. m. mass difference ^b	Ξ^{*0}	345	65
	Ξ^{*-}	355	50
	Total	700	55
$\Xi^*(1817)$ spin and parity (from $\Xi K \pi \pi$ final states)	24	20	85

^aData from 1.7 to 2.7 BeV/c, excluding 2.0 BeV/c, D_2 , and lead plate film. Beam momentum and fiducial volume criteria have not been imposed. Estimates in column 1 are lower limits, being based on currently observed ratios of (passing events)/(events measured).

^bOnly $\approx 50\%$ of the events listed are in the $\Xi^*(1530)$ resonant peak.

B. Scanning Biases and Other Systematic Errors

In this appendix we consider possible systematic errors due to the following effects:

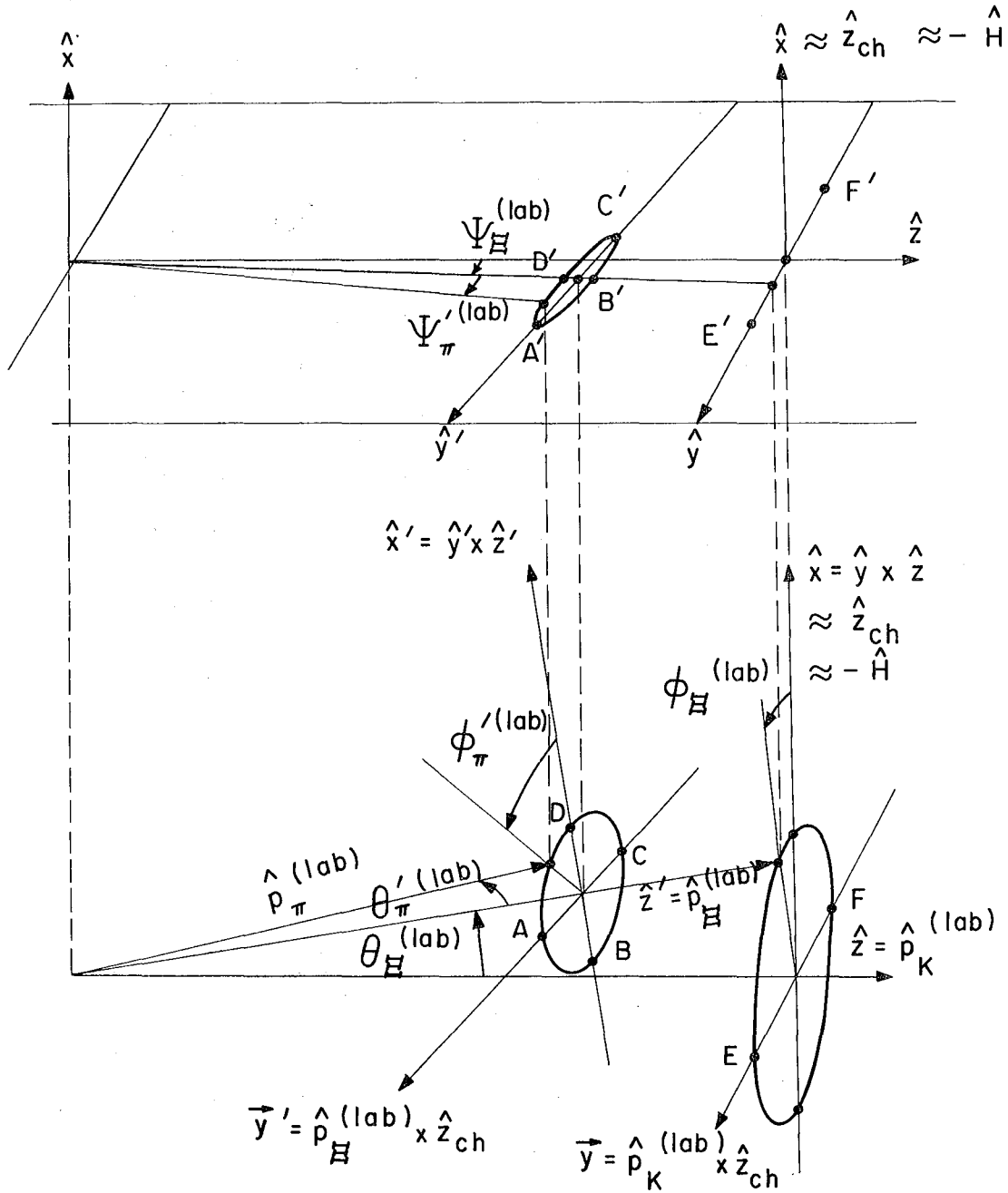
- (i) (Ξ^- only) loss of events having π^- track (from Ξ^- decay) nearly collinear with Ξ^- track;
- (ii) loss of events having short Ξ or Λ track;
- (iii) escape from chamber, prior to decay, of Ξ or Λ ;
- (iv) precession of Ξ and Λ polarization in magnetic field.

Our discussion centers on K-63 data. The same considerations apply to K-72 data, although quantitative estimates of effects such as scanning biases and escape losses are somewhat different. The most significant effect is found to be (i); observed distortions in the Ξ^- decay distribution are consistent with those expected from such an effect alone. We find (in Sec. 2 of this appendix) that weighting of Ξ^- events with an empirical factor corrects the observed distortions without altering our conclusions regarding Ξ spin and decay parameters.

In the following discussion we refer to two new coordinate systems, (x, y, z) and (x', y', z') , having their $z(z')$ axes oriented along $\hat{p}_K^{(lab)}$ and $\hat{p}_\Xi^{(lab)}$, the lab directions of the incident K^- and Ξ respectively (see Fig. B-1). We define $\vec{y} = \hat{p}_K^{(lab)} \times \hat{z}_{ch}$ and $\vec{y}' = \hat{p}_\Xi^{(lab)} \times \hat{z}_{ch}$, where \hat{z}_{ch} is the bubble chamber z -axis (essentially the optic axis and the direction of the magnetic field).¹⁰⁸ Directions of particles with respect to (x, y, z) and (x', y', z') are specified by angles (θ, ϕ) and (θ', ϕ') respectively, as illustrated for $\hat{p}_\Xi^{(lab)}$ and $\hat{p}_\pi^{(lab)}$, the lab directions of the Ξ and decay pion. Incident beam tracks are nearly horizontal in the bubble chamber (i. e., $\hat{x} \approx \hat{z}_{ch}$), so we may regard $\psi^{(lab)}$ and $\psi'^{(lab)}$ (projected angles in the y - z plane) as the projected angles (relative to $\hat{p}_K^{(lab)}$ and $\hat{p}_\Xi^{(lab)}$, respectively) seen by the scanner.

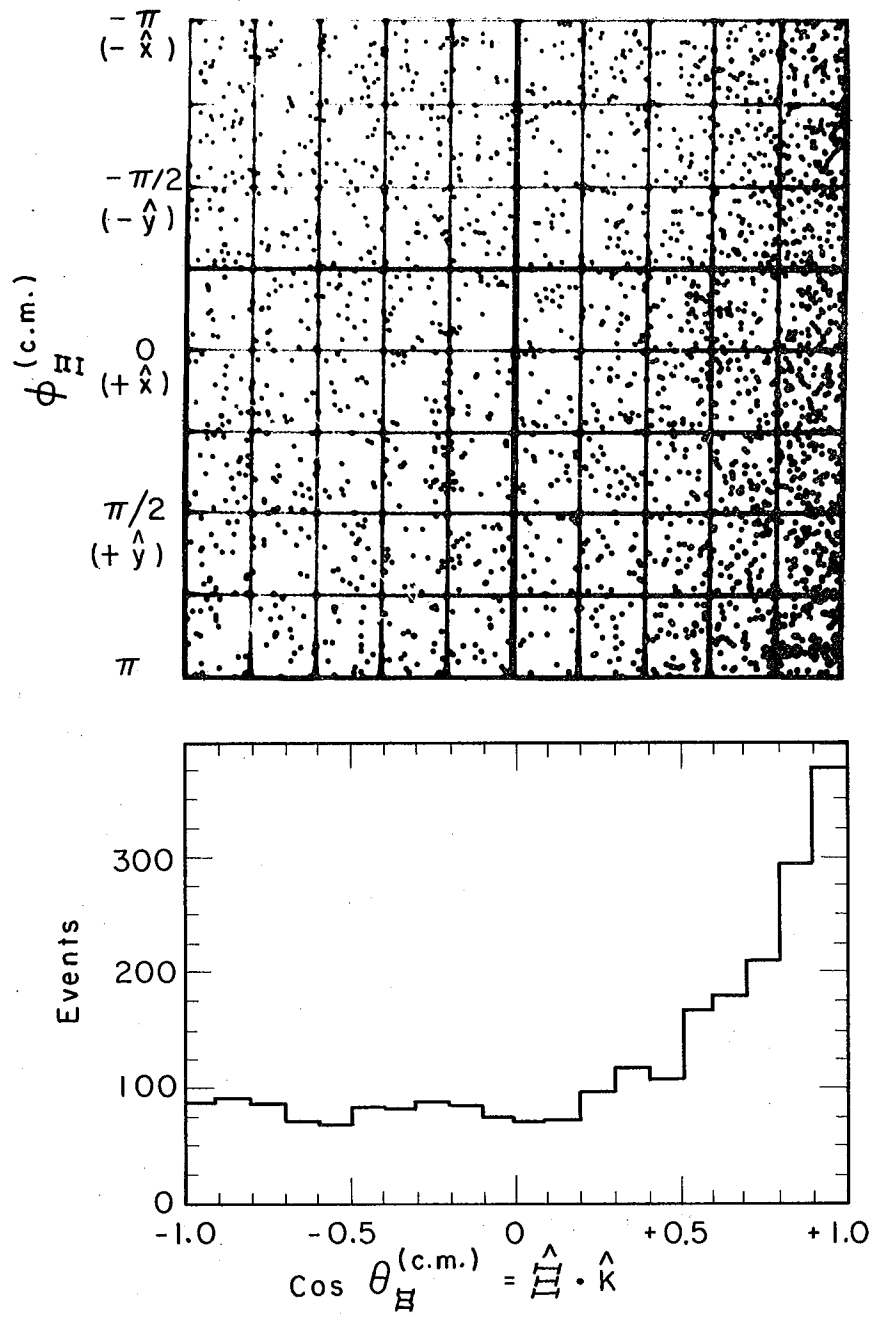
1. Causes of Systematic Errors

a. Small-angle Ξ^- decay. In Figs. B-2 and B-3 we present, for the 2529 K-63 Ξ^- events listed in Table V-I, scatter plots and projections of $\phi_\Xi^{(c.m.)}$ vs $\cos \theta_\Xi^{(c.m.)}$, angles describing Ξ production in the



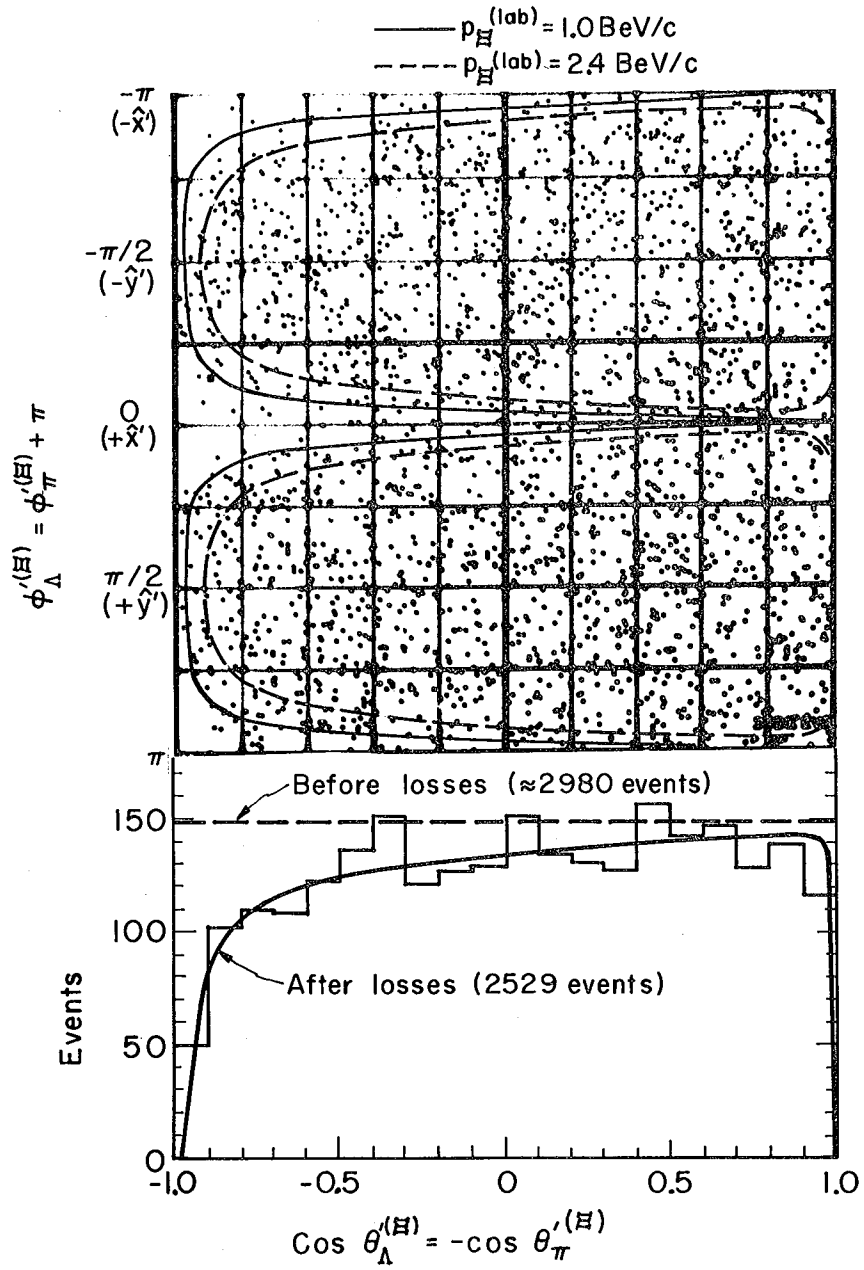
MUB13880

Fig. B-1



MUB-13881

Fig. B-2



MUB-13882

Fig. B-3

c. m. frame, relative to axes (x, y, z) ; and $\phi_{\Lambda}^{\prime(\Xi)} = (\phi_{\pi}^{\prime(\Xi)} + \pi)$ vs. $\cos \theta_{\Lambda}^{\prime(\Xi)} = -\cos \theta_{\pi}^{\prime(\Xi)}$, angles describing Ξ decay in the Ξ rest frame, relative to axes (x', y', z') . The quantity $\cos \theta_{\Xi}^{\prime(\text{c.m.})}$ is equivalent to $(\hat{\Xi} \cdot \hat{K})$ as defined by Fig. II-1; however, $\cos \theta_{\Lambda}^{\prime(\Xi)}$ is not equivalent to $(\hat{\Lambda} \cdot \hat{\Xi})$, because in Fig. B-3 we have transformed \vec{p}_{Λ} from the lab frame to the Ξ rest frame via a single Lorentz transformation along $\vec{p}_{\Xi}^{\text{(lab)}}$ (rather than through the intermediate c. m. frame).^{109, 110} In Fig. B-3, $\phi_{\Lambda}^{\prime(\Xi)} = \phi_{\Lambda}^{\prime(\text{lab})}$; i. e. $\phi_{\Lambda}^{\prime} = \tan^{-1} \left[(\hat{p}_{\Lambda} \cdot \hat{y}') / (\hat{p}_{\Lambda} \cdot \hat{x}') \right]$ is the same in the Ξ rest frame as in the lab frame.

The distribution of $\phi_{\Xi}^{\prime(\text{c.m.})}$ in Fig. B-2 is consistent with isotropy. Hence, because the Ξ can be polarized only along $\vec{n} = (\hat{K} \times \hat{\Xi})$ and because \hat{n} is uncorrelated with the bubble chamber z-axis, the distribution in Fig. B-3 should be isotropic if the Ξ has spin 1/2 and if systematic biases are absent. [Even if $J_{\Xi} > 1/2$, the distribution must be even in $\cos \theta_{\Lambda}^{\prime(\Xi)}$.]

We have sketched on the scatter plot (Fig. B-3), for $p_{\Xi}^{\text{(lab)}} = 1.0$ and 2.4 BeV/c, contours representing $\psi_{\pi}^{\prime(\text{lab})} = 5^{\circ}$, where $\psi_{\pi}^{\prime(\text{lab})}$ is the projected lab angle between the Ξ^{-} and decay pion at the Ξ^{-} decay vertex.¹¹¹ The curve in the $\cos \theta_{\Lambda}^{\prime(\Xi)}$ projection represents the expected distribution of events, calculated under the assumption that no events having $\psi_{\pi}^{\prime(\text{lab})} \leq 5^{\circ}$ are detected. The observed distribution is consistent with assumed cutoff values $[\psi_{\pi}^{\prime(\text{lab})}]_{\text{min}} = 5^{\circ} \pm 2^{\circ}$, corresponding to a 10 to 20% loss of events.

b. Short Ξ or Λ tracks. For short Ξ^{-} tracks we assume a detection efficiency of the form

$$\text{det. eff. } (\Xi^{-}) = \exp[-\ell_{\text{min}} / \ell_{\text{av}}(\Xi^{-})] \quad (\text{B-1})$$

where ℓ_{\min} is an assumed projected length cutoff, of the order of 1 cm.; $\ell_{\text{av}}^{(\Xi^-)}$ is the mean projected Ξ^- path length, given by

$$\ell_{\text{av}}^{(\Xi^-)} = \left| \frac{\vec{p}(\text{lab})}{p_{\Xi^-}} - \left(\frac{\vec{p}(\text{lab})}{p_{\Xi^-}} \cdot \hat{x} \right) \hat{x} \right| c \tau_{\Xi^-} / m_{\Xi^-} \quad (\text{B-2})$$

Similarly, we assume (for Ξ^- events) a Λ detection efficiency of the form

$$\text{det. eff. } (\Lambda) = \exp[-\ell_{\min} / \ell_{\text{av}}^{(\Lambda)}] \quad (\text{B-3})$$

and for Ξ^0 events an (approximate) overall detection efficiency of the form

$$\text{det. eff. } (\Xi^0, \Lambda) = \exp[-\ell_{\min} / \ell_{\text{av}}^{(\Xi^0 + \Lambda)}] \quad (\text{B-4})$$

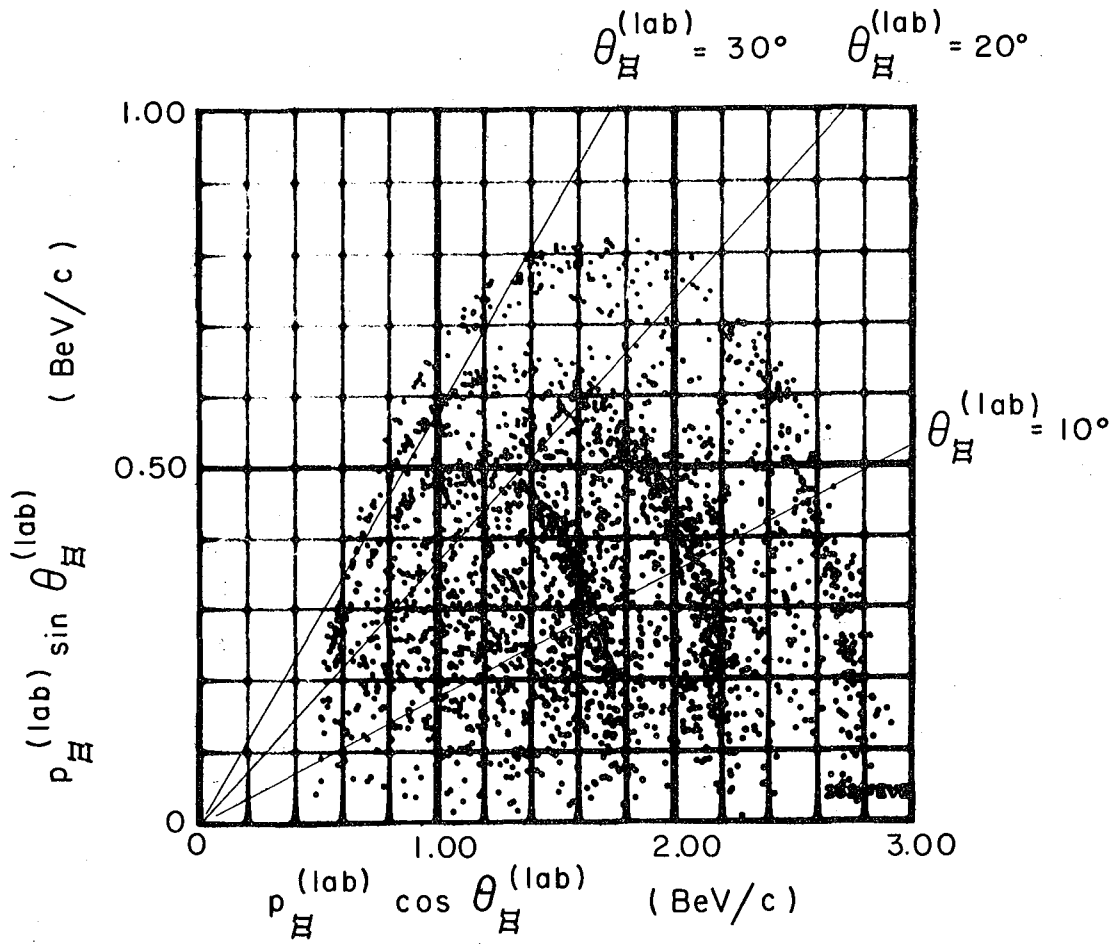
where

$$\begin{aligned} \ell_{\text{av}}^{(\Xi^0 + \Lambda)} = & \left| \left[\frac{\vec{p}(\text{lab})}{p_{\Xi^0}} - \left(\frac{\vec{p}(\text{lab})}{p_{\Xi^0}} \cdot \hat{x} \right) \hat{x} \right] c \tau_{\Xi^0} / m_{\Xi^0} \right. \\ & \left. + \left[\frac{\vec{p}(\text{lab})}{p_{\Lambda}} - \left(\frac{\vec{p}(\text{lab})}{p_{\Lambda}} \cdot \hat{x} \right) \hat{x} \right] c \tau_{\Lambda} / m_{\Lambda} \right| \quad (\text{B-5a}) \end{aligned}$$

$$\approx \left| \frac{\vec{p}(\text{lab})}{p_{\Xi^0}} - \left(\frac{\vec{p}(\text{lab})}{p_{\Xi^0}} \cdot \hat{x} \right) \hat{x} \right| c \left(\tau_{\Xi^0} + \tau_{\Lambda} \right) / m_{\Xi^0} \quad (\text{B-5b})$$

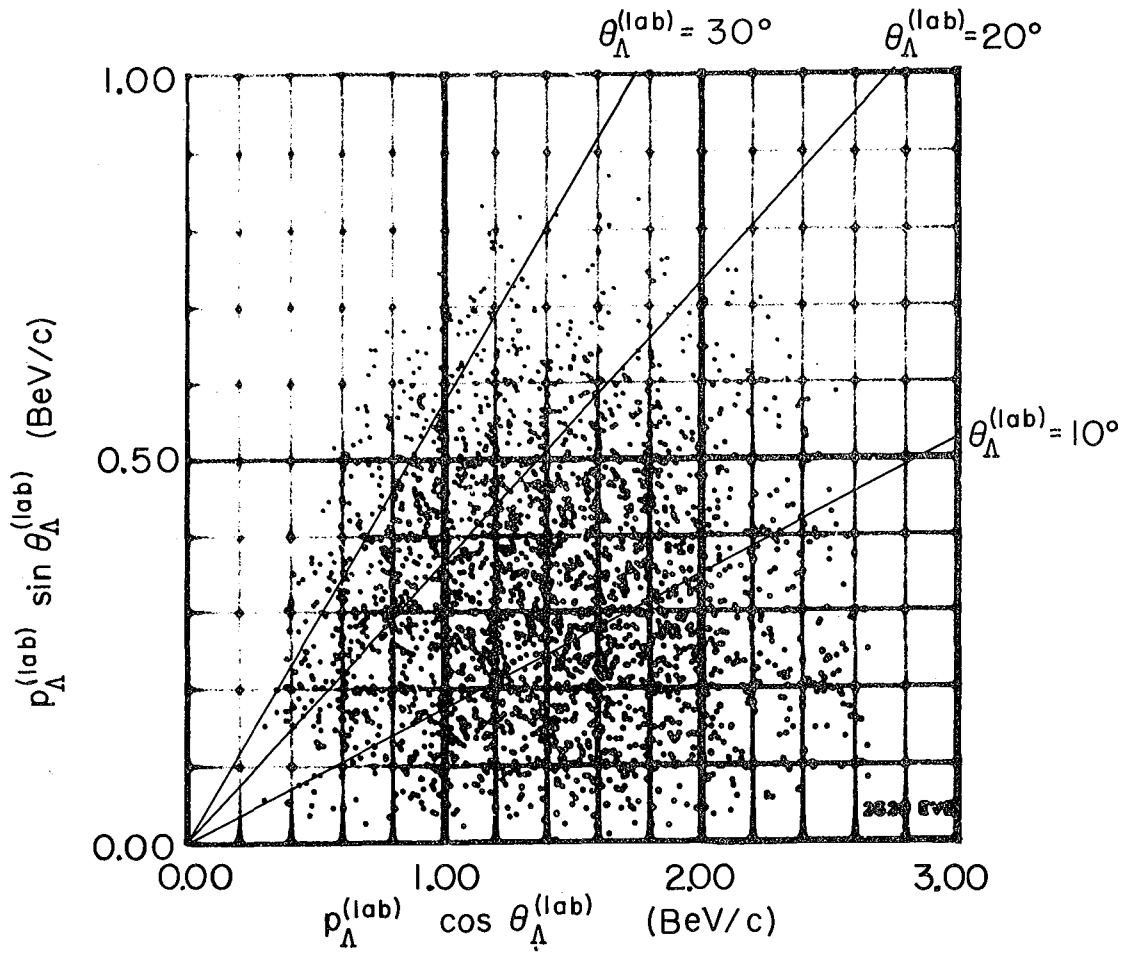
(We find the approximation $\vec{p}_{\Lambda}(\text{lab}) / m_{\Lambda} \approx \vec{p}_{\Xi^0}(\text{lab}) / m_{\Xi^0}$ to be valid to $\approx 5^\circ$ in angle and $\approx 10\%$ in magnitude.)

In Figs. B-4 and B-5 we present observed distributions of parallel and transverse Ξ and Λ momentum components (relative to the beam direction $\hat{z} = \hat{p}_K^{(\text{lab})}$) for the 2529 K-63 Ξ^- events of Table V-I. Distributions for Ξ^0 events are similar. From these data, assuming $\ell_{\min} = 1$ cm, we estimate the fractional loss of events as



MUB-13883

Fig. B-4



MUB-13884

Fig. B-5

$$\begin{aligned} \langle 1 - \text{det. eff.} \rangle &\approx 16\% \text{ for } \Xi^-, \\ &\approx 10\% \text{ for } \Lambda \text{ in } \Xi^- \text{ events, and} \\ &\approx 5\% \text{ for } \Xi^0 \text{ events.} \end{aligned}$$

These estimates exceed actual fractional losses, as the scanning detection efficiency for short Ξ^- and Λ (in K-63 Ξ^- events) is $\approx 100\%$ for Ξ^- and Λ at least as short as 1 cm.¹¹² In K-72 Ξ^- data (where we expect higher loss rates than in K-63 data), the actual loss rates for short Ξ^- and Λ (in Ξ^- events) are about 6% and 2%, respectively.⁷

Because backward-produced Ξ (and Λ from them) have small lab momenta, we expect a preferential depletion of events having $(\hat{\Xi} \cdot \hat{K}) \approx -1$. This effect in itself cannot bias the Ξ decay distribution. However, we also expect a preferential depletion of events having small values of $\cos \theta'_\Lambda(\Xi) \approx (\hat{\Lambda} \cdot \hat{K})$.¹¹⁰ Noting that $\vec{p}_\Lambda^{(\text{lab})}/m_\Lambda \approx \vec{p}_\Xi^{(\text{lab})}/m_\Xi$ and that $\gamma_\Lambda^{(\Xi)} = E_\Lambda^{(\Xi)}/m_\Lambda \approx 1$, we see that

$$p_\Lambda^{(\text{lab})} \approx p_\Lambda^{(\Xi)} \cdot \hat{p}_\Xi^{(\text{lab})} \quad (\text{B-6a})$$

$$\approx \eta_\Xi^{(\text{lab})} E_\Lambda^{(\Xi)} + \gamma_\Xi^{(\text{lab})} p_\Lambda^{(\Xi)} \cos \theta'_\Lambda(\Xi) \quad (\text{B-6b})$$

$$\approx m_\Lambda \eta_\Xi^{(\text{lab})} \left[1 + \frac{\beta_\Lambda^{(\Xi)}}{\beta_\Xi^{(\text{lab})}} \cos \theta'_\Lambda(\Xi) \right], \quad (\text{B-6c})$$

where $(\vec{\eta}_\Xi^{(\text{lab})}, \gamma_\Xi^{(\text{lab})}) = \frac{1}{m_\Xi} (\vec{p}_\Xi^{(\text{lab})}, E_\Xi^{(\text{lab})})$ and $(\vec{\eta}_\Lambda^{(\Xi)}, \gamma_\Lambda^{(\Xi)}) = \frac{1}{m_\Lambda} (p_\Lambda^{(\Xi)}, E_\Lambda^{(\Xi)})$ (with $\eta \equiv \beta\gamma$) refer to the Ξ in the lab frame and to the Λ in the Ξ rest frame, respectively. Hence

$$\text{det. eff. } (\Lambda) \approx \exp\left[-\frac{\ell_{\text{min}}}{\eta_\Lambda^{(\text{lab})}} c\tau_\Lambda\right] \text{ (if } \Lambda \text{ dip angle is ignored)} \quad (\text{B-7a})$$

$$\approx 1 - \frac{\ell_{\min}}{\eta_{\Xi}^{(\text{lab})} c \tau_{\Lambda}} \left[1 - \frac{\beta_{\Lambda}^{(\Xi)}}{\beta_{\Xi}^{(\text{lab})}} \cos \theta'_{\Lambda}(\Xi) \right]. \quad (\text{B-7b})$$

Assuming $\ell_{\min} = 1$ cm, we crudely estimate (for K-63 Ξ^{-} events)

$$\langle \text{det. eff. } (\Lambda) \rangle \approx 1 - 0.10 \left(1 - \frac{0.125}{0.8} \cos \theta'_{\Lambda}(\Xi) \right) \quad (\text{B-8a})$$

$$\approx 0.90 + 0.015 \cos \theta'_{\Lambda}(\Xi) \quad (\text{B-8b})$$

The expected asymmetry, $\langle \cos \theta'_{\Lambda}(\Xi) \rangle \approx 0.017$, is to be compared with 0.014, the statistical error for 2529 events.

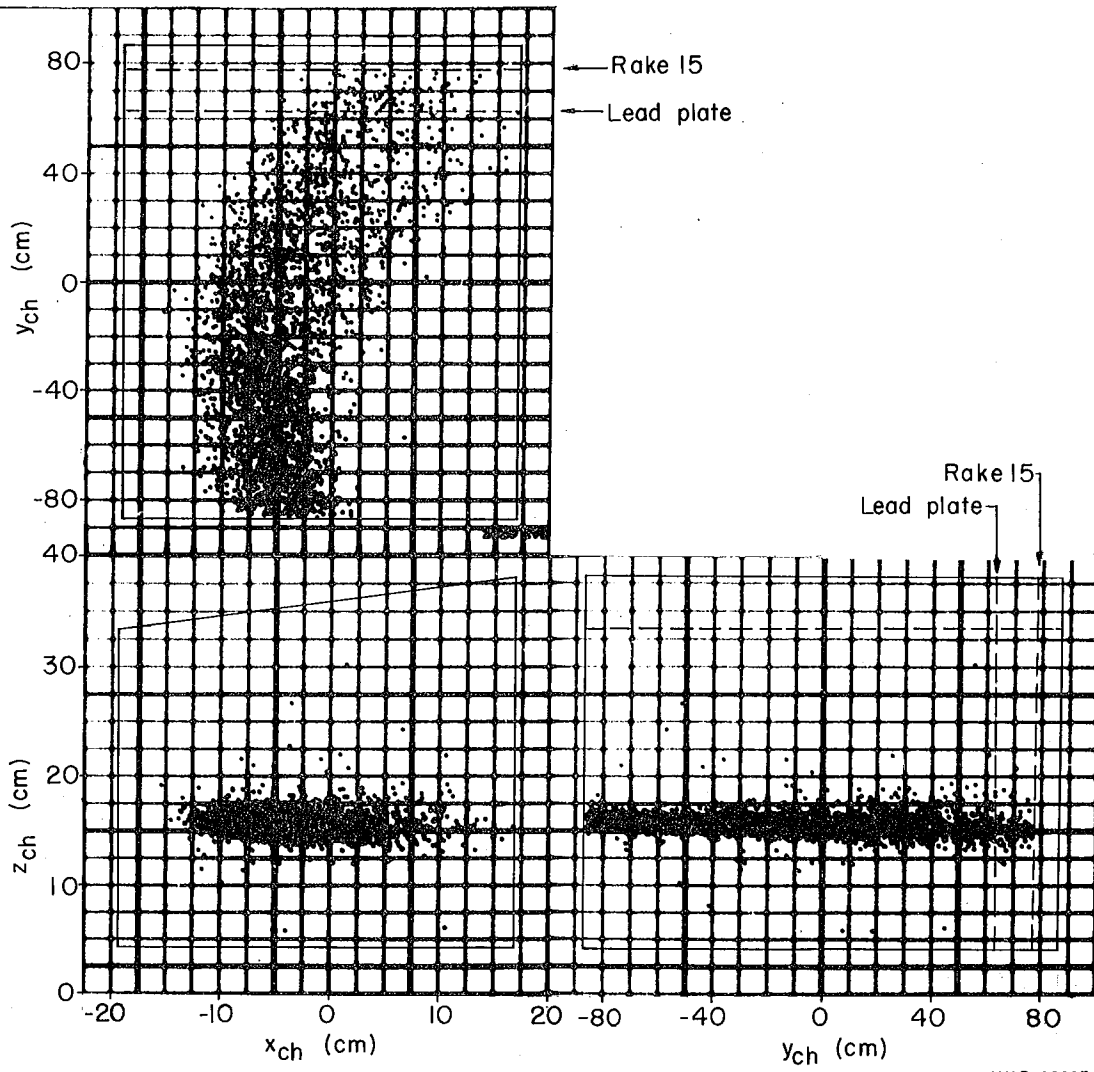
c. Escape losses. In Fig. B-6 we illustrate the position in the bubble chamber of the production vertex of the 2529 K-63 Ξ^{-} events appearing in Table V-I. Distributions for Ξ^0 events are similar. Also illustrated are the approximate limits of volume visible in all three camera views, the position of rake 15 (the scan limit), and the position of a lead plate that limited the chamber for all of the 1.7 BeV/c exposure and 37% of the 2.1 BeV/c exposure.¹¹³ (Visibility limits were estimated from blueprints and scan table measurements and then checked against distributions of the Λ decay vertex of the same Ξ^{-} events; vees from Λ decay are observed, although sparsely, as far out as the stated boundaries.)

Using the data of Fig. B-6 and the momentum distributions of Figs. B-4 and B-5, we have crudely estimated the fractional losses of Ξ and Λ through the walls of the chamber prior to decay; the results are presented in Table B-I. In the calculations, the a priori distribution of events (prior to escape losses) was assumed to be

$$\frac{dN}{dy_{\text{ch}}} \propto \exp[-y_{\text{ch}}/\ell'] , \quad (\text{B-9})$$

where ℓ' is a (momentum-dependent) effective decay length describing beam attenuation due to interaction and decay of the incident K^{-} .

Escape losses cause a preferential depletion of events having large values of $(\hat{\Xi} \cdot \hat{K})$, an effect which biases the Ξ production distribution. In the Ξ decay distribution, the estimated asymmetry in



MUB-13885

Fig. B-6

Table B-I. Estimated Ξ and Λ escape losses (percent).

Wall of chamber	Ξ^- events			Ξ^0 events			
	Ξ unseen	Ξ seen	Total	Ξ outside chamber	Ξ inside chamber	Total	
Rear and far right	with lead plate	3.6	5.3	8.9	6.2	5.3	11.5
	no lead plate	1.0	3.5	4.5	2.9	4.0	6.9
	overall ^a	1.6	4.0	5.6	3.5	4.2	7.7
Bottom	0.05	1.1	1.2	0.5	1.6	2.1	
Left	0.06	0.9	1.0	0.4	1.3	1.7	
Top	0.004	0.4	0.4	0.1	0.7	0.8	
Near right	0.004	0.4	0.4	0.1	0.7	0.8	

^a Approximately 25% of Ξ^- and 19% of Ξ^0 in our sample are from film exposed while lead plate was in place.

$\cos \theta_{\Lambda}^{\prime}(\Xi) \approx (\hat{\Lambda} \cdot \hat{K})$ resulting from the $\cos \theta_{\Lambda}^{\prime}(\Xi)$ dependence of $p_{\Lambda}^{(\text{lab})}$ (see Sec. B.1.b) is $\langle \cos \theta_{\Lambda}^{\prime}(\Xi) \rangle \approx -0.002$ (to be compared with a statistical error ≈ 0.011 .)¹¹⁰

d. Precession of Ξ and Λ polarization. As a function of time t , the precession of the polarization vector $\vec{P}(t)$ of a particle in a magnetic field \vec{H} is described by

$$\dot{\vec{P}}(t) = \frac{d\vec{P}(t)}{dt} = \vec{\omega}(t) \times \vec{P}(t). \quad (\text{B-10})$$

(Here \vec{P} is the polarization three-vector defined in the particle's rest frame, and t is measured in the lab frame.) As discussed by Simmons,¹¹⁴ the effective angular precession velocity $\vec{\omega}(t)$ may be considered as consisting of two terms:

$$\vec{\omega}(t) = \vec{\omega}_{\text{Larmor}} + \vec{\omega}_{\text{Thomas}}(t) \quad (\text{B-11})$$

$$\text{where } \vec{\omega}_{\text{Larmor}} = \frac{-\mu}{J} \frac{e p}{2 m_p c} \vec{H} \quad (\text{B-12})$$

represents the Larmor precession of a particle at rest, and

$$\vec{\omega}_{\text{Thomas}}(t) = \frac{\gamma-1}{2} \frac{1}{v} [\dot{\vec{v}}(t) \times \vec{v}(t)], \quad (\text{B-13})$$

called the Thomas precession, is a relativistic effect caused by the acceleration of the particle (if charged) in the magnetic field. Here

μ = magnetic moment in units of the Bohr nuclear magneton
 $e_p \hbar / 2 m_p c$ (e_p and m_p are the proton charge and mass),

J = spin in units of \hbar ,

γ = (total lab energy/rest mass), and

$\vec{v}(t)$ = particle velocity in the lab frame, described by

$$\dot{\vec{v}}(t) = \frac{e}{\gamma m c} \vec{v}(t) \times \vec{H},$$

where e and m are the (signed) charge and mass of the particle in question. Hence

$$\vec{\omega}(t) = C_1 \hat{H} + C_2 [\hat{H} \cdot \hat{v}(t)] \hat{v}(t), \quad (\text{B-14})$$

where¹¹⁵

$$C_1 = \left[\frac{-\mu}{2J} \frac{e_p}{m_p c} + \frac{\gamma-1}{\gamma} \frac{e}{mc} \right] H \quad (\text{B-15})$$

$$C_2 = - \left(\frac{\gamma-1}{\gamma} \right) \frac{e}{mc} H. \quad (\text{B-16})$$

Assuming for magnetic moments the mass-corrected SU(3) values¹¹⁶

$\mu_{\Xi^-} = -0.66$, $\mu_{\Xi^0} = -1.32$, and $\mu_{\Lambda} = -0.78$, one obtains

$$\text{for } \Xi^-: \quad C_1 = \left[0.66 - 0.71 \frac{\gamma-1}{\gamma} \right] \frac{e_p}{m_p c} H \quad (\text{B-17})$$

$$C_2 = \left[0.71 \frac{\gamma-1}{\gamma} \right] \frac{e_p}{m_p c} H$$

$$\text{for } \Xi^0: \quad C_1 = \left[1.32 \right] \frac{e_p}{m_p c} H; \quad C_2 = 0 \quad (\text{B-18})$$

$$\text{for } \Lambda: \quad C_1 = \left[0.78 \right] \frac{e_p}{m_p c} H; \quad C_2 = 0 \quad (\text{B-19})$$

$$\text{where } \frac{e_p}{m_p c} H = 9.58 \times 10^3 \text{ sec}^{-1} \text{ gauss}^{-1} \times 17.9 \text{ k gauss} \quad (\text{B-20a})$$

$$= 1.71 \times 10^8 \text{ sec}^{-1}. \quad (\text{B-20b})$$

Precession angles prior to decay are small (of the order of 10° or less), so to a good approximation we may ignore the variation of $\hat{v}(t)$ as a function of time; during a time interval $dt = \gamma d\tau$ (where τ is proper time), $\vec{P}(t)$ changes by approximately

$$d\vec{P} \approx \left\{ C_1 \hat{H} \times \vec{P}(0) + C_2 [\hat{H} \cdot \hat{v}(0)] \hat{v}(0) \times \vec{P}(0) \right\} dt, \quad (\text{B-21})$$

where $\hat{v}(t)$ and $\vec{P}(t)$ are evaluated at $t = 0$, the instant of Ξ production or decay, for Ξ and Λ , respectively.

(i) Precession of Ξ^- and Ξ^0 polarization. At time $t = 0$, the Ξ have direction $\hat{v}(0) = \hat{\Xi}$, and polarization $\vec{P}(0) = \vec{P}_{\Xi} = P_0 \hat{n}$ along the production normal $\hat{n} = \widehat{(\mathbf{K} \times \Xi)}$. (As in Fig. II-1, \hat{K} , $\hat{\Xi}$, and \hat{n} are defined in the production c. m.; \hat{H} is defined in the lab frame.) After an interval $dt = \gamma d\tau$, the Ξ will have acquired a longitudinal polarization component (relative to axes defined at production)¹¹⁵ given by

$$d\vec{P}_{\Xi} \cdot \hat{\Xi} = P_0 [C_1 (\hat{H} \times \hat{n} \cdot \hat{\Xi}) + C_2 (\hat{H} \cdot \hat{\Xi}) (\hat{\Xi} \times \hat{n} \cdot \hat{\Xi})] \gamma d\tau \quad (\text{B-22a})$$

$$= P_0 C_1 (\hat{H} \times \hat{n} \cdot \hat{\Xi}) \gamma d\tau \quad (\text{B-22b})$$

$$= P_0 C_1 \cos \theta_{\Xi}^{(\text{c.m.})} \cos \phi_{\Xi}^{(\text{c.m.})} \gamma d\tau, \quad (\text{B-22c})$$

and a component along $\widehat{(\Xi \times n)} = \widehat{(\Xi \times \hat{n})}$ given by

$$d\vec{P}_{\Xi} \cdot \widehat{(\Xi \times n)} = P_0 [C_1 (\hat{H} \times \hat{n}) \cdot \widehat{(\Xi \times \hat{n})} + C_2 (\hat{H} \cdot \hat{\Xi}) (\hat{\Xi} \times \hat{n}) \cdot \widehat{(\Xi \times \hat{n})}] \gamma d\tau \quad (\text{B-23a})$$

$$= P_0 (C_1 + C_2) (\hat{H} \cdot \hat{\Xi}) \gamma d\tau \quad (\text{B-23b})$$

$$= P_0 (C_1 + C_2) \sin \theta_{\Xi}^{(\text{c.m.})} \cos \phi_{\Xi}^{(\text{c.m.})} \gamma d\tau, \quad (\text{B-23c})$$

where $\theta_{\Xi}^{(\text{c.m.})}$ and $\phi_{\Xi}^{(\text{c.m.})}$ define the direction of the Ξ in the production c. m., as illustrated in Fig. B-1. As the production of events is uniform about the beam axis, the average precession angles

$$\left\langle \frac{d\vec{P}_{\Xi} \cdot \hat{\Xi}}{P_0} \right\rangle \quad \text{and} \quad \left\langle \frac{d\vec{P}_{\Xi} \cdot \widehat{(\Xi \times n)}}{P_0} \right\rangle \quad \text{are zero. From observed}$$

distributions of γ and $\theta_{\Xi}^{(\text{c.m.})}$ we estimate the rms angles

$$\langle [d\vec{P}_{\Xi} \cdot \hat{\Xi} / P_0]^2 \rangle^{1/2} \approx 1.5^\circ \text{ for } \Xi^-, \approx 7.0^\circ \text{ for } \Xi^0; \quad (\text{B-24})$$

$$\langle [d\vec{P}_{\Xi} \cdot \widehat{(\Xi \times n)} / P_0]^2 \rangle^{1/2} \approx 1.8^\circ \text{ for } \Xi^-, \approx 6.5^\circ \text{ for } \Xi^0. \quad (\text{B-25})$$

The effect of precession on measured values of $\vec{P}_{\Xi} \cdot \hat{n}$ is of the order of 0.05% and 0.7% for Ξ^- and Ξ^0 , respectively.

(ii) Precession of Λ polarization. At $t = 0$, the instant of Ξ decay, the Λ have direction $\hat{v}(0) = \hat{\Lambda}$ and polarization $\vec{P}(0) = \vec{P}_{\Lambda}$ specified by helicity components $\vec{P}_{\Lambda} \cdot \hat{\Lambda}$, $\vec{P}_{\Lambda} \cdot \hat{x}$, and $\vec{P}_{\Lambda} \cdot \hat{y}$ (\hat{x} and \hat{y} are now defined as in Fig. II-1). After a time interval $dt = \gamma d\tau$, a Λ initially having a longitudinal polarization $\vec{P}_{\Lambda} = P_0 \hat{\Lambda}$ will have acquired transverse polarization components given by

$$d\vec{P}_{\Lambda} \cdot \begin{Bmatrix} \hat{x} \\ \hat{y} \end{Bmatrix} = P_0 C_1 [\hat{H} \times \hat{\Lambda} \cdot \begin{Bmatrix} \hat{x} \\ \hat{y} \end{Bmatrix}] \gamma d\tau \quad (\text{B-26a})$$

$$= P_0 C_1 \left\{ \begin{array}{c} \text{-----} \sin \phi_{\Lambda} \cos \phi_{\Xi}^{(\text{c.m.})} \text{-----} \\ -\sin \theta_{\Lambda} \sin \phi_{\Xi}^{(\text{c.m.})} + \cos \theta_{\Lambda} \cos \phi_{\Lambda} \cos \phi_{\Xi}^{(\text{c.m.})} \end{array} \right\} \gamma d\tau,$$

(B-26b)

where $(\theta_{\Lambda}, \phi_{\Lambda})$, corresponding to (θ, ϕ) of Fig. II-1, describe the Λ direction in the Ξ rest frame. (Terms proportional to C_2 vanish for neutral particles.) Similarly, a Λ initially having polarization $P_0 \hat{x}$ will have acquired a y-component given by

$$d\vec{P}_{\Lambda} \cdot \hat{y} = P_0 C_1 [\hat{H} \times \hat{x} \cdot \hat{y}] \gamma d\tau \quad (\text{B-27a})$$

$$= P_0 C_1 [-\sin \theta_{\Lambda} \cos \phi_{\Lambda} \cos \phi_{\Xi}^{(\text{c.m.})} - \cos \theta_{\Lambda} \sin \phi_{\Xi}^{(\text{c.m.})}] \gamma d\tau.$$

(B-27b)

(Equations (B-26) and (B-27) with signs reversed represent the precession of x- and y-components onto the Λ -axis, and of the y-component onto the x-axis.) Each of the above expressions averages to zero upon integration over $\phi_{\Xi}^{(\text{c.m.})}$; were this not the case, the precession described by Eqs. (B-26) and (B-27) could result in a biased determination of a_{Ξ} and/or J_{Ξ} , and Φ_{Ξ} , respectively. Averaging each of the expressions over the observed γ and $(\theta_{\Lambda}, \phi_{\Lambda})$ distributions, we estimate the rms angles as

$$\langle [d(P_0 \hat{\Lambda}) \cdot \hat{x}/P_0]^2 \rangle^{1/2} \approx 2.9^\circ; \quad (\text{B-28})$$

$$\langle [d(P_0 \hat{\Lambda}) \cdot \hat{y}/P_0]^2 \rangle^{1/2} \approx 3.7^\circ; \quad (\text{B-29})$$

$$\langle [d(P_0 \hat{x}) \cdot \hat{y}/P_0]^2 \rangle^{1/2} \approx 3.3^\circ. \quad (\text{B-30})$$

In conclusion, the precession of the Ξ and Λ polarization has no effect on Ξ decay distributions, and a negligible effect on Ξ production distributions.

2. Empirical Scanning-Bias Correction

In Fig. B-7 we present observed distributions of $(\hat{\Lambda} \cdot \hat{K})$ and $(\hat{\Lambda} \cdot \hat{\Xi})$ for the 4080 Ξ^- and Ξ^0 events listed in Table V-I.¹¹⁷ These distributions should be isotropic if $J_\Xi = 1/2$ and if scanning biases and other systematic effects are absent. [Even if $J_\Xi > 1/2$, these distributions must be even in $(\hat{\Lambda} \cdot \hat{K})$ and $(\hat{\Lambda} \cdot \hat{\Xi})$.]

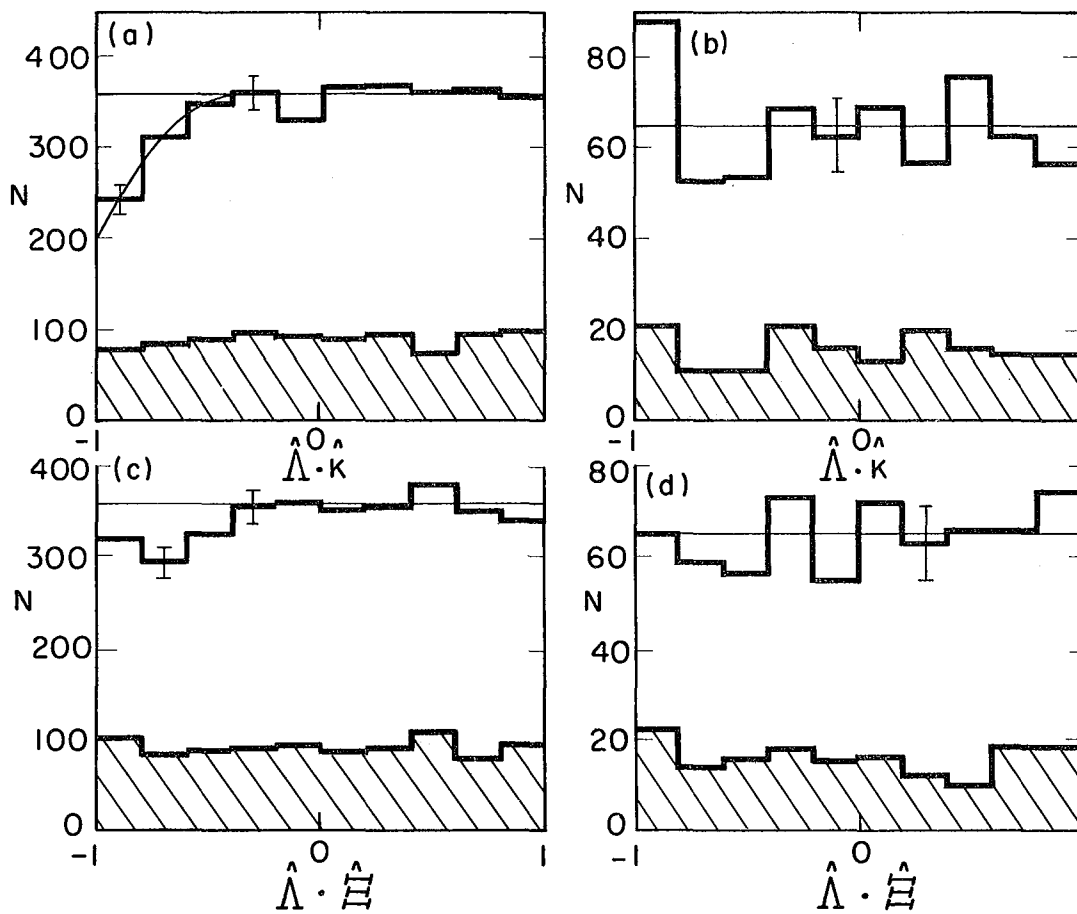
The observed anisotropy in Ξ^- events is related to the anisotropy in $\cos \theta_\Lambda^{(\Xi)}$ illustrated in Fig. B-3, and may be entirely attributed to the loss of small-angle π^- from Ξ^- decay. As would be expected from this bias, the anisotropy is most evident in $\cos \theta_\Lambda^{(\Xi)}$, less so in $(\hat{\Lambda} \cdot \hat{K})$, still less so in $(\hat{\Lambda} \cdot \hat{\Xi})$, and absent in Ξ^0 events.¹¹⁰

We have empirically corrected the $(\hat{\Lambda} \cdot \hat{K})$ anisotropy by weighting Ξ^- events with a factor

$$w(z) = [1 - C(z-z_0)^2]^{-1}, \quad (\text{B-31})$$

where $z \equiv (\hat{\Lambda} \cdot \hat{K})$, $z_0 = -0.35$, and $C = 0.50$ (1.24) for K-72 (K-63) events. (If the other biases discussed in Sec. B.1 were significant, their effects would be most evident in the $(\hat{\Lambda} \cdot \hat{K})$ distribution and would be indistinguishable from the small-angle π^- effect.) After correction, the resulting K-72 and K-63 distributions are consistent with isotropy.

In Table B-II we present measured values of a_Ξ, Φ_Ξ, t_{10}
 $= P_\Xi / \sqrt{3}$, and $X = \Delta \ln \mathcal{L} = \ln \mathcal{L}(J = 1/2) - \ln \mathcal{L}(J = 3/2)$ for the corrected and uncorrected Ξ^- events, binned in 12 subsamples as in



MUB-9193

Fig. B-7

Table B-II. Effect of Ξ^- scanning bias correction. Subsamples listed are defined in Table V-II. First and second entries for each subsample represent results of analysis before and after correction, respectively.

Subsample	N	Average weight	a_{Ξ^-}	Φ_{Ξ^-} (deg)	$t_{10} = P_{\Xi^-}/\sqrt{3}$	$X = \Delta \ln \mathcal{L}^b$
1	194	1.0 1.025	$\begin{cases} -0.467 \\ -0.459 \end{cases} \pm 0.166$	$\begin{matrix} -13 \\ -13 \end{matrix} \pm 40$	$\begin{matrix} -0.256 \\ -0.256 \end{matrix} \pm 0.098$	$\begin{matrix} 0.59 \\ 0.58 \end{matrix} \pm 0.69$
2	470	1.0 1.023	$\begin{cases} -0.317 \\ -0.315 \end{cases} \pm 0.120$	$\begin{matrix} -87 \\ -87 \end{matrix} \pm 44$	$\begin{matrix} -0.104 \\ -0.108 \end{matrix} \pm 0.072$	$\begin{matrix} 0.02 \\ 0.02 \end{matrix} \pm 0.44$
3	166	1.0 1.025	$\begin{cases} -0.514 \\ -0.524 \end{cases} \pm 0.158$	$\begin{matrix} 15 \\ 15 \end{matrix} \pm 39$	$\begin{matrix} 0.307 \\ 0.308 \end{matrix} \pm 0.101$	$\begin{matrix} 0.92 \\ 0.85 \end{matrix} \pm 0.24$
4	272	1.0 1.058	$\begin{cases} -0.537 \\ -0.529 \end{cases} \pm 0.156$	$\begin{matrix} -1 \\ 7 \end{matrix} \pm 40$	$\begin{matrix} 0.153 \\ 0.151 \end{matrix} \pm 0.080$	$\begin{matrix} -0.56 \\ -0.52 \end{matrix} \pm 0.48$
5	342	1.0 1.049	$\begin{cases} -0.428 \\ -0.438 \end{cases} \pm 0.136$	$\begin{matrix} -13 \\ -22 \end{matrix} \pm 46$	$\begin{matrix} 0.139 \\ 0.141 \end{matrix} \pm 0.076$	$\begin{matrix} 0.01 \\ -0.04 \end{matrix} \pm 0.50$
6	179	1.0 1.060	$\begin{cases} -0.182 \\ -0.168 \end{cases} \pm 0.123$	$\begin{matrix} 30 \\ 34 \end{matrix} \pm 18$	$\begin{matrix} 0.516 \\ 0.526 \end{matrix} \pm 0.107$	$\begin{matrix} 1.66 \\ 1.68 \end{matrix} \pm 1.34$
7	229	1.0 1.073	$\begin{cases} -0.274 \\ -0.268 \end{cases} \pm 0.148$	$\begin{matrix} -2 \\ -5 \end{matrix} \pm 23$	$\begin{matrix} 0.310 \\ 0.323 \end{matrix} \pm 0.106$	$\begin{matrix} -0.34 \\ -0.17 \end{matrix} \pm 0.92$
8 ^a	154	1.0 1.042	$\begin{cases} -0.423 \\ -0.369 \end{cases} \pm 0.233$	$\begin{matrix} 51 \\ -108 \end{matrix} \pm 149$	$\begin{matrix} +0.041 \\ -0.051 \end{matrix} \pm 0.121$	$\begin{matrix} -0.02 \\ 0.00 \end{matrix} \pm 0.11$
9	301	1.0 1.068	$\begin{cases} -0.314 \\ -0.300 \end{cases} \pm 0.162$	$\begin{matrix} -27 \\ -27 \end{matrix} \pm 60$	$\begin{matrix} -0.069 \\ -0.081 \end{matrix} \pm 0.089$	$\begin{matrix} -0.24 \\ -0.28 \end{matrix} \pm 0.25$
10	367	1.0 1.065	$\begin{cases} -0.563 \\ -0.562 \end{cases} \pm 0.125$	$\begin{matrix} 12 \\ 18 \end{matrix} \pm 30$	$\begin{matrix} -0.198 \\ -0.205 \end{matrix} \pm 0.072$	$\begin{matrix} -0.15 \\ -0.27 \end{matrix} \pm 0.74$
11	473	1.0 1.069	$\begin{cases} -0.496 \\ -0.481 \end{cases} \pm 0.116$	$\begin{matrix} -123 \\ -138 \end{matrix} \pm 57$	$\begin{matrix} 0.103 \\ 0.089 \end{matrix} \pm 0.065$	$\begin{matrix} 0.08 \\ 0.00 \end{matrix} \pm 0.40$
12	284	1.0 1.041	$\begin{cases} -0.375 \\ -0.339 \end{cases} \pm 0.137$	$\begin{matrix} -19 \\ -18 \end{matrix} \pm 34$	$\begin{matrix} -0.253 \\ -0.250 \end{matrix} \pm 0.091$	$\begin{matrix} 1.27 \\ 1.28 \end{matrix} \pm 0.82$
Average ^c	3277	1.0 1.051	$\begin{cases} -0.402 \\ -0.394 \end{cases} \pm 0.042$	$\begin{matrix} 1.3 \\ 0.1 \end{matrix} \pm 9.8$	$\begin{matrix} 0.027 \\ 0.024 \end{matrix} \pm 0.025$	$\begin{matrix} 3.24 \\ 3.13 \end{matrix} \pm 2.29$

^aSample #8 excluded from average. Solutions listed correspond to two different local maxima in $\ln \mathcal{L}$.

^b"Error" of X is given by $\sigma_X = (0.037N)^{1/2} |t_{10}|$. (See Sec. V. A. 3.)

^cIn calculation of average values of a_{Ξ^-} and Φ_{Ξ^-} , subsamples are weighted by $(\delta a_{\Xi^-})^{-2}$, and $(\delta \Phi_{\Xi^-})^{-2}$, respectively. Totals rather than averages are calculated for $X = \Delta \ln \mathcal{L}$.

Table V-II. Parameters were obtained from separate maximum-likelihood fits (with $L_{\max} = 1$) to the 12 subsamples; axes defining the t_{LM} were $\hat{Z} = \hat{n}$, $\hat{Y} = \hat{K}$, and $\hat{X} = \hat{K} \times \hat{n}$. Except for t_{20} and $\text{Re } t_{22}$ (in fits with $L_{\max} = 3$), which are sensitive to the $(\hat{\Lambda} \cdot \hat{K})$ anisotropy, all parameters are shifted, on the average, by amounts small compared with the statistical errors quoted in the body of this report. We conclude that the biases discussed in this appendix do not affect our conclusions regarding the Ξ spin and decay parameters. The analysis of $\Xi^*(1530)$ and $\Xi^*(1817)$ is even less likely to be affected by the same biases.

C. Checkerboard Theorem for N-Body Final States

In this appendix we prove the generalization of Capps' Checkerboard Theorem stated in Sec. II.A.3. The proof is analogous to that of Ref. 21 (unpublished appendix) for two-body final states. We shall refer to Fig. C-1, in which the c. m. momentum vectors $\vec{A}, \vec{B}, \vec{J}$, and \vec{C} , and the axis $\vec{z} = \vec{A} \times \vec{J}$ are illustrated.

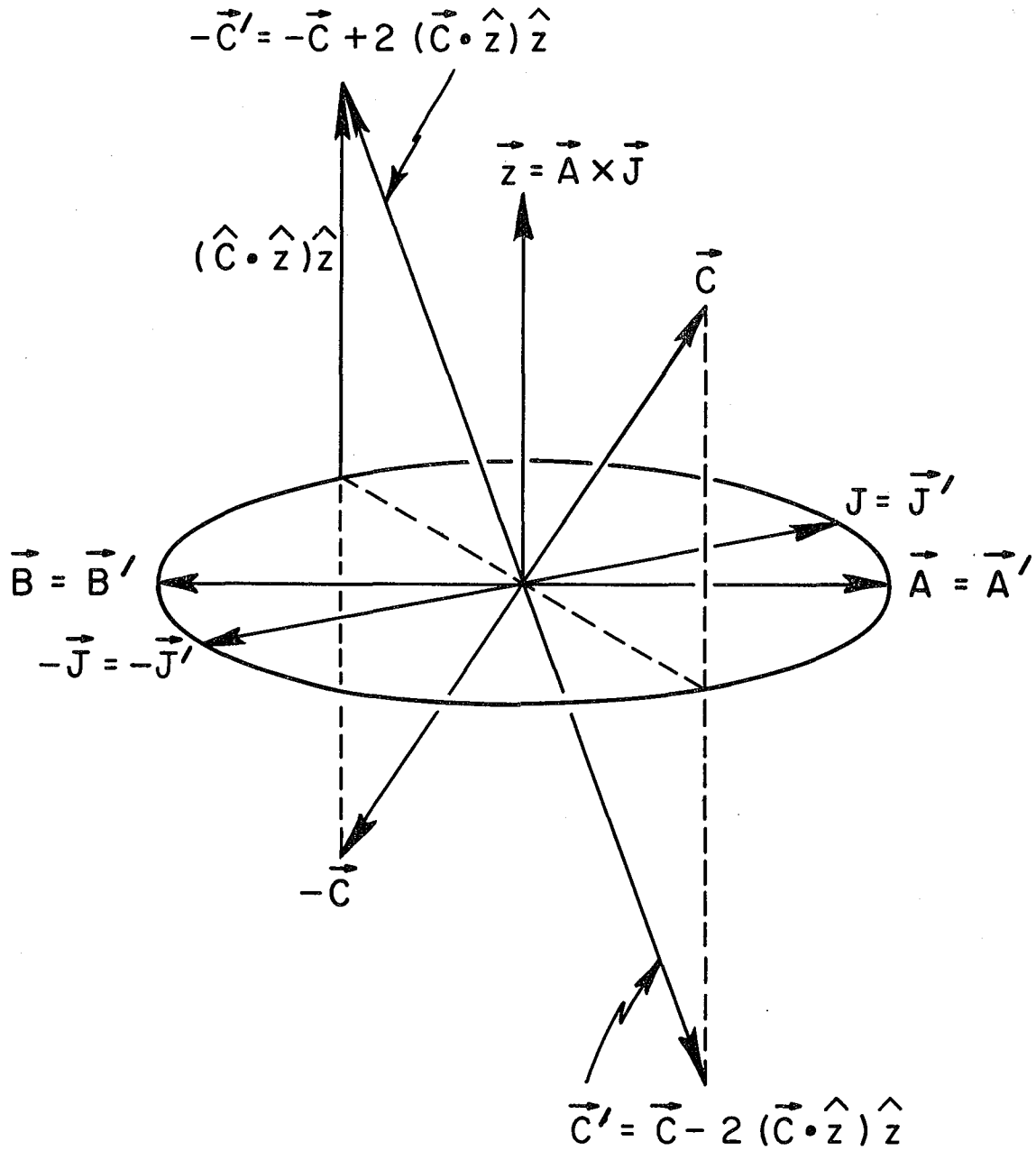
Because A and B are unpolarized and because we average over final spin states of C, D, etc., any expectation value t_{LM} (before reflection) may be regarded as a function depending only upon the c. m. momenta $\vec{A}, \vec{J}, \vec{C}, \vec{D}$, etc., i. e.,

$$t_{LM} \equiv t_{LM}(\vec{A}, \vec{J}, \vec{C}, \vec{D}, \dots) \quad (\text{C-1})$$

For an event having the configuration $(\vec{A}', \vec{J}', \vec{C}', \vec{D}', \dots)$ the corresponding expectation value is equal to the same function of the transformed momenta, i. e.,

$$t'_{LM} \equiv t_{LM}(\vec{A}', \vec{J}', \vec{C}', \vec{D}', \dots) \quad (\text{C-2})$$

We consider a transformation in which the vectors $\vec{A}, \vec{J}, \vec{C}, \vec{D}$, etc. are reflected in the x-y plane: $\vec{A} \rightarrow \vec{A}'$, $\vec{J} \rightarrow \vec{J}'$, $\vec{C} \rightarrow \vec{C}'$, $\vec{D} \rightarrow \vec{D}'$, etc., where \vec{A}' , \vec{J}' , and \vec{C}' are as illustrated in Fig. C-1. We note that $\vec{A}' = \vec{A}$ and $\vec{J}' = \vec{J}$. This transformation is equivalent to a spatial inversion, followed by a 180° rotation about the z-axis. From Fig. C-1 we see that



MUB-9855

Fig. C-1

$$t'_{LM} = t_{LM} [\vec{A}, \vec{J}, \vec{C} - 2(\vec{C} \cdot \hat{z})\hat{z}, \vec{D} - 2(\vec{D} \cdot \hat{z})\hat{z}, \dots] \quad (C-3a)$$

$$= (-)^M t_{LM} (-\vec{A}, -\vec{J}, -\vec{C}, -\vec{D}, \dots) \quad (C-3b)$$

(by the rotation transformation properties of the t_{LM}).

We define t_{LM}^P as $t_{LM}(-\vec{A}, -\vec{J}, -\vec{C}, -\vec{D}, \dots)$, the value of t_{LM} for the inverted system, whereby

$$t'_{LM} = (-)^M t_{LM}^P. \quad (C-4)$$

In general, t_{LM} and t'_{LM} differ because of the difference in the vectors \vec{C}, \vec{D} , etc.; but if one averages over the directions \vec{C}, \vec{D} , etc., any dependence upon \vec{C}, \vec{D} , etc. vanishes, so that

$$\langle t_{LM} \rangle_{C, D, \text{etc.}} = \langle t'_{LM} \rangle_{C, D, \text{etc.}} \quad (C-5)$$

(where $\langle \quad \rangle_{C, D, \text{etc.}}$ denotes an average over directions \vec{C}, \vec{D} , etc.).

Further, by the assumption of parity conservation in the production process,

$$\langle t_{LM} \rangle_{C, D, \text{etc.}} = \langle t_{LM}^P \rangle_{C, D, \text{etc.}} \quad (C-6)$$

so that

$$\langle t_{LM} \rangle_{C, D, \text{etc.}} = (-)^M \langle t'_{LM} \rangle_{C, D, \text{etc.}} \quad (C-7a)$$

$$= (-)^M \langle t_{LM} \rangle_{C, D, \text{etc.}} \quad (C-7b)$$

Hence $\langle t_{LM} \rangle_{C, D, \text{etc.}}$ can be non-zero only if M is even.

D. Approximate K-63 Path Length and Beam Contamination

In Table D-I we present rough estimates of the K-63 path length and percent beam contamination at each momentum. After a fiducial volume correction is applied, the values of K^- path length listed in Table D-I agree with values calculated independently by Lindsey.¹²¹ The K^- path length is given by

$$K^- \text{ path length (cm)} = \frac{\ell_K^{\text{decay}}(\text{cm})}{\text{BR}(3P)} \times N(3P), \quad (\text{D-1})$$

where $N(3P)$ is the total observed number of three-prong events, $\text{BR}(3P)$ is the branching ratio for K^- decay into the three-prong topology,¹²²

and $\ell_K^{\text{decay}} = \frac{p_K}{m_K} c \tau_K$ is the mean path length of a decaying K^- .

The fraction F of K^- in the beam (at the bubble chamber window) is

$$F = \left[\begin{array}{c} \text{no. of 3-prongs} \\ \text{per beam track} \\ \text{(observed)} \end{array} \right] / \left[\begin{array}{c} \text{no. of 3-prongs} \\ \text{per beam track} \\ \text{(expected)} \end{array} \right] \quad (\text{D-2a})$$

$$= \left[\frac{N(3P)}{N(\text{BT})} \right] / \left[\frac{\text{BR}(3P)}{\ell_K^{\text{decay}}} \times \ell_K^{\text{av}} \right], \quad (\text{D-2b})$$

where $N(\text{BT})$ is the total observed number of beam tracks, and ℓ_K^{av} is the average distance traveled by a K^- before it decays, interacts, or leaves the chamber. To obtain ℓ_K^{av} , let N_0 be the number of K^- beam tracks entering the chamber, so that $N(x) = N_0 e^{-x/\ell_K^{\text{av}}}$ is the number of beam tracks remaining after distance x , where

$$(\ell_K^{\text{av}})^{-1} = \left(\ell_K^{\text{decay}} \right)^{-1} + \rho \sigma_{K^- p}$$

is an effective decay rate for K^-

(including attrition due to $K^- p$ interactions, corrected for unseen small-angle scatters) and ρ (in cm^{-3}) is the proton density in the bubble chamber. By definition,

Table D-I. Approximate K-63 path length and percent beam contamination.

		Momentum (BeV/c) ^a						
		1.71 ± 0.04	2.097 ± 0.038	2.435 ± 0.045	2.584 ± 0.024	2.610 ± 0.034	2.700 ± 0.034	Total
Data used	Total rolls	249	235	143	245	335	204	1384
	Frames/roll ^b	669 ± 17 ^d	663 ± 2	595 ± 2	649 ± 2	603 ± 2	592 ± 4	
	Beam tracks/frame ^c	7.0 ± 1.0 ^d	9.5 ± 0.5	7.1 ± 0.5	6.4 ± 0.5	8.2 ± 0.5	8.5 ± 0.5	
	N(3P) = observed 3-prong events ^e	5042	6442	1859	3431	5814	2912	25,500
	σ_{K^-p} corrected (mb) ^f	30.9 ± 0.7	27.5 ± 0.6	25.6 ± 0.6	25.1 ± 0.6	25.0 ± 0.6	24.7 ± 0.6	
	σ_{π^-p} corrected (mb) ^g	31.6 ± 0.7	33.0 ± 0.6	31.9 ± 0.6	31.2 ± 0.6	31.1 ± 0.6	30.8 ± 0.6	
Results	L (cm) ^h	151 ± 5	160 ± 4	165 ± 3	165 ± 3	165 ± 3	165 ± 3	
	K^- path length (events/ μ b) ^j	3.83 ± 0.21	6.00 ± 0.32	2.01 ± 0.10	3.93 ± 0.20	6.74 ± 0.34	3.50 ± 0.18	26.0 ± 1.4
	Effective π^- path length (events/ μ b) ^j	1.1 ± 0.9	1.3 ± 0.6	0.5 ± 0.2	1.4 ± 0.5	1.8 ± 0.6	1.8 ± 0.4	7.9 ± 3.2
	% Non- K^- background ^k	22 ± 17	18 ± 7	18 ± 8	25 ± 9	21 ± 7	34 ± 7	23 ± 9

^aSee Ref. 118.

^bFrom first scan sheets (Colette B. Merrill, April 1965).

^cFrom beam scan sheets (Jay Kahn, April 1965).

^dIncomplete data at 1.7 BeV/c.

^eFrom first scan tallies, June 1966.

^fInterpolated values from Ref. 119, decreased by 23 ± 5% of K^-p elastic cross section to correct for unseen small angle scatters (Gerald Lynch, private communication).

^gInterpolated values from Ref. 120, decreased by 8.0 ± 0.5% to correct for unseen small angle scatters (Lyndon Hardy, private communication).

^hScanned length of bubble chamber (-86 cm ≤ y_{ch} ≤ 78 cm), corrected for track curvature. A lead plate at $y_{ch} = 63$ cm limited the chamber for all of the 1.7 BeV/c and 37% of the 2.1 BeV/c exposure. About half of the tracks at 1.7 BeV/c exit through the side wall of the chamber.

^jPath lengths correspond to entire scanned length of bubble chamber.

^kFraction of non- K^- entering chamber.

$$\ell_K^{av} = (K^- \text{ path length})/N_0 \quad (D-3a)$$

$$= \frac{1}{N_0} \int_0^L N(x) dx \quad (D-3b)$$

$$= \int_0^L e^{-x/\ell'_K} dx \quad (D-3c)$$

$$= \ell'_K \left[1 - e^{-L/\ell'_K} \right], \quad (D-3d)$$

where L is the scanned length of a beam track in the bubble chamber. If all the beam contamination is π^- , the K^- and π^- path lengths are related by

$$\frac{\pi^- \text{ path length}}{K^- \text{ path length}} = \frac{1 - F}{F} \times \frac{\ell_\pi^{av}}{\ell_K^{av}}, \quad (D-4)$$

where ℓ_π^{av} is defined for π^- exactly as ℓ_K^{av} for K^- . In our calculation the following constants were used:

$$\tau_K = 1.229 \pm 0.008 \times 10^{-8} \text{ sec}$$

$$\tau_\pi = 2.551 \pm 0.026 \times 10^{-8} \text{ sec}$$

$$BR(3P) = 0.0588 \pm 0.0017$$

$$\rho = 0.350 \times 10^{23} \text{ cm}^{-3},$$

in addition to data appearing in Table D-I. Estimates of $N(BT)$ were obtained from separate estimates at each momentum of rolls scanned, frames/roll, and beam tracks/frame.

Approximate effective path lengths (e. g., for comparison with the entries of Table V-I) may be estimated as ¹²³

$$\begin{aligned}
 \left[\begin{array}{l} \text{effective path} \\ \text{length} \end{array} \right] &\approx \left[\begin{array}{l} \text{K}^- \text{ path} \\ \text{length} \end{array} \right] \quad (\text{Table D-I}) \\
 &\times \frac{\left[\begin{array}{l} \text{events passing} \\ \text{any hypothesis} \end{array} \right]^{124}}{\left[\begin{array}{l} \text{events observed} \end{array} \right]} \quad (\text{Table A-I}) \\
 &\times \frac{\left[\begin{array}{l} \Xi^- \text{ candidates (4/65)} \end{array} \right] (\text{Table V-I})^{125}}{\left[\begin{array}{l} \Xi^- \text{ candidates (9/65)} \end{array} \right]} \quad (\text{Table A-I}) \\
 & \hspace{15em} (\text{D-5})
 \end{aligned}$$

For example, for event-type 72 at 4.7 BeV/c,

$$\begin{aligned}
 \left[\begin{array}{l} \text{effective} \\ \text{path length} \end{array} \right] &\approx 3.83 \text{ events}/\mu\text{b} \\
 &\times \frac{403}{455} \\
 &\times \frac{(272 + 31 + 54 = 357)}{387} \hspace{10em} (\text{D-6a})
 \end{aligned}$$

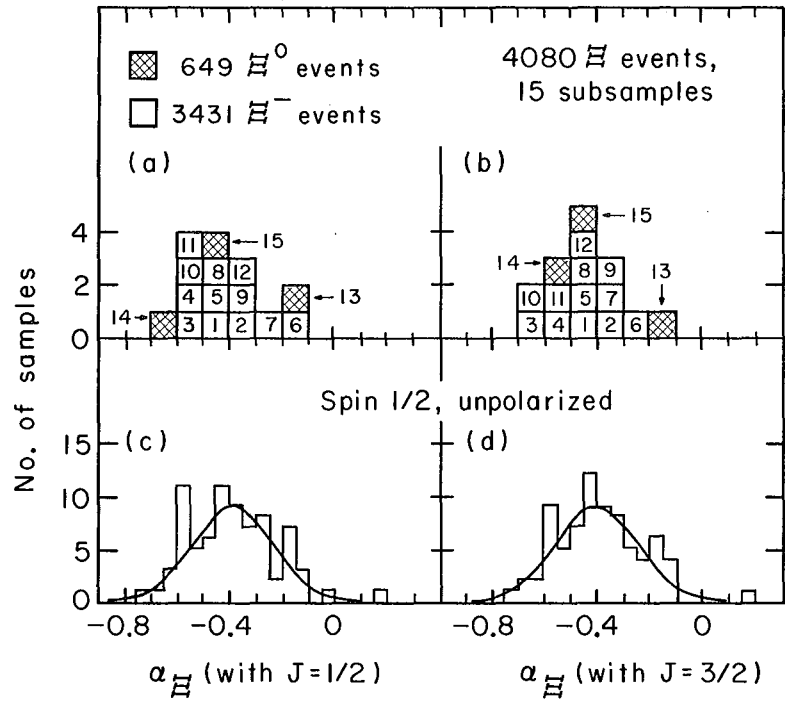
$$\approx 2.6 \text{ events}/\mu\text{b}; \hspace{10em} (\text{D-6b})$$

so that

$$\sigma(\text{K}^- \text{p} \rightarrow \Xi^- \text{K}^+) \approx 3/2 \times \frac{272}{2.6 \text{ events}/\mu\text{b}} \approx 160 \mu\text{b}. \quad (\text{D-7})$$

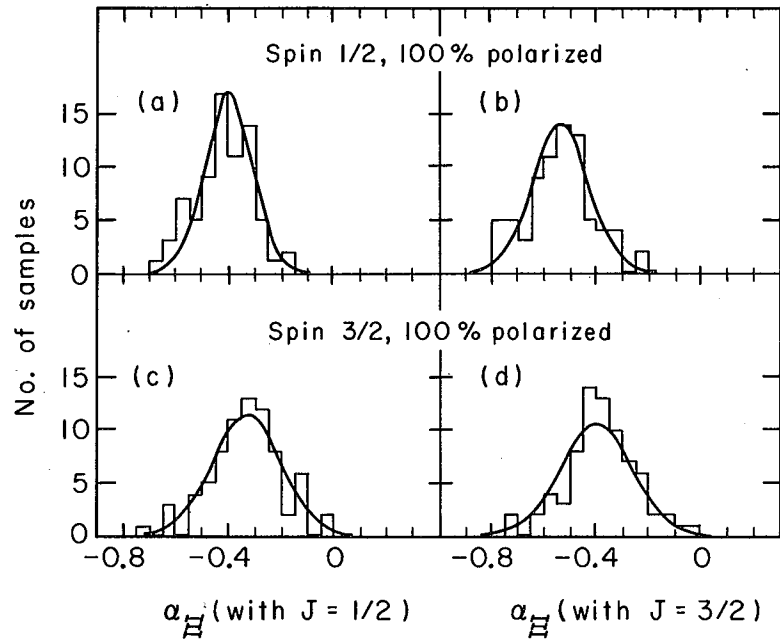
E. Analysis of Monte Carlo Events

The maximum-likelihood programs used in this analysis were checked by generating and analyzing samples of Monte Carlo events.¹²⁶ In Figs. E-1 through E-6 we present distributions of observed values of a_{Ξ^-} , Φ_{Ξ^-} , and t_{10} for the 15 Ξ^- and Ξ^0 subsamples of Table V-II, and for the three sets of Monte Carlo events described in Section V.A.3. In Table E-I we specify the fixed and variable parameters in the various fits. Values listed for variable parameters and their errors, corresponding to the curves plotted in Figs. E-1 through E-6, are averages of values calculated for the individual 272-event Monte Carlo samples. Agreement between the observed distributions and plotted curves



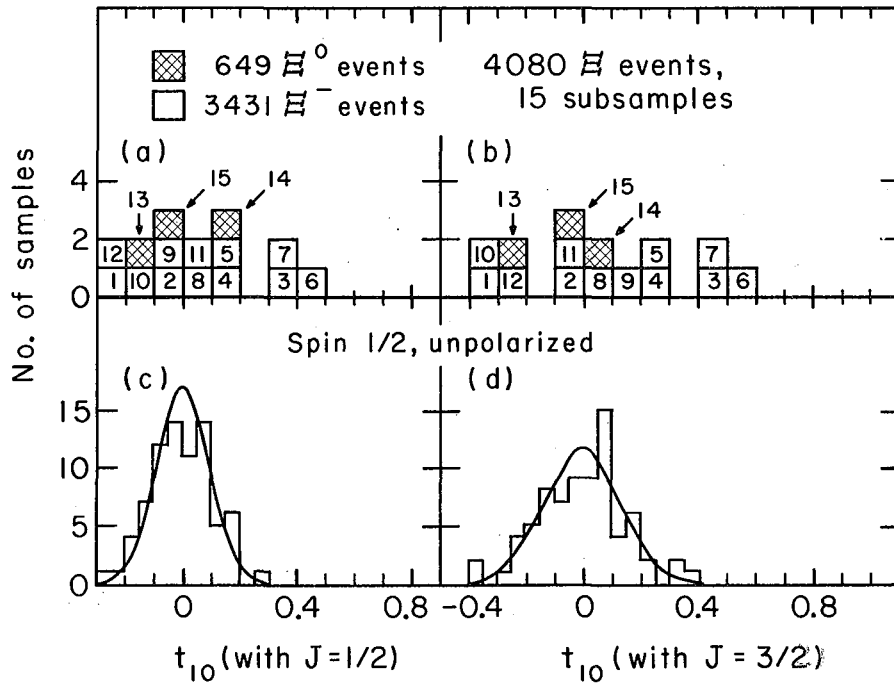
MU-36856

Fig. E-1



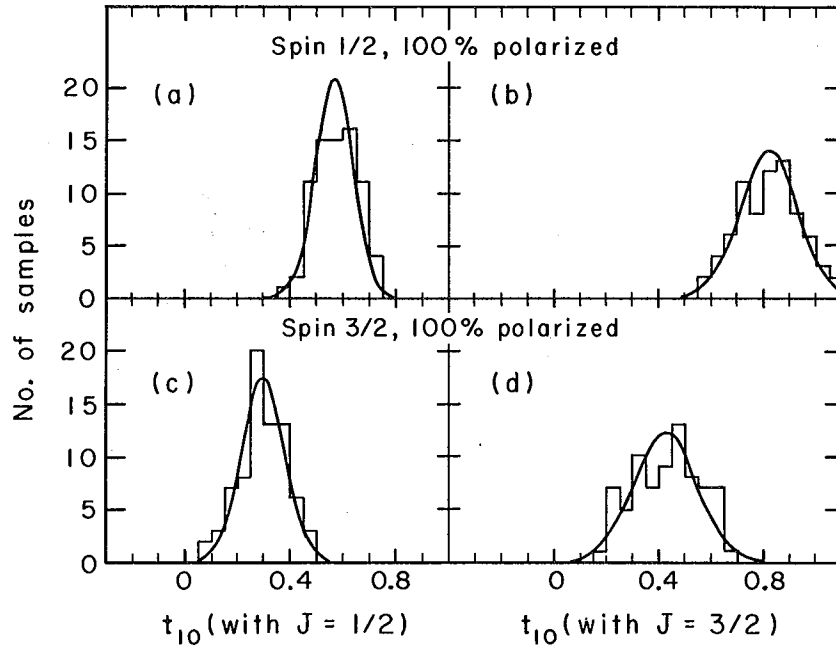
MU-36857

Fig. E-2



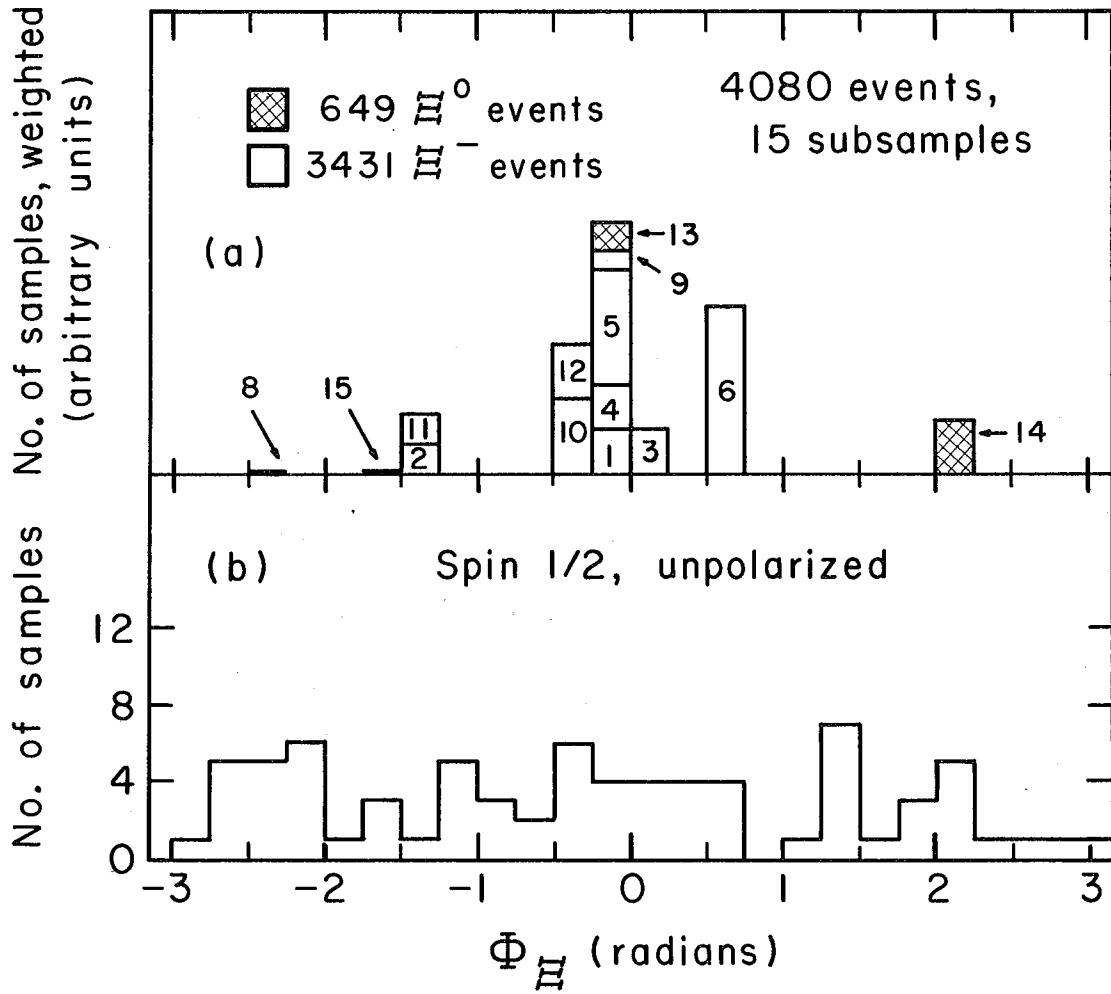
MU-36858

Fig. E-3



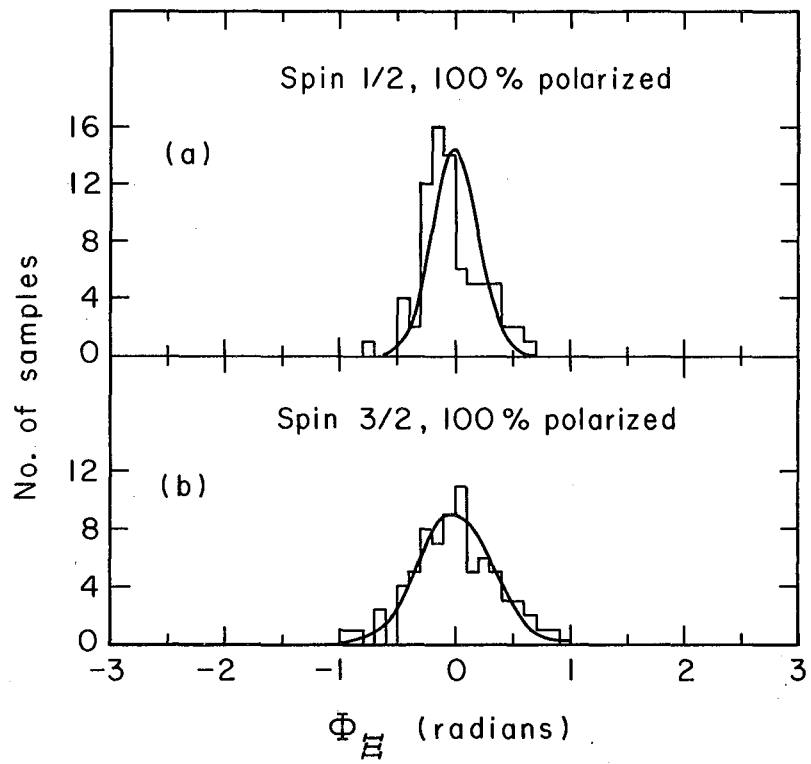
MU-36859

Fig. E-4



MUB 13652

Fig. E-5



MU-36861

Fig. E-6

Table E-1. Analysis of Monte Carlo events.

Fig.	Sample ^a	Parameter Investigated	Fixed parameters in fits ^b			Curves illustrated	
			J	a_{Ξ}	Φ_{Ξ}		
E-1	(a) Ξ data	a_{Ξ}	1/2	--	0	--	--
	(b) Ξ data	a_{Ξ}	3/2	--	0	--	--
	(c) S1	a_{Ξ}	1/2	--	0	$\langle a_{\Xi} \rangle = -0.40$	$\langle (\delta a_{\Xi})^2 \rangle^{1/2} = 0.16$
	(d) S1	a_{Ξ}	3/2	--	0	$\langle a_{\Xi} \rangle = -0.40$	$\langle (\delta a_{\Xi})^2 \rangle^{1/2} = 0.17$
E-2	(a) S2	a_{Ξ}	1/2	--	0	$\langle a_{\Xi} \rangle = -0.40$	$\langle (\delta a_{\Xi})^2 \rangle^{1/2} = 0.09$
	(b) S2	a_{Ξ}	3/2	--	0	$\langle a_{\Xi} \rangle = -0.54$	$\langle (\delta a_{\Xi})^2 \rangle^{1/2} = 0.11$
	(c) S3	a_{Ξ}	1/2	--	0	$\langle a_{\Xi} \rangle = -0.33$	$\langle (\delta a_{\Xi})^2 \rangle^{1/2} = 0.13$
	(d) S3	a_{Ξ}	3/2	--	0	$\langle a_{\Xi} \rangle = -0.40$	$\langle (\delta a_{\Xi})^2 \rangle^{1/2} = 0.14$
E-3	(a) Ξ data	t_{10}	1/2	--	0	--	--
	(b) Ξ data	t_{10}	3/2	--	0	--	--
	(c) S1	t_{10}	1/2	--	0	$\langle t_{10} \rangle = 0.00$	$\langle (\delta t_{10})^2 \rangle^{1/2} = 0.09$
	(d) S1	t_{10}	3/2	--	0	$\langle t_{10} \rangle = 0.00$	$\langle (\delta t_{10})^2 \rangle^{1/2} = 0.13$
E-4	(a) S2	t_{10}	1/2	--	0	$\langle t_{10} \rangle = 0.57$	$\langle (\delta t_{10})^2 \rangle^{1/2} = 0.07$
	(b) S2	t_{10}	3/2	--	0	$\langle t_{10} \rangle = 0.82$	$\langle (\delta t_{10})^2 \rangle^{1/2} = 0.11$
	(c) S3	t_{10}	1/2	--	0	$\langle t_{10} \rangle = 0.30$	$\langle (\delta t_{10})^2 \rangle^{1/2} = 0.09$
	(d) S3	t_{10}	3/2	--	0	$\langle t_{10} \rangle = 0.43$	$\langle (\delta t_{10})^2 \rangle^{1/2} = 0.12$
E-5	(a) Ξ data	Φ_{Ξ}	1/2	-0.40	--	--	--
	(b) S1	Φ_{Ξ}	1/2	-0.40	--	--	--
E-6	(a) S2	Φ_{Ξ}	1/2	-0.40	--	$\langle \Phi_{\Xi} \rangle = 0^\circ$	$\langle (\delta \Phi_{\Xi})^2 \rangle^{1/2} = 12^\circ$
	(b) S3	Φ_{Ξ}	3/2	-0.40	--	$\langle \Phi_{\Xi} \rangle = 0^\circ$	$\langle (\delta \Phi_{\Xi})^2 \rangle^{1/2} = 19^\circ$

^aThe Ξ data are the 15 subsamples defined in Table V-II. The Monte Carlo samples S1, S2, and S3 were generated under the assumptions (S1) $J = 1/2$, $t_{10} = 0$; (S2) $J = 1/2$, $t_{10} = t_{10}^{\max} = 0.57$; (S3) $J = 3/2$, $t_{10} = t_{10}^{\max} = 0.43$. All Monte Carlo samples (S1, S2, S3) are in 272-event subsamples having $a_{\Lambda} = 0.62$, $a_{\Xi} = -0.40$, $\Phi_{\Xi} = 0$.

^bAll fits assume $a_{\Lambda} = 0.62$.

illustrates that a_{H} , Φ_{H} , and t_{10} are correctly calculated, and that the calculated error δx (for $x = a_{\text{H}}, \Phi_{\text{H}}, t_{10}$) corresponds to the rms deviation of independent measurements of x , i. e.,

$$\langle (\delta x)^2 \rangle = \langle (x - \langle x \rangle)^2 \rangle = \langle x^2 \rangle - \langle x \rangle^2. \quad (\text{E-1})$$

Similarly, we find that the parameters t_{2M} and t_{3M} (and corresponding errors) are correctly estimated by our maximum-likelihood programs.

Further checks demonstrated that the two maximum-likelihood programs used (one written by the author and Morris¹²⁷ and the other by Berge) yield identical results. The results are also in agreement with a moment-projection program written by Shafer.¹²⁸

FOOTNOTES AND REFERENCES

1. R. Armenteros, K. H. Barker, C. C. Butler, A. Cachon, and C. M. York, *Phil. Mag.* 43, 597 (1952); E. W. Cowan, C. D. Anderson, R. B. Leighton, and V. A. J. Van Lint, *Phys. Rev.* 92, 1089 (1953); R. Armenteros, B. Gregory, A. Lagarrigue, L. Leprince-Ringuet, F. Muller, and C. Peyrou, *Nuovo Cimento Suppl.* (9) 12, 327 (1954).
2. L. W. Alvarez, P. Eberhard, M. Good, H. K. Ticho, and S. G. Wojcicki, *Phys. Rev. Letters* 2, 215 (1959).
3. Murray Gell-Mann, *The Eightfold Way: A Theory of Strong Interaction Symmetry*, in *The Eightfold Way*, M. Gell-Mann and Y. Ne'eman, Ed. (W. A. Benjamin, Inc., New York, 1964), p. 11.
4. Y. Ne'eman, *Nucl. Phys.* 26, 222 (1961).
5. F. Gürsey and L. A. Radicati, *Phys. Rev. Letters* 13, 173 (1964).
6. A. Pais, *Phys. Rev. Letters* 13, 175 (1964).
7. J. Peter Berge, Philippe Eberhard, J. Richard Hubbard, Deane W. Merrill, Janice B. Shafer, Frank T. Solmitz, and M. Lynn Stevenson, *Phys. Rev.* 147, 945 (1966).
8. J. Richard Hubbard, *Properties of the Neutral Cascade Hyperon* (Ph.D. thesis), UCRL-11510, April 1966.
9. Janice Button-Shafer and Deane W. Merrill, *Spin and Decay Parameters of the Ξ^- Hyperon*, UCRL-11884, Jan. 1965.
10. P. Eberhard, J. Button-Shafer, and D. Merrill, *Decay Properties of the Ξ^- Hyperon*, UCRL-11427, July 1964.
11. Gerald A. Smith, James S. Lindsey, Joseph J. Murray, Janice Button-Shafer, Angela Barbaro-Galtieri, Orin I. Dahl, Philippe Eberhard, William E. Humphrey, George R. Kalbfleisch, Ronald R. Ross, Frank T. Shively, and Robert D. Tripp, *Phys. Rev. Letters* 13, 61 (1964).
12. Gerald A. Smith, James S. Lindsey, Janice Button-Shafer, and Joseph J. Murray, *Phys. Rev. Letters* 14, 25 (1965).
13. Janice Button-Shafer, James S. Lindsey, Joseph J. Murray, and Gerald A. Smith, *Phys. Rev.* 142, 883 (1966).

14. Gerald A. Smith and James S. Lindsey, Final-State Interaction Involving Hyperons, in Proceedings of the Second Topical Conference on Recently Discovered Resonant Particles, Ohio University, Athens, Ohio, June 1965 (Ohio University Press, Athens, Ohio, 1965) p. 251; and UCRL-16162, June 1965.
15. J. Badier et al., *Physics Letters* 16, 171 (1965); and J. Badier et al., $B = 1$, $S = -2$ States in K^-p Interactions at 3 GeV/c, in Proceedings of the International Conference on High-Energy Physics, Dubna, USSR, 1964 (Atomizdat, Moscow, 1966), Vol. I, p. 593.
16. A. Halsteinslid et al., Preliminary Results on $\Xi^- + K^{0,+} + n(\pi)$ Final States Produced by 3.5 GeV/c K^- , in Proceedings of the Sienna International Conference on Elementary Particles, Sienna, Italy, 1963 (Società Italiana di Fisica, Bologna, Italy, 1963), Vol. I, p. 173.
17. A. H. Rosenfeld, A. Barbaro-Galtieri, W. H. Barkas, P. L. Bastien, J. Kirz, and M. Roos, Data on Elementary Particles and Resonant States, UCRL-8030 (Part I) Rev., August 1965.
18. M. Ademollo and R. Gatto, *Phys. Rev.* 133, B531 (1964).
19. R. Gatto and H. P. Stapp, *Phys. Rev.* 121, 1553 (1961).
20. R. H. Capps, *Phys. Rev.* 122, 929 (1961).
21. N. Byers and S. Fenster, *Phys. Rev. Letters* 11, 52 (1963), and unpublished appendix of Byers and Fenster, Dept. of Physics, University of California, Los Angeles, May 1963.
22. Janice Button-Shafer, *Phys. Rev.* 139, B605 (1965).
23. Charles Zemach, *Phys. Rev.* 140, B109 (1965).
24. S. M. Berman and M. Jacob, Spin and Parity Analysis in Two-Step Decay Processes, Stanford Linear Accelerator Center Report SLAC-43 (Stanford University, Stanford, California, May 1965).
25. Henry P. Stapp, Relativistic Transformation of Spin Directions, UCRL-8096, December 1957.
26. Consider a momentum four-vector (\vec{p}, E) in frame 1, having velocity $\vec{v} = \beta c$ relative to frame 2. Mathematically, the direct Lorentz transformation corresponds to (i) a rotation to align \vec{v}

with the z -axis; (ii) a Lorentz transformation along the z -axis (p_x and p_y are unchanged); (iii) the inverse of the rotation in (i). If this prescription is followed, components of vectors in frames 1 and 2 refer to the same coordinate system, so that scalar products may be calculated in the usual fashion.

27. W. S. C. Williams, An Introduction to Elementary Particles (Academic Press, New York, 1961), pp. 173-174; and Janice Button, Use of the Density Matrix and Scattering Matrix in Calculating Intensities and Polarizations in Some General Types of Interactions, Alvarez Group Physics Memo 337, September 1961.
28. T. D. Lee and C. N. Yang, Phys. Rev. 109, 1755 (1958).
29. Richard H. Capps, Phys. Rev. 122, 929 (1961).
30. Our definition of the $B_{m_1 m_2}^J$ functions corresponds to that of Ref. 31.
31. M. Jacob and G. C. Wick, Ann. Phys. 7, 404 (1959).
32. See Ref. 22, Eq. (3).
33. See Ref. 22, Eq. (38).
34. See Ref. 22, Eq. (11).
35. See Appendix D of Ref. 9.
36. This is identical to the distribution $I(\theta)$ for a "formation" resonance. See J. Button-Shafer, Parity of Fermions: Tests and Ambiguities, UCRL-16857, May 1966 (to be published in Phys. Rev.).
37. Cf. Eqs. 21 through 24 of Ref. 22. (Zemach in Ref. 23 also presents a similar relation, although he utilizes different language.)
38. John M. Blatt and Victor F. Weisskopf, Theoretical Nuclear Physics (Wiley Press, New York, 1952), p. 361.
39. We denote by L_{\max} the maximum value attained by L in the sums (II-48) and (II-50). Normally $L_{\max} = 2J$.
40. J. Murray, J. Button-Shafer, F. Shively, G. Trilling, J. Kadyk, A. Rittenberg, D. Siegel, J. Lindsey, and D. Merrill, A Separated 2.5 to 2.8 GeV/c K^- Beam at the Bevatron, in Proceedings of the International Conference on High Energy Physics, Dubna, USSR, 1964 (Atomizdat, Moscow, 1966), Vol. II, p. 541; and UCRL-11426, July 1964.

41. Deane W. Merrill, Design of the K-63 Beam Using an Analog Computer, Alvarez Group Physics Memo 519 (Rev.), August 1964.
42. S. Flatté, S. Chung, L. Hardy, and R. Hess, K-63: Changing the Incident K^- Momentum from 2.7 GeV/c to 2.1 GeV/c, Alvarez Group Physics Memo 524, August 1964.
43. Joseph J. Murray, Glass Cathodes in Vacuum-Insulated High-Voltage Systems, in Proceedings of International Conference on Instrumentation for High-Energy Physics, Berkeley, California, September 1960 (Interscience Publishers, New York, 1961), p. 25.
44. Daniel Siegel, Joseph J. Murray, Alan Rittenberg, and Janice Button-Shafer, Quadrupole Magnet Analysis and Shimming, Alvarez Physics Memo NFD-518, July 1964.
45. Compelling interest in 1.7 BeV/c K^- (especially by Shafer) prompted redesign and realignment of the beam.
46. Events containing Ξ^- (event-types 12, 72, and 74) were measured exclusively on Franckensteins; events containing Ξ^0 (types 32, 40, and 42) were measured on SMP's as well as Franckensteins.
47. For a description of the standard analysis procedure and computer programs, see A. H. Rosenfeld, Nucl. Instr. Methods 20, 422 (1963), or A. H. Rosenfeld and W. E. Humphrey, Ann. Rev. Nucl. Sci. 13, 103 (1963).
48. A description of the K-63 scanning procedure, and a list of kinematic hypotheses tested in K-63 PACKAGE, appears in R. Casey, O. Dahl, G. Smith, and L. Polissar, K-63 Scanning Instructions, Alvarez Group Physics Memo NFD-456, July 1963 (Rev. April 1964). See also Marten, Casey et al., Addenda to K-63 Scanning Instructions, Alvarez Group Physics Memo NFD-472, Sept. 1963.
49. DST-EXAM is described in O. Dahl, G. Kalbfleisch, and A. Rittenberg, DST-EXAM-2 and Pi-63, K-63 Data Analysis Systems, Alvarez Group Programming Memo P-54 (Rev.), July 1965.
50. The calculation of confidence levels is described in Ref. 49. In this analysis we have used for the variable χ^2 weighting and cut-off parameters the standard K-63 values, namely: CHISQ(1-4) = 13.0, 18.0, 32.0, 30.0; FAC(1-4) = 0.8, 0.7, 0.5, 0.6;

FLABEL(19,20) = 0.2, 0.005. Beam momentum and fiducial volume criteria were not imposed on the events selected.

51. For all Ξ^- hypotheses we observe slightly non-uniform confidence level distributions, i. e., an excess of events for c.l. values near 1.0. We judge that the χ^2 correction factors in DST-EXAM (see Ref. 50) are too extreme for Ξ^- events, and perhaps for multi-vertex events in general. The use of incorrect χ^2 correction factors has little effect on the classification of Ξ^- events, however, because virtually all ambiguities are between two or more Ξ^- hypotheses, which are affected similarly.
52. The ratio R as defined contains more information than a simple ratio of confidence levels x/y . Because confidence levels <0.005 may be recorded as zero (if contributing χ^2 exceed certain limits specified in Ref. 50) the observed ratio x/y is meaningless for "low c.l." events, i. e., events having $y < 0.005$. For these events the ratio R is a lower limit of the actual confidence-level ratio, provided all confidence levels ≥ 0.005 are correctly recorded. The χ^2 limits in DST-EXAM are set high enough that this is the case.
53. A list of kinematic hypotheses tested in π -63 PACKAGE appears in Dahl, Koellner, Miller, Starr, and Strong, π -63 Scanning Instructions, Alvarez Group Physics Memo NFD-507, May 1964.
54. As nearly as possible, the momenta of the π -63 samples were chosen to agree with those of the K-63 samples. Unfortunately, the π -63 data at 2.6 BeV/c are limited; however, they yield results similar to those at 3.1 BeV/c.
55. The conclusions of this paragraph are not sensitive to assumed values of decay parameters; the values used are approximately those best fitting the data.
56. James W. Cronin and O. E. Overseth, Phys. Rev. 129, 1795 (1963).
57. Given N subsamples having $|t_{10}^{\text{actual}}| \approx t_{10}^{\text{max}}$, we expect half of these, on the average, to yield experimental values $|t_{10}^{\text{obs}}| > t_{10}^{\text{max}}$, thereby producing a decrease of $\approx N/4$ in $\ln \mathcal{L}$ when the constraint is applied. Our data are consistent with

- $J = 3/2$, with ≈ 30 of the 47 subsamples having $|t_{10}^{\text{actual}}| \approx t_{10}^{\text{max}}$.
58. Frank T. Solmitz, *Ann. Rev. Nucl. Sci.* 14, 375 (1964).
59. J. Peter Berge, private communication. The constant factor actually varies from ≈ 0.10 at $|P_{\Xi}| = 1.0$ to ≈ 0.07 at $|P_{\Xi}| \approx 0.05$.
60. Two of the 47 Ξ^- subsamples in Table V-III yielded unacceptable fits ($|a_{\Xi}| > 1$) and were ignored.
61. D. Duane Carmony, Gerald M. Pjerrou, Peter E. Schlein, William E. Slater, Donald H. Stork, and Harold K. Ticho, *Phys. Rev. Letters* 12, 482 (1964).
62. For a discussion of the technique, proposed by N. Byers, see Appendix C of Ref. 9.
63. G. W. London, R. R. Rau, N. P. Samios, S. S. Yamamoto, M. Goldberg, S. Lichtman, M. Primer, and J. Leitner, *Phys. Rev.* 143, 1034 (1966).
64. L. Jauneau et al., in Proceedings of the Sienna International Conference on Elementary Particles, Sienna, Italy, 1963 (Società Italiana di Fisica, Bologna, Italy, 1963), p. 1; and L. Jauneau et al., ibid., p. 4.
65. H. Schneider, *Phys. Letters* 4, 360 (1963).
66. We define the S and P amplitudes as
- $$S = |S| e^{i\Delta S} = \rho_S e^{i\delta_S}$$
- $$P = |P| e^{i\Delta P} = \rho_P e^{i\delta_P}$$
- where δ_S and δ_P are final-state $\Lambda\pi$ scattering phase shifts. Invariance under T (C) requires that ρ_S and ρ_P be relatively real (imaginary). As no spin-1/2 $\Lambda\pi$ resonances are known in the vicinity of 1320 MeV, δ_S and δ_P are expected to be small.
67. S. B. Treiman, *The Weak Interactions*, in Dispersion Relations and Elementary Particles (Lectures for Summer School of Theoretical Physics, Les Houches, 1960), edited by C. DeWitt and R. Omnes (Wiley Press, New York, 1960), p. 526.
68. Benjamin Lee, *Phys. Rev. Letters* 12, 83 (1964).
69. See, for example, Murray Gell-Mann, *Phys. Rev. Letters* 12, 155 (1964); Hirotaka Sugawara, *Progr. Theoret. Phys.* (Kyoto)

- 31, 213 (1964); and Sidney Coleman and S. L. Glashow, Phys. Rev. 134, B671 (1964).
70. Roger O. Bangerter, Angela Barbaro-Galtieri, J. Peter Berge, Joseph J. Murray, Frank T. Solmitz, M. Lynn Stevenson, and Robert D. Tripp, Phys. Rev. Letters 17, 495 (1966).
 71. M. L. Stevenson, J. P. Berge, J. R. Hubbard, G. R. Kalbfleisch, J. B. Shafer, F. T. Solmitz, S. G. Wojcicki, and P. G. Wohlmut, Phys. Letters 9, 349 (1964); and erratum, Phys. Letters 17, 358 (1965).
 72. The calculation was performed by J. Peter Berge.
 73. D. Berley, S. Herzbach, R. Kofler, S. Yamamoto, W. Heintzelman, M. Schiff, J. Thompson, and W. Willis, Σ^+ Decay Parameters, presented at the 13th International Conference on High-Energy Physics, Berkeley, California, August 31-Sept. 7, 1966, and summarized in Proceedings of the International Conference on High Energy Physics, Berkeley, California, September 1966 (University of California Press, Berkeley, California, to be published).
 74. World average values are tentative values from a forthcoming compilation by Arthur H. Rosenfeld, Angela Barbaro-Galtieri, Janos Kirz, William J. Podolsky, Matts Roos, William J. Willis, and Charles Wohl, Data on Elementary Particles and Resonant States, UCRL-8030 (Rev.), August 1966.
 75. A. Pais, Rev. Mod. Phys. 38, 215 (1966).
 76. P. E. Schlein, D. D. Carmony, G. M. Pjerrou, W. E. Slater, D. H. Stork, and H. K. Ticho, Phys. Rev. Letters 11, 167 (1963).
 77. G. M. Pjerrou, P. E. Schlein, W. E. Slater, L. T. Smith, D. H. Stork, and H. K. Ticho, Phys. Rev. Letters 14, 275 (1965).
 78. Because not all event-type topologies have been fully measured, no conclusions regarding cross sections or branching ratios should be drawn from these data.
 79. The K^* mass limits are 840 to 940 MeV, corresponding to $2 \times \Gamma_{\text{obs}}$.
 80. A priori errors have been multiplied by appropriate scaling factors of ≈ 1.0 to 1.3 in order to produce correct χ^2 distributions for fits at the production vertex.

81. S. P. Rosen, Phys. Rev. Letters 11, 100 (1963); and A. J. Macfarlane and E. C. G. Sudarshan, Nuovo Cimento 31, 1176 (1964).
82. C. H. Chan and A. Q. Sarker, Phys. Rev. Letters 13, 731 (1964); T. K. Kuo and Tsu Yao, Phys. Rev. Letters 14, 79 (1965); and A. D. Dolgov, L. B. Okun, I. Ya. Pomeranchuk, and V. V. Solov'yev, Phys. Letters 15, 85 (1965).
83. B. Sakita, Phys. Rev. Letters 13, 643 (1964).
84. H. R. Rubinstein, Phys. Rev. Letters 17, 41 (1966).
85. Sidney Coleman and Sheldon L. Glashow, Phys. Rev. 134, B671 (1964).
86. R. H. Socolow, Electromagnetic Masses in the Unitary Symmetry Theory (Ph. D. thesis), Harvard University, Cambridge, Massachusetts, 1964 (unpublished).
87. Roger F. Dashen and Steven C. Frautschi, Phys. Rev. Letters 13, 497 (1964); Phys. Rev. 137, B1331 (1965); and Phys. Rev. 137, B1318 (1965).
88. Aditya Kumar, Phys. Rev. 140, B202 (1965).
89. Frederick J. Gilman, Phys. Rev. 147, 1094 (1965).
90. H. Harari, Phys. Rev. 139, B1323 (1965).
91. The standard version of PACKAGE, which was used in the analysis of this report except in the Ξ^* (1530) mass-difference analysis, assumes $m(\Xi^0) = 1316.0$ MeV and $m(\Xi^-) = 1321.0$ MeV.
92. See J. Friedman and R. Ross, Maximum Likelihood Estimate of Resonant State Production in Multiparticle Final States, Alvarez Group Programming Memo P-102, October 1964; and J. Friedman, MURTLBERT Reference Guide, Alvarez Programming Memo P-144, July 1966.
93. J. D. Jackson, Nuovo Cimento 34, 1644 (1964). In SUPER FIT, $\phi_{R}^{\pm}(w)$ is calculated by a subroutine BREWIG, coded by Angela Barbaro-Galtieri.
94. John M. Blatt and Victor F. Weisskopf, Theoretical Nuclear Physics (Wiley Press, New York, 1952), p. 361.
95. We observe an upward shift of $\approx 2 \pm 3$ MeV in w_0 for fits omitting the pion from Ξ decay, as compared to fits omitting the K or

the other pion. If not merely a statistical fluctuation, this effect could partially explain a 5-MeV discrepancy, observed both in this experiment and in the UCLA experiment,⁷⁷ between $\Xi\pi^0$ and $\Xi^0\pi^-$ resonant masses.

96. Calculating the Ξ^- turning angle directly from the measured length and curvature of the Ξ^- track, we obtained poor 1C fits for many events having Ξ^- shorter than ≈ 1 cm. Acceptable fits were obtained for 97% of the events when the Ξ^- curvature was calculated from a Ξ^- -mass-dependent fit at the Ξ^- decay vertex.
97. Susumo Okubo, *Progr. Theoret. Phys. (Kyoto)* 27, 949 (1962).
98. Sidney Coleman and Sheldon L. Glashow, *Phys. Rev. Letters* 6, 423 (1961).
99. For a comparison of various SU(3) and SU(6) symmetry schemes, see Refs. 75 and 90.
100. Roger F. Dashen and Steven C. Frautschi, *Phys. Rev.* 135, B1190 (1964).
101. Values quoted are from the compilation of A. H. Rosenfeld et al. (Ref. 17) and from the following experiments: P. Schmidt, *Phys. Rev.* 140, B1329 (1965); Martin G. Olsson, *Phys. Rev. Letters* 14, 118 (1965); George Gidal, Anne Kernan, and Sedong Kim, *Phys. Rev.* 141, 1261 (1966); W. A. Cooper, H. Filthut, A. Fridman, E. Malamud, E. S. Gelsema, J. C. Kluyver, and A. G. Tenner, *Phys. Rev. Letters* 8, 365 (1964); R. Armenteros, M. Ferro-Luzzi, D. W. G. Leith, R. Levi-Setti, and A. Minten, *Phys. Letters* 19, 75 (1965); G. W. London et al. (Ref. 63); and G. M. Pjerrou et al. (Ref. 77).
102. From Figs. VI-2 and VI-4 we estimate that these mass limits accept $(393 + 88)/(475 + 100) \approx 84\%$ of the $\Xi^*(1530)$, in a sample containing $(70 + 18)/(463 + 106) \approx 15\%$ non- Ξ^* background. More appropriate limits might have been 1520 to 1545 MeV, accepting 72% of the Ξ^* with 11% background.
103. With our choice of axes ($\hat{Z} = \hat{K} \times \hat{\Xi}^*$, $\hat{Y} = \hat{\Xi}^*$, $\hat{X} = \hat{Y} \times \hat{Z}$) only the odd-M moments [those containing odd powers of $(\hat{\Xi} \cdot \hat{Y})$] are affected by the removal of events having $(\hat{\Xi} \cdot \hat{Y}) < 0$. But these moments are zero due to parity conservation in the $\Xi^*(1530)$ production process.

104. The quoted χ^2 and confidence levels are taken from Ref. 13, where results from UCLA data (Ref. 76) and Berkeley data (Ref. 13) are compared in a consistent fashion. Button-Shafer points out that confidence levels are underestimated (especially for spin χ^2 values) due to the smallness of samples analyzed. Comparison of χ^2 with those obtained from randomly generated events indicates that (in Ref. 13) "the $D_{3/2}$ hypothesis is discriminated against with perhaps a $\leq 3\%$ confidence level."
105. The parity of Ξ^* (1817) is defined relative to that of Ξ^* (1530).
106. H. C. Corben, Phys. Rev. 145, 1251 (1966).
107. The ionization information, obtained for the author by Tom Strong, has been forwarded to J. Richard Hubbard and J. Peter Berge so that current tapes may be properly updated.
108. Like the bubble-chamber coordinate system (x_{ch}, y_{ch}, z_{ch}), the systems (x, y, z) and (x', y', z') are right-handed in Fig. B-1 and left-handed in real space; i. e., $\hat{x}(\hat{x}')$, $\hat{y}(\hat{y}')$, and $\hat{z}(\hat{z}')$ lie roughly along \hat{z}_{ch} , \hat{x}_{ch} , and \hat{y}_{ch} , respectively. For purposes of this discussion we assume the magnetic field to point along $-\hat{z}_{ch}$ (which is not really the case) so that negative particles curve toward $+\hat{x}_{ch}$, as desired.
109. Here $\vec{p}_{\Xi}^{(lab)}$ is measured at the Ξ decay vertex.
110. For most events, $\cos \theta_{\Lambda}^{(\Xi)}$ is more nearly equivalent to $(\hat{\Lambda} \cdot \hat{K})$ than to $(\hat{\Lambda} \cdot \hat{\Xi})$, since $\vec{p}_{\Xi}^{(lab)}$ is more nearly parallel to $\hat{K} = \hat{p}_K$ (c. m.) than to $\hat{\Xi} = \hat{p}_{\Xi}$ (c. m.). Nevertheless, due to the forward $(\hat{\Xi} \cdot \hat{K} \approx +1)$ peak in the Ξ production distribution, $\cos \theta_{\Lambda}^{(\Xi)}$ is roughly equivalent to $(\hat{\Lambda} \cdot \hat{\Xi})$ as well as to $(\hat{\Lambda} \cdot \hat{K})$.
111. The observed distribution of $p_{\Xi}^{(lab)}$ extends from 0.5 to 3.0 Bev/c, with a mean value near 1.7 Bev/c. Approximately 80% of the events lie between the representative values 1.0 and 2.4 Bev/c.
112. Philippe Eberhard, private communication.
113. The visible volume of the chamber is approximately defined by:
 $-19 \text{ cm.} \leq x_{ch} \leq 17 \text{ cm.}$, $-86 \text{ cm.} \leq y_{ch} \leq 86 \text{ cm.}$,
 $4 \text{ cm.} \leq z_{ch} \leq (0.132 x_{ch} + 36 \text{ cm.})$. Rake 15 and the lead plate are at $y_{ch} = 78 \text{ cm.}$ and $y_{ch} = 63 \text{ cm.}$, respectively.

114. James E. Simmons, Effect of Proton-Proton Scattering on an Initial Longitudinal-Spin Polarization (Ph.D. thesis), UCRL-3625, Jan. 1957. A covariant derivation is given by V. Bargmann, Louis Michel, and V. L. Telegdi, Phys. Rev. Letters 2, 435 (1959).
115. For Ξ^- , Eq. B-14 expresses the rate of precession relative to fixed axes defined at the Ξ^- production vertex, which we have used. Relative to axes rotating with the Ξ^- momentum, the \hat{n} -component of $\vec{\omega}(t)$ is $C_1' = C_1 - \omega_{cy}$, where ω_{cy} , the cyclotron frequency, is $-eH/\gamma mc$. For the case of protons, C_1' reduces to the familiar form $\gamma(\mu - 1)\omega_{cy}$.
116. M. A. B. Beg and A. Pais, Phys. Rev. 137, B1514 (1965). The experimental value of μ_Λ is -0.73 ± 0.17 . [See D. A. Hill and K. K. Li, Phys. Rev. Letters 15, 85 (1965).]
117. Distributions of $(\hat{\Lambda} \cdot \hat{n})$ appear in Fig. V-12. Distributions of $\hat{\Lambda} \cdot (\hat{K} \times \hat{n})$ and $\hat{\Lambda} \cdot (\hat{\Xi} \times \hat{n})$ are consistent with isotropy.
118. D. Siegel, J. Friedman, and R. Ross, Study of K-63 Beam Momenta using Taus, Alvarez Group Physics Memo NFD-582, February 1966, and Alan Rittenberg, private communication.
119. V. Cook, Bruce Cork, T. F. Hoang, D. Keefe, L. T. Kerth, W. A. Wenzel, and T. F. Zipf, Phys. Rev. 123, 320 (1961).
120. A. N. Diddens, E. W. Jenkins, T. F. Kycia, and K. F. Riley, Phys. Rev. Letters 10, 262 (1963).
121. James S. Lindsey, Production Properties and Decay Modes of the ϕ Meson (Ph.D. thesis), UCRL-16526, December 1965.
122. Most three-prong events are due to the τ decay mode $K^- \rightarrow \pi^+ + \pi^- + \pi^-$; however, one cannot always distinguish a τ decay from other three-prong decay modes of the K^- . In our calculation we assume the true number of three-prong events to be the number observed in the first scan (see Ref. 121, p. 30). A 4% uncertainty is included to allow for uncertainty in the scanning procedure followed; i. e., although scanners were instructed to record all three-prong events, some obvious Dalitz pairs were omitted.

123. For Ξ^0 events, an extra factor of $(\Xi \text{ candidates processed in } \pi\text{-63 PACKAGE})/(\Xi \text{ candidates})$ (See Table A-I) should be included in effective path lengths.
124. This factor, to correct for unmeasured events, is appropriate if failing events are assumed to be correctly identified but badly measured. If failing events are assumed to be junk, i. e., stray vees, misidentified event types, etc., the correct factor is $(\text{events measured})/(\text{events observed})$. In actuality the failing events include both bad measurements and junk, with the ratio depending upon the topology and the status of remeasurements.
125. This factor corrects for the fact that Table A-I represents a more complete Ξ^- sample than Table V-I. The factor is not necessary for Ξ^0 events.
126. Jim Morris and J. B. Shafer, SPIN-P-MOCK, a Program to Generate Randomly a Two-Step Decay Chain of Polarized Fermions, Alvarez Group Programming Memo P-74, February 1964.
127. D. W. Merrill, J. B. Shafer, and J. R. Morris, LIKEF, a Maximum-Likelihood Program for Byers-Fenster Analysis of Nonleptonic Hyperon Decay, Alvarez Group Programming Memo (in preparation).
128. J. B. Shafer and J. R. Morris, SPINPAR-I, a Program to Determine Spin and Parity of a Fermion, Alvarez Group Programming Memo P-69, November 1963.

FIGURE CAPTIONS

- Fig. II-1. Diagram of Ξ production and decay. See text for definition of angles and coordinate systems.(page 4).
- Fig. III-1. Schematic layout of K-63 beam. S1 and S2 are electrostatic separators; M1, M2, M3, and M4 are bending magnets; Q1, Q2, ... Q13 are quadrupoles.
- Fig. III-2. Profiles of K-63 beam in (a) vertical plane and (b) horizontal plane. The y-axis (beam direction) is compressed by a factor of 80 relative to x and z, and effects of bending magnets are ignored.
- Fig. III-3. Schematic drawing of first mass slit seen (a) end on, and (b) from above lower jaw. The y-axis (beam direction) is compressed by a factor of 6 relative to x and z. High and low momentum K^- (2% above and below the nominal momentum) are focused at A and B respectively.
- Fig. IV-1. Results of ionization investigation, for 138 type-72 events having $1/3 \leq Q \leq 3$. Ionization showed the positive track at the production vertex to be K^+ in 61 cases and π^+ in 61 cases; 16 events could not be resolved.
- Fig. IV-2. Confidence-level plot for 2720 passing type-72 events. Most points lie on the x- or y-axis.
- Fig. IV-3. Classification of events by confidence levels (drawing not to scale).
- Fig. IV-4. Distribution of $\log_{10} R$ for the hypothesis $K^- + p \rightarrow \Xi^0 + K^+ + \pi^-$ [Eq. IV-14] for (a) K-63 events at 1.7 and 2.1 BeV/c, and (b) π^- -63 events at 2.1 BeV/c. The effective π^- path length in (b) is 4.1 ± 3.0 times that of the estimated π^- beam contamination in (a).

Fig. IV-5. Same as Fig. IV-4, except for (a) K-63 events, 2.45 through 2.7 BeV/c, and (b) π^- -63 events at 2.6 and 3.1 BeV/c. The effective π^- path length in (b) is 1.7 ± 0.5 times that of the estimated π^- beam contamination in (a).

Fig. IV-6. Distribution of $\log_{10} R$ for the hypothesis $K^- + p \rightarrow \Xi^0 + K^0$ [Eq. IV-15] for (a) K-63 events at 1.7 and 2.1 BeV/c, and (b) π^- -63 events at 2.1 BeV/c. The effective π^- path length in (b) is 2.0 ± 1.2 times that of the estimated π^- beam contamination in (a).

Fig. IV-7. Same as Fig. IV-6, except for (a) K-63 events, 2.45 through 2.7 BeV/c, and (b) π^- -63 events at 2.6 and 3.1 BeV/c. The effective π^- path length in (b) is 2.3 ± 0.7 times that of the estimated π^- beam contamination in (a).

Fig. IV-8. Distribution of $\log_{10} R$ for the hypothesis $K^- + p \rightarrow \Xi^0 + K^0 + \pi^+ + \pi^-$ [Eq. IV-16] for (a) K-63 events, 2.45 through 2.7 BeV/c, and (b) π^- -63 events at 2.6 and 3.1 BeV/c. The effective π^- path length in (b) is 3.2 ± 1.1 times that of the estimated π^- beam contamination in (a).

Fig. V-1. Dependence of $w = \ln \mathcal{L}$ upon assumed spin factor $(2J + 1)$, for 3278-event Ξ^- sample. Black and white points represent values obtained with and without density matrix constraint applied, respectively.

Fig. V-2. Distribution of $X = \Delta \ln \mathcal{L}$ for (a) the 15 Ξ subsamples of Table V-II; and (b) 75 Monte Carlo samples having $J = 1/2$, $a_\Lambda = 0.62$, $a_\Xi = -0.40$, $\Phi_\Xi = 0$, $t_{10} = 0$. The curve shown in (b) represents $\bar{X} = 0$, $\sigma_X = 0.27$.

Fig. V-3. Distribution of $X = \Delta \ln \mathcal{L}$ for (a) 75 Monte Carlo samples having $J = 1/2$, $a_\Lambda = 0.62$, $a_\Xi = -0.40$, $\Phi_\Xi = 0$, $t_{10} = t_{10}^{\max} = 0.57$; and (b) 75 Monte Carlo samples having $J = 3/2$; $a_\Lambda = 0.62$, $a_\Xi = -0.40$, $\Phi_\Xi = 0$, $t_{10} = t_{10}^{\max} = 0.43$. Curves shown represent (a) $\bar{X} = 1.66$, $\sigma_X = 1.93$; (b) $\bar{X} = -0.67$, $\sigma_X = 1.07$.

Fig. V-4. Observed values X_{obs} and calculated functions $P(X, J)$ for (a) 4080-event combined Ξ sample (see Table V-II), and (b) 3130 events of the 3278-event Ξ^- sample (see Table V-III).⁶⁰ Arrows indicate values of X_{obs} .

Fig. V-5. Observed values X_{obs} and calculated functions $P(X, J)$ for (a) 649-event Ξ^0 sample (see Table V-III) and (b) 3779-event combined Ξ sample.⁶⁰ Arrows indicate values of X_{obs} .

Fig. V-6. Plot of $X = \Delta \ln \mathcal{L}$ vs $|t_{10}|$ for 45 Ξ^- subsamples and 7 Ξ^0 subsamples (see Table V-III). Values of $|t_{10}|$ were obtained with $J = 1/2$. Dashed curves represent the expected range of X ($\bar{X} \pm \sigma_X$) for the $J = 1/2$ and $J = 3/2$ assumptions, as a function of $|t_{10}|$. The solid curve represents the expected distribution in $|t_{10}|$ (due to measurement errors) if all subsamples have zero polarization. Points a, b, and c designate $\langle (\delta t_{10})^2 \rangle^{1/2} = 0.16$, $\langle t_{10}^2 - (\delta t_{10})^2 \rangle^{1/2} = 0.24$, and $\langle t_{10}^2 \rangle^{1/2} = 0.29$.

Fig. V-7. Plot of $w = \ln \mathcal{L}$ as a function of assumed Φ_{Ξ^0} , for Ξ^0 data appearing in Table V-VI. Error bars represent 1 standard deviation. For K-72 and K-63 data combined, no value of Φ_{Ξ^0} is excluded by more than 2.9 standard deviations, and all values between -10° and $+220^\circ$ are consistent (within 2 standard deviations) with the data.

Fig. V-8. Correlation between α_Λ and $\alpha_{\Xi^-,0}$ for combined K-72 and K-63 data. Diagonal lines represent the variation of α_{Ξ^-} and α_{Ξ^0} as functions of α_Λ ; points A and A' indicate the values ($\alpha_\Lambda = 0.673 \pm 0.072$, $\alpha_{\Xi^-} = -0.389 \pm 0.044$, $\alpha_{\Xi^0} = -0.398 \pm 0.106$) that maximize the likelihood for combined Ξ^- and Ξ^0 data. If the value $\alpha_\Lambda = 0.62 \pm 0.07$ is included as independent information,⁵⁶ the likelihood is maximized at B and B' ($\alpha_\Lambda = 0.647 \pm 0.048$, $\alpha_{\Xi^-} = -0.398 \pm 0.041$, $\alpha_{\Xi^0} = -0.413 \pm 0.104$). Quoted errors $\delta\alpha_\Lambda$ and $\delta\alpha_{\Xi^-}$ correspond to (one-half) the horizontal and vertical dimensions of the ellipses. If correlations between α_Λ and $\alpha_{\Xi^-,0}$ were ignored, the errors $\delta\alpha_{\Xi^-}$ and $\delta\alpha_{\Xi^0}$ would be equal to the distances $AC = AD$ and $A'C' = A'D'$, respectively.

Fig. V-9. Values of Ξ decay parameters obtained in various experiments (plotted in order of number of events processed). See text regarding calculation of approximate world average values (indicated by arrows). Dashed entry for Φ_{Ξ^0} represents secondary solution in K-72 data, less likely by ≈ 1.6 standard

deviations. For combined K-72 and K-63 Ξ^0 data, all values of Φ_{Ξ^0} between -10° and $+220^\circ$ are consistent (within two standard deviations) with the data.

Fig. V-10. Comparison of experimental data with Lee's SU(3) triangle prediction ($\Sigma_0^+ = \frac{1}{\sqrt{3}} [2\Xi_-^- - \Lambda_-^0]$) and $|\Delta I| = 1/2$ rule ($\Sigma_0^+ = \frac{1}{\sqrt{2}} [\Sigma_-^- - \Sigma_+^+]$). The SU(3) prediction [Eq. (V-28)] requires overlap of ellipses 1 and 2; the $|\Delta I| = 1/2$ prediction [Eq. (V-29)] requires overlap of 2 with either 3 or 4 (corresponding to solutions with Σ^- decaying via S- or P-wave, respectively). Both predictions combined [Eq. (V-32)] require overlap of 1 with either 3 or 4. Solution 4 is incompatible with the results of a recent experiment.⁷³

Fig. V-11. Distributions of $(\hat{p} \cdot \hat{\Lambda})$ for (a) 3431 Ξ^- events and (b) 649 Ξ^0 events. K-72 events are shaded.

Fig. V-12. Decay distribution, 4080 Ξ^- and Ξ^0 events. Events in subsamples having $P_{\Xi} < 0$ (shaded) have been rotated 180° about the beam axis, effectively raising $\langle P_{\Xi} \rangle$ from 0.02 ± 0.04 to 0.23 ± 0.04 . The theoretical curves are plotted for $J = 1/2$, $\alpha_{\Lambda} = 0.62$, $\alpha_{\Xi} = -0.40$, $\Phi_{\Xi} = 0$, and $P_{\Xi} = 0.23$.

Fig. V-13. Decay distribution, 649 Ξ^0 events. Events in subsamples having $P_{\Xi} < 0$ (shaded) have been rotated 180° about the beam axis, effectively raising $\langle P_{\Xi} \rangle$ from 0.18 ± 0.12 to 0.30 ± 0.12 . The theoretical curves are plotted for $J = 1/2$, $\alpha_{\Lambda} = 0.62$, $\alpha_{\Xi} = -0.40$, $\Phi_{\Xi} = 130^\circ$, and $P_{\Xi} = 0.30$.

Fig. V-14. Decay distribution, 4080-event Monte Carlo sample having $J = 1/2$, $\alpha_{\Lambda} = 0.62$, $\alpha_{\Xi} = -0.40$, $\Phi_{\Xi} = 0$, and $t_{10} = 0.57$. The theoretical curves correspond to the parameters used in generating the events.

Fig. V-15. Decay distribution, 4080-event Monte Carlo sample having $J = 3/2$, $\alpha_{\Lambda} = 0.62$, $\alpha_{\Xi} = -0.40$, $\Phi_{\Xi} = 0$, and $t_{10} = 0.43$. The theoretical curves correspond to the parameters used in generating the events.

Fig. VI-1. Dalitz plot for 1819 unambiguous $\Xi K \pi$ final states, 1.7 to 2.7 BeV/c (see text). Curves shown are kinematic limits for 1.7, 2.1, and 2.7 BeV/c. Error bars represent $2\Gamma_{\text{obs}}$ [$\Gamma_{\text{obs}} \approx 12$ MeV and ≈ 50 MeV for $\Xi^*(1530)$ and $K^*(890)$, respectively].

Fig. VI-2. Observed $\Xi \pi$ mass distribution for unambiguous $\Xi K \pi$ final states. Only the 1017 unshaded events (non- K^* , with visible Λ decay) are used in further analysis. Solid curve represents a P-wave resonance having $m(\Xi^*) = 1533$ MeV, Γ_0 (true width) = 7 MeV, folded with the experimental resolution function having width $\Gamma_{\text{RF}} = 6$ MeV. Dashed curve is phase space.

Fig. VI-3. Plot of $K\pi_2$ mass squared vs $\Xi\pi_1$ mass squared, for 265 unambiguous $\Xi K \pi \pi$ final states, 2.1 to 2.7 BeV/c (see text). Only $K\pi_2$ and $\Xi\pi_1$ pairs having $I_z = \pm 1/2$ are plotted (two points/event for $\Xi^- K^0 \pi^+ \pi^0$ final states). Curve shown is kinematic limit for 2.7 BeV/c. Error bars represent $2\Gamma_{\text{obs}}$ ($\Gamma_{\text{obs}} \approx 12$ MeV and ≈ 50 MeV for $\Xi^*(1530)$ and $K^*(890)$ respectively).

Fig. VI-4. Observed $\Xi \pi$ mass distribution for unambiguous $\Xi K \pi \pi$ final states. Only $\Xi \pi$ pairs having $I_z = \pm 1/2$ are plotted (two points/event for $\Xi^- K^0 \pi^+ \pi^0$ final states). Only the 172 unshaded $\Xi \pi$ pairs are used in further analysis. Solid curve represents a P-wave resonance having $m(\Xi^*) = 1532$ MeV, Γ_0 (true width) = 7 MeV, folded with the experimental resolution function having width $\Gamma_{\text{RF}} = 5$ MeV. Dashed curve is phase space.

Fig. VI-5. Observed $\Lambda \pi \pi$ effective-mass distributions for unambiguous non- K^* $\Xi K \pi$ events, fit according to 1C hypotheses (VI-7) through (VI-9). Plotted curves represent best fits, with the assumptions of (i) P-wave resonance, zero-width resolution function; (ii) Gaussian resolution function, zero-width resonance; (iii) P-wave resonance having Γ_0 (reduced width) = 7 MeV, folded with experimental resolution function (illustrated). Values of $m(\Xi^*)$ and Γ_{obs} refer to solid curves (iii).

Fig. VI-6. Dependence of $m(\Xi^*)$ (triangles) and $m(\Lambda\pi)$ (circles) upon assumed masses $m(\Xi^-)$ and $m(\Xi^0)$, for (a) $\Xi^- K^0 \pi^+$ events; (b) $\Xi^- K^+ \pi^0$ events; (c) $\Xi^0 K^+ \pi^-$ events; (d) and (e), $\Xi^- K^+ \pi^0$ and $\Xi^0 K^+ \pi^-$ events combined. In (d) and (e), $m(\Xi^-)$ and $m(\Xi^0)$ are varied in parallel and opposite directions, respectively. In the fits, we assumed a zero-width resolution function, as in Eq. (VI-11). Numbers in parentheses indicate the number of events passing the selection criteria in each case. Diagonal solid lines represent least-squares fits to the plotted points. Diagonal dashed lines represent the condition $m(\Lambda\pi) = m(\Xi)$; i. e., (measured Ξ mass) = (assumed Ξ mass).

Fig. VI-7. Predicted electromagnetic mass splittings of the spin-1/2 octet and spin-3/2 decuplet, in (a) SU(3) and SU(6); (b) quark model; (c) tadpole model. In SU(3), the 10 mass differences are described by five independent parameters (a, b, c, a', b'). In SU(6)⁸² $a = a'$ and $b = b'$. In the more restricted SU(6) model of Sakita,⁸³ $a = a'$, $b = b'$, and $c = 0$. In the quark model,⁸⁴ there are four independent parameters (a'', b'', c'', d''); if the spin- and isospin-dependence of quark forces is ignored, $d'' = 0$. In the tadpole model,⁸⁶ there is one independent parameter x; the three terms associated with each mass difference represent, respectively, (i) tadpole term alone; (ii) contribution due to spin-1/2 octet; (iii) contribution due to spin-3/2 decuplet.

Fig. VI-8. Comparison of observed decuplet mass splittings with predictions of SU(3). Solid straight lines represent observed mass differences, in terms of SU(3) parameters a' and b' defined in Fig. VI-7; dashed lines represent standard-deviation errors. Ellipses centered at A and B represent best-fit values of a' and b' (with standard-deviation errors) without and with Ξ^* data, respectively. Values of parameters and χ^2 are presented in Table VI-IV.

Fig. VI-9. Values of $w = \ln \mathcal{L}$ from fits to (a) 159 $\Xi^- K^0 \pi^+$; (b) 39 $\Xi^- K^+ \pi^0$; (c) 53 $\Xi^0 K^+ \pi^-$; (d) 96 $\Xi K \pi \pi$. Fits with $L_{\max} = 1$ have four free parameters (one per sample); fits with $L_{\max} = 3$ have 28 parameters (7 per sample).

Fig. VII-1. Plot of $\Xi\pi$ mass squared vs $\Xi\pi\pi$ mass squared for 164 K-63 $\Xi K \pi \pi$ events. Only $\Xi\pi$ combinations having $I_z = \pm 1/2$ are plotted; $\Xi^- K^0 \pi^+ \pi^0$ events appear twice in the scatter plot and $\Xi\pi$ distribution, but only once in the $\Xi\pi\pi$ distribution. The shaded regions and resonance widths illustrated correspond to mass limits defined in the text. The kinematic boundary illustrated corresponds to an incident momentum of 2.7 BeV/c. The plotted curve represents $\Xi\pi\pi$ phase space for all events containing $\Xi^*(1530)$, with and without $K^*(890)$, normalized to events outside the region $3.2 \text{ BeV}^2 \leq m^2(\Xi\pi\pi) \leq 3.4 \text{ BeV}^2$.

Fig. VII-2. Scatter plot of c.m. energy vs $\cos \alpha = \hat{\Xi}^*(1530) \cdot \hat{\Xi}^*(1817)$ for 41 events containing both $\Xi^*(1817)$ and $\Xi^*(1530)$. Events in K^* band ($m(K\pi_1) \geq 840 \text{ MeV}$) lie above the left-hand curves and are discarded; the 21 K^* events removed are replaced by assigning double weight to the 8 events above the right-hand curves.

Fig. VII-3. Distribution of (a) $|\cos \theta| \equiv |\hat{\Xi}^*(1530) \cdot \hat{n}|$ and (b) $|\cos \psi| \equiv |\hat{\Xi} \cdot \hat{\Xi}^*(1530)|$ for 41 events containing both $\Xi^*(1817)$ and $\Xi^*(1530)$. Theoretical curves, indicating the expected anisotropy for various $\Xi^*(1817) J^P$ assumptions, are normalized to the shaded area ($12 + 8 + 8 = 28$ events).

Fig. B-1. Coordinate systems used in discussion of systematic errors. Points A', B', ... F' represent projections of A, B, ... F. See Ref. 108 regarding the direction of \hat{H} .

Fig. B-2. Observed Ξ production distribution, in production c.m., for 2529 K-63 Ξ^- events. Angles and axes are defined with respect to the beam direction $\hat{p}_K^{(\text{lab})}$ and the bubble chamber z-axis, as illustrated in Fig. B-1.

- Fig. B-3. Observed Ξ decay distribution, in Ξ rest frame, for 2529 K-63 Ξ^- events. Angles and axes are defined with respect to $\hat{p}_{\Xi}^{(\text{lab})}$ and the bubble chamber z-axis, is illustrated in Fig. B-1.
- Fig. B-4. Parallel and perpendicular components (relative to incident beam direction $\hat{p}_K^{(\text{lab})}$) of Ξ lab. momentum $\vec{p}_{\Xi}^{(\text{lab})}$. (See Fig. B-1.)
- Fig. B-5. Parallel and perpendicular components (relative to incident beam direction $\hat{p}_K^{(\text{lab})}$) of Λ lab momentum $\vec{p}_{\Lambda}^{(\text{lab})}$. (See Fig. B-1.)
- Fig. B-6. Position in bubble chamber of the production vertex of 2529 K-63 Ξ^- events. Solid boundaries indicate visible volume of bubble chamber.
- Fig. B-7. Distribution of $(\hat{\Lambda} \cdot \hat{K})$ and $(\hat{\Lambda} \cdot \hat{\Xi})$ for (a, c) 3431 Ξ^- events and (b, d) 649 Ξ^0 events listed in Table V-I. The K-72 events are shaded. Curve in (a) represents $[w(z)]^{-1}$, where $w(z)$ is given by Eq. (B-31).
- Fig. C-1. Diagram illustrating c. m. momenta of particles A, B, J, and C in the reaction $A + B \rightarrow J + C + D + \dots$.
- Fig. E-1. Measured values of α_{Ξ} for (a, b) 15 Ξ samples; and (c, d) 75 Monte Carlo samples having $J = 1/2$, $t_{10} = 0$.
- Fig. E-2. Measured values of α_{Ξ} for (a, b) 75 Monte Carlo samples having $J = 1/2$, $t_{10} = 0.57$; and (c, d) 75 Monte Carlo samples having $J = 3/2$, $t_{10} = 0.43$.
- Fig. E-3. Measured values of t_{10} for (a, b) 15 Ξ samples; and (c, d) 75 Monte Carlo samples having $J = 1/2$, $t_{10} = 0$.
- Fig. E-4. Measured values of t_{10} for (a, b) 75 Monte Carlo samples having $J = 1/2$, $t_{10} = 0.57$; and (c, d) 75 Monte Carlo samples having $J = 3/2$, $t_{10} = 0.43$.
- Fig. E-5. Measured values of Φ_{Ξ} for (a) 15 Ξ samples; and (b) 75 Monte Carlo samples having $J = 1/2$, $t_{10} = 0$. The 15 Ξ samples in (a) have been weighted by $(\delta\Phi_{\Xi})^{-2}$.
- Fig. E-6. Measured values of Φ_{Ξ} for (a) 75 Monte Carlo samples having $J = 1/2$, $t_{10} = 0.57$; and (b) 75 Monte Carlo samples having $J = 3/2$, $t_{10} = 0.43$.



This report was prepared as an account of Government sponsored work. Neither the United States, nor the Commission, nor any person acting on behalf of the Commission:

- A. Makes any warranty or representation, expressed or implied, with respect to the accuracy, completeness, or usefulness of the information contained in this report, or that the use of any information, apparatus, method, or process disclosed in this report may not infringe privately owned rights; or
- B. Assumes any liabilities with respect to the use of, or for damages resulting from the use of any information, apparatus, method, or process disclosed in this report.

As used in the above, "person acting on behalf of the Commission" includes any employee or contractor of the Commission, or employee of such contractor, to the extent that such employee or contractor of the Commission, or employee of such contractor prepares, disseminates, or provides access to, any information pursuant to his employment or contract with the Commission, or his employment with such contractor.